Lehrstuhl für Robotik und Systemintelligenz
TUM School of Computation, Information and Technology
Technical University of Munich

AI-Driven Multimodal Joint Analysis and Prediction

From Data to Prediction: An Adaptive AI-Driven Framework for Multimodal Biomechanical Joint Analysis in Clinical Applications

Nikolas J. Wilhelm

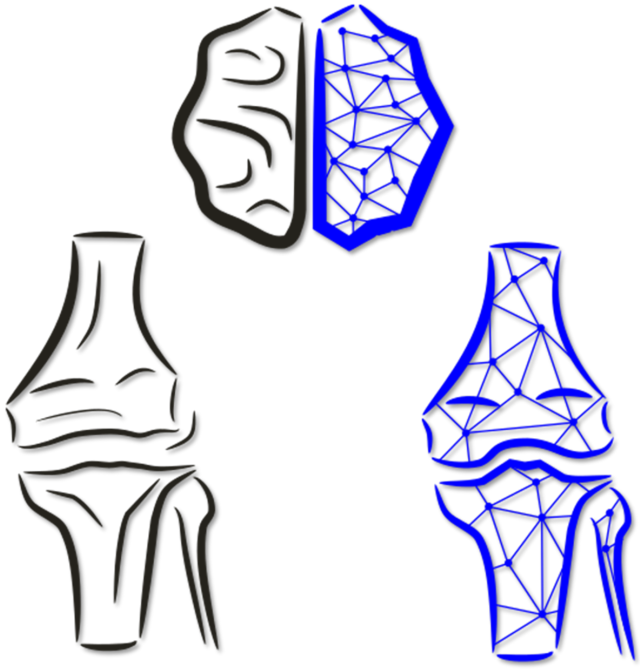

AI-Driven Multimodal Joint Analysis and Prediction

From Data to Prediction: An Adaptive AI-Driven Framework for Multimodal Biomechanical Joint Analysis in Clinical Applications

Nikolas J. Wilhelm

Technische Universität München
TUM School of Computation, Information and Technology

AI-Driven Multimodal Joint Analysis and Prediction

Nikolas J. Wilhelm

Vollständiger Abdruck der von der TUM School of Computation, Information and Technology der Technischen Universität München zur Erlangung eines

Doktors der Naturwissenschaften (Dr. rer. nat.)

genehmigten Dissertation.

Vorsitz:
Prof. Dr. Cristina Piazza

Prüfende der Dissertation:
1. Prof. Dr.-Ing. Sami Haddadin
2. apl. Prof. Dr. Rainer Burgkart
3. Prof. Dr. Robert Riener

Die Dissertation wurde am 20.06.2024 bei der Technischen Universität München eingereicht und durch die TUM School of Computation, Information and Technology am 31.10.2024 angenommen.

This dissertation is dedicated to my parents Dr. Helene Varady-Wilhelm and Dr. Wolfgang Wilhelm. I would also like to take this opportunity to thank the important people without whom this dissertation would not have been possible. First and foremost, I would like to thank Prof. Dr. Rainer Burgkart, who created the framework for this dissertation with his comprehensive medical and technical knowledge and his innovative thinking. My thanks also go to Prof. Dr. Sami Haddadin, who supervised the technical side of this work and provided decisive impulses at crucial moments. I would also like to thank Dr. Maximilian Karl, who made a very valuable contribution to the technical preparation of this dissertation with his AI knowledge and his great availability. Furthermore, I would like to thank Dr. Marco-Christopher Rupp for his expertise in preoperative planning and his attention to detail, as well as Thomas Dickmann for his mechatronic skills in exoskeleton development.
Last but not least, I would like to thank my fiancée Dr. Anna Tina Joseph, who accompanied me through all the ups and downs of this phase of my life and always had my back.

Abstract

This dissertation introduces an innovative framework that unifies medical informatics, robotics, and orthopedics. It responds to the key challenge of achieving real-time, objective data for advanced joint analysis and interventions, particularly in orthopedic patient care. To address this need, the work is organized into four components—Wearable Technology, Diagnostic and Planning Algorithms, Robotic Testing Platforms, and Optimization Algorithms—forming a comprehensive toolkit for clinicians and researchers.

Orthopedic care relies on timely, quantitative assessment of patient status. Two wearable solutions were therefore developed. First, an Internal Measurement Unit (IMU) system for gait analysis consistently matched near–Vicon-level precision, with a mean squared deviation of approximately 4.0° versus 18.8° using single-camera methods. Second, a force-controlled exoskeleton for finger rehabilitation in Chronic Regional Pain Syndrome (CRPS) patients improved QuickDASH scores (e.g., 50% down to 45%) in a six-week pilot study. Although sample size was small, both systems showed promise for integrating quantitative data into everyday orthopedic management.

AI-driven methods were also leveraged to automate diagnostic and surgical tasks. In detecting bone tumors from radiographs, a multitask deep learning model achieved an accuracy of correctly classifying primary bone tumors malignancy of over 80 %, approaching expert-level performance. For lower-limb alignment analyses, a separate AI system processed long-leg radiographs four times faster than orthopedic specialists while attaining an interrater reliability up to 0.99. Extending this to osteotomy planning resulted in accuracy levels that matched or surpassed clinical benchmarks, substantially cutting manual workload and illustrating AI's capacity to streamline workflow and boost clinical precision.

Another persistent challenge in orthopedics lies in robustly measuring how joints react to varying surgeries and rehab regimes. To meet this challenge, new robotic test benches were designed for the knee and hand. Repeated cadaveric tests showed that merely 2° of malalignment in a femoral implant can disrupt knee stability by over 6°, underscoring the critical importance of precise alignment. For hand biomechanics, an eight-motor force-controlled platform reproduced complex finger movements, capturing grip forces up to 1.9 N. Although these platforms require specialized technical expertise, their reliability, repeatability, and capacity for rich biomechanical data collection hold great potential for personalized intervention planning.

Finally, a key bottleneck in biomechanical research is building accurate digital twins that reflect complex musculoskeletal interactions. Two AI-driven optimizers were therefore created: (1) an autoencoder-based tool for refining kinematic parameters, showing reconstruction errors as low as $10e-5$, and (2) a reinforcement learning algorithm that adjusts dynamic parameters via proximal policy optimization, improving simulation fidelity by over 30%. While both methods depend on specialized data curation, the resulting gains in model accuracy broaden the opportunities for individualized orthopedic treatment.

In essence, this dissertation provides a comprehensive approach that incorporates wearable sensing, AI-based surgical planning, robotic benchmarking and advanced optimization, demonstrating how robotics and machine learning can solve long-standing problems in orthopaedic care. The key innovation is to combine these elements into a single adaptive framework that ultimately leads to personalized, efficient and evidence-based orthopaedic interventions.

Contents

1 Introduction

1.1 Motivation

The global increase in the elderly population is sharply raising the demand for specialized healthcare services, especially in orthopedics. In Germany alone, projections indicate that by 2055, the elderly population requiring long-term orthopedic care will increase by 1.8 million [14]. This demographic trend underscores the critical need for innovative solutions in managing and treating age-related orthopedic conditions, such as joint degeneration and osteoarthritis. As people grow older, the health of their joints becomes a key factor in their overall quality of life. Being able to move without pain is not just a part of well-being; it is essential to it [15]. Therefore, the increasing number of orthopedic issues among the elderly highlights the urgent need to prioritize joint health in medical care, ensuring that the later years of life are characterized by continued mobility and satisfaction [16]. Compounding this challenge is a simultaneous shift in the healthcare sector itself. The escalating demand for orthopedic care, coupled with a diminishing healthcare workforce, is leading to a crisis in this field [17]. It highlights the urgent need for innovative approaches to streamline orthopedic care, while making it more efficient and effective. This situation highlights the need for rapid and innovative development of our current healthcare models to close the gap between patient needs and available care.

In this scenario, the potential of robotics and Artificial Intelligence (AI) presents a significant opportunity. These technologies, known for their precision, analytical capabilities, and consistent performance, are well-suited to address the complex challenges in healthcare. The integration of AI and robotics in medical settings is poised to improve care quality, enhancing diagnostic accuracy, surgical precision, and consistent patient outcomes across different groups [18]. In addressing these orthopedic healthcare challenges, the emerging roles of AI and robotics are not just futuristic concepts but present-day realities. These technologies have already begun to transform various sectors, and their application in orthopedic care offers a promising pathway to address these critical healthcare needs. Their track record in improving efficiency, reducing human error, and driving innovation is a strong indicator of their potential impact on orthopedic healthcare [19].

Orthopedics, a field often at the forefront of technological innovation, is uniquely positioned to leverage the advancing capabilities of AI and robotics. The specific challenges that these technologies can address include early detection of joint degeneration, tailored surgical planning, and postoperative monitoring for optimal rehabilitation. By incorporating AI and robotics into orthopedic practice, the field can evolve to meet the growing demands for joint health care, particularly in the context of an aging population. Embracing these technologies offers a crucial opportunity to transform the treatment of orthopedic conditions, aiming to enhance mobility, reduce pain, and improve the quality of life for the elderly. This shift not only promises better patient outcome but also helps alleviate the pressure on healthcare systems. This thesis investigates the interface between technology and orthopaedic care and outlines a vision for a future where technology plays a central role in healing and support [20, 21].

1.2 Problem Statement

The drive to incorporate AI and robotics into orthopedic clinical practices faces considerable challenges, despite the recognized potential to revolutionize the sector. The integration is primarily hindered by technological limitations, resistance to change in clinical environments, and the inherently complex nature of orthopedic care. These barriers underscore the critical need for tailored innovations that can seamlessly

mesh with the unique demands of orthopedic treatments and enable smoother adoption into clinical workflows [22, 23].

Compounding these integration challenges, the orthopedic clinical setting presents its own unique hurdles, including patient diversity, case complexity, and the necessity for real-time decision-making. The existent technological advancements, as promising as they may be, frequently fall short of offering targeted solutions to these specialized needs. This discrepancy between potential and practical benefits necessitates the development of AI and robotics solutions that are specifically tailored to the particular clinical requirements of orthopaedic care [22].

Furthermore, the adoption of AI tools and robotic devices within healthcare practices is impeded by their failure to integrate seamlessly into everyday clinical operations, which often necessitates additional training or infrastructural modifications. This challenge is extended by an increasing demand for innovative wearable devices driven by a surge in orthopedic conditions, especially among the aging population. These wearables, essential for effective data collection and tailored for various stages of treatment, must enable ongoing patient monitoring and feedback, highlighting the importance of developing devices that are both efficient and specifically designed for orthopedic applications [22, 23].

Critical stages in the orthopedic treatment continuum, such as the preoperative and intraoperative phases, further illustrate the necessity for sophisticated AI tools that offer automated decision support, detailed operational planning, and comprehensive risk assessments. Advanced testbenches that provide real-time feedback during surgical procedures underscore the need for precision and the ability to make real-time adjustments. Moreover, the future of orthopedic care leans towards personalized treatments, requiring the development of optimization algorithms capable of generating individualized models based on extensive patient data. This approach promises to significantly enhance treatment efficacy by customizing interventions to match each patient's specific anatomical and health conditions [22, 24].

Ultimately, progress in orthopaedic care depends not only on the development of new AI and robotic technologies, but above all on their successful integration. This involves not only optimizing and tailoring these innovations to meet the specific demands of orthopedic treatments but also ensuring they function cohesively to improve patient outcomes and streamline clinical operations [22, 23].

1.3 Research Questions and Contributions

Building on the identified challenges within the orthopedic field, this thesis aims to address the critical gaps in technology integration and the application of AI and robotics in clinical settings. The focus is on exploring innovative solutions that can be seamlessly integrated into existing clinical workflows, thereby enhancing the precision and effectiveness of orthopedic care. The research questions are formulated to examine the potential of these technologies in improving diagnostic accuracy, surgical planning, and patient outcomes. They also seek to understand the challenges that must be overcome to realize the full benefits of these technological advancements. In the following, the questions are listed first, followed by the resulting contributions. These contributions can be summarized in Figure 1.1.

I. Integration of wearable and robotic technologies into clinical practice:

How can wearable and robotic technologies be effectively integrated into clinical orthopaedic workflows to provide real-time objective data for the prevention and rehabilitation of joint disease?

This central question aims to find viable methods of incorporating these advanced technologies into current medical protocols to improve the effectiveness of patient care and pave the way for customized treatment approaches.

To address this question, two mechatronic innovations are presented in our research. The first is the development of a low-cost IMU system designed for precise gait analysis to be rigorously tested in a volunteer study. This system is able to improve the prevention of joint disease by providing important real-time data that can be seamlessly integrated into clinical operations. The second innovation is a mechatronic exoskeleton adapted to finger rehabilitation. This exoskeleton is unique in its ability to measure internal

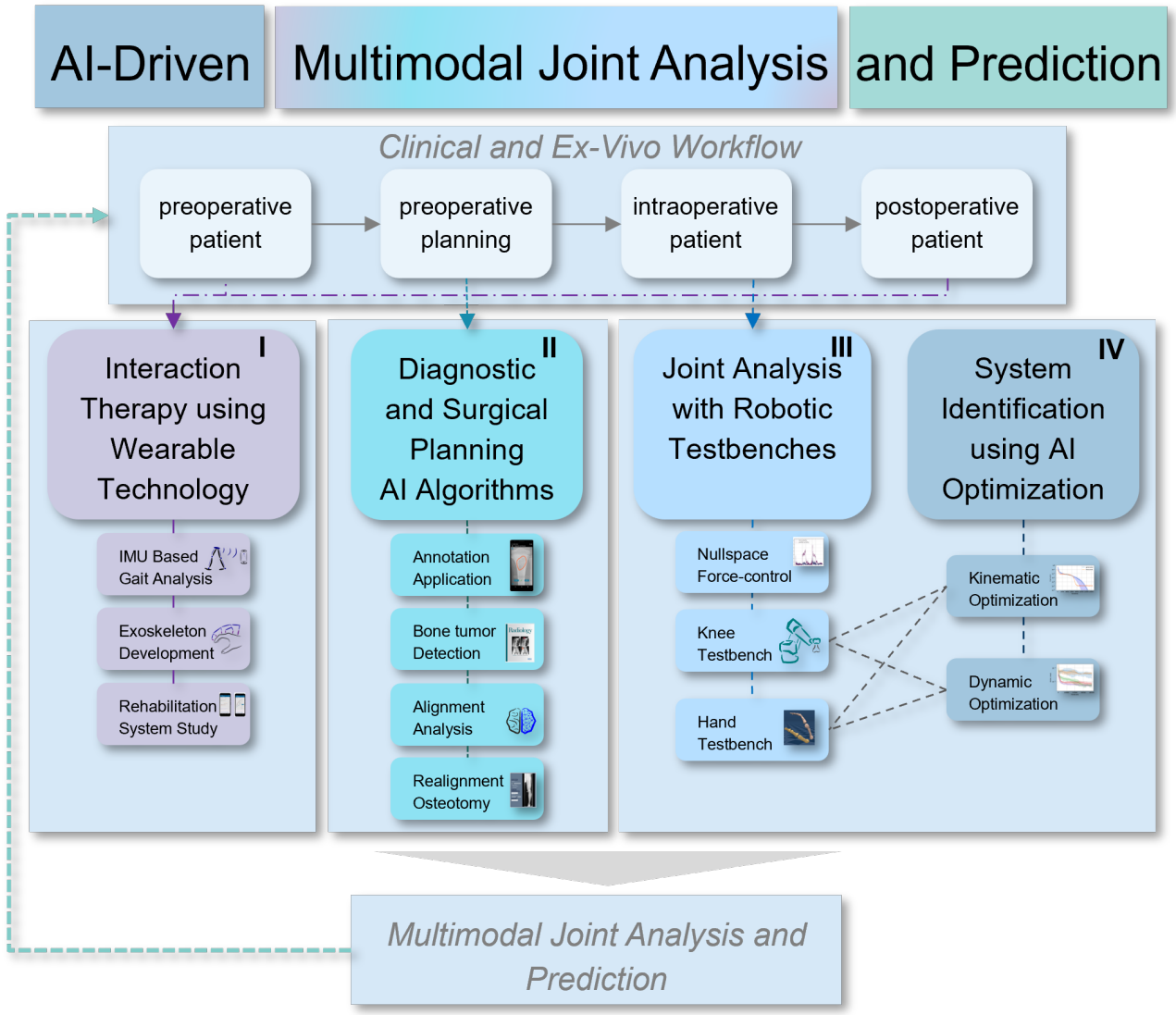

Figure 1.1 Overview of the individual research areas of the dissertation, which result from the four central research questions (main topics) and the associated contributions to these questions.

finger loads while capturing comprehensive motion data and has been clinically validated to confirm its effectiveness and integration capability in therapeutic situations. Overall, these devices will provide clinicians with accurate, objective data for the prevention and rehabilitation of joint disorders and demonstrate their practical application and potential for integration into clinical workflows through patient studies.

II. Leveraging AI in Orthopedic Diagnostics and Surgical Planning:

What are the potential benefits and challenges of using AI for image analysis in the diagnostic and surgical planning phase, especially for orthopedic tasks such as bone tumor detection, kinematic alignment analysis, and formulation of preoperative surgical planning strategies?

This question is about the use of AI technologies to improve the accuracy of orthopaedic diagnostics and surgical planning. By focusing on critical areas such as bone tumor detection and alignment analysis, the goal is to determine how AI can not only improve diagnostic accuracy, but also minimize planning errors and tailor treatments to individual patient needs.

In answering this question, three AI-powered technological advances are at the center of this research. The first innovation involves the development of a dedicated data annotation application tailored to orthopaedic imaging, designed to enable fast, accurate and intuitive analysis and interpretation of medical

images. Next, AI algorithms for the detection of bone tumors will be presented to increase the early detection rate and accuracy of diagnoses. Finally, the development of an automatic alignment analysis method for the lower limbs represents a new approach to improving the precision of surgical planning. Based on the alignment analysis, a preoperative planning system is developed to relieve the burden on the orthopaedic diagnostics department. By providing clinicians with highly accurate, objective data and automated analysis tools, these advances demonstrate their potential for practical application and seamless integration into clinical workflows, as evidenced by extensive validation studies.

III. Robotic testbenches for joint analysis:

How can the projected benefits of robotics be used to perform detailed and comprehensive analyses of human joints, with an orthopaedic focus on the complexity of the knee and hand?

This central question investigates how robotic testbeds can be utilized to conduct comprehensive analysis of human joints, with a particular emphasis on the biomechanics of knee and hand movements. The objective is to investigate how advanced robotic systems, capable of free translation and rotation, can enhance our understanding of joint mechanics and support surgical interventions.

For this, our research advances the field of robotic testbeds for joint analysis. The first contribution is the formulation of a suitable control algorithm in conjunction with the use of a 6-Degree of Freedom (DOF) robotic arm test rig specifically tailored to the knee joint. This system enables a detailed investigation of the knee joint mechanics and grants new insights into its biomechanical properties.

In addition, a special robotic test bench for the hand joint has been developed, introducing an innovative testing device that captures measurement data with unprecedented detail, including precise motion sequences and force measurements of the muscles involved. This advance offers new insights into the careful analysis of the musculoskeletal system of the hand. These innovations allow the test bed to generate high quality data for biomechanical modeling, demonstrating its significant potential to improve orthopaedic care and predictive accuracy.

IV. AI for biomechanical optimization:

How can AI algorithms be applied to highly individualized biomechanical systems to improve kinematic and dynamic modeling and thereby create more accurate and efficient models for the analysis of joint behavior?

This question addresses the role of AI in the field of biomechanics and aims to improve the development of models that mimic human joint behavior. By achieving higher levels of accuracy and efficiency, these models will significantly increase the potential for the advancement of surgical techniques and rehabilitation methods.

Our research contributes to the field of AI in biomechanical optimization through two key innovations. First, the application of differentiable forward kinematics in human joint modeling is presented. This approach enables the creation of models that can simulate and learn the complex movements of human joints accurately, allowing a more comprehensive understanding of joint mechanics. Second, a model-free Proximal Policy Optimization (PPO) approach is implemented for the dynamic optimization of biomechanical systems. This technique represents an advance in optimizing the dynamic aspects of joint motion models and provides a new level of precision and efficiency in the prediction and analysis of joint behavior.

1.4 Foundations and Related Work

This section provides a comprehensive review of the scientific literature in the field of joint analysis. Focusing on the complex structures of the hand and knee joints, the key findings from a number of studies are summarized, highlighting their contributions to our understanding of these complex anatomical areas. The discussion ranges from basic anatomical details to the latest technological advances, reflecting the multidisciplinary nature of joint analysis. The aim is to place the current research in the context of a broader academic dialog and to highlight trends, challenges and opportunities in the field.

To enable an in-depth investigation and assist in navigating the extensive literature, a thematic map is presented in Figure 1.2. This visual representation provides a connected overview of the key topics and research areas discussed and gives readers an understanding of how each topic is interconnected and contributes to the field of orthopaedic care.

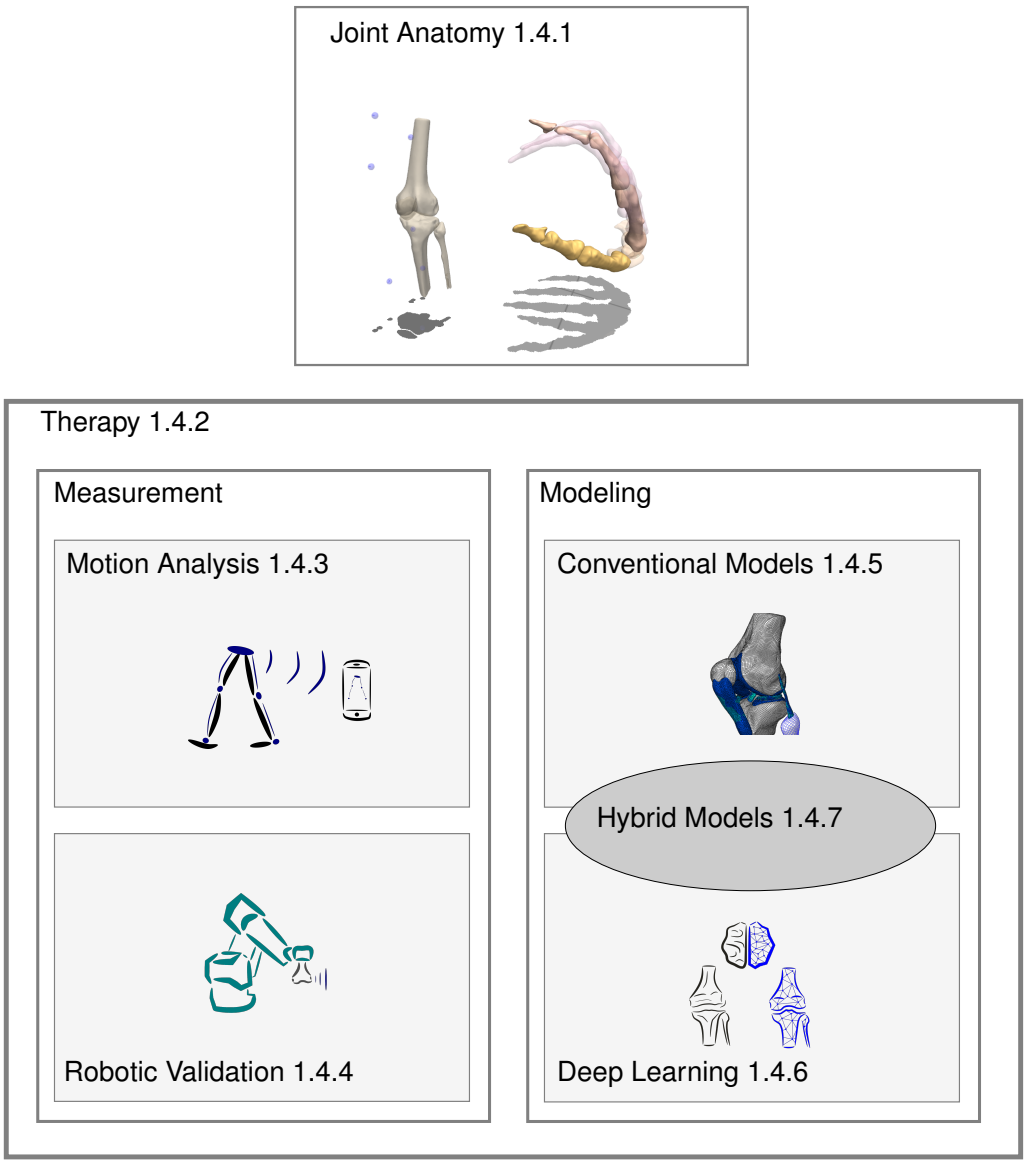

Figure 1.2 This figure provides a structured overview of the literature review, in which the main topics are categorized. It begins with an examination of general joint anatomy and then addresses two main areas: Measurement Techniques and Modeling Approaches, both of which are critical to comprehensive joint analysis. The image above right shows a conventional modeling method as described in Beidokhti et al. [25].

The organization of the following sections has been designed to ensure a consistent progression that transitions naturally from basic anatomical knowledge to the latest technological advances in the field. Beginning with an examination of human joint morphology, focusing specifically on the hand and knee in *On the Complexity of Human Joint Morphology* (Section 1.4.1), the foundation is laid for a comprehensive understanding of the structural details that are critical for both diagnosis and treatment. This foundational knowledge is crucial as the discussion progresses to *Clinical Therapy Pipelines* (Section 1.4.2), where the presentation shifts to modern therapeutic strategies. The provided emphasis here lies on the fact that a deep understanding of structural anatomy is essential for the development of effective interventions.

A critical evaluation of the development of motion analysis methods follows, highlighting their importance for clinical application and the impact of technological advances on traditional health paradigms. This

review forms the basis for examining the role of *Smart Robots as Measurement and Validation Devices* (Section 1.4.4), which examines the precision and effectiveness of modern robotic technologies in improving orthopaedic care through enhanced joint model validation.

The analysis then proceeds to *Biomechanical joint analysis* (section 1.4.5), where traditional analysis methods are examined for their fundamental importance, but also their limitations in fully capturing the complex interplay of biomechanical forces and anatomical structures in a personalized health context are highlighted. These limitations are addressed in the section *AI-assisted joint analysis* (section 1.4.6), where the integration of deep learning techniques into the joint analysis is investigated. This section demonstrates how sophisticated AI methods are when processing complex datasets and improve the precision of conventional analysis techniques.

Through this structured progression, the review aims to provide a detailed and differentiated overview of the evolving landscape of joint analysis in orthopaedic care. This journey from basic concepts to advanced applications forms the basis for the research presented in this thesis.

1.4.1 On the Complexity of Human Joint Morphology

This section presents the structural complexity and biomechanical background of the knee and hand joint.

The Knee Joint

The knee joint is composed of bone structures (patella, distal femur, proximal tibia), cartilage, menisci, ligaments, muscles and a synovial membrane [26]. Each of these different tissue categories has anisotropic material parameters and behaves differently according to the direction of their loads and kinematic structure. An overview of the tibiofemoral joint is displayed in Figure 1.3.

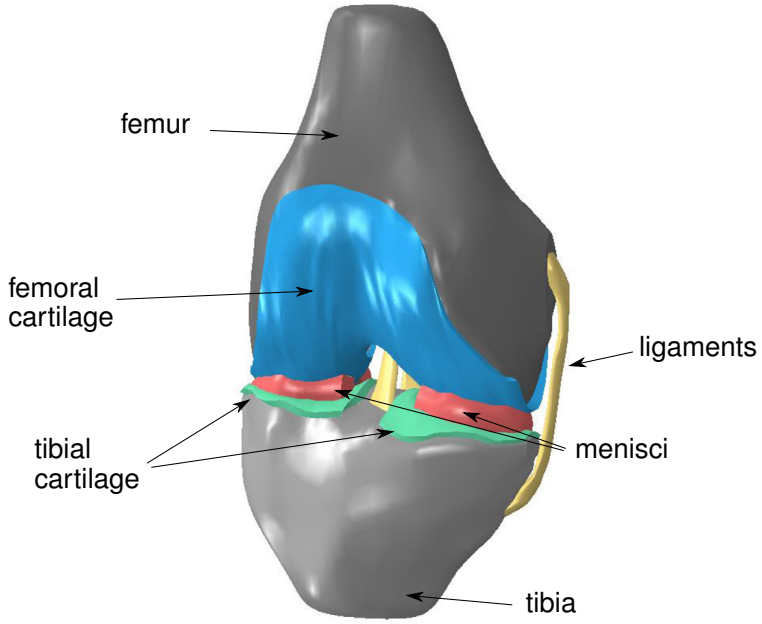

Figure 1.3 Illustration of the tibiofemoral joint as modification of Cooper et al. [27].

The knee joint consists of the medial tibiofemoral, lateral tibiofemoral, patellofemoral, and proximal tibiofibular joints [28]. However, the geometry of these joints is not congruent, so the connection between the tibia and femur is never complete and geometry deviations are compensated by the menisci and ligaments. The knee joint provides a range of motions in six DOF. The rotational motion consists of flexion-extension, internal-external, and varus-valgus [28]. Furthermore, translational motion is composed of anterior-posterior, medial-lateral, as well as compression and distraction of the knee joint. These six DOF

compose the complex functionality of knee joint motion [29]. In our daily activities, this joint supports a large portion of our body weight and allows a wide range of motion for flexion-extension and internal-external rotation [28]. To provide sufficient stability for managing wide range of motion under heavy loads several ligaments provide passive stability in all directions of the knee joint. The central pivot point is formed by the Anterior Cruciate Ligament (ACL) and Posterior Cruciate Ligament (PCL) as well as the meniscofemoral ligaments [30]. The menisci guide rotational stability of the knee and have fibre connections with the ACL and PCL [30]. The peripheral ligaments like the collaterals are primary passive stabilizers against varus-valgus rotation as well as internal and external rotation [30]. This kinematic structure enables a highly optimized compromise between stability, sufficient loading capability and flexibility for covering the desired range of motion. In detail, the loading and flexibility requirements result in a nonlinear kinematic behaviour of the knee joint described by the burmester curve [31, 32]. This curve describes the flexion motion generated by the four bar linkage between femur, tibia and the ACL and PCL ligaments as a result of rolling and sliding between the femur and tibia. At full extension, when loads tend to be maximal, stability is maximized and the femur and tibia are in almost complete rolling motion with respect to each other. With increasing flexion, the loads tend to decrease and the movement between femur and tibia is more and more dominated by sliding, stability decreases and flexibility increases. The knee joint is a dynamic system in the sense that its internal parameters are highly time-dependent. Due to the circadian rhythm the cartilage decreases in size throughout the day and increases during the night altering the kinematic and dynamic behaviour trough the day. Further, bone shapes vary over age and sex and are in continues change.

Due to the high complexity of the knee joint in connection with high loads from the movement cycle and the specific stability requirements for the ligaments, this joint is prone to injuries. Furthermore, the knee is the joint that is most commonly affected by osteoarthritis [33, 34] being one of the leading causes to disability [35]. Global trends suggest a significant increase in osteoarthritis prevalence over time and a shift towards younger age groups [36]. It is therefore a crucial part of ongoing research to better understand the exact processes within the joint. Increasing efforts are being made to develop early-stage interventions to prevent knee degeneration and delay the need for joint replacement surgery. This includes regenerative therapies for cartilage and bones [37] as well as repairs of the meniscus [38] and the ligaments [39]. However, if an implant is still needed, the patient-specific adaptation and development of the surgery and the knee implant is of great importance.

The Human Hand

The human hand is composed of a multitude of bones, joints, tendons and muscles that are all in a complex interaction with each other and enable humans to grasp, touch and in general interact with their environment. As shown in Figure 1.4, the bones of the hand can be divided into the carpal bones, which form the wrist, the metacarpal bones, and the phalanges, which in turn are divided into a distal phalanx, a middle phalanx, and a proximal phalanx, with the thumb being the exception it has no middle phalanx [42]. Each long finger is composed of three joints, named the Distal Interphalangeal Joint (DIP), the Proximal Phalangeal Joint (PIP) and the Metacarpophalangeal Joint (MCP), while the thumb is composed of the Interphalangeal Joint (IP), MCP and Carpometacarpal Joint (CMC). According to [43] the hand has 21 DOF as the MCP joints and CMC joint of the thumb have two DOF while the PIP and DIP joints all only have one DOF.

1.4.2 Clinical Therapy Pipelines

In order to provide data and optimization possibilities for joint therapy a number of key challenges need to be met. The proper acquisition of patient specific data and model validation for precise surgery or treatment and long term predictions of the therapy process need to be handled. In order to improve this process, Figure 1.5 shows a potential optimization pipeline streamlining the data acquisition process along the clinical reality. During treatment, patient-specific data can be collected at four different stages. First, preoperative data can be collected before surgery or treatment. This includes static demographic data such as age and gender, but should also require more detailed dynamic data such as gait cycles recorded with measuring devices. Secondly, imaging data from Magnet Resonance Imaging (MRI), Computer Tomography (CT)

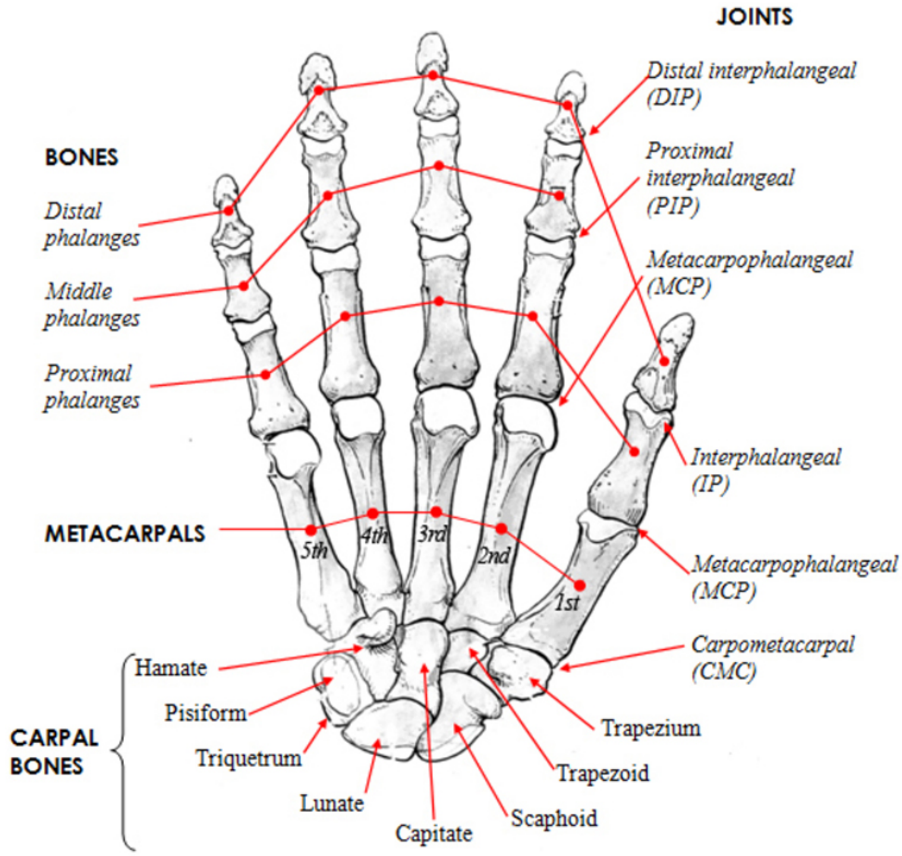

Figure 1.4 Bones and joints of the human hand. Original image from [40], as used in [41].

or X-rays are collected during preoperative planning. This step determines the geometry of the joint and identifies further disease details or anatomical landmarks. Thirdly, data can be collected during the surgery itself to determine the current Range of Motion (ROM) of the joint in combination with the implant parameters or the exact positioning of the implant. Furthermore, this data can be complemented by ex-vivo validation to compare surgical treatments with robotic interactions. Finally, patient-specific data such as gait cycles can be collected again after surgery and during rehabilitation to objectively evaluate the success of the therapy.

Recent studies have further enriched our understanding of these processes. MacMahon, Rao, et al. investigate the shift towards a more integrative approach in preoperative optimization for total joint arthroplasty, underlining the shift from mere preoperative clearance to a more comprehensive preoperative patient optimization [44]. Additionally, Heckmann and Glusenkamp investigates the potential of linking databases in joint arthroplasty and orthopaedics and present this as an advanced way to improve clinical outcomes through data integration [45]. Complementing these perspectives, Andrinopoulou, Harhay, et al. addresses dynamic prediction models using joint models of longitudinal and time-to-event data, a method that stands to improve long-term predictions in therapy processes [46]. These studies collectively contribute to the evolving landscape of joint therapy, emphasizing the importance of data-driven and patient-centric approaches.

Having established the fundamental anatomy and therapeutic strategies for joint care, the focus shifts to the technological evolution in movement analysis. This transition reflects the progression from basic understanding to the application and integration of advanced tools in monitoring and rehabilitation.

1.4.3 Kinematic Motion Analysis

Motion analysis, particularly gait analysis, is a central component in joint therapy, aiding in disease progression monitoring, rehabilitation, and training. Technologies like Vicon [47] and OptiTrack [48] represent the commercial gold standard, offering high-precision motion capture with an Root Mean Square (RMS)

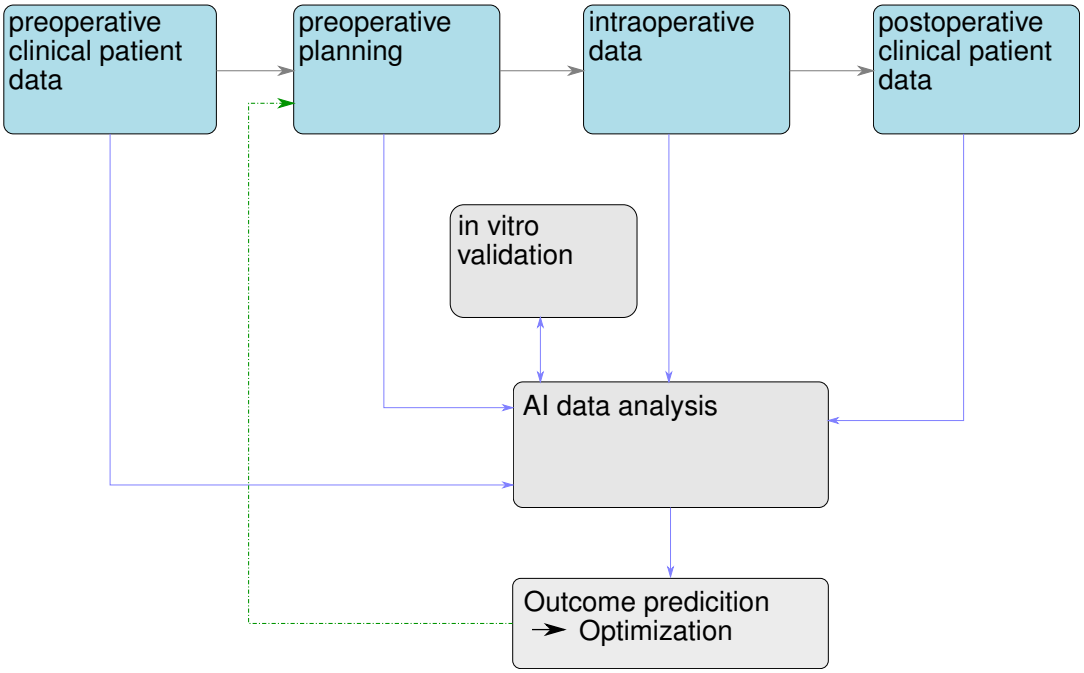

Figure 1.5 Enhanced surgical data pipeline for joint procedures within a clinical setting. The process encompasses four distinct stages aligned with the timeline from preoperative to postoperative patient data collection and care. Comprehensive data analysis is conducted on all accumulated data, helping in the prediction and optimization of subsequent preoperative planning phases.

error below 1 mm [49]. This precision has been instrumental in tasks such as characterizing joint torque profiles post-ACL reconstruction [50].

However, these systems rely on marker placement, which causes challenges in practice. Accurate marker positioning on anatomical landmarks is difficult, and skin-based markers may not precisely correspond to true 3D joint positions due to soft tissue movement [51]. Additionally, high cost, the need for controlled conditions, and marker attachment limit practicality in routine clinical settings, thus constraining the broader application of motion analysis [51]. Overcoming these limitations therefore remains an essential goal for the widespread clinical adoption of motion analysis technologies.

AI-Based Gait Analysis

Recent breakthroughs in computer vision and machine learning have led to more reliable markerless motion capture systems. These innovations promise to transform sports biomechanics and rehabilitation, extending motion analysis applications to routine training and competition environments [51]. This shift may resolve the biomechanics dilemma of balancing accuracy with external validity. Widespread motion analysis could yield substantial datasets, enhancing the benefits of deep learning in biomechanics. Key elements of markerless systems include advanced camera setups and sophisticated algorithms. Optimal systems utilize high-definition cameras (High Definition (HD)-Ultra High Definition (UHD)) with high frame rates (>100 Hz) and depth sensing capabilities. A notable example is Microsoft's "Kinect For Xbox One." However, limitations persist in precision biomechanics due to accuracy issues, with active camera systems suffering from range limitations, low frequency (30 Hz), and reduced effectiveness in bright light [51, 52].

Recent advancements have led to the use of passive camera systems in motion analysis, primarily driven by deep learning techniques. These methods typically separate the problem of 3D human pose estimation into two stages: initial 2D keypoint detection and subsequent 3D pose estimation [53–60]. A Convolutional Neural Network (CNN) processes each image frame to detect 2D keypoints, followed by various algorithmic steps to construct a coherent 3D model. This two-stage process, with intermediate supervision, allows for refined tuning of networks and efficient data compression into keypoints, enabling streamlined processing.

Pavllo et al. (2019) demonstrate a notable approach, using a CNN to integrate frame keypoints into a stable 3D model over time, validated on the Human3.6 dataset with a Mean Per-Joint Position Error (MPJPE) of 36.5 mm [61, 62]. Despite promising, the application of these models in biomechanical analysis remains immature and far too inaccurate.

Internal Measurement Based Gait Analysis

Recent IMU systems have gained relevance as an effective alternative to conventional camera-based methods in gait analysis. Integrating an accelerometer, gyroscope, and magnetometer, IMUs accurately measure spatial orientation: The accelerometer tracks triaxial acceleration, the gyroscope detects angular velocities, and the magnetometer assesses orientation against Earth's magnetic field. This sensor combination ensures precise IMU alignment, crucial for capturing rapid movements, as evidenced by a reported Root RMS error of 3.3 deg in knee flexion/extension measurements [63].

Gait analysis, vital for diagnosing and managing musculoskeletal and neurological conditions, has seen significant advancements with IMU-based systems [64]. Offering portability and cost-effectiveness, these systems are gaining traction in clinical and research settings. Research by [65–69] underscores the versatility and dependability of IMU-based gait analysis. Beyond enhancing accessibility, IMU technology enables remote monitoring in real-world settings, representing a substantial evolution from traditional lab-based approaches.

Building upon the advancements in movement analysis, the next critical aspect is the anticipated key role of robotic measurement and validation in enhancing the precision of biomechanical studies.

1.4.4 Smart Robots for Measurement and Validation

Robotic validation is a fundamental aspect of model development in biomechanics, ensuring that theoretical models align with real-world conditions [70]. This is important in the study of complex joints such as the knee and hand.

Recent advancements in robotic testbenches have improved our ability to conduct detailed biomechanical analysis. In the field of knee biomechanics, innovative robotic testbenches have been developed to overcome the constraints of fixed geometry found in earlier methods. These advanced systems enable a more comprehensive exploration of knee joint behavior under various loading conditions, providing valuable insights for surgical planning and prosthetic design [71–74].

The challenge of accurately capturing biomechanical data for the knee joint, considering its complexity and the necessity to account for all six DOF, is substantial. Robotic methodologies offer significant advantages in terms of applying precise movements and forces. The pioneering work by Frey et al. [75] introduced advanced robotic testing for knee joint analysis, utilizing a 6 DOF robot with high-frequency control and integrated force-torque sensors. This approach enabled the collection of critical data on varus-valgus loading and its relationship with flexion loading. Subsequent studies have expanded these techniques to other joints, such as the spine [76], and have introduced tools like CT data segmentation for enhanced analysis in contexts like total knee replacement surgeries [77].

In hand biomechanics, the development of sophisticated testbenches has been instrumental in understanding the complex interactions within the hand structure, including cartilage, ligaments, and muscles. These platforms have significantly advanced our knowledge of hand movements and force dynamics, addressing the complex nature of joint behavior [78–82]. Insights gained from these studies are crucial for developing more effective treatments and rehabilitation strategies for hand-related injuries and conditions.

Overall, the integration of advanced robotic testbenches in biomechanical research marks an improvement in the validation process of the respective models. By ensuring that computational models accurately reflect the complex dynamics of human joints, these developments not only enhance the robustness of biomechanical models but also contribute to more effective and personalized medical interventions.

Advancements in Robotic Exoskeletons for Hand Rehabilitation

Robotic exoskeletons have emerged as a transformative solution in hand rehabilitation, addressing limitations in hand functionality due to various conditions such as neuromuscular diseases, hand injuries, and age-related impairments [83]. Traditional therapy methods often fall short due to early hospital discharges, limited therapist availability, and high costs [84, 85]. In contrast, robotic systems offer a promising alternative, particularly in stroke rehabilitation, where repetitive motion training is crucial [86–88].

Studies have shown that robotic hand rehabilitation, through repetitive motion training, can be more effective than conventional therapy [89]. Exoskeletons equipped with advanced sensors provide precise, repeatable data, enabling the quantification of a patient's functional status [90]. These systems simplify high-frequency rehabilitation exercises without increasing financial burdens, allowing for consistent daily training routines that are often unfeasible in manual therapy.

Still, despite their potential, the clinical application of exoskeleton systems remains limited due to their complexity and usability challenges in clinical settings [90]. Addressing these issues, recent developments have focused on enhancing usability through improved position sensing, user-friendly bi-directional actuators, and integrated force sensors. These advancements aim to provide a more effective and accessible approach to hand rehabilitation.

Over the past two decades, various hand exoskeleton systems have been developed for rehabilitation, force assistance, or haptic feedback in virtual reality applications. A critical requirement for these systems is biomechanical compatibility with the human hand to ensure safe operation [83]. Notable approaches include underactuated kinematic structures with three degrees of freedom, encompassing all three finger phalanges [91, 92]. Such designs enable the calculation of forces transmitted to the finger phalanges, given the mechanism's configuration and the actuator force.

In the context of CRPS, treatment goals focus on enhancing hand mobility and functionality while alleviating pain. Conventional physiotherapy and ergotherapy often yield limited results due to time and resource constraints [84, 85]. Robotic exoskeletons offer a viable alternative, providing precise, cost-effective data for monitoring patient progress and enabling more frequent therapy sessions. However, challenges remain in adapting these systems to individual patient needs, particularly in terms of direct fitting and sensor integration [93–98].

Robotic Control Challenges

Especially in a medical context, developed models need to be reliable and proven in order to not develop harmful consequences in application. However, especially for joint analysis which combines imaging data with motion and load trajectories a sufficient validation becomes a challenging task. The recurring application of position and load targets in combination with highly individual differences between joints requires a complex testing environment. The described tactile task is an active part of robotics research [99]. There are multiple control strategies for solving this robot-joint interaction: Position control methods, force control methods, impedance and admittance methods and hybrid-position and force control methods. Single position control can not be used for individual biomechanical testing due to the risk of overloading and destruction at alternating surfaces. Force control methods do not achieve any exact positional target such as applying a flexion of 90 degrees of the knee joint and therefore make the comparison between specimen not practical. Impedance and admittance control methods project the position or force control target via stiffness and damping matrices into the same space [100]. However, neither position nor force precision are deterministic and stability is limited by the achievable impedance [101, 102]. Further, the individual specimens of the joint require to determine the parameters of these matrices. Hybrid position-force control methods have a high potential, as they ensure position and force precision by dividing the work space into force and position related DOF [103] and will therefore be considered for individual joint testing.

The drawback of the hybrid position-force control is the complete decoupling of position and force related DOF via a selection matrix as proposed by Raibert and Craig [103]. This separation decouples the desired goals for testing in task-space, however a coupling in the joint-space of the robot remains, leading to instability. Schuetz, Pfaff, et al. [104] proposed an approach which used the null space in order to solve this

coupling problem and proposed a tactile control scheme for stability. However, while Schuetz, Pfaff, et al. [104] mainly focused on the task of obstacle avoidance these approaches have not been used for actual force control in a complex testing environment such as an individual joint specimen.

While robotic technologies represent an important advancement in biomechanical validation, their utility depends on the availability of accurate models for validation. This brings us into the domain of conventional joint analysis techniques, where understanding their historical development and current relevance is crucial. These traditional methodologies provide the foundational models that newer validation techniques, such as those offered by robotics, seek to test and refine.

1.4.5 Biomechanical Joint Analysis

For predicting the knee joint behaviour and analyse its limitations and potential for therapeutic use, a significant amount of research involves Finite Element (FE) modelling. Kazemi, Dabiri, et al. [105] and Cooper, Wilcox, et al. [27] provide a comprehensive overview of current applications of such FE models and their respective challenges. They range from cartilage degeneration and osteochondral effects [106–108] to the influence of meniscal shape [109, 110] and the biphasic effects of cartilage on loading [111]. However, the computational study of the contact mechanics of the knee joint remains a challenge due to the contact dynamics between tissues and joint surfaces. Consequent validation of knee joint models is particularly difficult. So far only limited progress has been reported in translating the findings and tools of modelling research into clinical practice [27]. To overcome these problems, Cooper, Wilcox, et al. [27] summarizes three main problems for joint analysis, defined as follows:

- Capture and representation of appropriate geometry and material properties,
- Representation of motions, loads and constraints.
- Establishment of relevant outputs in connection to clinical benefits.

Addressing these problems builds the foundation for current joint analysis research.

Geometry based Modeling

In order to achieve a certain level of detail, the geometry of all participating structures along the respective motion has to be considered. This is usually done by utilising medical imaging (CT or MRI) [112–114], providing an approximation of joint geometry altered by imaging artefacts and simplifications from the segmentation process [115]. Models based on these approaches are broadly capable of investigating the combined role of menisci and ligaments in load transmission and stability [116]. This study demonstrates the potential of segmentation based models to predict complex stress and strain patterns [27]. However, these models do not cover anisotropic material behaviour. An alternative to segmentation-based models focuses on the mathematical description of geometry [117–119], enabling qualitative predictions of expected trends. However, data extracted from such models does not match well with experimental predictions [109, 120] limiting their use to trend prediction only.

A problem with geometry-based modelling is its lack of automation and unknown inner material properties. While mathematical models do not provide the required accuracy for clinical use, imaging-based models lack validation and are often unpractical due to highly individual parameter optimization.

Motion and Load Modeling

An important part of appropriate modelling is ensuring that the model generates physiological motions motivated by real world measurements. This does not only require understanding the moving joint parts, but also a measurement system in order to extract relevant moving and load scenarios. A distinction is made between applying loads and measuring the resulting movement, or measuring the movement and extracting the loads from it [27]. To date, it has been difficult to deduce in-vivo movements. However, the

joint kinematics can be inferred using CT bone models validated by a gold standard skin marking method for movement detection [121]. Furthermore, in-vivo forces can be derived from quasi-static multibody models [122, 123]. An essential part of understanding the entire motion of a complex joint such as the knee is to further consider the role of ligaments and menisci. [112] suggests that providing patient-specific ligament characteristics improves the prediction of kinematics and contact forces. Meniscal translation in response to loading was captured using MRI [124] to create more advanced models [125].

The disadvantage of these movement and load-dependent models is their limited applicability for in-vivo testing. The gold standard in motion capture involves considerable effort and creates unnatural conditions for the test subject. In addition, all data collected are only associated with a single time stamp and do not cover longitudinal effects over time.

Output Definition and Clinical Relevance

For medical modeling, it is important to consider the clinical relevance of extracted outputs to predict intervention responses or disease progression [126]. In order to connect modelling to osteoarthritis an important database is the Osteoarthritis Initiative (OI) introduced in [127], which contains clinical evaluation data coupled with imaging (X-ray and MRI) of over 5000 subjects. Mononen, Tanska, et al. [106] demonstrated how to combine model based approaches with clinical relevance by developing their models based on the imaging data and defining the outputs in relation to it. In detail, they applied collagen fibril damage on their models if tensile stresses exceeded a threshold during gait loading over successive iterations. This enabled them to develop an algorithm capable of predicting cartilage degeneration in the knee joint.

In general, databases like those by Peterfy, Schneider, et al. [127] suggest a more generic and general approach towards modeling and clinical predictions. Especially with the rising potential of deep learning analysis these databases can be exploited with new methods generating direct clinical benefit.

Transitioning from conventional approaches, we look at the impact of deep learning on joint analysis, showcasing how this modern computational technique is reshaping our methods and insights in the field.

1.4.6 Artificial Intelligence-aided Joint Analysis

The applications of deep learning have achieved one of the most significant changes in research history. Since the successful introduction of AlexNet in 2012 [128], which was capable of recognising images better than any previously tuned algorithm, this research branch developed to the most active of modern history. Today deep learning based algorithms succeed human performance in image recognition [129], are capable of summarising complex text analysis [130] and solve the protein folding problem [131]. All these major successes emphasise the capability of these algorithms to be successfully applied for joint analysis. For these reasons, the most relevant algorithms with a potential for joint analysis are presented next.

Lesion Detection and Segmentation

In this subsection, the transformative impact of deep learning technologies in the field of medical imaging, with a particular focus on orthopaedic applications is analyzed. The power of deep learning in tasks such as classification and object recognition is well documented and represents an important milestone in medical diagnostics. An example of this is the breakthroughs in skin cancer classification [132] and breast cancer detection [133], which set a precedent for the application of these technologies in disease identification and treatment.

The extension of these advances to the orthopaedic field has shown that deep learning holds great promise. A notable development by Tiulpin, Klein, et al. [134], for example, presents a deep learning tool for analyzing knee osteoarthritis that uses X-rays and medical history to predict the progression of the disease. This is complemented by another significant project that uses MRI scans to classify various knee joint conditions, such as ACL ruptures and meniscus damage. These examples underline the potential of deep learning to refine orthopaedic diagnostics. In addition, the improvement of segmentation capabilities

through object recognition networks, in particular Mask R-CNN [135], as shown in the example of automatic 3D knee segmentation [136], represents a major advance. The growth of datasets such as MRNet [137] and the Osteoarthritis Initiative continues to drive progress in this area, particularly the improvement of diagnostics related to knee joint analysis.

Building on this foundation, the discourse transitions to addressing the global challenge of lower extremity Osteoathritis (OA) and malalignment issues, spotlighting the urgent need for more precise and reliable diagnostic tools. Conventional methods for analyzing leg alignment are characterized by inefficiency and inaccuracy, a gap that the recent innovations of Machine Learning (ML) and Deep Learning (DL) attempt to close. The accuracy of the DL models in determining alignment parameters marks a shift towards automated, sophisticated diagnostic systems that promise to improve orthopaedic care. Supported by a breadth of research [138–149], these technological advancements suggest a future where orthopedic practitioners are equipped with advanced tools to diagnose and manage complex pathologies with an unprecedented level of precision and reliability. This narrative progression from the success of deep learning in general medical applications to its specific impact on orthopedics, and finally to addressing critical challenges in the field, illustrates a logical flow of how these technologies are shaping the future of orthopedic diagnostics and treatment.

Dimensionality Reduction

A big problem of dealing with complex tasks such as joint analysis is the high dimensionality of the problem, as large image sequences from MRI scans need to be analysed or long sequences or measurement trajectories need to be handled. In order to compress this complexity into meaningful low-dimensional representations a variety of deep learning based algorithms have been developed. Famous representatives are the Variational Autoencoder (VAE) [150], Generative Adversarial Network (GAN) [151] or recent approaches such as Momentum Contrastive (MoCo) encoders [152]. All these algorithms have a low dimensional representation of the original high dimensional input enabling a simplified analysis and efficient processing. Further, these training approaches work in an unsupervised manner enabling to extend these algorithms for large datasets as no particular labelling is required. These generative algorithms are capable of predicting disease progression or can improve image quality. A study by [153] has enabled an improved resolution of knee MRI data due to GAN based image reconstruction. As these algorithms can both compress and generate imaging data they also develop an understanding of the underlying data structure. The full potential of these algorithms to actually create physics-based models for direct joint analysis however remains an open challenge and further research is necessary in order to replace conventional methods.

1.4.7 Hybrid Models and Optimization based Approaches

In the field of physical modeling, deep learning approaches often encounter challenges, particularly when physics-based rules are absent. This can lead to issues like overfitting and limited applicability in complex scenarios. Addressing this, a promising direction has emerged: the fusion of physics-based knowledge with deep learning to enhance generalization. A key development in this area is the integration of differential equations with deep learning algorithms, as exemplified by the work of Chen, Rubanova, et al. [154]. This hybrid approach enables the creation of models where neural networks compensate for unknown parameters within a physics-based framework, thereby improving the model's generalization capabilities while maintaining adherence to physical laws.

In the fields of robotics and biomechanics, the efficacy of neural network-based solutions in kinematic analysis has been increasingly recognized. The studies by Köker et al. [155], Duka [156], and Jiang et al. [157] have demonstrated the accuracy and adaptability of neural networks in these domains. The concept of differentiable kinematics, examined by Ono et al. [158] and Fang et al. [159], further underscores the potential of learning-based methods in kinematic calculations. This potential is supported by the development of emerging software solutions [160–162]. Additionally, autoencoders have been identified as potent tools for kinematic optimization. The research conducted by Kubovčıék, Luptáková, et al. [163],

Nagano, Nakamura, et al. [164], and S and Kurian [165] highlights their effectiveness. However, a notable challenge arises in differentiable physics-based models, particularly with backpropagation in dynamic parameters in complex biomechanical systems [166, 167]. This issue is being tackled by model-free approaches like evolutionary algorithms and reinforcement learning, which have shown efficacy in aligning simulated behaviors with real-world scenarios [168]. Reinforcement learning-based optimization techniques, in particular, have demonstrated their utility across various fields, ranging from quantum control [169] to enhancing the efficiency of thermal power units [170]. These techniques are especially valuable when dealing with dynamic parameters such as stiffness and damping characteristics [171, 172], presenting a compelling alternative to traditional differentiable models.

To conclude, the field is experiencing a significant convergence of methodologies, combining differentiable modeling, neural networks, and reinforcement learning. This integration is forging a robust framework capable of tackling the challenges inherent in physical systems modeling.

1.5 Thesis Structure

This dissertation offers a detailed examination of various innovative domains, including wearable technology, diagnostic algorithms, robotic testbeds, control systems, and optimization algorithms, with a specific focus on joint analysis and rehabilitation. The goal is to develop a personalized and adaptive framework that supports comprehensive joint analysis and predictive modeling. This framework aims to enhance the precision and effectiveness of diagnostics and interventions in orthopedic care. The structure of the thesis is intentionally designed to illustrate how these technological components can be integrated into the clinical workflow, as shown in Figure 1.1. This integration is critical for translating theoretical advancements into practical applications that benefit patient care.

1.5.1 Chapter 2: Prevention and Rehabilitation through Wearables

This chapter presents a detailed analysis of wearable devices designed for gait analysis in knee joint assessments, alongside an adaptive exoskeleton for hand assessment. It investigates the use and clinical application of the adaptive exoskeleton specifically tailored for finger rehabilitation. To enable a structured discussion, the chapter is organized into three main sections:

1. **Section 2.1: Scalable Gait Analysis through accessible IMU Systems** - Examines the development and implementation of a cost-effective IMU system specifically for analyzing gait and knee joint movements. It also includes an evaluation of this system through a clinical study.

2. **Section 2.2: Finger Rehabilitation through an Introspective Mechatronic Exoskeleton** - Introduces a novel architecture for an adaptive mechatronic exoskeleton for finger rehabilitation and analysis.

3. **Section 2.3: Clinical Application and Integration Study** - Examines the development of an exoskeleton platform designed for finger rehabilitation. It focuses on enhancing patient monitoring and increasing patient motivation through the incorporation of gamification strategies.

1.5.2 Chapter 3: Diagnostics and Surgical Planning through Artificial Intelligence Image Analysis

The third chapter deals with diagnostic and surgical planning algorithms. It covers data annotation, bone tumor detection, automatic alignment algorithms and preoperative planning for the lower limbs. The chapter is divided into four main sections:

1. **Section 3.1: Data Annotation** - Discusses the development of a rapid dataset creation application.

2. **Section 3.2: Bone Tumor Detection Algorithms** - Presents algorithms for bone tumor identification and classification.
3. **Section 3.3: Automatic Alignment Analysis for the Lower Limb** - Introduces a deep learning model for alignment analysis of the lower extremity.
4. **Section 3.4: Automated Preoperative Planning for Realignment Osteotomy** - Covers automated planning of medial open wedge high tibial osteotomy using AI.

1.5.3 Chapter 4: Reproducible Joint Analysis through Robotic Benchmarking Systems

The fourth chapter investigates the use of robotic testbenches for the analysis of knee and hand joints. It focuses on methodologies, results, and broader implications of these studies. The chapter includes:

1. **Section 4.1: Constraint-Tolerant Control for Biomechanical Systems** - Discusses null space control in robotic arm tasks and its applications.
2. **Section 4.2: Ex-Vivo Human Knee Joint Analysis** - Presents a validation study of a robotic testbench for biomechanical evaluations of the knee joint.
3. **Section 4.3: Ex-Vivo Human Hand Joint Analysis** - Introduces a robotic testbench for analyzing pincer grip execution in human specimen hands.

1.5.4 Chapter 5: Personalized Digital Twins through Artificial Intelligence-based Optimization

The fifth chapter focuses on optimization algorithms for biomechanical systems, focusing on kinematic and dynamic optimization. It presents methodologies in autoencoder-based kinematic optimization and system identification through reinforcement learning. The chapter comprises:

1. **Section 5.1: Differentiable Forward Kinematics for Kinematic Optimization** - Researches differentiable kinematic modeling.
2. **Section 5.2: Model-Free Proximal Policy Optimization for Dynamic Optimization** - Discusses the adaptation of models for the human knee using reinforcement learning.

1.5.5 Chapter 6: Conclusions

The sixth chapter summarizes the key discoveries and critical evaluations made throughout the thesis. It looks at the integration of robotics and AI in orthopaedic care and shows how this fusion answers fundamental research questions and leads to notable advances.

1. **Section 6.1: Contributions** - Elaborates on the key contributions of the thesis, detailing the novel approaches and methodologies developed within the context of robotics and AI in orthopedics.
2. **Section 6.2: Addressing Objectives and Research Questions** - Critically examines how the thesis meets its set objectives and answers the research questions posed at its inception, linking these back to the contributions made.
3. **Section 6.3: Limitations** - An introspective look at the main limitations encountered in the research. This section discusses the boundaries and challenges of the methods and technologies employed, providing a balanced view of the research.
4. **Section 6.4: Achievements** - Assesses the overall impact of the thesis, discussing how its findings and contributions have influenced the field of orthopedics, both in academic and practical contexts.

5. **Section 6.5: Future Work** - Outlines the potential paths for future research, this section suggests improvements and areas of exploration that build upon the thesis's findings, indicating directions for continued innovation in orthopedic care.

1.6 Core Publications

The research conducted for this dissertation has led to several publications in the fields of wearable technology, diagnostic algorithms, robotic testbenches, and control and optimization algorithms. These publications are integral to the thesis, each contributing to the understanding and development of joint analysis and rehabilitation. The following detailed list of these publications categorizes them along the relevant chapters of the thesis.

1.6.1 Publications from Chapter 2: Prevention and Rehabilitation through Wearables

1. **Wilhelm, N.**, Micheler, C. M., Lang, J. J., Hinterwimmer, F., Schaack, V., Smits, R., Haddadin, S., and Burgkart, R. (2023). Development and Evaluation of a Cost-effective IMU System for Gait Analysis: Comparison with Vicon and VideoPose3D Algorithms. *Current Directions in Biomedical Engineering*, 9(1), 254–257. [1] *Published* - This publication discusses a scalable, cost-effective IMU system for gait analysis.

2. **Wilhelm, N.**, Dickmann, T., Glowalla, C., Haddadin, S., van der Smagt, P., and Burgkart, R. (2021). An Adaptive Mechatronic Exoskeleton for Force-Controlled Finger Rehabilitation. *Frontiers in Robotics and AI*, 8. [2] *Published* - Introduces an adaptive mechatronic exoskeleton for finger rehabilitation.

3. **Wilhelm, N.**, Haddadin, S., Lang, J. J., Micheler, C., Hinterwimmer, F., Reiners, A., Burgkart, R., and Glowalla, C. (2022). Development of an Exoskeleton Platform of the Finger for Objective Patient Monitoring in Rehabilitation. *Sensors*, 22(13), 4804. [3] *Published* - Focuses on an exoskeleton platform for finger rehabilitation and patient monitoring.

1.6.2 Publications from Chapter 3: Diagnostics and Surgical Planning through Artificial Intelligence-based Image Analysis

1. von Schacky, C. E., **Wilhelm, N.**, Schäfer, V. S., Leonhardt, Y., Gassert, F. G., Foreman, S. C., Gassert, F. T., Jung, M., Jungmann, P. M., Russe, M. F., Mogler, C., Knebel, C., von Eisenhart-Rothe, R., Makowski, M. R., Woertler, K., Burgkart, R., and Gersing, A. S. (2021). Multitask Deep Learning for Segmentation and Classification of Primary Bone Tumors on Radiographs. *Radiology*, 301(2), 398–406. [4] *Published* - Presents multitask deep learning for bone tumor detection.

2. von Schacky, C. E., **Wilhelm, N.**, Schäfer, V. S., Leonhardt, Y., Jung, M., Jungmann, P. M., Russe, M. F., Foreman, S. C., Gassert, F. G., Gassert, F. T., Schwaiger, B. J., Mogler, C., Knebel, C., von Eisenhart-Rothe, R., Makowski, M. R., Woertler, K., Burgkart, R., and Gersing, A. S. (2022). Development and evaluation of machine learning models based on X-ray radiomics for the classification and differentiation of malignant and benign bone tumors. *European Radiology*, 32(9), 6247–6257. [5] *Published* - Discusses ML models for classifying bone tumors.

3. **Wilhelm, N.**, von Schacky, C. E., Lindner, F. J., Feucht, M. J., Ehmann, Y., Pogorzelski, J., Haddadin, S., Neumann, J., Hinterwimmer, F., von Eisenhart-Rothe, R., Jung, M., Russe, M. F., Izadpanah, K., Siebenlist, S., Burgkart, R., and Rupp, M.-C. (2024). Multicentric Development and Validation of a Multi-Scale and Multi-Task Deep Learning Model for Comprehensive Lower Extremity Alignment Analysis. *AI in Medicine*. [6] *Accepted* - This work introduces a deep learning model for comprehensive lower extremity alignment analysis, accepted at 11. March 2024.

4. **Wilhelm, N.**, von Schacky, C. E., Lindner, F. J., Feucht, M. J., Ehmann, Y., Pogorzelski, J., Haddadin, S., Neumann, J., Hinterwimmer, F., von Eisenhart-Rothe, R., Jung, M., Russe, M. F., Izadpanah, K., Siebenlist, S., Burgkart, R., and Rupp, M.-C. (2024). Fully Automated Planning of Medial Open Wedge High Tibial Osteotomy on Weight Bearing Anterior Posterior Long Leg Radiographs via Artificial Intelligence – A Multicentric Development and Validation Study. Planned for *The American Journal of Sports Medicine*. [7] *Planned submission, Draft finished, Demo available online* - This upcoming submission covers the fully automated planning of medial open wedge high tibial osteotomy using AI. Unsubmitted manuscript.

1.6.3 Publications from Chapter 4: Reproducible Joint Analysis through Robotic Benchmarking Systems

1. **Wilhelm, N.**, Burgkart, R., Lang, J., Micheler, C., and von Deimling, C. (2019). Exploiting Null Space Potentials to Control Arm Robots Compliantly Performing Nonlinear Tactile Tasks. *International Journal of Advanced Robotic Systems*, 16(6). [8] *Published* - Studies null space control in robotic arm tasks.

2. **Wilhelm, N.**, von Deimling, C., Haddadin, S., Glowalla, C., and Burgkart, R. (2023). Validation of a Robotic Testbench for Evaluating Biomechanical Effects of Implant Rotation in Total Knee Arthroplasty on a Cadaveric Specimen. *Sensors*, 23(17), 7459. [9] *Published* - Focuses on a robotic testbench for knee joint analysis.

3. **Wilhelm, N.**, Glowalla, C., Haddadin, S., Schote, J., Hoeppner, H., van der Smagt, P., Karl, M., and Burgkart, R. (2024). Design and Implementation of a Robotic Testbench for Analyzing Pincer Grip Execution in Human Specimen Hands. Accepted for the 2024 IEEE International Conference on Robotics and Automation (ICRA). [10] *Accepted.* - Presents a robotic testbench for hand joint analysis.

1.6.4 Publications from Chapter 5: Personalized Digital Twins through Artificial Intelligence-based Optimization

1. **Wilhelm, N.**, Haddadin, S., Burgkart, R., van der Smagt, P., and Karl, M. (2024). Accurate Kinematic Modeling using Autoencoders on Differentiable Joints. Accepted for the 2024 IEEE International Conference on Robotics and Automation (ICRA). [11] *Accepted.* - Discusses kinematic modeling using autoencoders.

2. **Wilhelm, N.**, Burgkart, R., Hinterwimmer, F., Haddadin, S., and Karl, M. (2024). System Identification of the Human Knee by Adaption of Plausible Models using Reinforcement Learning in Robotic Data Acquisition. Submitted to IEEE IROS. [12] *Under Revision* - Focuses on model adaptation for the human knee using reinforcement learning.

2 Prevention and Rehabilitation through Wearables

In this chapter, a detailed investigation of wearable technologies for orthopaedics is conducted as part of the research presented, which is closely aligned with the research question: How can wearables and robotic technologies be effectively integrated into clinical orthopaedic workflows to provide real-time objective data for joint disease prevention and rehabilitation? With the help of Figure 2.1, the development of diagnostic tools into rehabilitative devices within the orthopaedic discipline is outlined. It emphasizes the dual role of wearable technologies not only as instruments for data acquisition, but also as active participants in changing biomechanical processes through their motor functions.

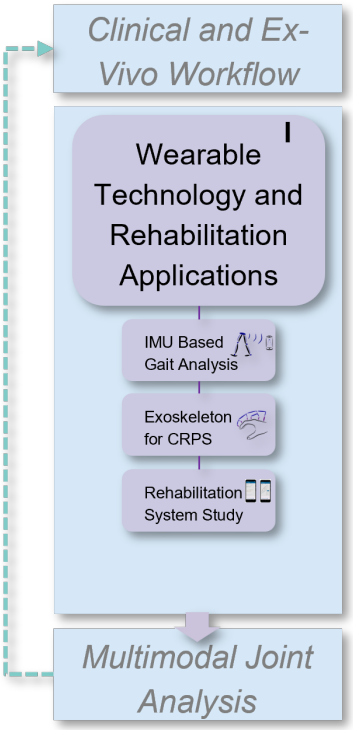

Figure 2.1 Chapter overview.

In the field of orthopaedics, wearable technologies are moving beyond their role as mere advanced measurement devices; they are an integral part of musculoskeletal health management. This chapter discusses the development of some of these technologies and their impact on diagnostic and rehabilitation procedures. The research begins with an introduction to an innovative gait analysis system that utilizes IMU technology (Section 2.1), which is essential for the early detection of limb deformities and the prevention of long-term orthopedic complications suited for knee joint analysis. A state-of-the-art exoskeleton developed for the rehabilitation of CRPS patients of the hand is then presented (Section 2.2), marking the transition to a rehabilitative focus and illustrating the adaptability of wearable technologies in orthopaedic care. The chapter concludes with an analysis of a patient-study evaluating the effectiveness of the exoskeleton in real-world applications (Section 2.3), which provides valuable insights into the practical implications of these technologies.

2.1 Scalable Gait Analysis through accessible IMU Systems

This section addresses the development and evaluation of a cost-effective IMU-based system tailored for gait analysis, as reported in [1]. Gait analysis is crucial for diagnosing and managing various medical conditions, including musculoskeletal injuries and neurological disorders [64]. Traditional systems for gait analysis, though accurate, are often expensive and cumbersome, limiting their accessibility for widespread clinical and research use. In response to this challenge, IMU-based systems offer a portable, affordable alternative, as underscored by previous studies [65–69].

The IMU system developed in this study consists of five calibrated sensors integrated with a mobile application, designed to capture the lower body orientation during various activities, including walking and stair climbing. The system efficacy was benchmarked against the gold-standard Vicon system and the modern VideoPose3D algorithm [61], involving eight healthy participants who each performed ten repetitions of the specified activities. This setup aimed to accurately analyze the hip and knee flexion angles.

The findings revealed that the IMU system exhibited a significantly lower Mean Squared Error (MSE) in comparison to single camera-based deep learning approaches, with its performance being notably comparable to that of the Vicon system. Such results highlight the systems potential as a viable tool for both clinical and research settings, offering a blend of affordability, robustness, and user-friendliness.

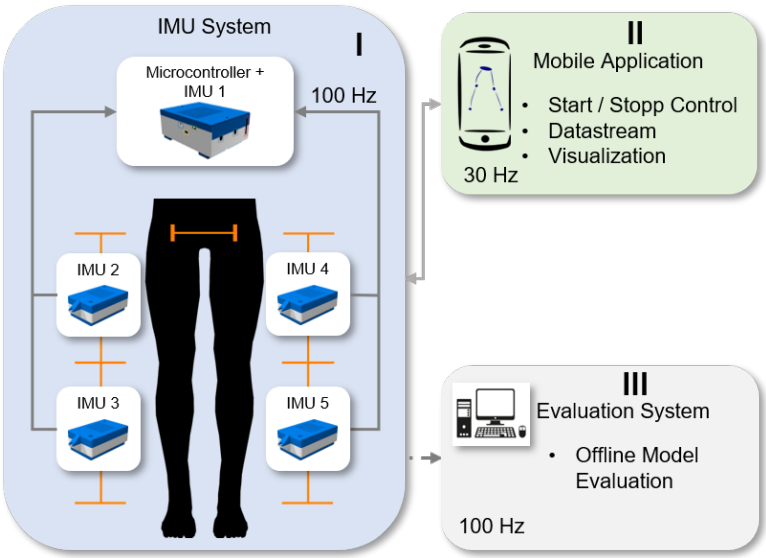

Figure 2.2 Test bench architecture consisting of the primary IMU system (I) with five IMUs, a mobile application (II) for data visualization and control and an offline evaluation system (III) from Wilhelm et al. [1].

This comparative study aims to position the IMU-based gait analysis system as a practical and efficient alternative that provides broader access to accurate gait analysis for the diagnosis and management of health conditions.

The IMU system developed in this study, as shown in Figure 2.2, is integrated into a mobile app and uses five calibrated sensors to capture the orientation of the lower body. The application allows the system to be started and stopped and serves as a visualization toolbox during data generation at 30 Hz. The entire analysis is performed offline on the evaluation system with a sampling rate of 100 Hz.

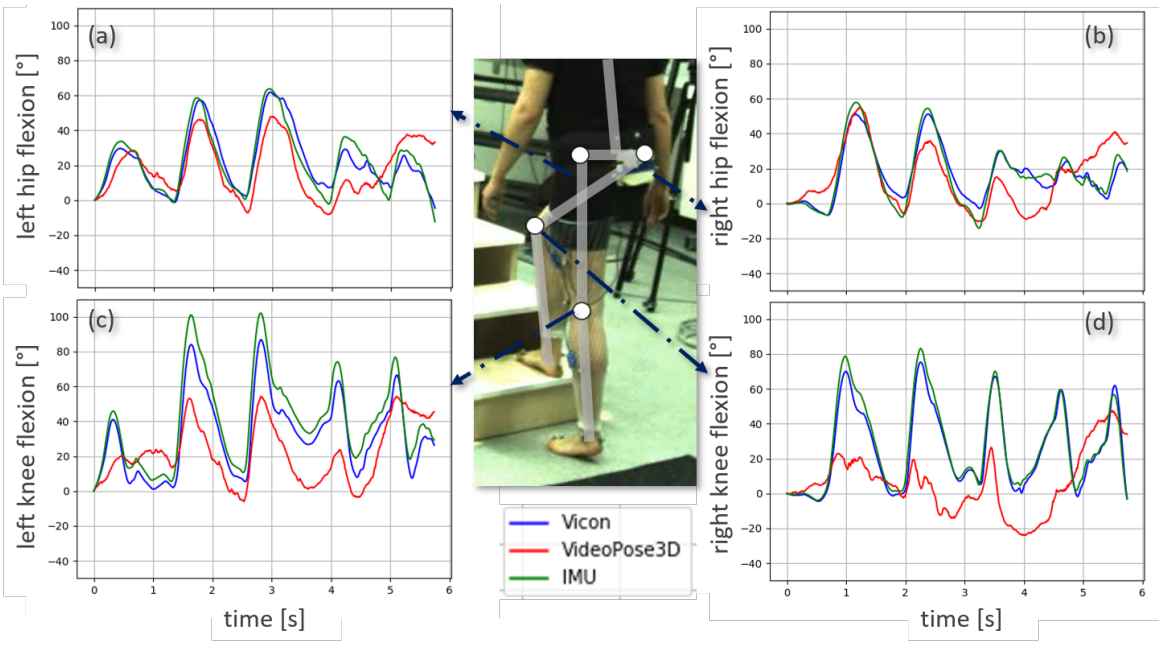

Figure 2.3 Stairclimbing task study setup with joint angle graphs for Vicon (blue), VideoPose3D (red), and IMU (green) systems. Left and right hip flexion angles are shown in (a) and (b), and left and right knee flexion angles in (c) and (d). The central snapshot shows the camera image and an overlay of the model used for gait analysis [1].

The study was successful in acquiring all measurements, including those for a stair climbing task, as depicted in Figure 2.3. Data for the flexion angles of the knee and hip was obtained from all three systems,

with the Vicon system serving as gold standard. The results showed that the IMU system closely matched the Vicon system in terms of the flexion angles of both the left and right hip and the right knee. However, there was an offset observed for the left knee flexion. The VideoPose3D model showed moderate agreement with the Vicon system for the flexion of the left and right hip but had significant accuracy loss for the flexion angles of the knee.

Table 2.1 Assessment of the Mean Squared Deviation (MSD) in knee or hip flexion for the Gait and Stairclimbing task from IMU and VideoPose3D systems compared to the Vicon system. Data represented as mean ± standard deviation. Results from Wilhelm et al. [1].

Task	Joint	IMU	VideoPose3D
Gait	Knee	4.0 ± 1.1	18.8 ± 4.3
	Hip	5.1 ± 1.7	24.4 ± 6.5
Stairclimbing	Knee	5.9 ± 1.6	27.7 ± 4.9
	Hip	6.6 ± 1.6	10.1 ± 3.0

Table 2.1 presents the MSD comparison of the IMU model, Vicon system, and VideoPose3D algorithm in gait and stair climbing accuracy. The IMU system displayed a significantly lower MSD than VideoPose3D, indicating its potential for clinical and research applications.

The design of the IMU system, which is low-cost, promotes its integration into daily use cases, potentially bridging the gap between clinical and home-based monitoring. This accessibility allows patients and healthcare professionals to track changes in gait over time. The findings of the present study emphasize the promising potential of the IMU system as a valuable tool for both clinical and research contexts, meriting further exploration of its performance in complex tasks and diverse populations.

The current system design supports up to five independent IMUs, and the devised model is tailored to the proposed IMU configuration, necessitating further adaptations for incorporating additional IMUs. Although the system offers satisfactory accuracy, the results indicate that, for highly precise movement analysis, Vicon-based motion detection remains the gold standard. While the application provided should be user friendly, this has not been adequately tested and will need to be worked out in the future.

To summarize, this study introduces a cost-effective IMU system for gait analysis that surpasses single camera based deep learning methods and closely matches the performance of the more expensive gold-standard system. The development of an affordable and precise IMU system for gait analysis presents substantial potential for advancing clinical and research applications.

2.2 Finger Rehabilitation through an Introspective Mechatronic Exoskeleton

The previous section was focused on gait analysis, with the knee joint being the central subject of assessment. To demonstrate the applicability of wearable technologies to various joints, attention is now shifted to the assessment of the hand. In this section, an innovative mechatronic exoskeleton designed for finger rehabilitation is discussed [2]. Equipped with motion detection and control sensors, this exoskeleton is provided with three significant advantages for enhancing hand therapy.

First, it allows for precise measurement of patient-specific finger dynamics. The configuration of the exoskeleton can be fully reconstructed using data from three angular position sensors placed on the kinematic structure. Additionally, the actuation force acting on the exoskeleton is recorded, enabling the determination of the ROM and the force and torque trajectories of each finger joint. Second, the adaptive kinematic structure enables the patient to perform various functional tasks. The force control of the exoskeleton acts as a safeguard, limiting the maximum possible joint torques during finger movement. Last, the system is compact, lightweight, and does not require extensive peripherals. Its safety features make it easy to use at home. The applicability of the system was tested on three healthy subjects. An overview of the developed system can be seen in Figure 2.4.

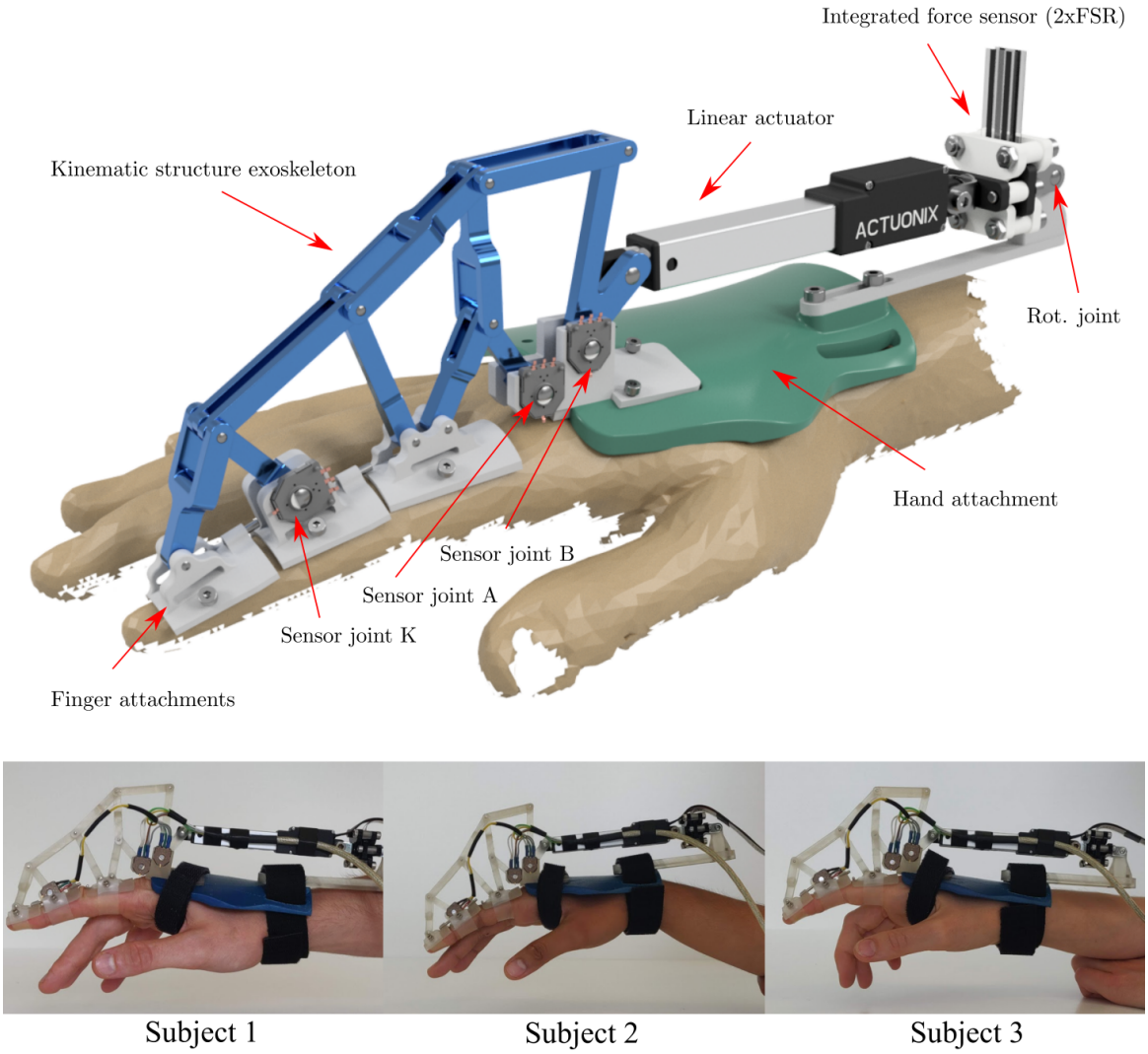

Figure 2.4 Rendering (top) and application of the real system (bottom) of the exoskeleton [2]. In the bottom row, the exoskeleton is attached to the index finger of three individual test subjects [2].

2.2.1 Exoskeletons

Impaired hand functionality can significantly hinder daily activities. Hand mobility can be limited due to various conditions such as neuromuscular diseases, hand injuries, motor function restrictions resulting from a stroke, age-related limitations, and CRPS [83]. Conventional therapy often leads to unsatisfactory results due to early hospital discharges, insufficient availability of therapists, and high financial costs [84, 85]. Therefore, there is a growing interest in improving hand functionality through robotic rehabilitation systems. Research on stroke rehabilitation has highlighted the potential of robotic hand rehabilitation [83]. Repetitive motion training plays a supportive role in the recovery of motor skills [86–88]. Hand rehabilitation using repetitive motion training with a robotic system is likely more effective than conventional therapy [89].

Exoskeletons equipped with suitable sensors can provide accurate and repeatable data to quantify the functional status of the patient hands [90]. Moreover, high-frequency rehabilitation exercises do not increase the financial burden of the treatment. Therefore, using exoskeletons in therapy can allow patients to follow a daily training routine, which is usually not possible in manual therapy. Despite the demonstrated potential of exoskeleton systems for rehabilitation, their use in therapy is still limited [90]. The complexity of these systems and the resulting poor usability in a clinical context are significant barriers. This work extends the approaches of previous studies by adding position sensing, a more user-friendly bi-directional actuator, and a force sensor. This simplifies the measurement process and extends the functionality in comparison to

previous approaches [83]. We also provide a mathematical model to represent the actuation forces on the load in the finger joints.

Over the past two decades, a variety of hand exoskeleton systems have been developed, most of which are intended either for hand rehabilitation, force assistance, or to provide haptic feedback, e.g., for virtual reality applications. Regardless of the intended use, all systems must meet the key requirement of biomechanical compatibility with the human hand to enable safe operation [83]. The approach by previous studies uses an underactuated kinematic structure with three degrees of freedom that incorporates all three finger phalanges [91, 92]. This kinematic structure allows the computation of all forces transmitted to the finger phalanges, provided that the configuration of the mechanism and the actuator force acting on the structure are known.

To fully harness this potential, the methods from previous research were expanded in [2] by integrating angular position sensors into the kinematic structure and coupling a bi-directional electric linear actuator with a force sensor [91, 92]. By measuring the angles between linkages at three joints of the kinematic structure, it is possible to develop a parameterized dynamic model of the index finger. This enhancement allows for precise tracking of joint motion, which is critical for monitoring patient progress, as well as for accurately mapping measured forces and calculating resulting loads and resistance torques across each joint.

System Requirements

The rehabilitation effectiveness hinges on key requirements. It must ensure patient safety, be biomechanically compatible with the human hand, and prevent finger joint hyperextension and excessive force application. The exoskeleton should accommodate various hand sizes and grasping tasks, leaving the palm free for object interaction during training. It should stimulate all finger-flexion joints and record diagnostic data of angle and torque trajectories for each joint. The system should be scalable for whole-hand use, user-friendly for clinical and home settings, as well as comfortable and easy to wear and remove. It should support various rehabilitation modes, including active, active-assistive, and resistive training. Safety is ensured through mechanical end stops to prevent finger joint hyperextension. The force control should allow fine-tuning of the maximum actuation forces on the fingers. The kinematic structure should be rigid for precise positioning and accurate sensor data interpretation. A three DOF underactuated system is preferred for natural finger motion, supporting bidirectional forces up to approximately 45 N. Direct control of the kinematic structure is necessary for precise force control.

The key requirements for the system can be summarized as follows: It must be safe to use, suitable for both clinical and home environments, scalable to accommodate the entire hand, comfortable and easy to put on and take off, optimized for a wide range of motion, and designed to allow free movement of the palm. Additionally, it should be capable of measuring the angle and torque of each joint and compatible with various rehabilitation modes. No system known to the author fully met these requirements considering the exhaustive literature review. However, the approach by [92], later modified by [91], was the closest match, forming the basis for the common structure of the exoskeleton in development [2].

2.2.2 Exoskeleton Modeling

Kinematic Model

The kinematic structure of our approach is visualised in Figure 2.5. The rigid links lie in the plane of the flexion/extension motion of the finger. They are connected by eleven rotational joints with six points of connection to the finger and the back of the hand. The kinematic chain can be decomposed into three five-bar linkages, each with two degrees of freedom, and two four-bar linkages, each with one degree of freedom. This structure allows for greater flexibility and ROM compared to simpler variants with fewer subsets of joints.

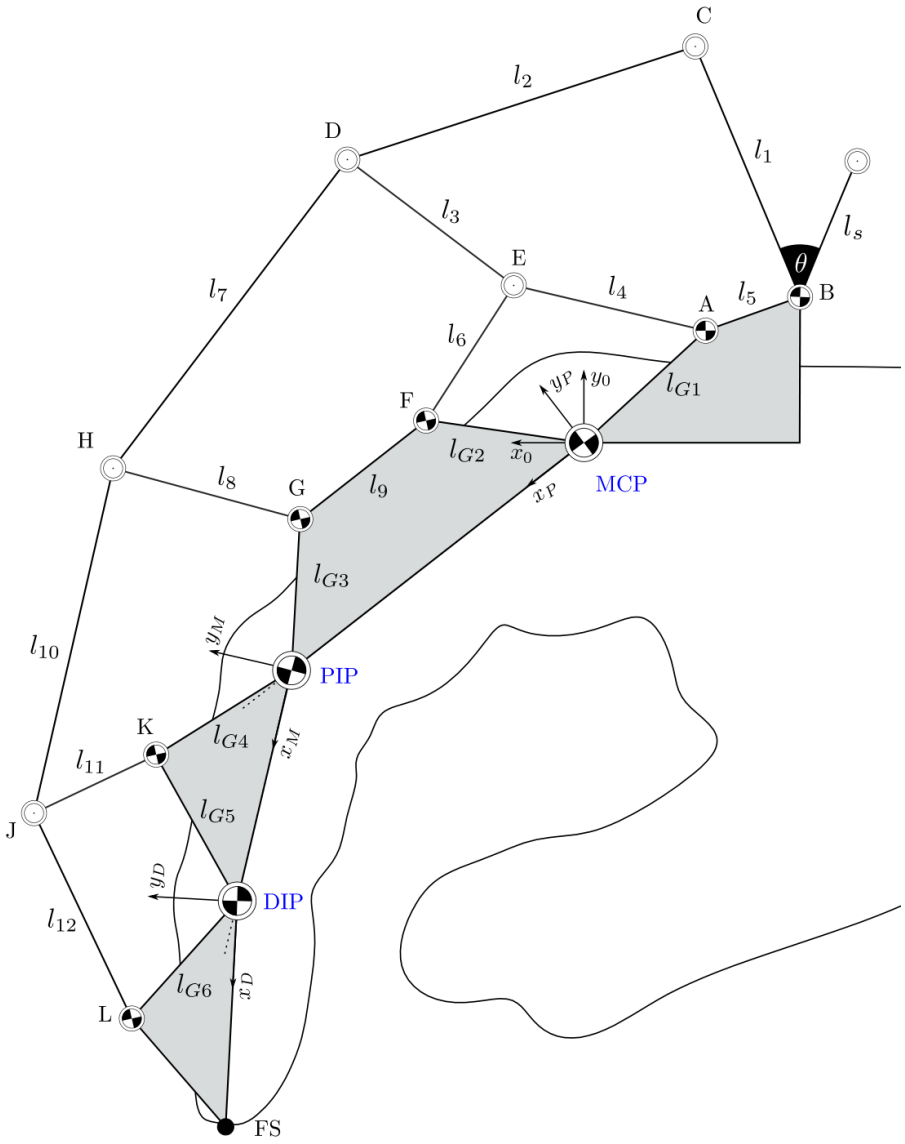

Figure 2.5 Linkage structure of the proposed exoskeleton system as an extension to [91]. The finger joints are marked in blue. Areas marked in grey are considered as rigid bodies within the structure [2].

The planar mechanism's degrees of freedom can be calculated using equation (2.1), with $n = 14$ for the number of links and g for the number of joints. Joints connecting three links are counted twice, resulting in $10 + 2 \cdot 4 = 18$ joints. Each rotational joint has one degree of freedom, represented by f_i.

$$\begin{aligned} F &= 3\,(n-1) - 3g + \sum_{i=1}^{g} f_i \\ &= 3\,(14-1) - 3 \cdot 18 + 18 = 3 \end{aligned} \tag{2.1}$$

The kinematic model is calculated using the tan-half-angle technique ([173], p. 412), which determines a joint's two potential positions based on its distance to two known joints. The system employs a linear actuator with respective actuation force F_{act}, allowing multiple actuators on the hand's dorsal side for simultaneous finger actuation.

Dynamic Model of the Finger

The dynamic model is derived from the contact forces between the exoskeleton and finger. This model comprises three finger joints moving in a plane, interconnected by revolute joints. Each joint experiences an unknown torque ($M_1 - M_3$), symbolizing either the joint's resistance to motion or the actuation torque applied by the patient. The minimum coordinates $\boldsymbol{q} = (\alpha, \beta, \gamma)^T$ are represented by the respective joint angles of the MCP, PIP and DIP joints. Contact forces are the attachment points between the exoskeleton and the finger and can be solved analytically [2].

The dynamic model can resolve the unknown torques $M_1 - M_3$ under unrestrained motion conditions, i.e., without additional contact forces acting on the finger, using the projected Newton-Euler equations:

$$\sum_{i=1}^{3} \left[{}_I\boldsymbol{J}_{T,i}^T \boldsymbol{F}_{\text{sum}} + {}_{K_i}\boldsymbol{J}_{R,i}^T \boldsymbol{M}_{\text{sum}} \right] = \boldsymbol{0}, \tag{2.2}$$

$$\text{with } \boldsymbol{F}_{\text{sum}} = m_i \, {}_I\boldsymbol{a}_{C_i} - {}_I\boldsymbol{F}_i,$$
$$\text{and } \boldsymbol{M}_{\text{sum}} = {}_{K_i}\dot{\boldsymbol{L}}_i + {}_{K_i}\boldsymbol{\omega}_i \times {}_{K_i}\boldsymbol{L}_i - {}_{K_i}\boldsymbol{M}_i.$$

The sum of forces and moments for each body is computed and projected in the directions compatible with the kinematic constraints via the transposed individual Jacobian matrices for translation ${}_I\boldsymbol{J}_{T,i}^T$ and rotation ${}_{K_i}\boldsymbol{J}_{R,i}^T$. The forces $\boldsymbol{F}_i$ and moments $\boldsymbol{M}_i$ are described with respect to the inertial reference frame I and body-fixed coordinate frames K_i, respectively. $\boldsymbol{L}_i$ denotes the angular momentum and $\boldsymbol{\omega}$ the angular velocity of each body.

Given the small magnitudes of moving masses, velocities, and accelerations in the system compared to the external forces and moments, the model can be approximated quasi-statically with $\dot{\boldsymbol{q}} = \ddot{\boldsymbol{q}} = \boldsymbol{0}$. This approximation allows for the calculation of $M_1 - M_3$ based solely on kinematic data. If necessary, the kinematic calculation could be extended by $\dot{\boldsymbol{q}}$ and $\ddot{\boldsymbol{q}}$ for the dynamic case.

System Integration and Control

The system's adaptability, functionality, and constraints were evaluated through a prototype tested on three subjects, as illustrated in Figure 2.4. Its rigidity was enhanced by reinforcing the flange between the motor mount and the back of the hand. Potentiometers were placed at joints A and B due to their extensive range of motion, which enable optimal sensor resolution utilization and mechanical suitability. The K joint was chosen for its large range of motion and flexible mounting options for the sensors. In addition, the data from joint K is essential for comprehensive system analysis, as the kinematic calculations beyond joints A and B rely on this information. Finger attachments were implemented using adjustable silicone bands, ensuring adequate force transmission to each finger limb. Hyperextension of the finger joints was prevented by extending the attachments on their proximal side with small screws. The connection between the motor and the exoskeleton kinematics was realized by a small pin, allowing a quick and safe motor release. The 12 V power supply of the linear motor was coupled with an emergency stop switch for electrical safety.

The sensor control system architecture incorporates three rotary potentiometers as angular position sensors. To enhance the accuracy of these sensors and counteract their inherent non-linear behavior, discrete Analog to Digital (ADC) counts were ascertained at intervals of 2°. Position and force sensor readings were obtained by an ADC on a Teensy 4.1 microcontroller with a 12-bit resolution. The raw ADC values were logged onto a Storage Device (SD) card at a frequency of 100 Hz. The actuator position is controlled via a pulse width modulation (PWM) signal based on the control system's output [2].

Force Sensor Integration

Force Sensing Resistor (FSR)-type force sensors were integrated into a custom-built mechanical enclosure (Figure 2.6) to measure the actuation force. The design and placement of the force sensor enclosure

eliminated typical error sources, ensuring an orthogonal application of the forces on the resistor in both tension and compression directions. The force sensor unit pivots freely around its rear attachment point. It

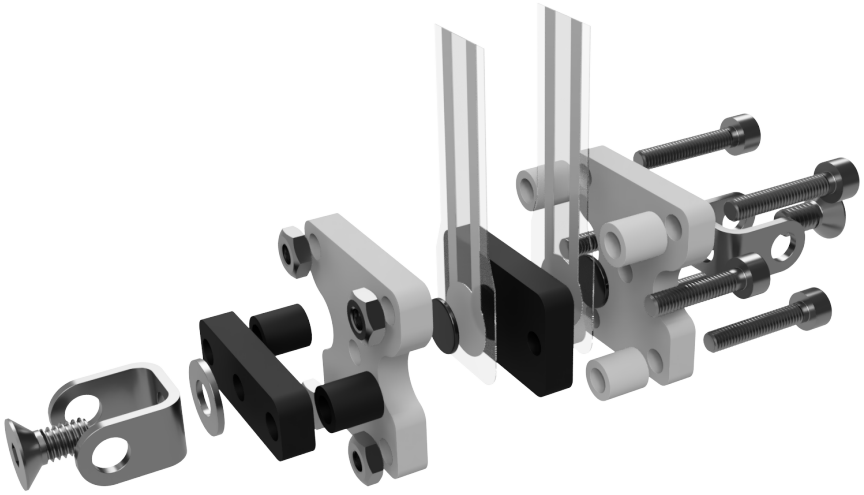

Figure 2.6 Exploded view of the FSR sensor integration. The setup ensures an orthogonal application of the applied forces on the resistor in tension and compression direction [2].

is rigidly clamped to the linear actuator at its front attachment point, acting as an extension of its center line. The enclosure is made up of two rigid claws, a black and a white one as shown in Figure 2.6. Two FlexiForce® A201 sensors with a maximum load rating of 45 N were used in the prototype. To achieve linear sensor response and to adjust the force ranges, two non-inverting operational amplifier circuits were used to process the voltage readings from the sensors.

Control System

A force thresholding system was implemented for initial testing. The desired actuator trajectory was calculated in real time and decomposed into a series of target actuator positions. Actuation torque at joint B was monitored and compared against a preset threshold value. To prevent system oscillations, this comparison was managed by a two-point controller with a dead-band feature, enhancing system stability and response. The system adaptivity excludes the control of individual joint trajectories by manipulating the actuator position. However, the joint angles and joint torques can be determined using the described kinematic and dynamic models, providing potential input to the control system.

2.2.3 Results

Exoskeleton ROM Evaluation

The ROM is a crucial characteristic of the rehabilitation-focused exoskeleton. An experiment was conducted in which subjects performed repetitive maximum flexion and extension of the index finger. The exoskeleton served as a measurement tool, enabling the determination of joint trajectories. The active ROM encompasses all potential positions that the fingertip can reach, whereas the functional ROM signifies a subset of these positions that are essential for executing the majority of daily tasks. The ROM achieved by the coupling of the exoskeleton with the index finger is also taken into account.

Table 2.2 enumerates individual data and the resultant ROM for each subject. Evaluation of the functional ROM indicates that the exoskeleton-index finger coupling encompasses 77%, 87% and 100% of the functional ROM for the three subjects, respectively. As the length of the index finger diminishes from 93 mm to 87 mm and 85 mm, the corresponding functional ROM expands due to the relative increase in the size of the kinematic structure, enabling greater distances during flexion. Consequently, positions necessitating substantial flexion of all three finger joints are unachievable for subject 1. Nevertheless, the exoskeleton

coupling provides nearly unrestricted movements in a significant segment of the functional ROM, rendering it suitable for training a wide range of daily life grasping tasks for all subjects.

Table 2.2 Tabulated parameters of the three individual subjects for the index finger and the achievable ROM. Results from [2].

	Subject 1	Subject 2	Subject 3
Gender	male	female	female
Age [years]	27	25	25
Overall Length [mm]	93	87	85
Proximal Phalanx [mm]	41	39	37
Middle Phalanx [mm]	27	24	24
Distal Phalanx [mm]	25	24	24
Functional ROM	77%	87%	100%
Overall ROM	40%	44%	60%

Force Control Interaction Evaluation

The force control system was evaluated by limiting the exoskeleton movement for subject 1. A force-sensitive plate was introduced as an obstacle to the free finger movement, and the resulting force at the fingertip was measured, as displayed in Figure 2.7. The exoskeleton driving torque was capped at 0.1 Nm, and the resistive forces at the fingertip were interpreted as increased joint stiffness by the model. Figure 2.8 illustrates a sharp increase in joint moments following the finger contact with the force-sensitive plate.

Figure 2.7 Experiment setup or force control interaction.

Upon contact with the plate, a controller-induced oscillation is observed, attributable to the maximum and minimum permissible torques of the drive torque. The maximum external force on the force-sensitive plate is 1.53 ± 0.1 N, leading to an immediate drop in the measured torques. The effect manifests differently across the finger joints. The DIP and PIP joints experience lower torques due to the external contact force, while the MCP joint experiences a more intense torque accumulation. The angular trajectories remain almost unchanged for the MCP and DIP joints, with only the PIP joint responding to the altered load. The low standard deviation of the trajectories indicates the system's sufficient load-bearing capacity in subject 1. The experiment demonstrates that the exercise intensity can be tailored to the patient's hand's functional state by adjusting the controller's thresholds, ensuring patient comfort during therapy.

2.2.4 Conclusion

The section introduced a force-controlled exoskeleton designed for automated rehabilitation of CRPS patients. The exoskeleton meets critical requirements for CRPS treatment, potentially reducing treatment costs and simplifying frequent rehabilitation exercises. The system's integrated position and force sensors

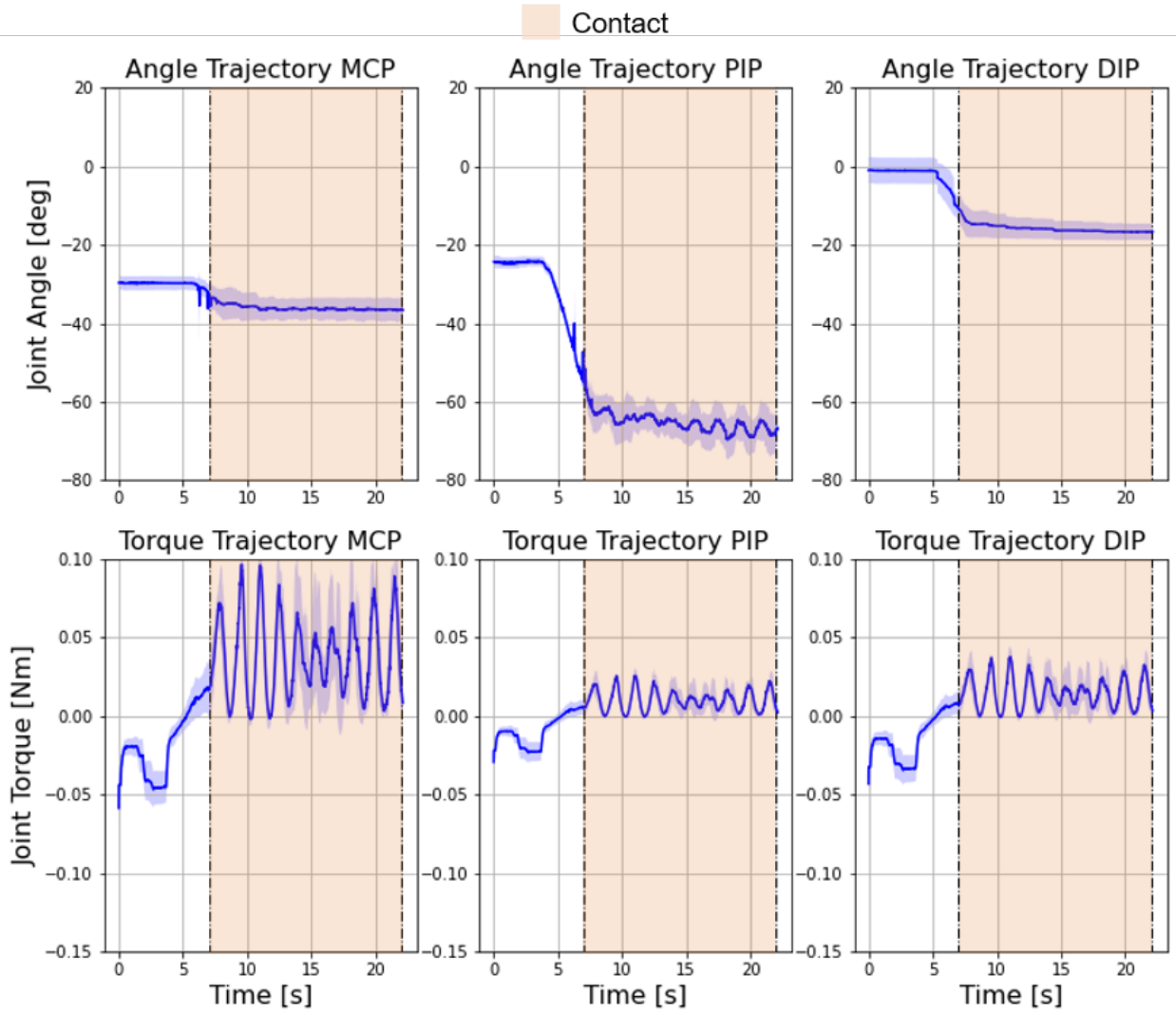

Figure 2.8 Control intervention for subject 1 during a flexing movement of the index finger with a torque limit of 0.1 Nm at the actuator over three independent test cycles. The resulting mean $\pm$ standard deviation over all cycles are displayed. The finger hits a force sensitive plate at 7 s, which measures a maximum external force to the fingertip of 1.53 ± 0.1 N [2].

collect data, including the finger's ROM and angular and torque trajectories of each joint, enabling objective quantification of the finger's functional status. This data assists therapists in monitoring rehabilitation progress and assessing treatment efficacy. Notably, the recorded resistive torque at varying angular positions can be used to track changes in joint stiffness over time.

The adaptive kinematic exoskeleton structure allows for a range of force-assisted grasping tasks. The actuation force on the structure is measured and limited by a two-point controller, thereby capping the maximum torque at each finger joint. The exoskeleton can provide passive support by applying force to the fingertip in both directions. The functional ROM covered by the exoskeleton is adequate for rehabilitation purposes. The system is easy to attach and detach from the patient finger, and suitable for home use due to its simplicity and affordability. The system is further user-friendly, as the next section demonstrates in more detail.

2.3 Clinical Application and Integration Study

In the previous section, the development of a force-controlled exoskeleton designed for the rehabilitation of patients suffering from CRPS was discussed. The system, equipped with integrated position and force sensors, demonstrated its potential in reducing treatment costs, facilitating frequent rehabilitation exercises, and providing valuable data for tracking rehabilitation progress and assessing treatment efficacy.

Building on this foundation, this section will investigate the application of this adaptive exoskeleton in a real-world context, focusing on its integration with a mobile application designed to enhance the rehabilitation process [3]. This innovative approach not only allows for interactive control of the exoskeleton but also enables the storage of patient-specific data and incorporates elements of gamification to motivate patients throughout their therapy. Over a six-week period, the system was applied to three CRPS patients, providing valuable insights into its practical applicability and the potential for objective therapy evaluation. The design of the exoskeleton, the mobile application, its game content, and the results of the patient study will be discussed in detail in the following.

Treatment of CRPS primarily aims to enhance hand mobility and functionality and alleviate pain. Physiotherapy and ergotherapy, the mainstays of conservative treatment, often yield unsatisfactory results due to time constraints, the need for expert therapists, and high costs [84, 85]. Conversely, exoskeletons can provide precise, cost-effective data for monitoring patient progress, enabling daily therapy [90]. However, many existing exoskeletons require direct fitting to the patient hand or offer adaptive actuation but lack sufficient sensor applications [93–98].

As discussed in Wilhelm et al. [3], the approach by Dickmann et al. [2] overcomes these limitations by providing adequate sensing for index finger actuation, motion tracking, and force control. This chapter extends this approach for clinical use by introducing a mobile application for control, enabling live tracking of patient data and ensuring easy applicability. The details of this development and its application in a clinical study are discussed in the following sections.

2.3.1 Methods

Mechatronic System

The mechatronic system, as detailed in Wilhelm et al. [3], builds upon the work of Dickmann et al. [2], incorporating a Bluetooth control unit and an improved housing for all electrical components. The electrical circuit, depicted in Figure 2.9, includes the individual electrical components and their specific roles within the exoskeleton system. The system utilizes three potentiometers for angle measurement of the exoskeleton kinematics and two FSR units to determine the external force applied by the actuator. The DSDTech HM10 Bluetooth module enables external Bluetooth communication, transmitting signals from the sensors to the mobile application and receiving commands for executing measurement protocols and actuator trajectories.

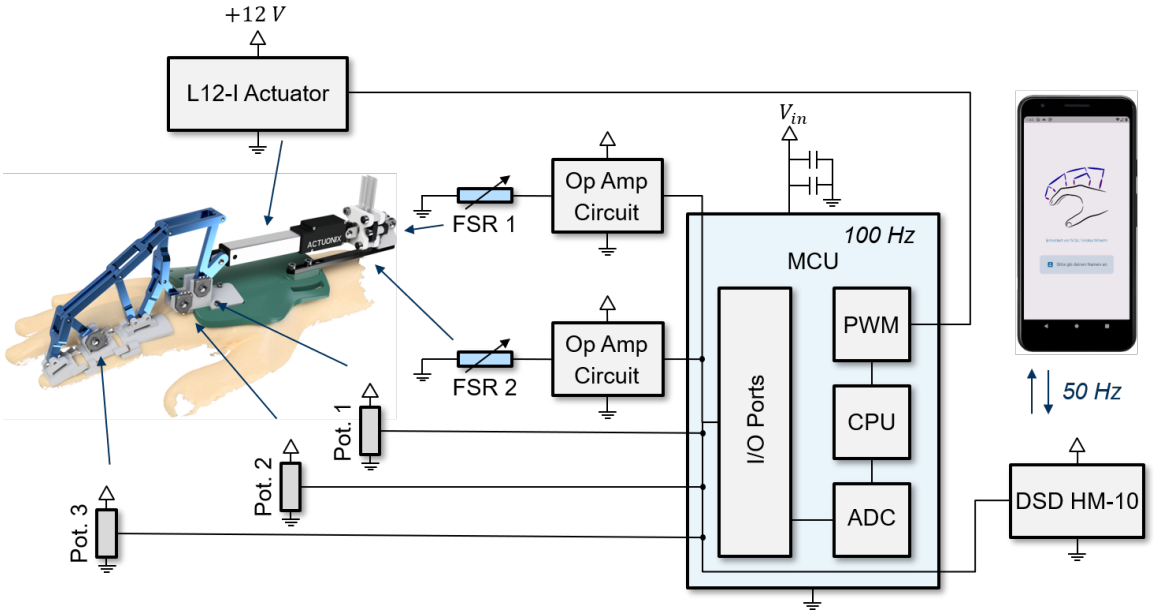

Figure 2.9 Overview of the electrical circuit of the extended exoskeleton from Dickmann et al. [2] and their corresponding use for the exoskeleton system in Wilhelm et al. [3].

Exoskeleton Framework

The exoskeleton architecture is based on the adaptive exoskeleton by Dickmann et al. [2]. The system can be attached to any hand and provides comprehensive force and torque measurements in the finger joints. The newly developed application creates an interactive interface between the patient and the exoskeleton, providing real-time information about the finger and the exoskeleton, enabling therapy via games, and collecting data for therapy objectification and progress diagnosis.

The application, as shown in Figure 2.10, provides a signal view for all relevant measurement signals of the finger, including the angular trajectories and corresponding moment curves. A live-view feature offers an intuitive image of the finger with the exoskeleton in its current position. To motivate patient participation in therapy, two games were developed: "Bubble Collector" and "Dodge Rectangles". The application also provides a separate input mask for patient-specific parameters, which are saved and can be edited at any time. The games were developed with a focus on incorporating established concepts of classical physiotherapy and ergotherapy, emphasizing the training of fine motor skills of the hand. The games provide a welcome change in the lengthy and complex treatment of CRPS and thus increase the patient compliance to regular therapy sessions.

Implementation of Clinical Studies

The study protocol was designed to treat patients with the exoskeleton during outpatient rehabilitation in addition to conventional physiotherapy. A total of 6 study sessions, each lasting 30 minutes, were conducted over 6 weeks. Every study session was carried out according to the defined protocol. Before and after each session, measurements were performed on the hands to assess other objectifiable parameters related to the progression of CRPS. At the end of the experimental sessions after 6 weeks, the Budapest diagnostic criteria and the Quick-DASH scores were additionally collected a second time.

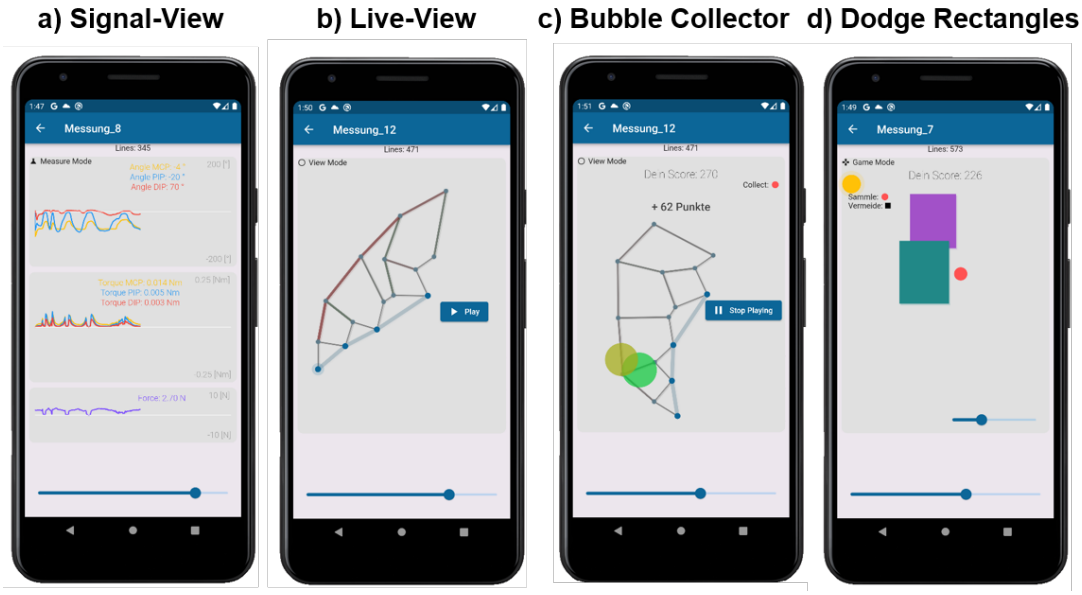

Figure 2.10 The application provides a display of the exoskeleton signals (a), and a real-time representation of the exoskeleton position (b). To engage the patient, two games, "Bubble Collector" (c) and "Dodge Rectangles" (d), are incorporated into the application. Figure from Wilhelm et al. [3].

Table 2.3 Demographics of patients from the study used in Wilhelm et al. [3].

Patient	Age	Sex	BMI	Duration CRPS	Trigger CRPS
1	26	female	32.1 $\mathrm{kg/m^2}$	5 years	Hand overload when writing
2	68	female	28.3 $\mathrm{kg/m^2}$	7 months	Elbow fracture
3	44	male	21.3 $\mathrm{kg/m^2}$	8 months	Wrist fracture

2.3.2 Results

Patient Demographics and Study Protocol

The adaptive exoskeleton was utilized in the treatment of three patients diagnosed with CRPS over a six-week period, adhering to the outlined study protocol. The patient group comprised two females and one male. The onset of CRPS in two of the patients was linked to a fracture and a surgical procedure on the affected limb, while in the third patient, CRPS was triggered by hand overuse during the writing of a graduate thesis.

Table 2.3 provides a summary of the demographic data of the patients. Each patient underwent a minimum of six treatment sessions, each lasting 30 minutes. The frequency of sessions was 1-2 per week for the initial four weeks, followed by a final treatment session at the six-week follow-up. The patients exhibited high motivation levels and reported a positive experience during the sessions. No complications or adverse events were reported during or after the trial sessions.

Based on the analysis of the recorded Patient-Reported Outcome Measures (PROM) and the subjective feedback from the patients, an improvement in symptoms and functionality was observed for all three patients [3]. The severity of CRPS, as indicated by the Budapest criteria, decreased for each patient. Furthermore, an enhancement was noted in all areas upon evaluating the Disabilities of the Arm, Shoulder and Hand (DASH) score. The evaluation outcomes are summarized in Table 2.4.

Measurements of the Exoskeleton

Next we examine the results obtained from the application of the exoskeleton over a six-week therapy period, as reported in Wilhelm et al. [3]. The exoskeleton was used to record joint and torque curves before

Table 2.4 Summary of patient progress over a six-week follow-up period, as measured by the QuickDASH and Budapest Score. A lower score in each case signifies an improvement in the patient condition. Table adapted from Wilhelm et al. [3].

Score	Patient 1	Patient 2	Patient 3
Budapest Pre [174]	6 / 11	5 / 11	7 / 11
Budapest Post [174]	5 / 11	1 / 11	2 / 11
QuickDASH Pre [175]	50%	43%	40%
QuickDASH Post [175]	45%	38%	38%

and after the therapy, providing valuable insights into the progress made by each patient. Figure 2.11 presents a comparative study of these results for the three patients.

The figure showcases the patients' hands equipped with the exoskeleton and the corresponding joint and moment curves. The joint curves for the MCP, PIP, and DIP joints, both before and after the six-week therapy period, are displayed. The motion depicted was generated by the linear motor, with the patient finger passively following the flexion provided by the exoskeleton.

The angular measurements were derived from solving the kinematic system of the exoskeleton using the patient-specific parameters. The force measurements also enables the computation of the corresponding torque curves for the finger joints. These torque curves represent the quasi-static solution of the loading equations [2] and are displayed beneath each of the joint curves. The curves and the shaded areas around them denote the mean and standard deviation over five measured trajectories, respectively.

2.3.3 Discussion

The exoskeleton system, comprising of the exoskeleton itself and the accompanying mobile application, was successfully utilized in the treatment of patients, as discussed in Wilhelm et al. [3]. The user-friendly design and comfort of the exoskeleton make it easier for patients to use intuitively. The system's ability to store individual user profiles and accept patient-specific parameters optimized the measurements and live views for each patient. The control system effectively responded to force limits, as demonstrated in Figure 2.11 for patient 2 (green), where exceeding the force limit of 6 N halted the movement and immediately unloaded the finger.

The implementation of gamification in rehabilitation was found to be highly effective. The system successfully incorporated established concepts from classical physiotherapy and occupational therapy. The engaging and playful nature of the games encouraged patients to push their limits. The therapeutic approach of analog mirror therapy and the therapy concept "Graded Motor Imagery" were effectively translated into a digital visualization and abstraction of the patient real finger onto a virtual model in the video game. The therapy concept "Exposure in Vivo (EXP)", where the patient consciously accepts pain to achieve an improvement in therapy outcome, was also observed. Feedback from patients regarding gamification was consistently positive [3].

The longitudinal study, which tracked the progress of patients over a six-week period, yielded several observations. All three patients showed a positive therapeutic course, as evidenced by the decrease in both QuickDASH and Budapest scores. This improvement is also reflected in the torque curves from Figure 2.11. For patient 2, the trajectory could now be applied with the exoskeleton, as the stiffness of the finger reduced, keeping the external force of the exoskeleton below 6 N during the trajectory. The patient data obtained from the study was compared with measurements from the healthy subject study of Dickmann et al. [2]. The comparison showed significant differences in the torque curves of healthy subjects and patients, with patients consistently showing a higher amplitude in the joint torque curve, primarily due to the higher stiffness of the patients' joints [3].

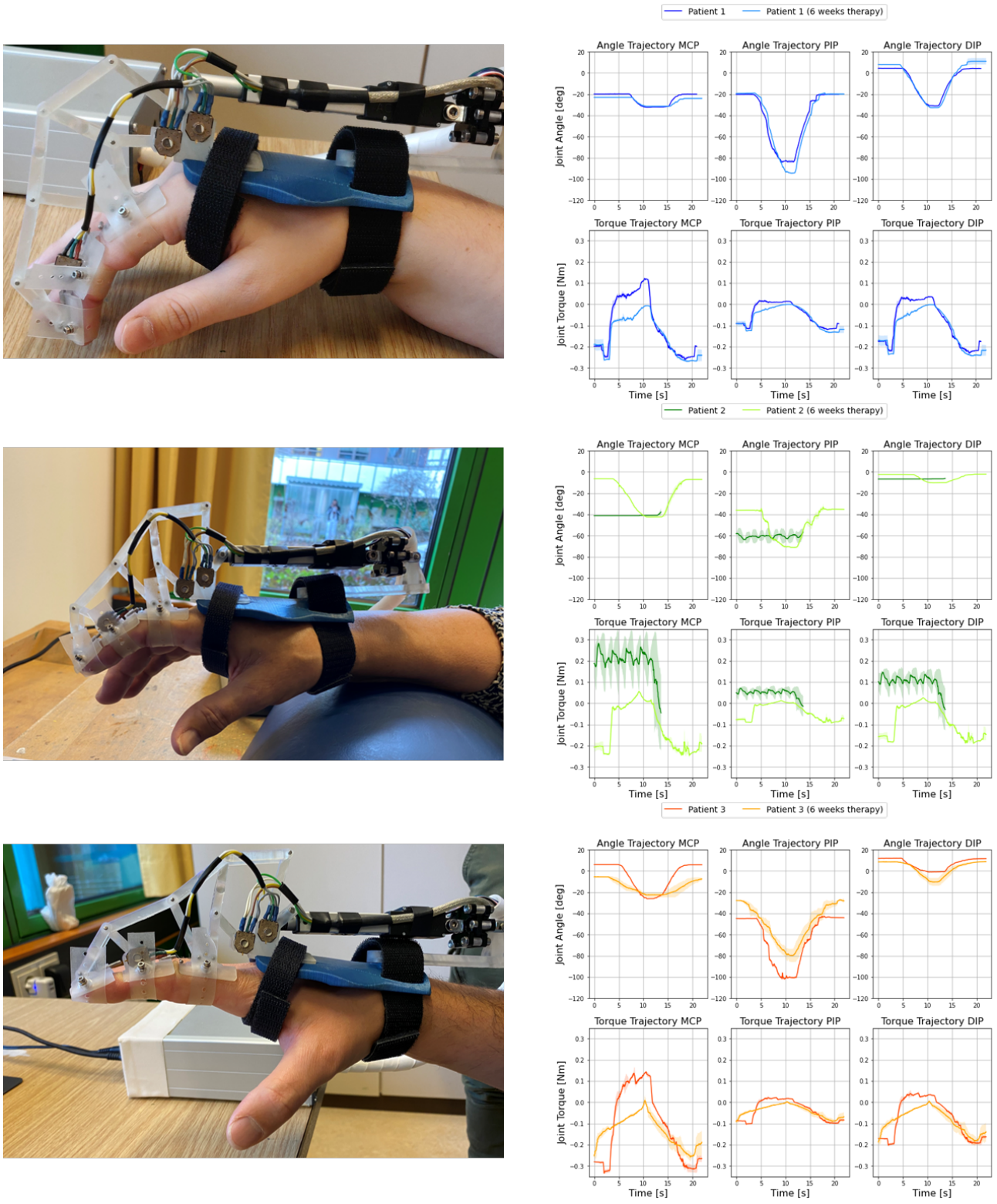

Figure 2.11 Comparative study of the exoskeleton application from Wilhelm et al. [3] presents the results of patient 1 (blue, top), patient 2 (green, middle), and patient 3 (orange, bottom) over a six-week period. The left side displays the patients' hands fitted with the exoskeleton. On the right, the joint curves of MCP, PIP, and DIP joints (top row) and the corresponding torque curves (bottom row) are shown. The displayed measurements represent the mean (line) ± standard deviation (shaded) of five individual measurements. Figure from Wilhelm et al. [3].

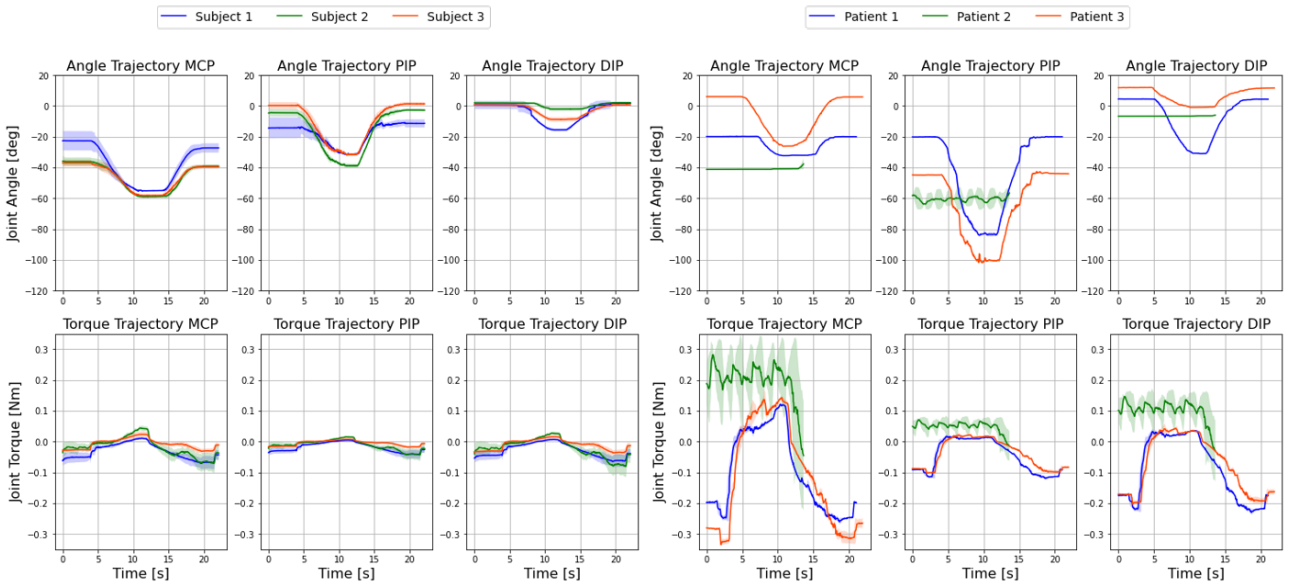

Figure 2.12 Comparison between three healthy subjects from the study by Dickmann et al. [2] (displayed on the left) and three CRPS patients prior to therapy (displayed on the right), as reported in Wilhelm et al. [3]. The top row illustrates the angular trajectories of the MCP, PIP, and DIP joints, while the bottom row presents the corresponding torque trajectories. The depicted measurements represent the mean (line) ± standard deviation (shaded) derived from five individual measurements.

Limitations

The study had several limitations, as discussed in Wilhelm et al. [3]. The small number of patients and the short treatment period with limited follow-up were significant constraints. Additionally, the collateral measurements used to objectify the clinical course of CRPS did not show a correlation with the clinical course due to a large spread of the absolute values. However, the exoskeleton measurements were very reliable and, along with the validated scores (Budapest criteria and DASH score), documented an improvement in function and disease outcome. Therefore, the use of exoskeleton measurements to provide objectifiable data on disease outcome is recommended for further studies.

2.3.4 Conclusion

The successful development and integration of the mobile application, as well as its application to patients, has effectively extended the exoskeleton system originally proposed by Dickmann et al. The incorporation of Bluetooth functionality has enabled the flexible and user-friendly operation of the exoskeleton. A comparative study between the original subject study by Dickmann et al. [2] and the conducted patient study revealed notable differences in the torque curves of patients, attributable to the increased stiffness of their finger joints. The follow-up study demonstrated a positive trend in both QuickDASH and Budapest scores, further supporting the efficacy of the exoskeleton as a valuable tool for rehabilitation and providing objective patient measurements. Future objectives of this project include expanding the exoskeleton to encompass the entire hand and further enhancing the mobile application [13].

3 Diagnostics and Surgical Planning through Artificial Intelligence-based Image Analysis

In this chapter, we address the transformative potential of AI in image analysis for orthopaedic diagnostics and surgical planning. Our discussion focuses on the role of AI in improving the accuracy and efficiency of bone tumor detection, kinematic alignment analysis, and the development of preoperative surgical strategies. This investigation is in line with the broader research question of the benefits and challenges associated with the use of AI for image analysis in orthopaedic diagnostics and surgical planning.

Structured to navigate from data acquisition through to clinical application, this chapter, as depicted in Figure 3.1, begins by addressing the foundational element of AI in healthcare: data. The development of automated planning algorithms necessitates access to comprehensive medical datasets, which are pivotal for training accurate and reliable AI models. Section 3.1 introduces a mobile application specifically designed for the annotation of radiographs, a tool that aids in the accumulation of medically annotated data essential for algorithm development.

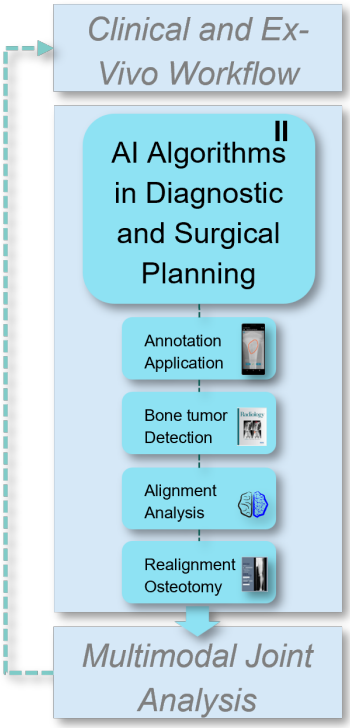

Figure 3.1 Section overview.

With a robust dataset in place, we transition to the heart of AI's application in orthopedics - the development of algorithms for critical diagnostics and planning tasks. Section 3.2 focuses on the vital area of bone tumor detection and classification, illustrating the impact of automation on enhancing diagnostic accuracy. The narrative extends beyond tumor detection to the identification of malpositions critical for orthopedic interventions. In Section 3.3, we present an algorithm designed for automatic kinematic alignment analysis, capable of detecting and quantifying malpositions, thereby facilitating precise surgical interventions and reducing the workload immensely.

Finally, the chapter progresses to discuss the integration of these diagnostic capabilities into automated surgical planning. Section 3.4 evaluates the application of AI in planning corrective osteotomies, showcasing how AI-powered algorithms can bridge the gap between diagnostic imaging and the formulation of tailored surgical strategies. This discussion not only highlights AI's potential to improve patient outcomes through enhanced diagnostic and planning accuracy but also addresses the complexities and challenges inherent in integrating these technologies into clinical practice.

3.1 Data Annotation

The rapid advancement of machine learning and deep learning methodologies has significantly influenced various sectors, including the medical field, where they are used for diagnosis, treatment planning, and patient monitoring [176, 177]. For the effective implementation of deep learning algorithms, accurate annotation and labeling of medical datasets are crucial [178]. However, the annotation process often requires expert knowledge and is labor-intensive, posing a significant challenge [179]. Insufficient dataset quality control can also compromise the performance and generalization of the resulting algorithms [180].

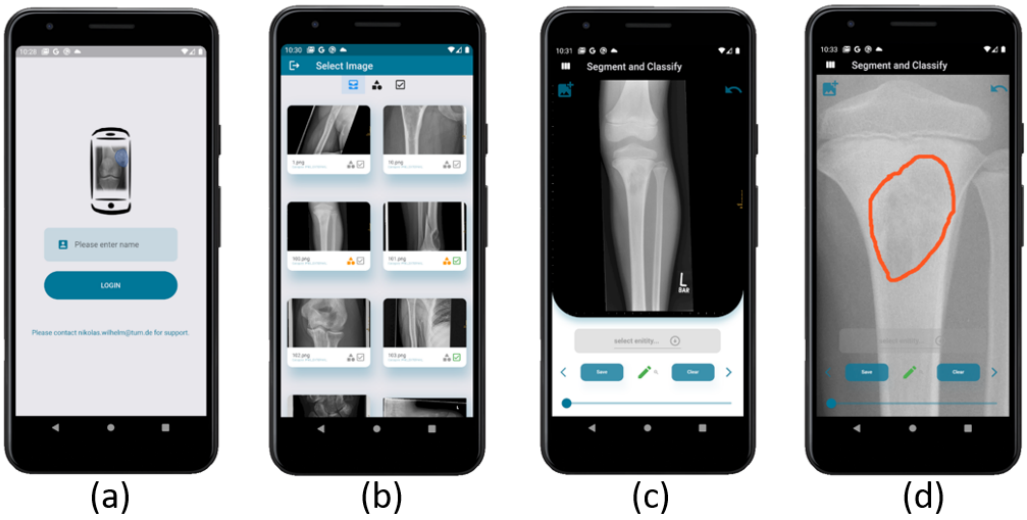

Figure 3.2 Overview of the Mobile Annotation App: Users initiate by logging in (a) and proceed to access specific tasks (b). Images can be annotated either through classification or segmentation (c), with an additional feature for detailed examination of sub-images (d). Best precision in annotation is achieved when using a tablet and pen.

As a result, recent research has emphasized the development of efficient annotation tools to optimize the process and alleviate the demands on medical professionals [181, 182].

3.1.1 Methods

To address these challenges, we introduce a novel pipeline that includes the development of a mobile annotation application and a deep learning pipeline capable of integrating the supplied annotation data for training. The application was developed using the Flutter framework [183], ensuring compatibility with Windows, Mac, iOS, and Android platforms. The application supports a variety of annotation techniques, accommodating user requirements for either classification or segmentation of images and can be seen in Figure 3.2. Moreover, it allows in-depth analysis of subimages to ensure a thorough examination and annotation of complex details within medical images. This functionality contributes to the enhancement of dataset quality and precision.

The primary aim of this application is to facilitate the efficient creation of medical datasets and their associated models. Figure 3.3 depicts the model generation pipeline, demonstrating the stepwise transformation of raw medical data into a functional deep learning model. Upon satisfactory completion of annotation tasks, the modeling process for recognition networks can commence. The dataset obtained from the application, consisting of a .txt file for each annotated image and user, is first converted into the Common Objects in Context (COCO) format [184]. Subsequently, image recognition or classification networks can be trained and validated using the transformed dataset.

3.1.2 Applicability

The effectiveness of this application was underscored in a recent study by Bloier, Hinterwimmer, et al. [185]. In their research, the authors employed this application as a foundational tool for annotating bone tumors in radiographs, thereby leveraging the application to gather expert medical data. Utilizing the annotations obtained through this application, Bloier et al. [185] trained their deep learning algorithms and achieved an Intersection over Union (IoU) of 87.43% on hold-out test data, despite the constraints of a limited dataset.

Despite the user-friendly nature of the application and the corresponding model, the requirement for manual data transfer between the two components via a USB connection is a potential drawback. Additionally, the project currently lacks empirical evidence to validate the advantages of the mobile software. However,

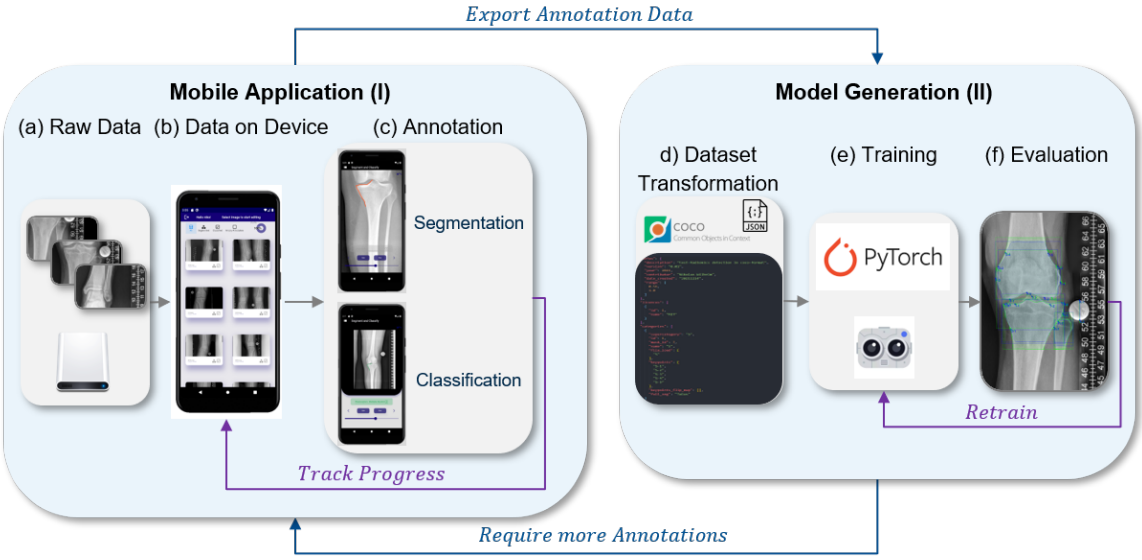

Figure 3.3 Pipeline Overview for Model Generation: (a) Raw data is transmitted to the device (b) for medical expert annotation (c), constituting the medical application component (I). Subsequently, data is exported and processed for model generation (II), involving dataset transformation (d), model training (e), and evaluation (f). Additional annotations may be necessary if evaluation outcomes are inadequate.

with the public release of the application, we anticipate its integration into a variety of projects, which we expect will provide further evidence of its capacity to streamline the annotation process.

3.1.3 Conclusion

In conclusion, this section presents a novel mobile annotation application and deep learning pipeline, aimed at expediting and streamlining the process of generating medical datasets and their corresponding models. The user-friendly interface and intuitive annotation capabilities of the application offer notable advantages over traditional annotation tools, thereby increasing workflow efficiency and annotation quality. Although certain limitations exist, such as the necessity for manual data transfer via USB, the application holds promise for widespread adoption in various research projects.

3.2 Bone Tumor Detection Algorithms

Cancer represents one of humanity's most significant vulnerabilities. In the field of orthopedics, bone tumors are among the most life-threatening conditions. Therefore, early and accurate detection is crucial for improving a patient's survival prospects. A primary motivation of this research is to enhance support in this critical area using AI tools, with the goal to provide an additional layer of security for tumor detection and classification in everyday clinical settings.

The detection and classification of bone tumors have been considerably improved through the use of DL algorithms. In a collaborative effort with the radiology department of Klinikum Rechts der Isar, a novel method for automatic bone tumor detection has been developed. This approach involves training a multitask DL model capable of performing bounding box placement, segmentation, and classification of primary bone tumors in radiographs [4].

The dataset used in the study [4] comprised radiographs of patients with primary bone tumors. The dataset was divided into two distinct sets: an internal set and an external set. The internal set was collected from a single institution and was used for training and validation of the DL model. The external set, collected from multiple institutions, was used to test the generalizability of the model. The internal set consisted of 135 patients with 145 primary bone tumors. The external set included 41 patients with 41 primary bone

tumors. The tumors in both sets were annotated by fellowship-trained musculoskeletal radiologists. The annotations included bounding box placement, segmentation, and classification of the tumors.

3.2.1 Methods

The model, as depicted in Figure 3.4, is based on a Microsoft COCO pretrained mask region–based convolutional neural network (Mask-RCNN-X101). The input of the model is an image with a resolution of 800 x 1200 pixels. The developed multitask model allows for simultaneous bounding box placement, segmentation, and classification of bone tumors on radiographs. Those three tasks represent a different head of the model, each with a different loss function. The loss functions for segmentation are per-pixel sigmoid loss and binary loss. The loss function for boundary box placement is the bounding box regression loss. The loss function for the classification task is the cross-entropy loss. An Adam optimizer with a 0.0025 learning rate at a batch size of two for 5000 epochs is used [4].

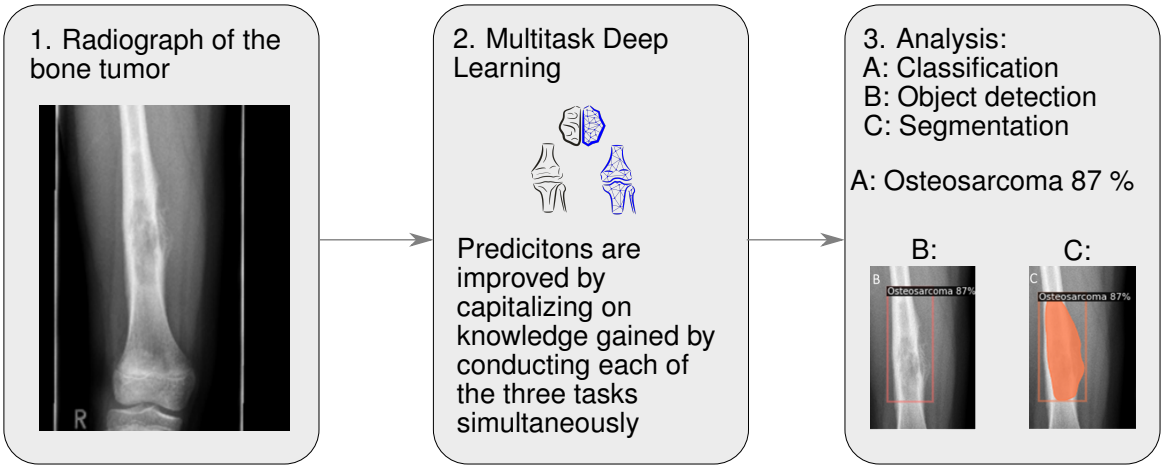

Figure 3.4 Overview of the multitask deep learning model based on a pretrained Mask-RCNN-X101. The model processes 800 x 1200 pixel images (1), simultaneously performing classification (3A), bounding box placement (3B) and segmentation (3C) of bone tumors on radiographs. Each task corresponds to a different head of the model with a unique loss function. The model is optimized using Adam with a 0.0025 learning rate for 5000 epochs [4].

The performance of the model was evaluated on both an internal and external test set and the main results are displayed in Table 3.1 [4]. For object detection, the multitask DL model placed 59.5% of the bounding boxes correctly (IoU > 0.5), demonstrating an IoU of 0.52 ± 0.34. In 82.0% of cases, there was at least some overlap between the bounding box and the tumor (IoU > 0). The segmentations performed by the multitask DL model yielded an average Dice score of 0.60 ± 0.37 on the external test set [4].

Table 3.1 Performance of the DL Model for Identification of Malignant Lesions on the Internal and External Test Sets and for Tumor Entity Classification, Bounding Box Placement, and Segmentation from Sckacky et. al. [4]. Results are displayed with direct numerical values in parentheses, 95% Confidence Intervall (CI)s in square brackets, and standard deviations, where applicable.

Multitask DL Model	Internal Hold-Out Test Set	External Test Set
Accuracy for malignancy	81.4 (114/140) [75.0, 87.8]	80.2 (89/111) [72.8, 87.6]
Sensitivity for malignancy	59.0 (23/39) [44, 77]	62.9 (22/35) [47, 79]
Specificity for malignancy	90.1 (91/101) [84.3, 95.9]	88.2 (67/76) [81, 96]
Linearly weighted Cohen k for malignancy	0.52 [0.44, 0.60]	0.53 [0.43, 0.62]
Accuracy for tumor entity (16 entities)	42.9 (60/140) [34.7, 51.1]	43.2 (48/111) [34.0, 52.4]
Intersection over union (bounding box)	0.54 ± 0.32	0.52 ± 0.34
Dice score (segmentation)	0.63 ± 0.34	0.60 ± 0.37

3.2.2 Conclusion

In conclusion, the developed multitask DL model [4] provides a promising tool for the accurate and simultaneous bounding box placement, segmentation, and classification of primary bone tumors on radiographs. The classification performance of the model surpassed that of radiologic residents and was comparable to that of musculoskeletal fellowship–trained radiologists. This model may improve the diagnostic accuracy and consequently improve the diagnostic workflow in patients with primary bone tumors. The developed model and its application in bone tumor detection have been recognized with the Trainee Research prize at the RSNA and the best abstract award at the DKMSR [186]. The studies have been published in Radiology [4] and European Radiology [5]. The code is publicly available at:
`https://github.com/NikonPic/BonetumorNet` and
`https://github.com/NikonPic/bonetumor-radiomics`.

3.3 Automatic Alignment Analysis for the Lower Limb

In addition to leveraging AI for critical diagnostic tasks such as bone tumor detection, similar models can be employed in other vital areas, such as the labor-intensive analysis of lower extremity malpositions and subsequent surgical planning. The development of these models, aimed at simplifying daily operations for Orthopedic Surgeon (OS), is discussed further below. OA of the lower limbs presents a significant global challenge, where misalignment plays a crucial role in a variety of musculoskeletal disorders, markedly influencing treatment outcomes [146, 187–199]. Accurate diagnosis and effective treatment planning necessitate a thorough preoperative analysis of alignment in the lower extremities, particularly using anterior-posterior (a.p.) Long Leg Radiograph (LLR). However, this complex process is not only time-consuming but also prone to inaccuracies [139, 140, 146–149, 188–192, 199].

Advancements in ML and DL technologies promise to improve the precision, reliability, and speed of these preoperative analyses. Although previous investigations have demonstrated that DL models can predict single alignment parameters with high accuracy, their practical use remains limited to these specific parameters [138–149].

In this context, we introduce a DL framework designed to automate the comprehensive assessment of leg alignment using a.p. LLR images fully. This framework benefits from the collaborative intelligence of master and expert networks to ensure maximum accuracy, offering a superior alternative to single-parameter models without the constraints of existing hardware. Multicenter validation studies have shown that our DL approach reaches a clinical-grade operational standard compared to OS, significantly outperforming manual evaluations in terms of efficiency [145, 4, 200–204].

Such findings highlight the considerable potential of cutting-edge DL models in enhancing the capabilities of orthopedic practitioners, especially for tasks that require high accuracy and reliability in diagnosing and managing lower limb pathologies.

3.3.1 Methods

This study (460/21s), approved by the Institutional Review Board and adhering to institutional privacy policies, retrospectively analyzed patients who underwent radiographic evaluation prior to lower extremity malalignment corrective surgery at University Hospital rechts der Isar in Munich from January 2014 to January 2021. Inclusion criteria comprised conventional preoperative weight-bearing anteroposterior LLRs, while exclusion criteria included unconsolidated fractures, metal implants or hardware overlaying cortical bone contours, and inadequate radiographic quality due to severe malrotation or incomplete visualization of bony structures. The data were partitioned into 60% for training, 10% for validation, and 30% for hold-out testing. An external validation dataset, equivalent in size to the internal dataset, was procured from the University of Freiburg.

Depending on patient height, two or three preoperative weight-bearing anteroposterior radiographs were obtained and merged to produce a full LLR. A ruler and a reference sphere served as length references.

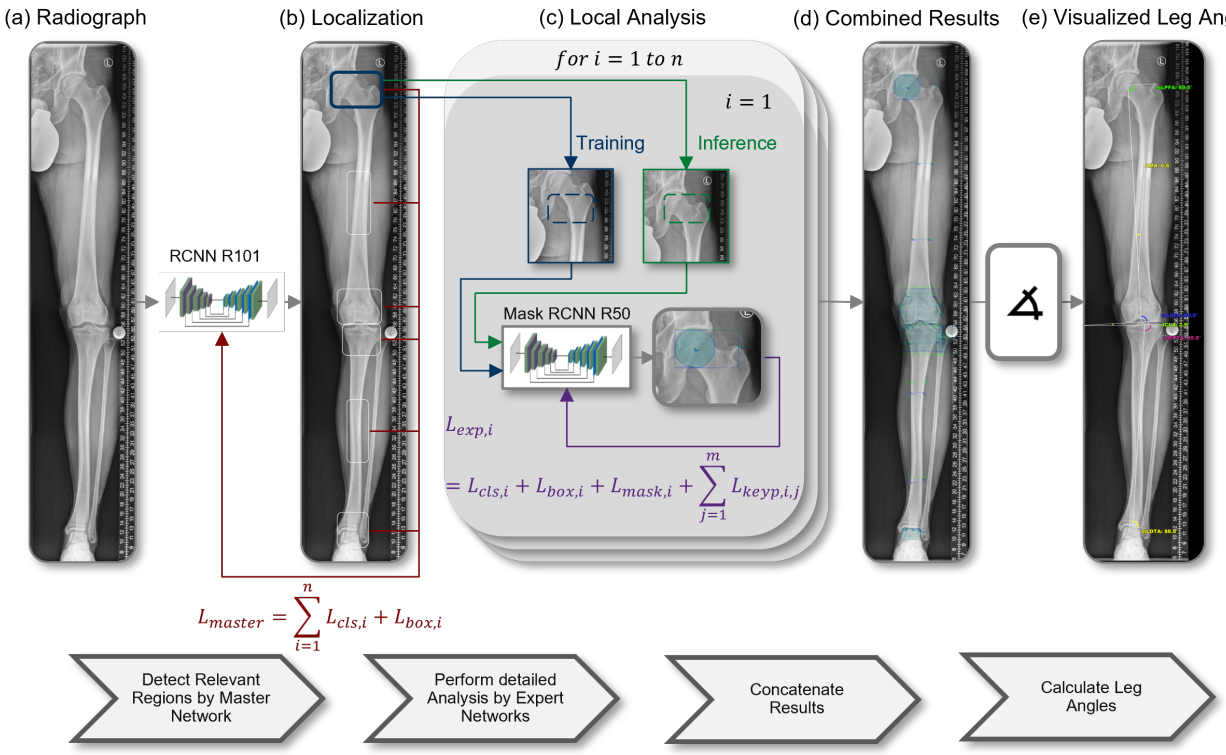

Figure 3.5 Comprehensive lower extremity alignment analysis via deep learning algorithm from Wilhelm et al. [6]: (a) Utilization of standard weight-bearing anteroposterior radiographs for hip, knee, and ankle evaluation.(b) Detection network processes radiographs, downscaled for memory conservation and optimizing $L_{cls,i}$ and $L_{box,i}$ during training, while specialized networks examine detected regions at full resolution. (c) Prior to employing expert networks, the image area optimized for inference aligns the object with the average location in the training dataset. Expert network training is further extended by segmentation ($L_{mask,i}$) and landmark identification ($\sum_{j=1}^{m} L_{keyp,i,j}$). (d) Projection of expert networks' data onto the hip-knee-ankle radiograph. (e) Result: Automated leg alignment assessment on radiographs.

Landmark segmentation and annotation were performed on all LLRs, with an internal validation of the annotation protocol conducted on 50 randomly selected images reviewed by three experienced OS. Labels and segmentations were created by one OS and verified by a second, with disagreements resolved by a third OS. These annotations served as the baseline reference for training.

Deep Learning Techniques for Leg Alignment Analysis

A multi-level approach was adopted for automatic detection and labeling of various landmarks and segmentations in a single image focused on leg anatomy. The architecture partitions the entire leg image anatomically into nine distinct objects, each with segmentation, landmarks, bounding box, and class. An upstream recognition step identifies sub-objects within the entire image, streamlining the task and bypassing hardware constraints. Each image region is then directed to expert networks based on their category, utilizing the original full image resolution. The primary image analysis, comprising landmark placement, bounding boxes, segmentation, and classification, is conducted by the respective expert multitasking network.

To enhance the precision of angle calculations, a process that integrates additional intermediate steps, tailored to the specific anatomy, was introduced. This approach merges information from bounding boxes, segmentation, and landmarks to augment the result's accuracy. To further optimize the accuracy of critical landmarks, specifically those situated on the convex contour of the femoral condyles, a local edge filter was employed, as discussed in more detail in Wilhelm et al. [6].

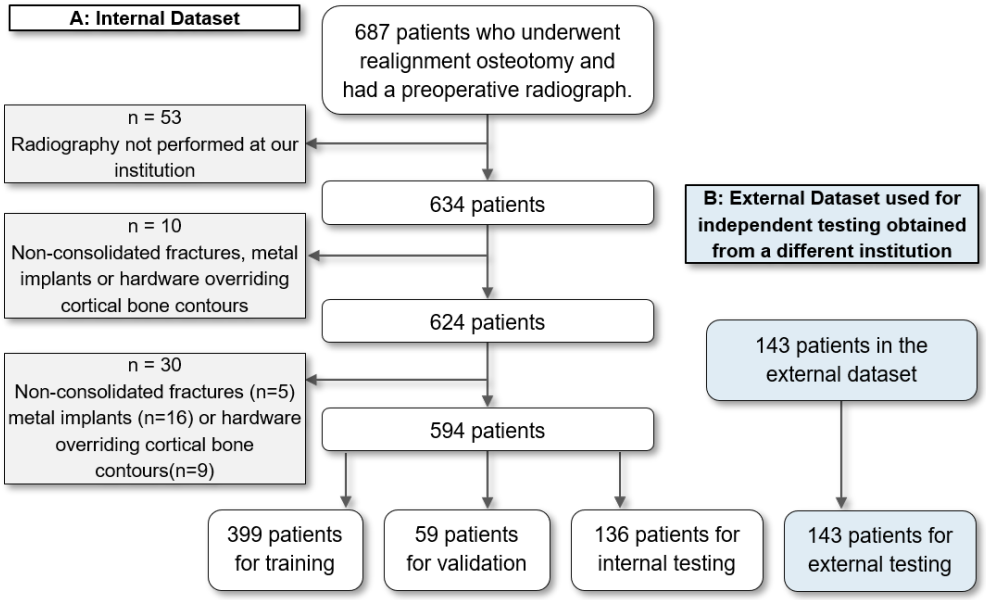

Figure 3.6 Flowchart illustrating the patient population for this study after considering inclusion criteria, exclusion criteria for the internal (A) and external dataset (B) [6].

Ablation Studies and Lower Extremity Alignment Analysis

Various deep learning architectures were assessed on the internal test dataset to optimize the DL model's accuracy. A subsequent ablation study assessed the advantages of anatomical landmark optimization filters. The DL model landmarks were compared with the combination of the DL model with local edge filters for points F-1 and F-2. The final automatic landmark detection algorithm generated numerical output for lower limb alignment, including relevant parameters such as Medial Lateral Patellar Femoral Angle (mLPFA), Medial Lateral Distal Femoral Angle (mLDFA), Joint Line Convergence Angle (JLCA), Medial Proximal Tibial Angle (mMPTA), Medial Lateral Distal Tibial Angle (mLDTA), Ankle Mechanical Axis (AMA), Mechanical Femorotibial Angle (mFTA), Knee Joint Line Obliquity (KJLO), Load on Tibia Plateau (TP), Mechanical Axis Deviation (MAD) and limb length.

The performance of the fully automated alignment analysis was evaluated by comparing the results with reference measurements performed by three different experienced human raters for both the internal and external test data sets. To evaluate inter- and intrarater reliability, segmentation and landmark detection and reference measurement were performed twice at four-week intervals in 30 randomly selected patients.

3.3.2 Results

From 01/2014 to 01/2021, 687 patients were identified from the institutional database who had a preoperative weight-bearing a.p. LLR. After applying inclusion and exclusion criteria, 594 patients (mean age 41.1 ± 13.2 years, 182 females, 388 left leg) were included in the study (Figure 3.6). The patient radiographs were randomly divided into training (n=399, 60%), validation (n=59, 10%), and test (n=136, 30%) datasets.

In the ablation study, the Multi Scale Training Simulation (MS-TrainSim) architecture achieved the highest average landmark accuracy (1.9 mm ± 2.9 mm), outperforming the Single Scale (SC) architecture (20.9 mm ± 73.9 mm) and the Multi Scale (MS) architecture (3.0 mm ± 6.0 mm). Therefore, the MS-TrainSim approach was used for all further analyses.

The DL model demonstrated high accuracy in identifying anatomical structures and landmarks necessary for angle calculation, as shown in Table 3.3. The model detected the reference sphere in all cases (132/132) and performed measurements on the ruler in the remaining cases (4/4). The mean RMSE for each object's landmarks ranged from 0.48 mm ± 1.0 mm (Sphere) to 7.1 mm ± 4.55 mm (Femur Shaft). The Sørensen-

Table 3.2 The Mean Root Mean Square Error (RMSE) of landmark detections for individual objects were compared across SC, MS, and MS-TrainSim approaches on the internal test dataset. The results are presented as mean ± standard deviation (range). Data from Wilhelm et al. [6].

Object [mm]	SC	MS	**MS-TrainSim**
Hip	6.6 ± 24.8	0.6 ± 0.4	**0.6 ± 0.3**
$\text{Femur}_{\text{trochanter}}$	6.9 ± 29.4	1.2 ± 1.5	**0.9 ± 0.5**
$\text{Femur}_{\text{shaft}}$	55.5 ± 105.3	17.5 ± 11.0	**7.1 ± 4.5**
$\text{Femur}_{\text{condyles}}$	6.9 ± 42.4	1.9 ± 2.0	**1.7 ± 1.6**
$\text{Tibia}_{\text{eminence}}$	12.5 ± 61.6	**1.0 ± 1.1**	1.1 ± 1.1
$\text{Tibia}_{\text{joint line}}$	6.9 ± 42.4	**1.3 ± 1.0**	1.3 ± 1.3
$\text{Tibia}_{\text{shaft}}$	95.4 ± 139.5	5.8 ± 4.1	**5.5 ± 3.5**
Ankle	1.1 ± 1.9	1.7 ± 3.5	**0.9 ± 1.7**
Sphere	8.2 ± 49.5	0.5 ± 1.0	**0.4 ± 1.0**
Average	20.9 ± 73.9	3.0 ± 6.0	**1.9 ± 2.9**

Dice coefficient for bounding box placement and segmentation varied between 0.89 ± 0.2 (Ankle) and 0.97 ± 0.01 (Femur Trochanter).

Table 3.3 Table shows RMSE for landmark detection, Dice Score for bounding box placement (Dice BBox) and segmentation (Dice Seg) for each object on the internal test dataset. Data is presented as mean ± standard deviation. Data from Wilhelm et al. [6].

	RMSE [mm]	Dice BBox	Dice Seg
Hip	0.57 ± 0.29	0.97 ± 0.02	0.97 ± 0.02
$\text{Femur}_{\text{trochanter}}$	0.89 ± 0.54	0.97 ± 0.01	0.97 ± 0.01
$\text{Femur}_{\text{shaft}}$	7.1 ± 4.55	0.9 ± 0.06	-
$\text{Femur}_{\text{condyles}}$	1.92 ± 2.67	0.96 ± 0.02	0.97 ± 0.01
$\text{Tibia}_{\text{eminence}}$	1.1 ± 1.12	0.96 ± 0.02	0.95 ± 0.09
$\text{Tibia}_{\text{jointline}}$	1.37 ± 1.36	0.96 ± 0.02	0.96 ± 0.01
$\text{Tibia}_{\text{shaft}}$	5.48 ± 3.49	0.92 ± 0.04	-
Ankle	0.83 ± 1.65	0.93 ± 0.09	0.89 ± 0.2
Sphere	0.48 ± 1.0	0.95 ± 0.15	0.95 ± 0.15

Interreader reliability for the internal and external test datasets is shown in Table 3.4. For both datasets, reliability between OS was good to excellent for angular measurements and excellent for absolute distances. Similarly, reliability between the DL model and ground truth measurements of the OS was moderate to excellent for angular measurements, and excellent for absolute distances.

Clinically acceptable accuracy details are in Table 3.5. In the internal dataset, agreement between OS (OS1, OS2, OS3) and the DL model ranged from 13.6% to 100%. In the external dataset, this agreement ranged from 31% to 100%.

In a comparison of analysis time, human raters took around 100 seconds for full alignment analysis using MediCAD version 6.0. The DL model, using a consumer-grade personal computer, completed the same task in about 22 seconds. This was significantly faster ($p \leq 0.01$) than human raters on both internal and external test datasets, making the DL model over four times faster.

3.3.3 Discussion

This study presents a DL model for leg alignment analysis from anteroposterior long-leg radiographs that exhibits comparable performance to orthopedic specialists in terms of precision, inter-reader reliability, and clinically acceptable accuracy [138, 145, 205, 206]. The model surpasses human raters in intra-rater

Table 3.4 Interreader reliability as quantified by Inter Class Correlation (ICC) values on the internal and external test dataset. Data listed in brackets are 95% CIs. TP, tibial plateau. Data from Wilhelm et al. [6].

Internal				
	OS1-OS2	OS1-OS3	OS2-OS3	AI-$\mathrm{OS}_{\mathrm{mean}}$
Leg length	**0.99 [0.99, 0.99]**	-	-	0.99 [0.97, 0.99]
Load on TP	0.92 [0.89, 0.95]	**1.0 [0.99, 1.0]**	0.99 [0.98, 1.0]	0.98 [0.97, 0.99]
MAD	0.99 [0.8, 1.0]	1.0 [0.95, 1.0]	**1.0 [0.99, 1.0]**	1.0 [0.98, 1.0]
mLPFA	0.98 [0.98, 0.99]	0.95 [0.74, 0.98]	0.95 [0.79, 0.98]	**0.99 [0.99, 0.99]**
AMA	**0.97 [0.95, 0.98]**	0.95 [0.68, 0.98]	0.95 [0.62, 0.99]	0.93 [0.9, 0.95]
mLDFA	**0.99 [0.98, 0.99]**	0.96 [0.93, 0.97]	0.96 [0.94, 0.98]	0.98 [0.97, 0.99]
JLCA	**0.92 [0.87, 0.95]**	0.87 [0.79, 0.92]	0.92 [0.87, 0.95]	0.73 [0.62, 0.81]
mMPTA	**0.99 [0.99, 0.99]**	0.81 [0.7, 0.88]	0.82 [0.71, 0.88]	0.97 [0.96, 0.98]
mFTA	**1.0 [1.0, 1.0]**	1.0 [0.98, 1.0]	1.0 [0.99, 1.0]	**1.0 [1.0, 1.0]**
KJLO	**0.96 [0.94, 0.97]**	-	-	0.95 [0.92, 0.97]
mLDTA	**0.99 [0.99, 0.99]**	0.98 [0.95, 0.99]	0.99 [0.98, 1.0]	0.97 [0.96, 0.98]
External				
	OS1-OS2	OS1-OS3	OS2-OS3	AI-$\mathrm{OS}_{\mathrm{mean}}$
Leg length	**1.0 [1.0, 1.0]**	0.92 [0.87, 0.95]	0.92 [0.86, 0.95]	0.99 [0.97, 0.99]
Load on TP	**1.0 [1.0, 1.0]**	**1.0 [1.0, 1.0]**	**1.0 [1.0, 1.0]**	**1.0 [1.0, 1.0]**
MAD	**1.0 [1.0, 1.0]**	0.99 [0.99, 0.99]	0.99 [0.99, 0.99]	1.0 [0.95, 1.0]
mLPFA	**0.99 [0.99, 0.99]**	0.95 [0.89, 0.97]	0.95 [0.91, 0.97]	0.98 [0.97, 0.98]
AMA	0.97 [0.94, 0.98]	**0.98 [0.97, 0.98]**	0.96 [0.9, 0.98]	0.94 [0.91, 0.96]
mLDFA	0.97 [0.95, 0.98]	**0.98 [0.97, 0.99]**	0.96 [0.95, 0.97]	0.98 [0.97, 0.99]
JLCA	**0.9 [0.87, 0.93]**	0.86 [0.8, 0.9]	0.79 [0.7, 0.85]	0.9 [0.85, 0.93]
mMPTA	**0.99 [0.99, 1.0]**	0.97 [0.95, 0.98]	0.96 [0.94, 0.97]	0.98 [0.98, 0.99]
mFTA	**1.0 [1.0, 1.0]**	**1.0 [1.0, 1.0]**	**1.0 [1.0, 1.0]**	**1.0 [1.0, 1.0]**
KJLO	**0.97 [0.96, 0.98]**	-	-	0.96 [0.95, 0.97]
mLDTA	**0.99 [0.99, 1.0]**	0.97 [0.96, 0.98]	0.97 [0.96, 0.98]	0.97 [0.95, 0.98]

reliability and processing time [207, 208]. Unlike previous solutions that employed single-task features, the proposed model adopts a multi-algorithmic ensemble learning approach, guided by a master network [145, 201–204]. This approach significantly outperforms prior work in landmark detection accuracy and segmentation tasks [138, 145, 209].

The model's reliability metrics are robust; it shows good to excellent interrater reliability on an external test dataset, akin to specialized orthopedic surgeons using FDA-approved digital planning programs [147]. Its deterministic behavior contributes to excellent intra-rater reliability [206]. In terms of clinical accuracy, a significant proportion of the model's measurements fall within the clinically tolerable safety margin, matching or exceeding human assessments [145, 203]. The model offers flexibility in calibration methods based on the availability of reference objects in the radiographs [147, 210, 211]. Despite a slight compromise in the precision of absolute distances, it maintains clinically acceptable performance metrics [206]. With a processing time of 22 ± 1 seconds, the model outperforms specialized orthopedic surgeons by a factor of 4.6 and commercial AI models by a factor of 8.6 [138, 206].

However, the model's performance is susceptible to anatomical abnormalities and suboptimal radiographic quality, necessitating human review in such instances [212]. Upon clinical deployment, the DL model promises substantial benefits in terms of reliability, time-efficiency, and cost-effectiveness for the radiologic and orthopedic workforce.

Table 3.5 Clinically acceptable accuracy according to clinically relevant tolerance margins on the internal and external test dataset. Values represent the percentage of individual cases, in which a clinically acceptable agreement was achieved. Data from Wilhelm et al. [6].

Internal test dataset				
	OS1-OS2	OS1-OS3	OS2-OS3	AI-OS_{mean}
Leg length (tol=5mm)	**56.0**	-	-	32.8
Load on TP (tol=2%)	**94.4**	15.2	14.4	90.4
MAD (tol=2mm)	41.6	20.0	26.4	**87.2**
mLPFA (tol=2°)	93.6	13.6	13.6	**96.0**
AMA (tol=2°)	**99.2**	16.8	16.8	98.4
mLDFA (tol=2°)	**97.6**	55.2	56.8	96.8
JLCA (tol=2°)	82.4	53.6	50.4	**91.2**
mMPTA (tol=2°)	**100.0**	56.8	56.0	96.0
mFTA (tol=2°)	**100.0**	59.2	59.2	**100.0**
KJLO (tol=2°)	**97.6**	-	-	94.4
mLDTA (tol=2°)	**96.8**	15.2	16.8	88.8
External test dataset				
	OS1-OS2	OS1-OS3	OS2-OS3	AI-OS_{mean}
Leg length (tol=5mm)	**68.5**	31.5	30.8	53.9
Load on TP (tol=2%)	**95.1**	72.7	69.9	86.0
MAD (tol=2mm)	**98.6**	73.4	74.1	62.9
mLPFA (tol=2°)	**90.9**	71.3	74.8	88.8
AMA (tol=2°)	**100.0**	95.8	95.8	99.3
mLDFA (tol=2°)	**97.9**	94.4	94.4	97.2
JLCA (tol=2°)	97.9	93.0	92.3	**98.6**
mMPTA (tol=2°)	**100.0**	93.0	93.0	98.6
mFTA (tol=2°)	**100.0**	96.5	95.8	**100.0**
KJLO (tol=2°)	**98.6**	-	-	97.2
mLDTA (tol=2°)	**99.3**	86.7	86.7	89.5

Limitations

The study faces several limitations affecting its outcomes. Variability in human performance and individual differences represent fundamental challenges. The DL model's accuracy heavily depends on the quality of radiographs; any variation can compromise its performance. Excluding radiographs with hardware overlapping cortical bones from the training data narrows the model's applicability, limiting its use in some clinical scenarios.

Furthermore, the model's success relies on the normality of anatomical structures and radiograph quality. Cases with anatomical abnormalities or suboptimal images require human review, impacting the model's reliability [212]. Despite these challenges, the DL model offers substantial potential benefits, including increased reliability, efficiency, and cost-effectiveness, promising significant support for the radiologic and orthopedic workforce.

3.3.4 Conclusion

The developed DL model provides a thorough analysis of leg alignment on a.p. LLR, matching the precision and reliability of OS. It did not fail on any image during validation. Moreover, it significantly outperformed human raters in processing time and consistency of repeated measurements. This demonstrates how ad-

vanced DL models can enhance orthopedic providers' capabilities in managing lower extremity pathologies, particularly in high-volume, precision-critical tasks.

3.4 Automated Preoperative Planning for Realignment Osteotomy

With the help of the presented algorithm for fully automated and comprehensive measurement of the lower limb, an extension was developed that enables fully automated surgery planning.

The methodology for determining the direction of the osteotomy cut is consistent with current best practices for medial opening wedge High Tibia Osteotomy (mow-HTO) and specifically aims to connect the osteotomy entry point to the tip of the fibula, as found in previous studies [213]. This approach is consistent with the results of safe zone studies demonstrating improved stability of a potential hinge fracture when externally supported by the ligamentous structures of the tibiofemoral joint [213]. The simulation of the osteotomy cut provides for 90% of the distance to be traveled to the lateral tibial cortex in order to maintain a safe margin and position the hinge point at the level of the tibiofibular joint [213].

The algorithm is then trained to replicate the correction result of the osteotomy based on the principles outlined by Miniaci, Ballmer, et al. [214]. The degree of preoperative malalignment is determined by the intersection of the load-bearing axis (Mikulicz line) with the tibial joint line. The correction angle at the osteotomy hinge is then calculated based on the deviation between the preoperative and the simulated postoperative center of the ankle joint line at the hinge point. The simulation continues until the osteotomy opening has reached the intended correction, with the gap measurement being derived from the postoperative simulation using a predefined reference object (e.g. a sphere or a ruler).

For determining the osteotomy's target, the DL algorithm incorporates two clinically accepted methods. The "percent-based method" classifies the width of the tibial plateau from 0% (medial tibial cortex) to 100% (lateral tibial cortex) at the Knee Joint Line (KJL), setting the postoperative weight-bearing line to intersect the tibial KJL between 55-65%, adjusted for associated lesions and procedures [215]. Alternatively, the "degree-based method" employs the postoperative mFTA to specify the correction magnitude. The operational flow of the DL model is detailed in Figure 3.7, illustrating the systematic approach to simulating and planning osteotomy corrections. The algorithm analyzes the complete deformity of the selected leg and calculates the size, angle and position of the osteotomy gap, which serves as the basis for the correct repositioning of the leg. The algorithm also takes into account that this osteotomy gap can be performed either in the femur or in the tibia, depending on the deformity. The physician can use the tool fully interactively, so that, for example, the positioning of the Mikulicz line and thus the subsequent orientation of the osteotomy can be changed. This value is fixed at 55% and can be manipulated via a slider [7].

3.4.1 Evaluating Preoperative Planning Accuracy

The validation of preoperative planning accuracy employed the same external dataset as described in Wilhelm et al. [6]. Three OS were tasked with planning the realignment osteotomy and predicting the postoperative alignment parameters for both 55% Mikulicz and 1° valgus planning strategies. These predictions were subsequently compared to those made by the completely autonomous DL model.

The accuracy of preoperative alignment parameters was evaluated against an external test dataset. The mean discrepancies between the DL model and the OS observations varied from 0.2 ± 0.2° (mFTA) to 1.0 ± 1.3° (mLPFA) for angular parameters, and 1.0 ± 1.0 mm (MAD) to 8.4 ± 10.5 mm (leg length) for distance measurements. Comparatively, discrepancies between OS measurements ranged from 0.1 ± 0.1° (mFTA, OS1-OS2) to 1.1 ± 1.4° (mLPFA, OS2-OS3) for angular parameters, and 0.6 ± 0.9 mm (MAD, OS1-OS2) to 12.6 ± 21.1 mm (leg length, OS2-OS3) for distance measurements, as documented in Table 3.6.

For osteotomy parameters, mean differences in gap width varied from 0.5 ± 0.7 mm (OS1-OS3) to 0.5 ± 0.9 mm (OS1-OS2) among OS, with a difference of 0.53 ± 0.63 mm between the DL model and OS in percent-based planning. Degree-based planning showed discrepancies ranging from 0.4 ± 0.6 mm (OS2-OS3) to 0.5 ± 0.8 mm (OS1-OS2) among OS, and a 0.4 ± 0.5 mm difference between the DL model and OS. Hinge angle discrepancies in percent-based planning ranged from 0.2 ± 0.4° (OS1-OS3) to 0.3 ±

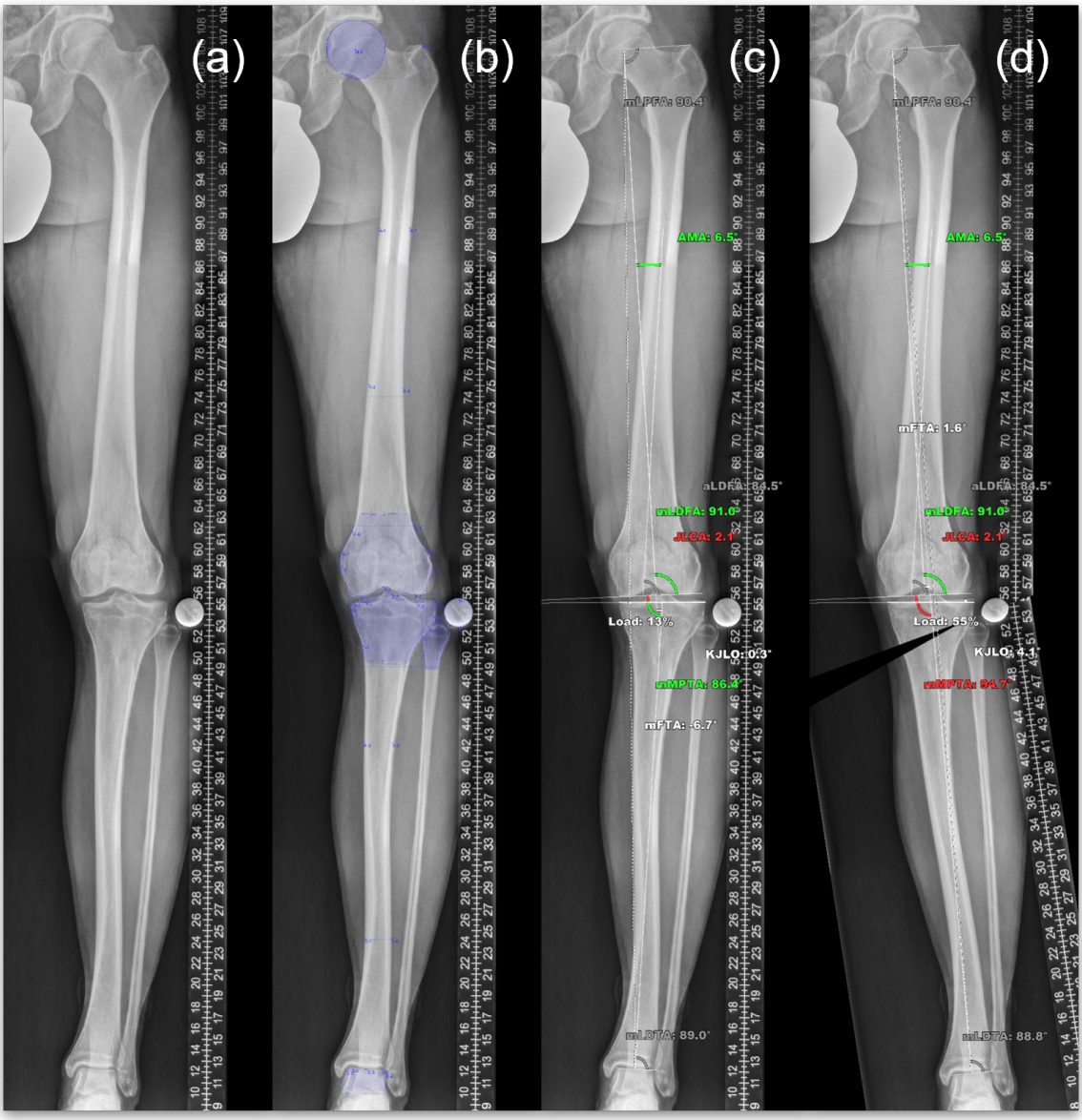

Figure 3.7 Example of preoperative-planning for realignment osteotomy using the deep learning algorithm: (a) The analysis is performed on a standard weight-bearing anterior-posterior radiograph of the hip, knee, and ankle, which is loaded into the program. (b) The AI algorithm analyzes the image and performs keypoint analysis and segmentations. (c) The comprehensive alignment is performed based on the network annotations. (d) The realignment surgery is planned based on the detailed analysis and the expected postoperative alignment is visualized (in this case 55% Mikulicz planning) [7].

0.8° (OS1-OS2) among OS, and 0.3 ± 0.7° between the DL model and OS. Degree-based planning showed differences from 0.2 ± 0.4° (OS2-OS3) to 0.3 ± 0.6° (OS1-OS2) among OS, and a 0.4 ± 0.5° discrepancy between the DL system and OS.

In evaluating the accuracy of simulated postoperative alignment parameters, mean differences between the DL system and OS ranged from 0.0 ± 0.0° (mFTA) to 1.0 ± 1.5° (mLDTA) for angular parameters, and from 0.2 ± 0.2 mm (MAD) to 7.7 ± 10.1 mm (leg length) for distance measurements. Mean differences among OS ranged from 0.0 ± 0.0° (mFTA, OS1-OS2) to 0.8 ± 1.6° (mLDTA, OS1-OS2) for angular parameters, and from 0.13 ± 0.17 mm (MAD, OS1-OS2) to 7.3 ± 14.6 mm (leg length, OS1-OS2) for distance measurements; see Table 3.6.

Table 3.6 Accuracy as quantified by the mean difference of the respective alignment parameters on external test dataset for 55% Mikulicz planning and 1 ° valgus planning. The highest accuracy for each parameter is highlighted in **bold**. Continuous variables are presented as mean ± standard deviation [7].

55% Mikulicz Planning				
	OS1-OS2	OS1-OS3	OS2-OS3	AI-OS_{mean}
Leg length [mm]	6.73 ± 13.38	**3.92 ± 8.3**	4.05 ± 11.44	6.8 ± 8.58
Load on TP [%]	**0.14 ± 0.19**	0.22 ± 0.45	0.15 ± 0.32	0.14 ± 0.33
MAD [°]	0.54 ± 0.49	0.46 ± 0.45	**0.35 ± 0.29**	1.13 ± 0.57
mMPTA [°]	0.38 ± 0.72	**0.32 ± 0.56**	0.39 ± 0.97	0.63 ± 0.66
mFTA [°]	0.12 ± 0.11	0.11 ± 0.11	**0.09 ± 0.07**	0.25 ± 0.14
KJLO [°]	**0.41 ± 0.72**	0.59 ± 1.27	0.48 ± 1.03	0.71 ± 0.92
mLDTA [°]	0.76 ± 1.55	0.52 ± 0.88	**0.49 ± 0.91**	1.0 ± 1.46
Correction angle [°]	0.34 ± 0.83	**0.24 ± 0.4**	0.27 ± 0.68	0.34 ± 0.68
Correction [mm]	0.5 ± 0.88	**0.46 ± 0.65**	0.49 ± 1.15	0.53 ± 0.63
1 ° Valgus Planning				
	OS1-OS2	OS1-OS3	OS2-OS3	AI-OS_{mean}
Leg length [mm]	7.31 ± 14.58	**4.13 ± 8.61**	4.98 ± 13.22	7.67 ± 10.13
Load on TP [%]	0.59 ± 0.44	0.53 ± 0.43	**0.41 ± 0.36**	1.19 ± 0.63
MAD [mm]	0.13 ± 0.17	0.15 ± 0.26	**0.1 ± 0.13**	0.19 ± 0.21
mMPTA [°]	0.41 ± 0.62	**0.36 ± 0.45**	0.41 ± 0.67	0.72 ± 0.62
mFTA [°]	**0.01 ± 0.04**	0.03 ± 0.07	0.01 ± 0.04	0.02 ± 0.04
KJLO [°]	**0.43 ± 0.78**	0.43 ± 0.86	0.46 ± 1.06	0.65 ± 0.72
mLDTA [°]	0.81 ± 1.59	**0.59 ± 0.98**	0.62 ± 1.15	1.05 ± 1.52
Correction angle [°]	0.34 ± 0.59	0.24 ± 0.44	**0.22 ± 0.37**	0.37 ± 0.48
Correction [mm]	0.52 ± 0.75	0.48 ± 0.55	**0.43 ± 0.55**	0.44 ± 0.53

3.4.2 Reliability of Preoperative Planning

Evaluating the reliability of the preoperopative measurements, for the OS, interreader reliability ranged from 0.84 (JLCA, OS2-OS3) to 1.0 for angles and from 0.9 (leg length) to 1.0 for distances. Interreader reliability between the average OS measurements and the DL system ranged from 0.6 (KJLO) to 1.0 for angles and from 0.98 (leg length) to 1.0 for distances (see Table 3.7). For osteotomy gap specific parameters, the interrater reliability for the measurement of the osteotomy gap width between the OS was from 0.9 (OS1-OS3) to 1.0. For the hinge angle interrater reliability between the OS was from 0.9 (OS1-OS3) to 1.0. Interrater reliabity between the DL system and the OS was 1.0 for both planning methods for the width of the osteotomy gap and for the correction angle. In the assessment of the interrater reliability of the postoperative measurements, interreader reliability, for the OS, ranged from 0.6 (mFTA, OS1-OS2) to 1.0 for angles and from 0.5 (MAD, OS1-OS2) to 1.0 for distances. Between the DL system and the average OS measurements interrater reliability was from 0.6 (mFTA) to 1.0 (mMPTA) for angles and 0.7 (MAD) to 1.0 (leg length) for distances. Details are provided in Table 3.7.

During validation on internal and external test data sets, the DL system developed demonstrated accuracy and reliability on a level of expert human raters in fully automated planning of mow-HTOs on a.p. LLR. Furthermore, it outperformed OS in terms of repeated measurement reliability and allowed for significant and substantial time savings in osteotomy planning. DL models such as this demonstrate the potential of AI to assist the orthopedic surgeons by accelerating osteotomy planning in clinical practice.

Table 3.7 Interreader reliability as quantified by ICC values for 55% Mikulicz and 1° varus planning on the external test dataset. Data listed in brackets are 95% CIs [7] (in preparation).

55% Mikulicz Planning				
	OS1-OS2	OS1-OS3	OS2-OS3	AI-OS_{mean}
Leg length	0.96 [0.94, 0.97]	0.94 [0.91, 0.96]	0.98 [0.97, 0.99]	**0.99 [0.98, 0.99]**
Load on TP	-0.04 [-0.58, 0.31]	-0.08 [-0.62, 0.28]	**0.08 [-0.37, 0.39]**	0.02 [-0.45, 0.33]
MAD	0.56 [0.3, 0.72]	0.73 [0.59, 0.82]	**0.79 [0.66, 0.87]**	0.66 [-0.2, 0.89]
mMPTA	0.94 [0.91, 0.96]	0.84 [0.76, 0.89]	0.89 [0.83, 0.92]	**0.95 [0.93, 0.97]**
mFTA	0.56 [0.23, 0.74]	0.68 [0.49, 0.79]	**0.76 [0.62, 0.85]**	0.63 [-0.22, 0.87]
KJLO	0.8 [0.7, 0.87]	0.86 [0.79, 0.91]	0.73 [0.59, 0.82]	**0.9 [0.84, 0.94]**
mLDTA	0.88 [0.82, 0.92]	0.88 [0.82, 0.92]	**0.98 [0.97, 0.99]**	0.94 [0.91, 0.96]
Correction angle	0.97 [0.95, 0.98]	0.93 [0.89, 0.95]	**0.99 [0.99, 0.99]**	0.99 [0.98, 0.99]
Correction	0.96 [0.94, 0.97]	0.9 [0.85, 0.93]	0.93 [0.89, 0.95]	**0.99 [0.98, 0.99]**
1° Valgus Planning				
	OS1-OS2	OS1-OS3	OS2-OS3	AI-OS_{mean}
Leg length	0.96 [0.93, 0.97]	0.93 [0.89, 0.95]	0.97 [0.96, 0.98]	**0.99 [0.98, 0.99]**
Load on TP	0.6 [0.17, 0.78]	0.69 [0.53, 0.8]	**0.76 [0.59, 0.85]**	0.58 [-0.22, 0.84]
MAD	0.46 [0.19, 0.65]	**0.79 [0.68, 0.86]**	0.55 [0.32, 0.7]	0.76 [0.51, 0.86]
mMPTA	0.93 [0.9, 0.95]	0.89 [0.83, 0.92]	0.93 [0.9, 0.95]	**0.95 [0.91, 0.97]**
mFTA	-0.0 [-0.52, 0.34]	0.0 [-0.5, 0.33]	**0.09 [-0.37, 0.39]**	0.05 [-0.41, 0.35]
KJLO	0.82 [0.73, 0.88]	0.74 [0.61, 0.82]	0.72 [0.58, 0.81]	**0.91 [0.84, 0.94]**
mLDTA	0.88 [0.81, 0.92]	0.86 [0.8, 0.91]	**0.95 [0.93, 0.97]**	0.93 [0.9, 0.95]
Correction angle	0.96 [0.94, 0.97]	0.97 [0.95, 0.98]	**0.99 [0.98, 0.99]**	0.99 [0.98, 0.99]
Correction	0.95 [0.91, 0.97]	0.95 [0.92, 0.96]	0.97 [0.96, 0.98]	**0.99 [0.98, 0.99]**

4 Reproducible Joint Analysis through Robotic Benchmarking Systems

This chapter examines the integration of robotics into the field of orthopaedics, focusing on how these technological advances enable detailed and comprehensive analysis of human joints, with a particular focus on the complexities of the knee and hand. This investigation aligns with the broader research question of how the benefits of robotics can be utilized for in-depth joint analysis.

Figure 4.1 provides the framework for the analysis and introduces robotic test benches as key tools to achieve this goal. Several key challenges and objectives are addressed in this chapter, including the accurate measurement of biomechanical variables such as forces, moments, positions and orientations during testing. It also addresses the variability between different joints, which is a major challenge for orthopedic analysis.

A foundational aspect of orthopedic research involves analyzing the complex interplay between applied biomechanical forces and the resulting joint movements. To this end, the chapter explains the specialized test setups and control mechanisms designed to navigate these dynamics. Section 4.1 presents an advanced control algorithm designed to improve the study of biomechanical systems, such as the human knee joint, which may initially appear undefined or insufficiently characterized. The null space is innovatively employed by this algorithm to strike a balance between force and position control, optimizing the accuracy of analyses.

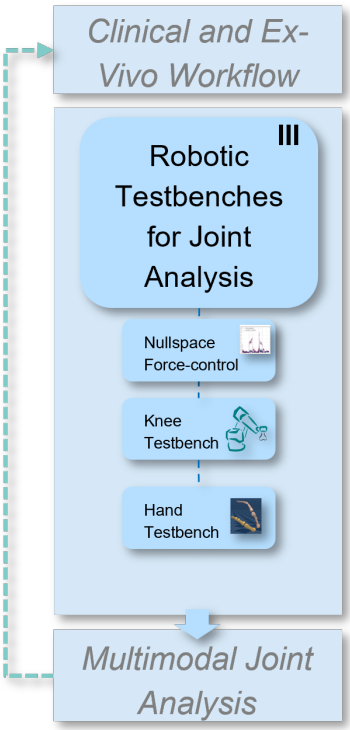

Figure 4.1 Section overview.

The specifics of the robotic test benches designed for the knee and hand joints are addressed in the subsequent sections. A detailed exploration of the knee joint testbench, outlining the methodologies and technological solutions employed to uncover new biomechanical insights, is offered in Section 4.2. Similarly, section 4.3 presents the hand joint test bench, which deals with the special challenges of hand biomechanics.

4.1 Constraint-Tolerant Control for Biomechanical Systems

The focus of this section is on the introduction of novel compliance control architectures that leverage null space solutions for the decoupling of force and position control [8]. Unlike traditional control schemes such as hybrid or impedance control, the proposed architectures offer superior performance in interacting with uncertain surfaces and materials.

The unique aspect of these architectures lies in their ability to treat 6-DOF manipulators as redundant systems. This is achieved by creating a virtual redundancy within a reduced workspace. The advantage of this approach is twofold: it allows for an orthogonal separation of Cartesian degrees of freedom and eliminates the occurrence of inner singularities.

To validate the effectiveness of these control architectures, experiments were conducted using a standard industrial robot (Stäubli, RX90B, 6 DOF). The robot was used to actuate two different biomechanically

inspired models of the human knee joint. The following sections deal with the details of the control algorithm, its implementation and performance evaluation.

4.1.1 Introduction to Advanced Control Algorithms

The industrial application of robots for tactile tasks has led to extensive research in the area of robot-object interaction [216, 217]. While significant advancements have been made, challenges in accuracy, stability, and robustness persist. These control challenges are amplified when robots interact with uncertain or nonlinear environments.

Existing control strategies generally fall into two categories: Hybrid Position and Force Control methods [103], and Impedance Control methods [218]. Both approaches have limitations. For instance, Impedance Control methods suffer from non-deterministic position accuracy and force precision, and their stability is constrained by achievable impedances [101, 102]. Hybrid methods, although offering fewer parameters, are limited by their vulnerability to inner singularities [219]. Schindlbeck and Haddadin [217] introduced a unified control framework that leverages task-energy tanks to enhance passivity and stability in both rigid and flexible joint robots. This approach addresses the limitations of traditional impedance and hybrid control methods, offering improved force tracking and compliant behavior.

A different strategy to address these limitations, some researchers have studied the use of null space solutions to decouple force and position control [220–222]. However, these methods still inherit the drawbacks of Impedance Control. A more recent framework by Schuetz et al. [104] showed promise but was not designed for persistent contact situations.

In this section, we introduce two advanced control algorithms for position controlled robots with force-torque sensing that build upon the framework of Schuetz et al. [104]. These algorithms are designed for explicit force control and offer a more flexible and efficient solution by leveraging null space separation [104, 223]. The algorithms were developed to address the unmet needs in the control of biomechanical systems, such as the human knee joint, and are an extension of the work presented in [8].

4.1.2 Related Work for Null Space Control

Hybrid Position/Force Control: A Mathematical Formulation

The hybrid position/force control architecture was initially proposed by Raibert et al. [103]. This control paradigm employs selector matrices $\boldsymbol{S}_x$ and $\boldsymbol{S}_f$ to partition the Cartesian task space into position-regulated ($\boldsymbol{\delta x}$) and force-regulated ($\boldsymbol{\delta f}$) DOF [103]. The control loops for these error vectors operate in parallel and are mapped into the joint space. The resultant control torque $\boldsymbol{\tau}_c$ is given by:

$$\boldsymbol{\tau}_c = \boldsymbol{g}_x \left(\boldsymbol{S}_x \boldsymbol{J}\right)^{-1} \boldsymbol{\delta x} + \boldsymbol{g}_f \left(\boldsymbol{S}_f \boldsymbol{J}\right)^T \boldsymbol{\delta f} \tag{4.1}$$

where $\boldsymbol{J}$ is the Jacobian matrix, and $\boldsymbol{g}_x$ and $\boldsymbol{g}_f$ are linear control functions for position and force, respectively. The mappings $\left(\boldsymbol{S}_x \boldsymbol{J}\right)^{-1}$ and $\left(\boldsymbol{S}_f \boldsymbol{J}\right)^T$ project the position and force errors into the joint space.

However, this control scheme has been criticized for its instability, particularly outside inner singularities [224, 225]. Fisher et al. [221] attributed part of this instability to the non-ideal separation of force and position DOFs, leading to cross-coupling. To mitigate this, Fisher et al. proposed using reduced Jacobians for the projections, formulated as:

$$\left(\boldsymbol{S}_x \boldsymbol{J}\right)^{\#} = \left(\boldsymbol{S}_x \boldsymbol{J}\right)^T \left(\boldsymbol{S}_x \boldsymbol{J} \boldsymbol{J}^T \boldsymbol{S}_x^T\right)^{-1}, \tag{4.2}$$

and subsequently revised the control torque equation as:

$$\boldsymbol{\tau}_c = \boldsymbol{g}_x (\boldsymbol{S}_x \boldsymbol{J})^{\#} \boldsymbol{\delta x} + \boldsymbol{g}_f \left(\left(\boldsymbol{S}_f \boldsymbol{J}\right)^T \boldsymbol{\delta f}\right). \tag{4.3}$$

Despite these improvements, residual force differences can still induce Cartesian velocities that interfere with position-controlled DOFs. Null space projections have been suggested as a potential solution to minimize these effects [8].

Null Space Control in Redundant Robots

Concurrent with the evolution of Hybrid Position/Force Control, kinematic solutions for redundant robots, characterized by $n > m$ where n and m are the number of joints and task DOFs respectively, have been developed. These solutions exploit the null space matrix $\boldsymbol{N}$, defined as:

$$\boldsymbol{N} = \boldsymbol{I} - \boldsymbol{J}^{\#}\boldsymbol{J}. \tag{4.4}$$

where $\boldsymbol{I}$ is the identity matrix, and $\boldsymbol{J}^{\#}$ is the identity-weighted pseudo-inverse of the Jacobian $\boldsymbol{J}$ [220, 226]. This matrix facilitates the orthogonal projection of the Jacobian and enables the minimization of any cost function $\boldsymbol{H}(\boldsymbol{q})$ in the null space through its gradient $\frac{\partial \boldsymbol{H}(q)}{\partial \boldsymbol{q}}$. The control joint velocity $\dot{\boldsymbol{q}}_c$ is thus formulated as:

$$\dot{\boldsymbol{q}}_c = \boldsymbol{J}^{\#}\dot{\boldsymbol{x}}_t - \alpha \boldsymbol{N}\left(\frac{\partial \boldsymbol{H}}{\partial \boldsymbol{q}}\right)^T, \tag{4.5}$$

where α is the stepsize, and $\dot{\boldsymbol{x}}_t$ is the task space velocity [226].

Various control architectures have been proposed based on this framework. For instance, Nemec et al. [227] introduced a hybrid impedance control for a 4-DOF arm robot that utilizes null space to absorb impacts while maintaining end-effector position and force. Sadeghian et al. [228] and Park et al. [229] employed similar strategies for lightweight arm robots and multi-contact scenarios, respectively. Platt et al. [230] presented a multi-priority impedance control that integrates Cartesian and joint impedance via null space. Recent advancements include surgical applications that leverage null space for patient safety [223].

However, no existing approach effectively decouples force and position targets at the end-effector via null space modulation at the velocity level. To address this gap, the Tactile Motion Control framework by Schuetz et al. [104] is adapted [8].

Tactile Motion Control for Redundant Manipulators

In order to enhance stability and performance, especially in applications involving biomechanical specimens with unpredictable behavior and responses, it is crucial to develop a controller capable of performing both position and force-controlled tasks in a completely decoupled manner. This necessity arises because relying solely on position or force control independently is often insufficient in such scenarios.

Building upon the foundational work of Walker et al. [219], Gertz et al. [231], and Chung et al. [232], Schuetz et al. [104] extended the null space control equation (4.5) by incorporating additional velocity inputs in task, joint, and null spaces, denoted as $\dot{\boldsymbol{u}}_t \in \mathbb{R}^m$, $\dot{\boldsymbol{u}}_j \in \mathbb{R}^n$, and $\dot{\boldsymbol{u}}_n \in \mathbb{R}^n$, respectively. This extension allows for the execution of supplementary tasks at different control levels:

$$\dot{\boldsymbol{q}}_c = \boldsymbol{J}^{\#}(\dot{\boldsymbol{x}}_t - \dot{\boldsymbol{u}}_t) - \dot{\boldsymbol{u}}_j - \boldsymbol{N}\left(\dot{\boldsymbol{u}}_n + \alpha\left(\frac{\partial \boldsymbol{H}}{\partial \boldsymbol{q}}\right)^T\right). \tag{4.6}$$

For the scope of this paper, which aims at task separation via null space, we focus on the null space velocity extension $\dot{\boldsymbol{u}}_n$:

$$\dot{\boldsymbol{q}}_c = \boldsymbol{J}^{\#}\dot{\boldsymbol{x}}_t - \boldsymbol{N}\dot{\boldsymbol{u}}_n. \tag{4.7}$$

Schuetz et al. [104] reduced the 3D contact phenomena to a 1D equation, employing the translatory Jacobian $\boldsymbol{J}_p \in \mathbb{R}^{3\times n}$ at the impact point and the normalized force vector $\boldsymbol{n}_f \in \mathbb{R}^{3\times 1}$. The contact space velocity $\dot{x}_p$ is then formulated as:

$$\begin{aligned} \dot{x}_p &= \boldsymbol{n}_f^T \boldsymbol{J}_p \dot{\boldsymbol{q}}_c \\ &= \boldsymbol{n}_f^T \boldsymbol{J}_p \boldsymbol{J}^{\#}\dot{\boldsymbol{x}}_t - \boldsymbol{n}_f^T \boldsymbol{J}_p \boldsymbol{N}\dot{\boldsymbol{u}}_n. \end{aligned} \tag{4.8}$$

The force-driven velocity at the point of contact, $\dot{x}_f$, is projected onto $\dot{\boldsymbol{u}}_n$ as:

$$\dot{\boldsymbol{u}}_n = \boldsymbol{J}_p^T \boldsymbol{n}_f \dot{x}_f. \tag{4.9}$$

Combining Equations (4.8) and (4.9), and introducing kinematic variable k_n and scalar velocity $\dot{x}_{pt}$, the contact relation in Cartesian space is obtained:

$$\dot{x}_p = \underbrace{\boldsymbol{n}_f^T \boldsymbol{J}_p \boldsymbol{J}^{\#} \dot{\boldsymbol{x}}_t}_{\dot{x}_{pt}} - \underbrace{\boldsymbol{n}_f^T \boldsymbol{J}_p \boldsymbol{N} \boldsymbol{J}_p^T \boldsymbol{n}_f}_{k_n} \dot{x}_f. \tag{4.10}$$

Applying a linear elastic material law, the contact force rate $\dot{f}_p$ is related to $\dot{x}_p$:

$$\dot{f}_p = -c\dot{x}_{pt} + ck_n\dot{x}_f. \tag{4.11}$$

The final control law for the null space force controller is then given by:

$$\dot{\boldsymbol{u}}_n = \frac{\boldsymbol{J}_p^T \boldsymbol{n}_f}{ck_n} \left(c\dot{x}_{pt} - \frac{2d}{T} f_p - \frac{1}{T^2} \int f_p \mathrm{d}t \right). \tag{4.12}$$

This method enables a 9-DOF manipulator to mitigate collision forces but is not optimized for sustained contact control or multi-directional force application [104, 8, 233].

4.1.3 Null Space Divided Compliant Control

The proposed controller aims to integrate the principles of hybrid motion and tactile motion control to achieve advanced compliant control capabilities. Specifically, the control law proposed by Schuetz et al. [104] for palpating undefined surfaces while modulating normal forces is extended. The architecture is further adapted to manage force control along multiple directions independently. An additional layer of complexity is introduced by dynamically prioritizing between position and force control within the null space.

Contact Control on an Undefined Surface

For sustained contact control with desired dynamics, the scalar force error δf is defined as the difference between the desired force f_d and the actual force f_a at the tool center point:

$$\delta f = f_d - f_a. \tag{4.13}$$

To account for persistent contact, the actual force rate $\dot{f}_a$ is given by:

$$\dot{f}_a = \dot{f}_d + \frac{2d}{T}\delta f + \frac{1}{T^2} \int \delta f \mathrm{d}t. \tag{4.14}$$

Here, $\dot{f}_p$ is equated to $\dot{f}_a$ as the contact point coincides with the tool center point, and the Jacobians at both points are identical. The position loop in the main task governs the motion around the surface, utilizing the position-selected Jacobian $\boldsymbol{J}_x$:

$$\boldsymbol{J}_x = \boldsymbol{S}_x \boldsymbol{J}. \tag{4.15}$$

Substituting the null space matrix of this reduced Jacobian $\boldsymbol{N}_x$, the joint velocity with modified projections is:

$$\dot{\boldsymbol{q}}_c = \boldsymbol{J}_x^{\#} \dot{\boldsymbol{x}}_t - \boldsymbol{N}_x \dot{\boldsymbol{u}}_n. \tag{4.16}$$

The null space velocity input $\dot{\boldsymbol{u}}_n$ is adapted to reflect the dynamics from Equation (4.14):

$$\dot{\boldsymbol{u}}_n = \frac{\boldsymbol{J}_p^T \boldsymbol{n}_f}{ck_n} \left(c\dot{x}_{pt} + \dot{f}_d + \frac{2d}{T}\delta f + \frac{1}{T^2} \int \delta f \mathrm{d}t \right). \tag{4.17}$$

This control law is parameterized by three scalar variables: time constant T, dimensionless damping d, and stiffness c. It is applicable for tasks requiring modulated contact normal force, such as painting a planar logo on a curved surface [8].

Multi-Directional Force Control

The initial framework focused on translational motions with force modulation along a single reference direction. We extend this to Cartesian space to enable force regulation along multiple orthogonal axes. The normal force vector $\boldsymbol{n_f}$ is decomposed into its Cartesian components n_{f_x}, n_{f_y}, and n_{f_z}:

$$\begin{aligned}\boldsymbol{n_f} &= \begin{pmatrix} n_{f_x} \\ 0 \\ 0 \end{pmatrix} + \begin{pmatrix} 0 \\ n_{f_y} \\ 0 \end{pmatrix} + \begin{pmatrix} 0 \\ 0 \\ n_{f_z} \end{pmatrix} \\ &= \boldsymbol{n}_{f_x} + \boldsymbol{n}_{f_y} + \boldsymbol{n}_{f_z}.\end{aligned} \tag{4.18}$$

The null space velocity, previously defined in Equation (4.9), is generalized to accommodate direction-dependent force-driven velocities $\dot{x}_f$, $\dot{y}_f$, and $\dot{z}_f$:

$$\boldsymbol{\dot{u}}_n = \boldsymbol{J}_p^T \left(\boldsymbol{n}_{f_x} \dot{x}_f + \boldsymbol{n}_{f_y} \dot{y}_f + \boldsymbol{n}_{f_z} \dot{z}_f \right). \tag{4.19}$$

Each directional velocity has an associated kinematic variable, exemplified by k_{n_y}:

$$k_{n_y} = \boldsymbol{n}_{f_y}^T \boldsymbol{J}_p \boldsymbol{N}_x \boldsymbol{J}_p^T \boldsymbol{n}_{f_y}. \tag{4.20}$$

Utilizing the dynamics from Equation (4.14), the scalar velocities at the tool center point are expressed as:

$$\dot{y}_f = \frac{1}{c k_{n_y}} \left(c \dot{x}_{pt_y} + \dot{f}_{d_y} + \frac{2d}{T} \delta f_y + \frac{1}{T^2} \int \delta f_y \mathrm{d}t \right). \tag{4.21}$$

Inserting Equations (4.21) and (4.20) into (4.19), we find that the null space joint velocity is inversely proportional to the external force component:

$$\begin{aligned}\boldsymbol{\dot{u}}_n &\propto \boldsymbol{J}_p^T \boldsymbol{n}_{f_y} \frac{1}{k_{n_y}} \dot{f}_{a_y} \\ &\propto \boldsymbol{J}_p^T \boldsymbol{n}_{f_y} \frac{1}{\boldsymbol{n}_{f_y}^T \boldsymbol{J}_p \boldsymbol{N}_x \boldsymbol{J}_p^T \boldsymbol{n}_{f_y}} \dot{f}_{a_y} \\ &\propto \frac{1}{n_{fy}} \dot{f}_{a_y}.\end{aligned} \tag{4.22}$$

This results in higher Cartesian velocities where the external force component is lower. However, this can lead to infinite velocities and must be deactivated below a certain threshold:

$$\lim_{n_y \to 0} \left(\frac{1}{n_{f_y}} \dot{f}_{a_y} \right) = \infty. \tag{4.23}$$

To ensure smooth transitions, the null space force-driven joint velocity $\boldsymbol{\dot{q}}_n$ is low-pass filtered. The extended framework is compatible with various attitude controls and is implemented solely via the null space calculated over the selected Jacobian matrix $\boldsymbol{J_x}$ [8].

Stability Analysis

The stability of the proposed controllers is analyzed based on the stability proof for tactile motion control by Sygulla et al. [233]. The dynamics from Equations (4.14), (4.17), and (4.19) are differentiated and solved for the control variables under two conditions:

$$\delta \ddot{f} = -\frac{2d}{T} \delta \dot{f} - \frac{1}{T^2} \delta f, \qquad \text{if } A \tag{4.24}$$

$$\delta \ddot{f}_{\{x,y,z\}} = -\frac{2d}{T} \delta \dot{f}_{\{x,y,z\}} - \frac{1}{T^2} \delta f_{\{x,y,z\}}, \qquad \text{if } B \tag{4.25}$$

where A and B represent Contact Control and Multi-Force Control, respectively. Both controllers are shown to be stable outside Jacobian singularities.

Decoupling Analysis

The framework aims for complete decoupling between position and force control in Cartesian space. Although hybrid control as introduced by Raibert et al. [103] initially appears decoupled, Fisher et al. [221] demonstrated that this is not the case. The controllers remain active along non-selected DOFs, leading to suboptimal performance. The joint velocity equation is reformulated as:

$$\begin{aligned}\dot{\boldsymbol{q}}_c &= (\boldsymbol{S}_x\boldsymbol{J})^{\#}\dot{\boldsymbol{x}}_x + (\boldsymbol{S}_f\boldsymbol{J})^T\dot{\boldsymbol{x}}_f \\ &= \dot{\boldsymbol{q}}_x + \dot{\boldsymbol{q}}_f.\end{aligned} \tag{4.26}$$

Upon projecting the position-selected Cartesian velocity and taking the dot product, the velocities are found to be orthogonally split:

$$\left(\boldsymbol{S}_x\boldsymbol{J}(\boldsymbol{S}_x\boldsymbol{J})^{\#}\dot{\boldsymbol{x}}_x\right)^T(\boldsymbol{S}_x\boldsymbol{J}\boldsymbol{N}_x\boldsymbol{J}^T\dot{\boldsymbol{x}}_f) = 0. \tag{4.27}$$

This orthogonality is also confirmed in joint space, validating the effectiveness of the null space division for decoupling [8].

$$\left((\boldsymbol{S}_x\boldsymbol{J})^{\#}\dot{\boldsymbol{x}}_x\right)^T\left(\boldsymbol{N}_x\boldsymbol{J}^T\dot{\boldsymbol{x}}_f\right) = 0. \tag{4.28}$$

Force-Prioritized Control Architecture

To enhance the decoupling between force and position control loops, a force-prioritized control architecture is introduced. This architecture employs a specialized null space matrix $\boldsymbol{N}_f$ to filter position-controlled joint velocities that are not orthogonal to force-regulated velocities [8]. The control equation is formulated as:

$$\dot{\boldsymbol{q}}_c = \boldsymbol{N}_f(\boldsymbol{S}_x\boldsymbol{J})^{\#}\dot{\boldsymbol{x}}_x + (\boldsymbol{S}_f\boldsymbol{J})^T\dot{\boldsymbol{x}}_f. \tag{4.29}$$

The null space matrix $\boldsymbol{N}_f$ is adapted based on the force-selected Jacobian:

$$\boldsymbol{N}_f = \boldsymbol{I} - (\boldsymbol{S}_f\boldsymbol{J})^{\#}(\boldsymbol{S}_f\boldsymbol{J}). \tag{4.30}$$

In this architecture, force-controlled DOFs operate in the workspace and have unrestricted access to the joint space. The position-controlled movements are filtered by $\boldsymbol{N}_f$, ensuring orthogonality between joint and Cartesian velocities:

$$\left(\boldsymbol{N}_f(\boldsymbol{S}_f\boldsymbol{J})^{\#}\dot{\boldsymbol{x}}_x\right)^T\left((\boldsymbol{S}_f\boldsymbol{J})^T\dot{\boldsymbol{x}}_f\right) = 0. \tag{4.31}$$

4.1.4 Experimental Evaluation

The experimental design aims to evaluate two key aspects of the proposed control architectures: 1) performance in nonlinear compliant control tasks, and 2) effects of task prioritization [8]. Two biomechanically-inspired tasks mimicking the human knee joint behavior serve as testbeds. For details on the contact control evaluation please refer to the original paper [8].

Evaluation of Multi-Force Control

The Multi-Force Control is assessed through a complex task involving a biomechanical model of the human knee joint, fabricated additively. The femur is rigidly coupled to the robot, while the tibia is environmentally fixed and non-linearly connected to the femur via ligament-mimicking ropes (Figure 4.2).

The task requires actuation in multiple Cartesian DOFs to characterize biomechanical properties, such as range of motion, while minimizing orthogonal loads. The flexion angle is actively adjusted within 0 to 11.5°, and force components are modulated between 10 and 30 N. The maximum angular velocity is 2.75°/s.

The control scheme demonstrates precise tracking with a maximum flexion error of 0.75° and a mean error of 0.15°. However, force errors increase during rapid flexion actuation, stabilizing during low-velocity periods. Key performance indicators are summarized in Table 4.1.

Figure 4.2 Test setup for the Multi-Force Control. The robot is attached to an additive manufactured replica of the human knee-joint constrained by tendons [8].

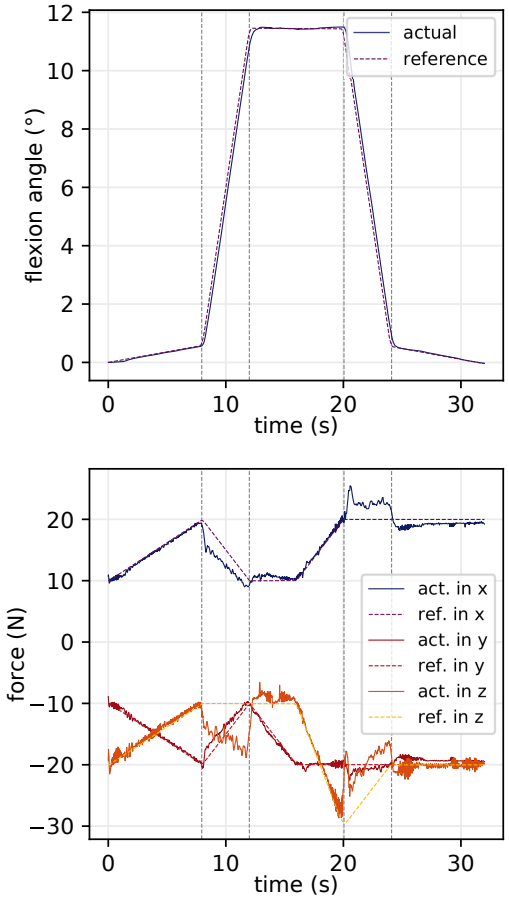

Figure 4.3 Flexion (above) and force tracking (below) of the Multi-Force Control during the described task execution [8].

4.1.5 Comparative Analysis of Position and Force Prioritisation

To illustrate the trade-offs between prioritizing force and position, a controlled experiment was conducted where the task trajectories for both control objectives remained constant. In this setup, force tracking was prioritized as the primary task, while flexion control was relegated to the null space. This adjustment led to improved force tracking but compromised positional accuracy, as evidenced by Figure 4.4 [8].

The experiment revealed that force errors were substantially reduced to a maximum and mean of 5.23 N and 0.62 N, respectively. Conversely, positional deviations exhibited a moderate increase, with a maximum of 1.45° and a mean of 0.38°. The quantitative metrics for this comparative analysis are tabulated in Table 4.5. The key findings can be summarized as follows:

- Force prioritisation yielded minimal force errors, largely unaffected by the positional task. However, it led to elevated position errors during active movements due to null space filtering.
- Position prioritisation excelled in positional tasks but exhibited a velocity-proportional increase in force errors.

4.1.6 Comprehensive Assessment of Null Space-Based Control Architectures

In summary, this section has introduced two innovative compliant control architectures—Contact Control and Multi-Force Control—that exploit null space for effective management of interaction tasks in nonlinear

Table 4.1 Quality measures of the Multi-Force Control experiment from Wilhelm et al. [8].

Quality Measure	Value	Unit
Position accuracy	< 0.01	°
Force accuracy	< 0.1	N
Maximum rotation error $\|\delta x\|_{max}$	0.75	°
Mean rotation error $\|\delta x\|_{mean}$	0.15	°
Root mean square rotation error $\mathrm{RMS}\ \delta x$	0.27	°
Maximum Euclidean force deviation $\|\boldsymbol{\delta f}\|^2_{max}$	11.58	N
Mean Euclidean force deviation $\|\boldsymbol{\delta f}\|^2_{mean}$	2.29	N
Root mean square force deviation $\mathrm{RMS}\ \delta f$	3.36	N

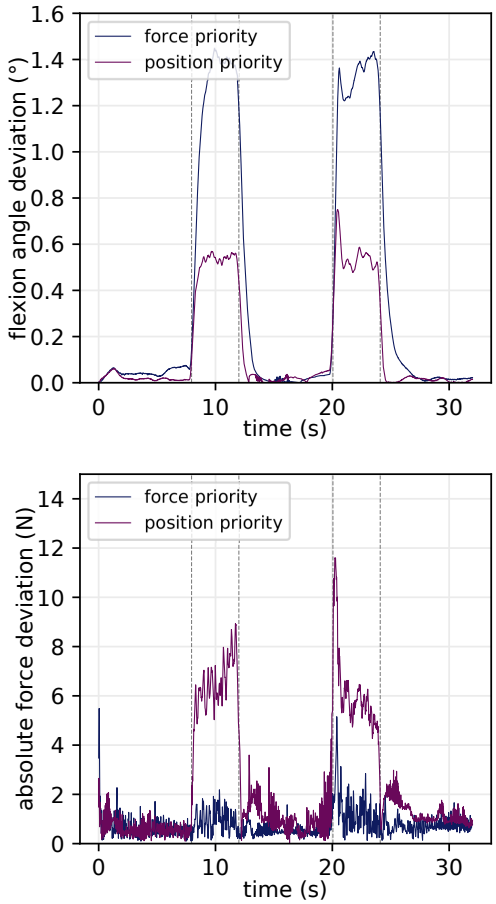

Figure 4.4 Comparative tracking performance under position and force prioritisation. Position errors and Euclidean norms of force errors are depicted [8].

Figure 4.5 Quality Measures of Multi-Force Control with Position Prioritisation compared to Force Prioritisation [8].

Quality Measure	Position Prioritisation	Force Prioritisation	Unit
$\|\delta x\|_{\max}$	$\mathbf{0.75}$	1.44	°
$\|\delta x\|_{\mathrm{mean}}$	$\mathbf{0.15}$	0.38	°
$\mathrm{RMS}\ \delta x$	$\mathbf{0.27}$	0.67	°
$\|\boldsymbol{\delta f}\|^2_{\max}$	11.58	$\mathbf{5.22}$	N
$\|\boldsymbol{\delta f}\|^2_{\mathrm{mean}}$	2.29	$\mathbf{0.62}$	N
$\mathrm{RMS}\ \delta f$	3.36	$\mathbf{0.81}$	N

systems [8]. These architectures sidestep the pitfalls of Jacobian inversion and inner singularities, offering a robust and stable solution for kinematic velocity projection.

The minimalistic approach to parameter tuning aligns with the chapter's broader goals, facilitating efficient operation of testbenches and easing the transition to digital twin development. The orthogonal decoupling of force and position tasks achieved through null space utilization is crucial for accurate biomechanical data evaluation, a prerequisite for subsequent kinematic and dynamic optimizations in Sections 5.1 and 5.2.

Ultimately, these control architectures serve as a dual-purpose foundation: they enhance the control of robotic test benches and set the stage for the data-driven creation of patient-specific digital twins. This dual utility advances the field towards more precise and individualized clinical assessments, meeting the overarching objectives of this research.

4.2 Ex-Vivo Human Knee Joint Analysis

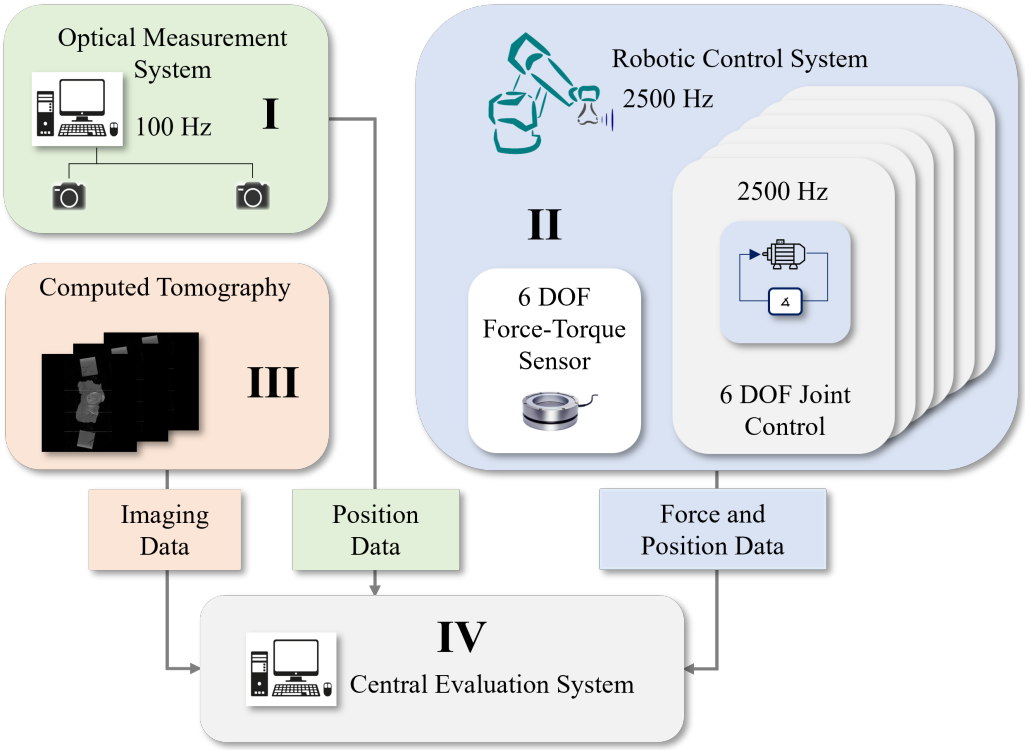

Figure 4.6 Test bench architecture consisting of an optical measuring system (I), the 6 DOF Robot Stäubli RX90B (II) with an additional 6 DOF force-torque sensor for external load acquisition, CT imaging (III), and the central evaluation system (IV) by Wilhelm et al. [9].

Building on the control framework introduced earlier, this section demonstrates its application in biomechanical testing. We will develop a robotic testbench that leverages these advanced control strategies to enhance research in biomechanics and orthopedics and evaluate different Total Knee Arthroplasty (TKA) strategies in knee joint replacement surgery.

The human knee, a complex joint crucial for movement and weight-bearing, is a key focus in prosthesis development and human motion analysis [28, 29]. Its complex structure, providing six degrees of freedom, and the variability of joints present challenges in biomechanical analysis [28]. This complexity underscores the importance of accurate biomechanical testing, which is essential for predicting in vivo knee loads [234], developing computational models [235], and informing surgical planning and implant design [236].

Our study aims to contribute to the understanding of knee joint biomechanics, given its significant role in knee osteoarthritis progression [33, 34, 237], the influence of knee alignment on disease progression [238], and the knee joint's susceptibility to injuries [35]. We aim to develop and validate a novel robotic testbench to study knee joint biomechanics, focusing on various loading conditions and the effects of implant alignment in TKA.

Previous studies have utilized robotic testbenches and cadaver studies to investigate knee joint biomechanics [71–74]. However, their applicability to new measurements remains limited due to their fixed geometries. This study aims to overcome this limitation by developing a unique robotic testbench for comprehensive knee joint biomechanics analysis, focusing on diverse loading conditions and aided by

a cadaveric study. This approach will allow the investigation of knee joint structure interactions and their response to varying loads, providing valuable insights for improving surgical planning and implant design [239].

4.2.1 Methods

Robotic Testbench

A 6 DOF robotic testbench, based on the experimental concept of Frey, Burgkart, et al. [75] and extended by Martinez, Deimling, et al. [240] and Tan, Saier, et al. [241], was used for dynamic investigation of the human cadaver knee joint (Figure 4.6). The robot records its position and orientation while performing various tests, such as varus-valgus and internal-external loading tests at different flexion angles.

A fresh-frozen human cadaveric left knee joint was prepared for biomechanical testing. A modified manual TKA procedure was performed, utilizing an adapter implant for the distal femur (Figure 4.7). The tibial component was implanted, and an adapter was secured to the bone. Different femoral shields with internal-external rotation of -5°, 0°, and +5° were attached to the adapter for biomechanical tests.

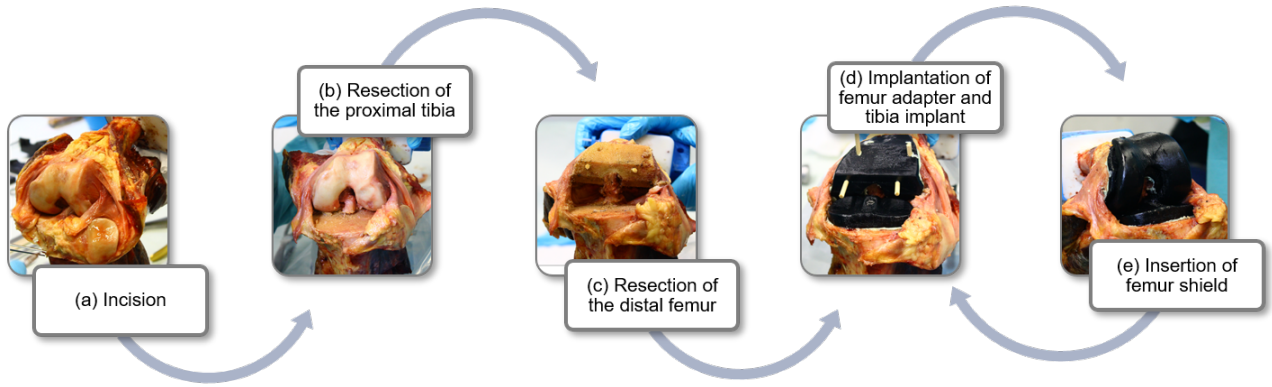

Figure 4.7 Sequential steps of the modified TKA procedure on a cadaveric knee joint: (a) opening of the joint capsule to expose the femur, tibia, and patella; (b) resection of the proximal tibia; (c) resection of the distal femur; (d) implantation of the tibial component and femoral adapter; and (e) switching femoral shields with different internal-external rotations (-5°, 0°, and +5°) during biomechanical testing [9].

Customized femoral implants were specifically designed and affixed to an adapter to investigate the effects of various rotational adjustments on cadaveric knee joints, as depicted in Figure 4.8. These implants were crafted based on segmented CT scans of the knee joint, ensuring precise anatomical alignment.

The robotic testbench system was used to conduct a comprehensive biomechanical assessment of the cadaveric knee joint. The evaluation involved varus-valgus and internal-external loading tests at multiple flexion angles for both the native knee joint and TKA conditions with varying implantation rotations.

The collected data was processed and analyzed to evaluate the biomechanical properties of the native knee joint and TKA conditions. Outcome measures included robotic testbench reproducibility, knee joint stability, comparison between native and TKA conditions and effects of varying femoral component rotations. Statistical analysis was conducted to identify significant disparities.

4.2.2 Results

Figure 4.9 illustrates the test and results of the clamped knee joint specimen using the 6 DOF Stäubli robot, providing motion and force-torque data. The setup includes femur fixation, a force-torque sensor, and trackers for the femur and tibia. The Stäubli RX90B robot, attached to a native knee specimen, enables a thorough knee joint biomechanics assessment under various loads, as displayed in Figure 4.9 (a). Figures 4.9 (b), (c), and (d) show the effects of different forces and torques on knee joint function and

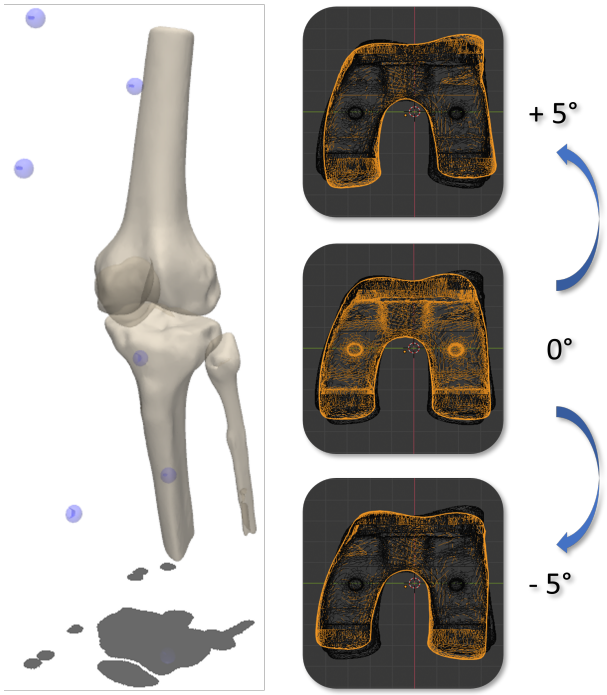

Figure 4.8 (a) 3D Slicer segmentation of the cadaveric knee joint, demonstrating the tibia, fibula, patella, and femur, along with the femoral (upper blue spheres) and tibial (lower blue spheres) trackers. (b) Tailored femoral component designs modeled on Stryker Triathlon TKA implants, resized and rotated to -5° (internal), 0° (neutral), and +5° (external). The femoral components are presented on the axial plane, viewed from the distal end [9].

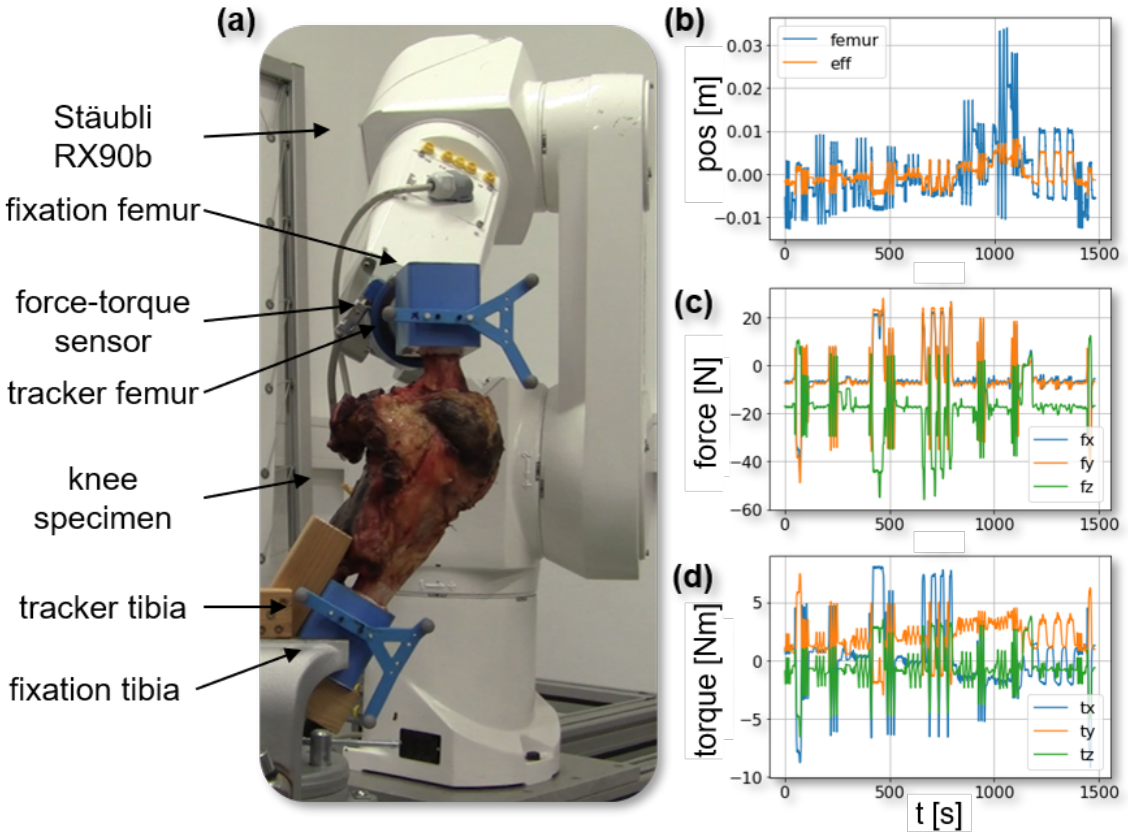

Figure 4.9 Complete test setup (a), synchronization and movement (b), as well as acquired force (c) and torque (d) data during the native knee test from Wilhelm et al. [9].

stability. The precision of the testing system is emphasized in Figure 4.9 (b), while Figures 4.9 (c) and (d) display the measured forces and torques. This experiment could enhance our knowledge of knee joint biomechanics and inform better treatment strategies for knee-related pathologies.

Examining Biomechanical Differences in Knee Joint with Various TKA Setups

Figure 4.10 presents the maximum deviation angles and corresponding standard deviations for internal-external and varus-valgus loading at varying flexion angles. The robotic testbench conducted each test three times, applying a 5 Nm torque. The figure uses distinct colors and symbols to differentiate between the native knee and TKA setups, with a provided legend for clarity.

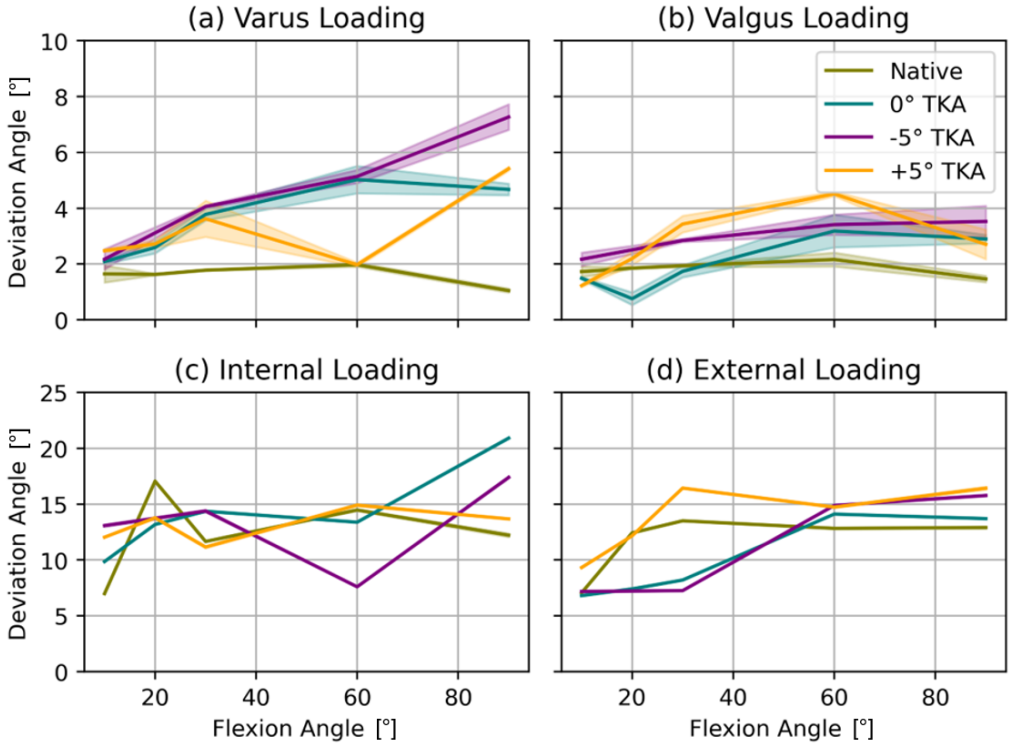

Figure 4.10 Comparison of maximum deviation angles and standard deviations for (a) varus, (b) valgus, (c) internal, and (d) external loading at 5 Nm across different flexion angles for native knee and total TKA with 0°, -5°, and +5° implant rotations. Results from Wilhelm et al. [9].

For varus loading as in Figure 4.10 (a) and valgus loading as in Figure 4.10 (b), the native knee shows superior stability with the smallest deviations ($< 2°$) from the neutral (zero loading) position. All TKA setups display reduced stability, with the -5° TKA showing the least stability for varus loading at 90° flexion ($> 6°$). The testbench maintains high precision, with standard deviations below 0.5°.

The internal and external loading results from Figure 4.10 (c) and (d) show more variability between the native knee and TKA variants. Unlike varus loading, the -5° TKA shows the highest stability for internal and external loading. The +5° TKA closely matches the native knee's stability, while the -5° TKA shows the largest deviation. The testbench's precision for internal-external loading tasks is excellent, with standard deviations below 0.1°.

Stability Assessment

The Total Deviation Angle (TDA), defined as the angular difference between extreme positions under specific loading conditions, is used to gauge joint instability. Higher TDA values indicate lower joint stiffness under the respective loading scenario. Figure 4.11 shows the varying impacts of different TKA modifications, compared to the native knee, on joint stability under diverse loading conditions. The diagram illustrates TDA for varus/valgus, as in Figure 4.11 (a) and internal/external in Figure 4.11 (b) loading across a range of flexion angles under a 5 Nm load, contrasting the native knee with three TKA orientations (neutral 0°, -5° internal rotation, and +5° external rotation of the femoral component).

The native knee shows the highest stability with least deviations, while TKA variations show increased deviations in both loading conditions. The -5° TKA shows the lowest stability in varus-valgus loading at 90° flexion but highest stability in internal-external loading. The +5° TKA closely mirrors the native knee performance, except for the -5° TKA showing the highest deviation. Error bars in the figure represent standard deviation, emphasizing the precision of the robotic testbench. This analysis highlights the significance of TKA strategies in preserving knee biomechanics and stability under diverse loading conditions.

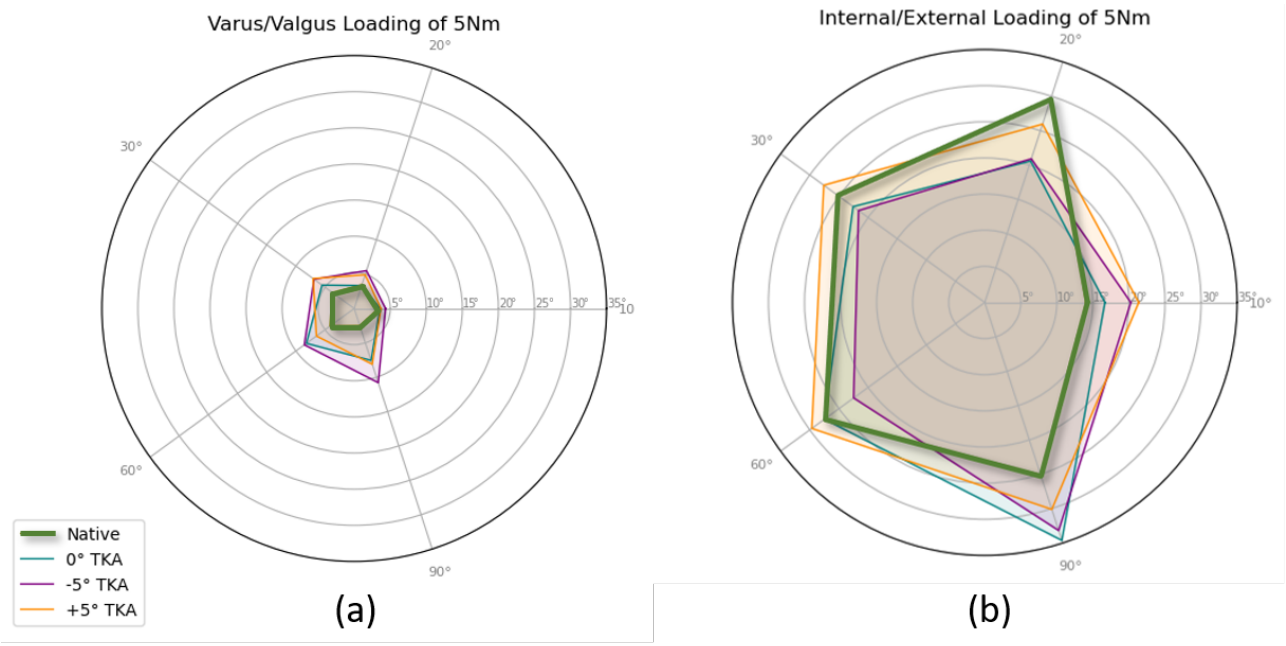

Figure 4.11 Kiviat Diagram of the TDA for instability in internal/external and varus/valgus loading for native knee and TKA variations (neutral 0°, -5° internal, +5° external) across flexion angles under 5 Nm load. (a) Varus/Valgus Loading and (b) Internal/External Loading. Results show the sum of deviations for both loadings, illustrating the impact of TKA strategies on knee biomechanics.

Figure 4.11 displays Kiviat diagrams of TDA for instability in internal/external and varus/valgus loading for the native knee and TKA variations across flexion angles under 5 Nm load. The diagrams, split into (a) Varus/Valgus Loading and (b) Internal/External Loading, provide a comprehensive view of the impact of TKA strategies on knee biomechanics. The radial nature of the diagrams facilitates easy comparison of TDA across different conditions and TKA variations, highlighting biomechanical differences and potential instabilities. The -5° internal TKA value at 20° flexion was determined through linear interpolation between values at 10° and 30° flexion.

TKA Variations vs. Native Knee Joint

This section quantifies the differences between the native knee and TKA configurations under varus, valgus, internal, and external loading. We calculate the MSE across all flexion angles and loading conditions, assessing TKA variations' deviation angles compared to the native knee. These deviations are crucial as they could impact clinical outcomes.

Table 4.2 (top) shows the MSE values for the deviation between the native knee and TKA configurations under varus and valgus loading. The neutral (0°) TKA showed the lowest mean deviation for both varus (5.5 ± 5.0) and valgus (0.9 ± 0.8) loading, suggesting superior biomechanical similarity to the native knee. Conversely, the -5° TKA showed the highest mean deviation for both varus (11.4 ± 14.0) and valgus (2.1 ± 1.6) loading, potentially leading to less desirable clinical outcomes.

Furhter, Table 4.2 (bottom) shows the MSE values for deviations between the native knee and TKA configurations under internal and external loading. The +5° TKA showed the minimal mean deviation for both internal (7.8 ± 9.7) and external (6.0 ± 4.2) loading, suggesting improved joint stability. In contrast, the

-5° TKA showed the maximal mean deviation, with values of 82.0 ± 105.4 for internal and 41.2 ± 58.3 for external loading, potentially leading to unfavorable clinical outcomes.

Table 4.2 Deviations between the native knee and different TKA for varus-valgus (top) and internal-external (bottom) loading evaluated by MSE and the respective standard deviations [9].

	Deviations to Native		
TKA	Varus	Valgus	Mean
+5°	**4.87** ± 7.19	1.93 ± 1.97	3.40 ± 3.67
±0°	5.51 ± 4.98	**0.88** ± 0.76	**3.20** ± 2.57
-5°	11.36 ± 14.04	2.05 ± 1.55	6.71 ± 7.14
TKA	Internal	External	Mean
+5°	**7.78** ± 9.70	**5.96** ± 4.23	**6.87** ± 4.83
±0°	21.50 ± 27.44	11.14 ± 12.73	16.32 ± 18.03
-5°	81.97 ± 105.40	41.22 ± 58.30	61.60 ± 74.86

4.2.3 Discussion

This study examined the biomechanical compatibility of different TKA variations under various loading conditions. The neutral 0° TKA showed the least mean deviation under varus and valgus loading, suggesting superior biomechanical compatibility. Conversely, the -5° TKA showed the highest mean deviation, potentially indicating less desirable clinical outcomes. For internal and external loading, the +5° TKA showed the least mean deviation, suggesting improved joint stability. Our findings align with previous research by Bellemans, Colyn, et al. [242], Howell, Roth, et al. [243], and Hutt, LeBlanc, et al. [244], which reported positive outcomes using kinematic alignment in TKA. The neutral 0° TKA, closer to kinematic alignment, showed superior performance under varus and valgus loading. Our results also support Rivière, Iranpour, et al. [245] proposal for a personalized approach to TKA modifications, as the +5° TKA showed superior joint stability under internal and external loading. The robotic testbench used in this study offers potential for broad application in biomechanical research. It can accurately simulate complex knee joint kinematics and manage diverse loading conditions, making it a valuable tool for assessing different TKA variations, surgical procedures, and implant designs.

This study has some limitations. It used a single knee specimen, limiting the generalizability of the findings. The study focused on biomechanical compatibility and joint stability, without considering factors like patient satisfaction and implant durability. The study also did not assess long-term clinical outcomes linked with different TKA modifications. Future studies should aim to overcome these limitations and investigate the effects of TKA modifications on a larger and more diverse population.

4.2.4 Conclusions

In summary, this study highlights the importance of TKA variation selection in optimizing biomechanical compatibility and joint stability. It shows that a neutral TKA variation performs best under varus and valgus loading, while a +5° variation provides better stability for internal and external loading. These findings underscore the need for personalized TKA strategies based on individual biomechanical needs. The study also demonstrates the potential of the robotic testbench in biomechanical research, aiding in the investigation of various TKA variations and facilitating pre-clinical assessments of new implant designs. By enhancing our understanding of knee joint biomechanics and TKA variations, we can improve surgical procedures and patient outcomes following TKA.

4.3 Ex-Vivo Human Hand Joint Analysis

Having examined the details of the robotic testbench designed for knee joint analysis, it is clear that biomechanics presents a wide array of research opportunities. The knee, a critical weight-bearing joint, has its own specific challenges and complexities. Similarly, the human hand, with its complex structure of tendons, muscles, and joints, offers a rich subject for study. The remarkable dexterity and versatility of the hand make it a central focus in biomechanical investigations. Moving from lower limb to upper extremity, the following section introduces a novel approach that combines robotics with hand biomechanics. This approach aims to investigate the mechanics of grip movements and tendon forces.

4.3.1 Introduction to Hand Biomechanics Analysis

The human hand, known for its structural complexity and multifunctionality, serves as an exceptional tool for interacting with our environment. The precise coordination of numerous muscles, required even for the simple act of moving a single finger, results in movements that are profoundly shaped by the viscoelastic properties of the ligaments, surrounding tissues, and the intrinsic kinematics of the joints [246–248]. This orchestration enables the hand to perform a wide range of tasks with remarkable precision and adaptability.

Historically, various hand models have been developed to capture the complex nature of the hand, with the goal of replicating its biomechanical behavior [249–251]. These models, primarily based on Computer Aided Design (CAD) data, are enhanced by incorporating muscle tractions and hand kinematics. Despite these advancements, a significant gap persists: the models, which focus heavily on geometry, often lack comprehensive biomechanical validation. The complexity of hand modeling and the need to define numerous boundary conditions make the validation process particularly challenging.

An outstanding challenge in this field is the accurate modeling of the thumb, which is due to its unique joint structure [78]. This has led to innovative modelling approaches that address the contact surfaces and stabilizing tissues of the thumb, viewing it as a force-controlled multibody system influenced by cartilage contacts, ligaments and muscles [78].

Although previous experimental studies have shed light on various aspects of hand behavior, they typically displayed a limited scope, focusing mainly on individual fingers. These studies often failed to consider the comprehensive relationship between muscle activation, resultant movement, and the forces exerted [79–82]. This narrow focus can overlook the integrated dynamics that characterize the function of the entire hand.

In this research context, we introduce a comprehensive testbench designed to address these existing shortcomings. Our system integrates force-controlled muscle actuation with the resulting movements and forces at the fingertips. Enhanced by the capabilities of eight independent motors, this setup allows for the simultaneous study of multiple fingers, closely replicating real-world grasping dynamics. We particularly focus on the pincer grip, a quintessential fine motor skill, where the thumb and index finger, in their flexed positions, come together [252]. This grip, symbolic of sophisticated motor functions, is recreated on a human specimen by precisely controlling the tendons of both the thumb and index finger.

This study introduces an enhanced version of the force-controlled hand stimulation testbench, equipped with eight motors. It efficiently captures external force-torque and motion data to analyze the hand's response to muscle actuation. Additionally, we apply this test rig to a cadaver hand to simulate complex tasks, including the pincer grip. This approach enables a more differentiated understanding of hand mechanics during precise movements.

4.3.2 Testbench Design and Methodology

The testbench, as depicted in Figure 4.12, is an assembly of four primary systems: the force control system, the optical measurement system (Optitrack©), the central control system, and a video capture camera. The force control system is a notable feature, integrating eight autonomous motors. Each motor is equipped with a strain gauge for force detection and an internal angle sensor. The motors, specifically the 9225-160KV brushless variants, are designed for efficient operation even under significant loads. The force control

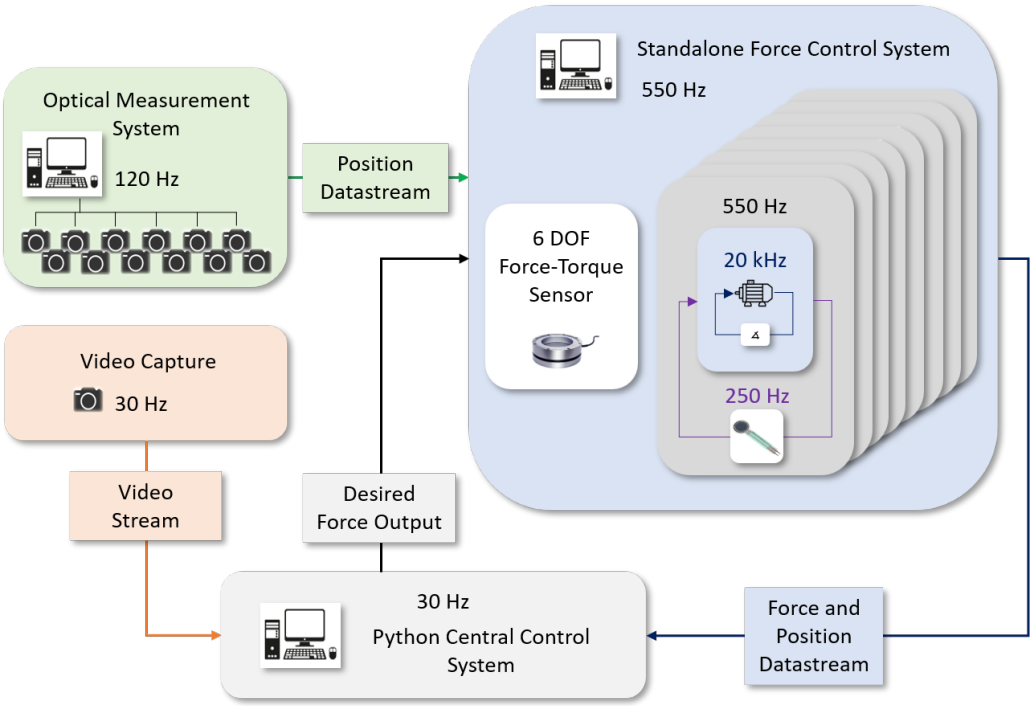

Figure 4.12 Schematic representation of the test bench, featuring an optical measuring system (I), eight force-controlled motors (II) governed by a central control unit (III), and a video capture system (IV). An integrated 6 DOF force-torque sensor facilitates external load measurement [10].

system's output is interfaced with the open-source Vedder electric velocity controller (VESC) [253], ensuring precise field-oriented control.

The integration of robotics with human hand biomechanics is evident in the testbench's design. The OptiTrack© setup, consisting of six cameras, provides real-time position and orientation data, which is relayed to the force control system. This data stream, synchronized with force and position metrics, is managed by an application developed on the Isaac Software Development Kit (SDK) [254]. The video capture system, while primarily used for evaluation, offers potential for AI-driven analyses, such as 3D hand reconstruction [255].

To emulate the pincer grip, each motor's actuation is governed by signals characterized by a sine wave, ensuring precise control over the tendons of both the thumb and index finger. The testbench's design emphasizes accurate force control, synchronized sensor data, and real-time operation, setting a robust foundation for future model-based control implementations.

The hand preparation process involves identifying and anatomical dissection of eight tendons responsible for the pincer grip. Custom Stereolithography (SLA) 3D-printed navigation trackers are affixed to the finger bones for position detection using an optical navigation system. The hand's positioning on the testbench ensures anatomical alignment of tendons and clear visibility of the trackers. The final test setup is visualized in Figure 4.13. The data acquisition process captures multiple variables, including position, orientation, forces, torques, and their derivatives. The setup comprises five rigid bodies tracked by OptiTrack©, providing comprehensive data for each time step.

The kinematic analysis involves a systematic process to determine the orientations of all rigid bodies at each timestep. The kinematic optimization for undefined rigid bodies employs an iterative process to finalize the positioning of the intermediate and proximal phalanges of the index finger and the proximal phalanx of the thumb. Joint angles in the phalanges are calculated using standard vector methods, ensuring accurate representation of the phalanx's deviation from its default position.

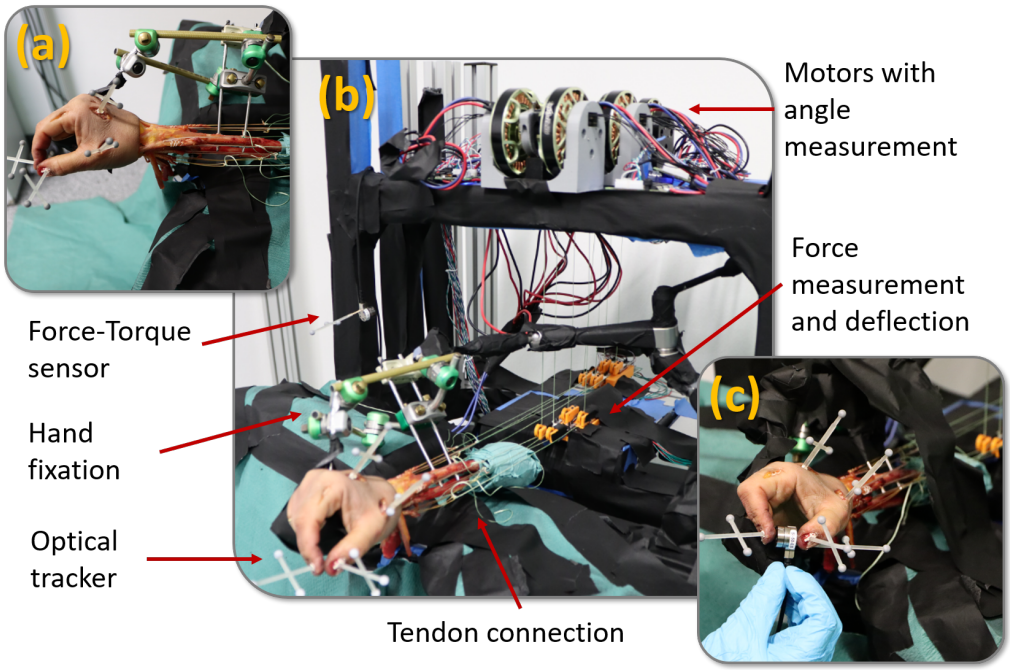

Figure 4.13 Illustration of the test rig and setup: (a) Depicts the precise fixation of the cadaver hand to the test stand; (b) Provides an in-depth view of the overall test configuration; (c) Demonstrates the execution of the pincer grip, highlighting the integrated force-torque measurement with a mobile sensor strategically positioned between the index finger and thumb [10].

4.3.3 Illustrative Results

The results of the study are best visualized through a series of figures that capture the essence of the research's findings. These figures provide a comprehensive overview of the hand's movements, tendon forces, and the resultant grip strength during both robotic and manual actuations.

1. **Robotic Actuation Results:** Figure 4.14 presents the outcomes from the robotic actuation. The figure depicts the movements of the thumb (left) and index finger (right) during the robotic actuation. The top row showcases the joint angles, while the middle and bottom rows illustrate the forces exerted by the respective tendons. Notably, there were fluctuations in force control and suboptimal joint angles, particularly with the MCP joint of the index finger being hyperextended.

2. **Manual Actuation Results:** Figure 4.15 illustrates the effects of manual actuation on the pincer grip. The figure highlights the movements of the thumb (left) and index finger (right), with the top row detailing joint angles and the middle and bottom rows emphasizing the forces from the respective tendons. Manual actuation resulted in smoother joint angle trajectories and reduced hyperextension of the MCP angles in the index finger.

3. **Pincer Grip Force Evaluation:** Figure 4.16 provides a visual representation of the grip force results. The figure delineates the outcomes from both the robotic and manual actuations, capturing the force exerted during the pincer grip.

These figures serve as a visual reference to the research's findings, offering a detailed perspective on the details of hand movements, tendon forces, and grip strength during different actuation methods.

4.3.4 Key Findings

The main goal of this research was to study the ability of a testbench setup to replicate and measure the movements and forces characteristic of a human hand during a pincer grip action. The data gathered from

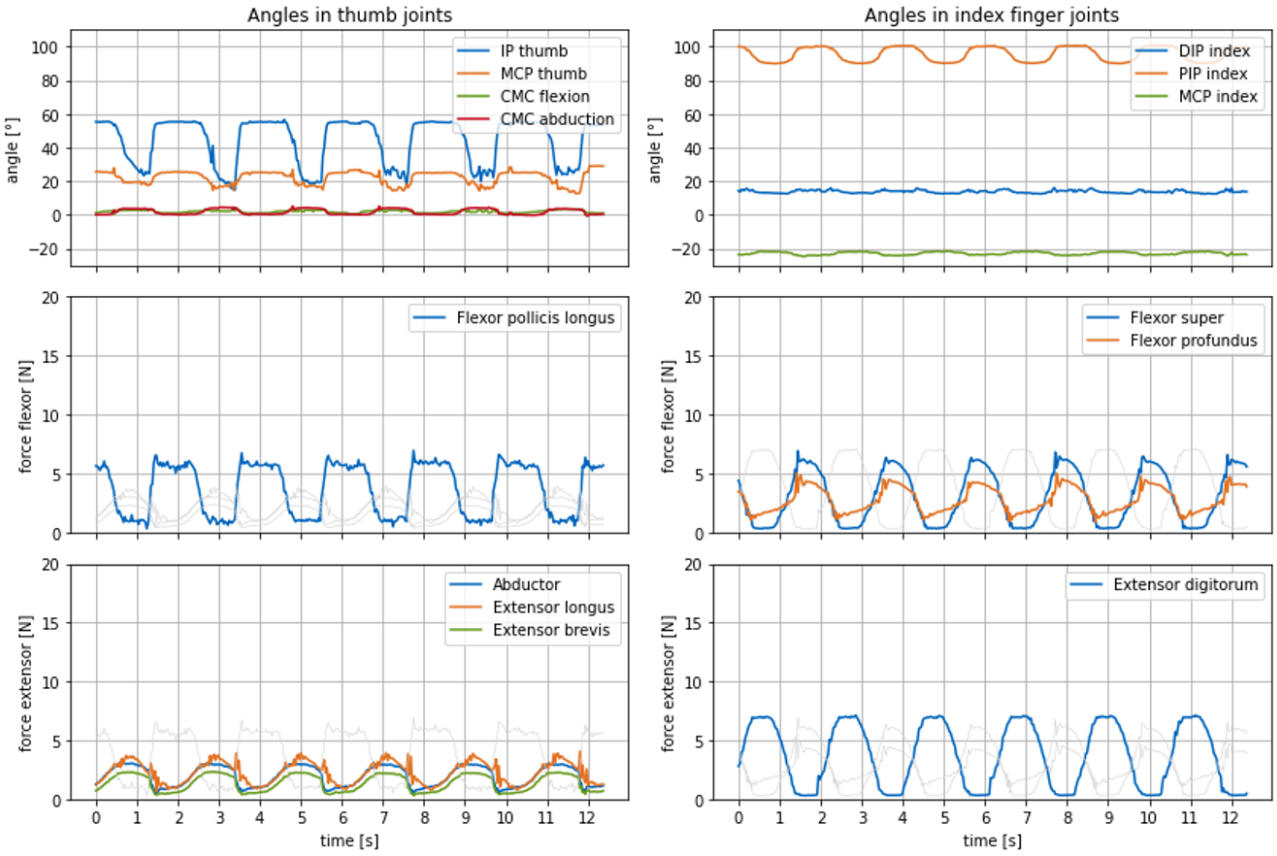

Figure 4.14 Results from hand testing for the male hand during **robotic** actuation. Joint angles and tendon forces are depicted for both the thumb and index finger [10].

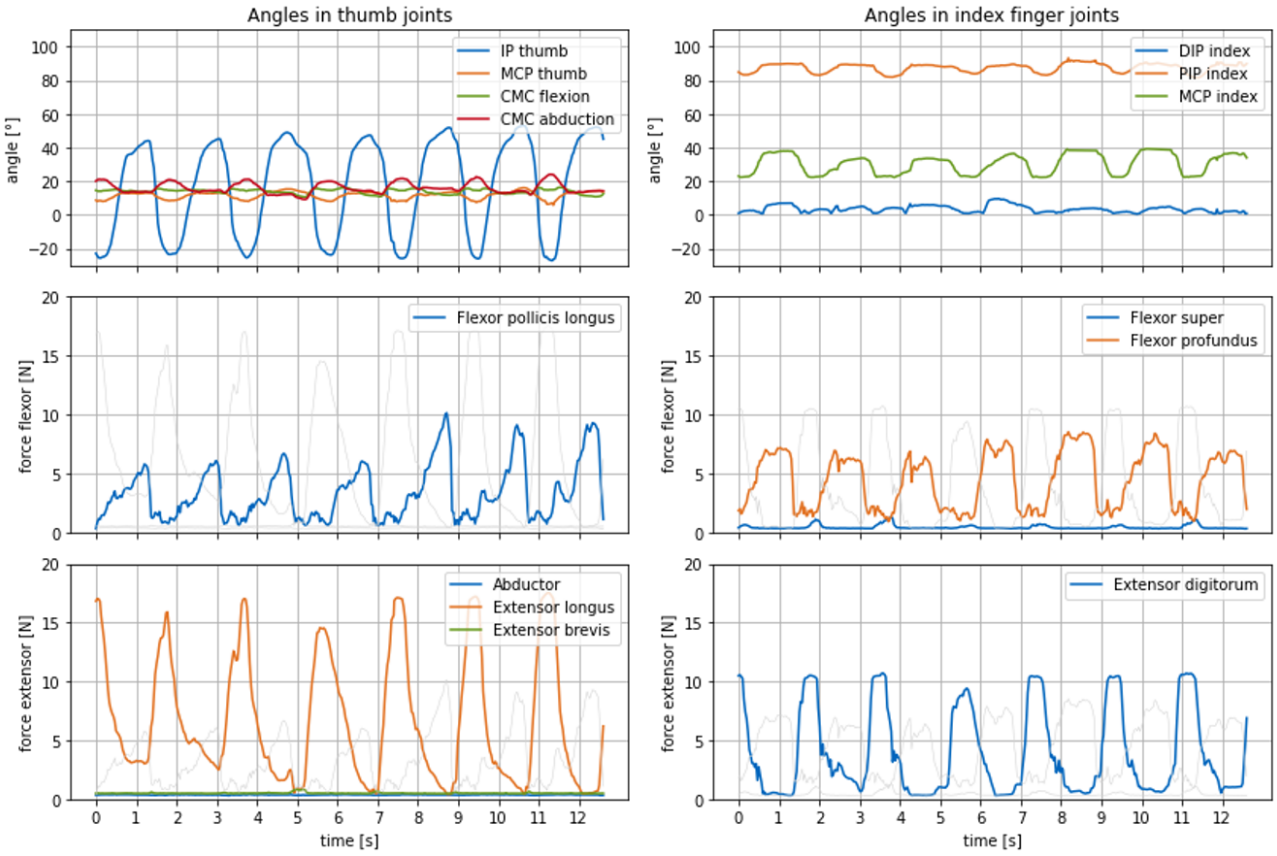

Figure 4.15 Results from hand testing for the male hand during **manual** actuation. The figure details joint angles and tendon forces for both the thumb and index finger [10].

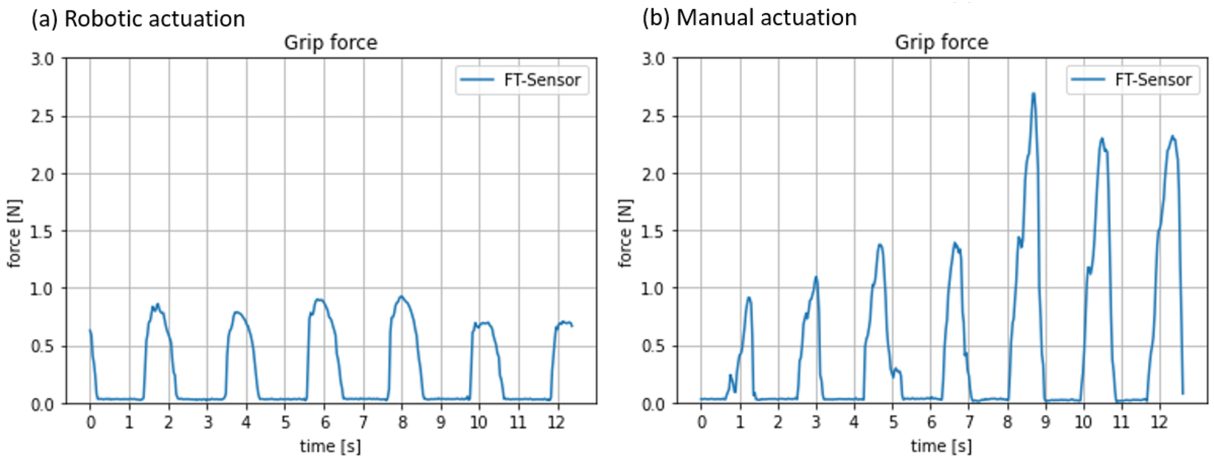

Figure 4.16 Demonstrative grip force measurements for the pincer grip, captured via the force-torque sensor. The figure contrasts the results from both robotic and manual actuations.

these experiments offer substantial insights into how tendon forces influence the resulting grip strength. Below are the principal findings from the study:

Successful Execution of the Pincer Grip: The testbench setup, through both robotic and manual actuation methods, successfully executed the pincer grip. The robotic actuation followed individual sinusoidal force trajectories for each motor, leading to the achievement of a pincer grip. Manual actuation, on the other hand, provided enhanced freedom, resulting in more physiologically accurate movements. Both methods yielded measurable external contact forces, with the robotic actuation producing a force of 0.8 ± 0.1 N and the manual actuation generating a force of 1.9 ± 0.6 N. The difference in these values highlights the variability in force outcomes based on the chosen actuation strategy.

In conclusion, the findings from this research underscore the potential of the testbench setup in replicating the dynamics of a human hand. The insights gained, especially the relationship between tendon forces and grip strength, can be instrumental in refining robotic hand actuation to achieve desired grip strengths and in understanding the biomechanics of the human hand.

4.3.5 Implications and Significance

Our research findings offer the path to deepened understanding of the biomechanics of the human hand, with wide-reaching implications for the domains of robotics and prosthetics. The discrepancies observed between the forces produced by robotic and manual actuation highlight the inherent challenges in emulating the biomechanical properties of human muscles through robotic actuators [256]. This non-linear relationship between tendon forces and grip strength, influenced by factors such as synergistic muscle activation, tendon interactions, and the mechanical advantages that vary with joint angles, provides invaluable insights. These can be harnessed to design robotic hands that are more efficient and adaptive, with control algorithms that facilitate natural grip patterns [257].

In the field of medical prosthetics, the biomechanical insights from our study can enhance prosthetic hand designs, offering users improved dexterity and functionality [258]. The observed non-linearities in force outputs, shaped by the combined forces from multiple tendons and changing joint angles, can guide the evolution of prosthetic hands to more closely mirror natural hand movements [259]. This paves the way for the creation of prosthetics that are not only more effective but also provide a more intuitive and comfortable user experience.

Additionally, a notable aspect of our research is the thorough data collection method, which fills gaps identified in previous studies [81]. By utilizing cadaver hands in our experiments, we achieve precise measurements, establishing a solid baseline for future research [260]. These data lay the groundwork for developing biomechanical models that accurately simulate hand movements and forces, effectively narrowing the gap between theoretical simulations and practical observations. These models are likely to

be invaluable in fields such as robotics and prosthetics, facilitating the creation of devices that more closely mimic human biomechanics.

Limitations

This research, while innovative in its exploration of hand biomechanics, was not without challenges. One of the primary issues faced was with the optical trackers used for data acquisition. These trackers, essential for our study, occasionally suffered from signal loss, which notably affected the evaluation of the female hand specimen. As the study progressed, changes in the biomechanical properties of the cadaveric specimens were observed. These alterations, reminiscent of mummification, could potentially influence the hand's response to actuation.

The process of determining joint angles, a crucial aspect of our analysis, also posed challenges. Relying on manual identification of joint positions introduced variability and potential inaccuracies in our measurements. Even under controlled conditions, environmental factors such as humidity and temperature have subtly affected tissue properties, thereby influencing the results. Furthermore, the limited diversity of hand specimens raises concerns about the generalizability of findings. Factors like age, prior hand usage, and medical history play a significant role in hand biomechanics, and the selected specimens do not capture the full spectrum of these variables.

4.3.6 Conclusion

In this research project, a detailed investigation of the biomechanics of the human hand was carried out, with a particular focus on the complex interaction between tendon forces and grip strength. The interdisciplinary approach, which seamlessly integrated robotics and biomechanics, enabled a successful evaluation of the test rig. By utilizing both manual and robotic techniques to operate the eight motors, the pincer grip was effectively executed. This highlights the robustness and efficacy of the test setup. The collected data is not only consistent with existing literature, but also fills notable gaps, particularly in terms of applicability in practice. This rich dataset captures the mechanics of the human hand and provides a solid foundation for future modeling efforts.

As the integration of biomechanics and robotics continues to deepen, the findings from this study provide a solid foundation for future research. These findings can contribute to the development of prosthetic and robotic hands and represent a remarkable advance in the field of robotic test rigs for joint analysis.

5 Personalized Digital Twins through Artificial Intelligence-based Optimization

This chapter addresses the optimization tasks essential for crafting advanced models in biomechanical systems, as depicted in Figure 5.1. Our research focuses on the careful analysis and optimization of biomechanical models based on available data to increase their precision and efficiency. This effort is pivotal for the generation of patient-specific digital twins, offering advancements in clinical applications. This task is in line with our central research question: How can AI algorithms be applied to highly individualized biomechanical systems to enhance kinematic and dynamic modeling, thereby facilitating more accurate and efficient models for analyzing joint behavior?

Our initial efforts focus on refining kinematic models, a project elaborated upon in Section 5.1. Here, a differentiable kinematic model is introduced, adapted to specific biomechanical conditions and further refined to achieve unparalleled accuracy and efficiency in simulating joint behavior. Given that kinematic boundary conditions are predetermined, our investigation narrows to defining selected dynamic parameters, such as stiffness and damping. To cope with the arising complexity, we pivot to sophisticated reinforcement learning techniques, as discussed in Section 5.2.

Incorporating AI algorithms is projected to enhance the accuracy and efficiency of both kinematic and dynamic modeling processes. These optimization algorithms are crucial for developing sophisticated digital twins, enabling more detailed and personalized analysis of patient-specific conditions. Through this chapter, we aim to underscore the transformative potential of AI in improving biomechanical modeling.

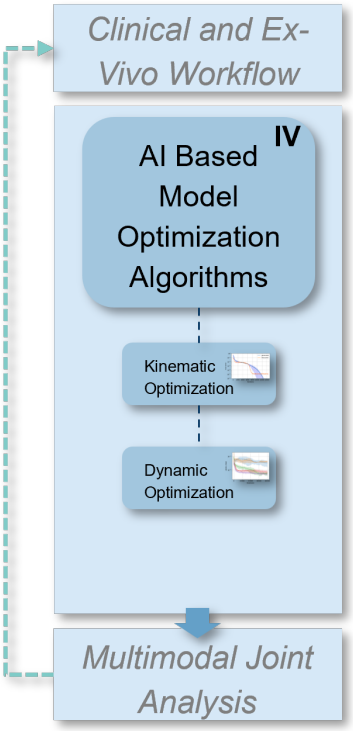

Figure 5.1 Section overview.

5.1 Differentiable Forward Kinematics for Kinematic Optimization

In the field of robotics and biomechanics, the accurate identification of joint parameters and the calculation of both forward and inverse kinematics are essential yet challenging tasks. This section presents an innovative kinematic optimization technique, which is supported by an architecture based on autoencoders [11].

The proposed method employs a neural network to emulate inverse kinematics. It transforms measurement data into parameters specific to individual joints during the encoding phase. These parameters are then fed into a pre-established, differentiable model for forward kinematics, resulting in a decoded version of the initial data. Not only does this approach provide a unified solution to the complexities of forward and inverse kinematics, but it also reveals new joint parameters that were previously undetected. The effectiveness of this optimizer has been confirmed through real-world experimental data, particularly focusing on knee and hand joints.

Moreover, the optimizer serves multiple functions. It not only simplifies the modeling and automation of kinematics but also facilitates a detailed assessment of various modeling techniques. By evaluating the differences in reconstruction losses, the advantages of each technique are emphasized. Overall, this

section highlights the advances in the field of kinematic optimization that can impact both biomechanics and robotics.

5.1.1 Introduction to Autoencoders and Kinematic Modeling

In both robotics and biomechanics, the tasks of identifying joint positions and performing calculations for forward and inverse kinematics are crucial. Challenges often emerge when multiple systems evaluate a single rigid body without awareness of their relative positions, leading to incomplete transformation functions in forward kinematics [261]. Conventional approaches, while foundational, encounter limitations in terms of speed and accuracy, particularly in complex robotic systems [157].

Recent advancements have highlighted the effectiveness of neural network-based solutions in overcoming kinematic challenges. Works by Köker et al. [155], Duka [156], and Jiang et al. [157] have demonstrated the versatility and accuracy of neural networks in various robotic applications. In the biomechanics domain, deep learning has provided insights into human movement, as evidenced by studies like those of Henry et al. [262] and Sun et al. [263]. As a complement to these developments, the concept of differentiable kinematics has gained traction. Contributions from Ono et al. [158] and Fang et al. [159] have emphasized the utility of mathematical groups and learning-based methods in kinematic calculations. Software solutions for differentiable robotics and kinematics have also been introduced [160–162].

In this evolving landscape, autoencoders have proven to be useful tools for kinematic optimization [163–165]. The research presented in this section introduces an autoencoder-based kinematic optimizer that processes measurement data (X_{mea}) to model inverse kinematics and derive joint positions (Q). These positions are then decoded to reconstruct $\hat{X}_{\text{mea}}$. The optimizer's effectiveness is validated using data from knee and hand joints, demonstrating its applicability in both biomechanical and robotic contexts [11]. The source code for the differentiable forward kinematics and optimization is publicly available at `https://github.com/NikonPic/DiffAutoKin`.

5.1.2 Materials and Methods

Differential Kinematics

The study of kinematics frequently employs transformation matrices to establish spatial relationships between various coordinate frames. These matrices generally consist of a rotation matrix R and a translation vector p. Vector differentiation plays a crucial role in understanding relative velocity and acceleration in kinematic systems [264]. Quaternions offer a more compact way to represent the rotation matrix, thereby simplifying the description of orientations and rotations in 3D space [265]. Our methodology leverages these matrices for differential kinematics, providing a framework that is fully differentiable, parallelizable, and algorithmically structured [11].

In robotics and biomechanics, the position of a rigid body in 3D space is often represented using a transformation matrix T_{o-b_i}, which indicates the position of body b_i relative to an origin frame o. These positions are usually obtained from tracking systems like OptiTrack [48] or Vicon [47], or calculated from a forward kinematics model given known joint angles q. Our approach distinguishes between transformations related to rigid bodies, T_{b_i}, and those dependent on joint positions q_i, denoted as $T_j(q_i)$.

Hinge joints mainly experience rotational transformations. The position of the rotational axis is represented by position_i, and its orientation by the axis vector axis_i. The transformation matrix for such a joint is determined through a series of steps, including translation to the joint axis, rotation about the joint axis, and inverse translation from the joint axis. The kinematic structure integrates both rigid bodies and joints to define the transformation from the base to the end effector, represented as T_{eff}. This transformation is expressed as the product of individual transformations associated with each body or joint in the kinematic chain.

We have also developed a comprehensive software solution that automates the creation of a differentiable kinematics model. This software parses Multiple Joints in Contact (MuJoCo)-based XML files [266] and is built on the PyTorch framework [267]. The source code is publicly accessible [11].

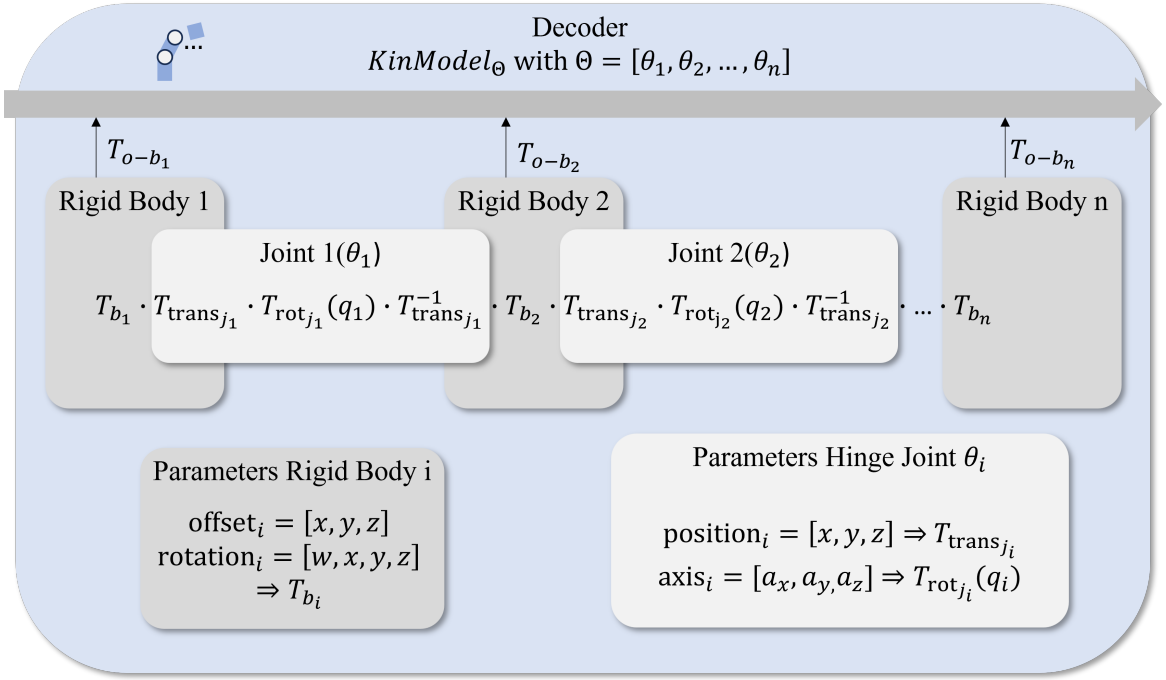

Figure 5.2 Forward Kinematics Model Visualization. The model demonstrates the dependency on joint parameters Θ and illustrates the transformations T_{o-b_i} derived from the kinematic chain [11].

Autoencoder-based Kinematic Optimizer

Building upon the principles of differentiable forward kinematics, we introduce an innovative kinematic optimizer rooted in autoencoder neural network architectures. Autoencoders are specialized neural networks designed for unsupervised learning, aiming to efficiently encode data and reconstruct it from the encoded form. The objective is to minimize the reconstruction error, typically quantified by the MSE [268].

In our approach, the encoder and decoder of the autoencoder serve as the inverse and forward kinematics models, respectively. Given a dataset X_{mea} of pose measurements, the encoder translates this data into joint angles Q. This is achieved through a neural network NN_Ψ, which models the inverse kinematics. These joint angles are then decoded using a differentiable forward kinematics model to produce the reconstructed data $\hat{X}_{\text{mea}}$. This ensures the preservation of mathematical integrity and facilitates gradient-based updates [11].

The primary goal is to minimize the reconstruction error between the measurement X_{mea} and its reconstruction $\hat{X}_{\text{mea}}$. This error serves as our loss function, and gradient-based optimization techniques are employed to iteratively refine the parameters Ψ and Θ.

$$\mathcal{L}(X_{\text{mea}}, \hat{X}_{\text{mea}}) = \frac{1}{m} \sum_{i=1}^{m} \|T_{\text{mea}}(t_i) - \hat{T}_{\text{mea}}(t_i)\|_2 \tag{5.1}$$

$$\Psi^*, \Theta^* = \arg\min_{\Psi,\Theta} \mathcal{L}(X_{\text{mea}}, \hat{X}_{\text{mea}}) \tag{5.2}$$

This optimization process allows the autoencoder to adeptly handle both inverse and forward kinematics, providing a comprehensive solution for kinematic analyses.

Regularization Techniques

Introduction to Regularization Techniques To enhance the robustness and generalizability of our autoencoder-based kinematic optimizer, we incorporated two advanced regularization techniques: Independent Component Analysis (ICA) and VAE.

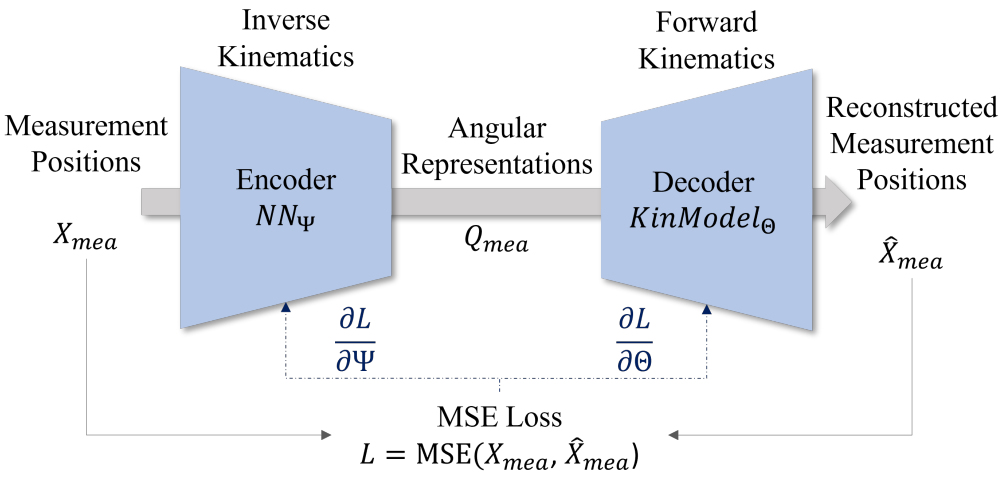

Figure 5.3 Schematic of the autoencoder-based kinematic optimizer. The encoder converts measurement data X_{mea} into joint angles Q, while the decoder reconstructs this data using the differentiable forward kinematics model. Gradients flow through the entire architecture during optimization [11].

ICA aims to decompose a multivariate signal into additive, independent non-Gaussian components [269]. In our model, the goal is to make the components of the encoded representation as independent as possible. We introduce an ICA-inspired regularization term, L_{ICA}, defined as:

$$L_{\text{ICA}} = \sum_{i \neq j} \text{cov}(q_i, q_j)^2 \tag{5.3}$$

This term penalizes the squared values of the off-diagonal elements of the covariance matrix of the encoded representations, encouraging feature independence. It is combined with the primary reconstruction loss during training.

VAEs extend the autoencoder framework by encoding input data into a probabilistic distribution, adding a stochastic dimension [270]. The VAE loss comprises both the reconstruction loss and the KL-divergence, L_{KL}:

$$L_{\text{KL}} = -\frac{1}{2} \sum_i (1 + \log(\sigma_i^2) - \mu_i^2 - \sigma_i^2) \tag{5.4}$$

The reconstruction loss considers the decoder's output as a Gaussian distribution, with its mean and variance determined by the neural network and a learnable log standard deviation:

$$L_{\text{rec}} = -\mathbb{E}_{Q \sim q_\Phi(Q|X_{\text{mea}})}[\log p_\Theta(X_{\text{mea}}|Q)] \tag{5.5}$$

The overall VAE loss, L_{VAE}, is:

$$L_{\text{VAE}} = L_{\text{rec}} + \lambda L_{\text{KL}} \tag{5.6}$$

where λ is a weighting factor. Both ICA and VAE offer unique advantages: ICA ensures feature independence, while VAE enhances latent space smoothness and generalizability. By integrating both, we aim to create a kinematic optimizer that balances accuracy, robustness, and interpretability.

Experimental Validation

This study evaluated the effectiveness of an autoencoder-based kinematic optimizer, enhanced with ICA and VAE regularization techniques, on kinematic data from two real-world setups, showcased in Figure 5.4. We initiated this by converting the primary MuJoCo models, representative of our datasets, into kinematic representations and subsequently back into MuJoCo's format for thorough evaluation [11].

The investigation for the hand testbench concentrated on analyzing the joint positions of the index finger, including the MCP, PIP, and DIP joints, alongside the thumb's CMC, MCP, and IP joints. For the knee

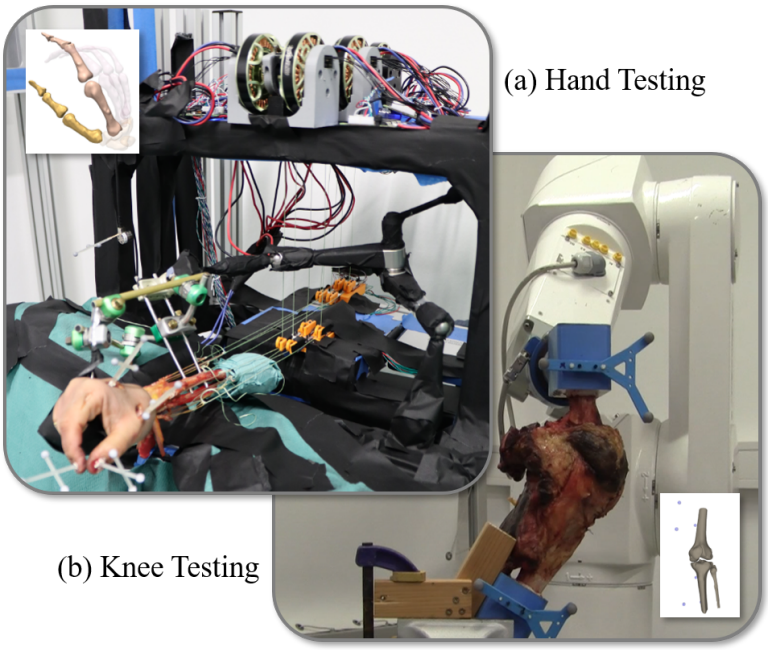

Figure 5.4 Experimental setups for kinematic data acquisition: (a) Hand testbench capturing movements of the index finger's MCP, PIP, and DIP joints, and the thumb's CMC, MCP, and IP joints. (b) Data from Wilhelm et al. [9, 10] representing knee joint motions across multiple DOFs.

joint, known for its complex DOFs, we studied three models reflecting varying degrees of freedom (1 DOF, 2 DOFs, and 3 DOFs) as per the data from Wilhelm et al. [11]. The focus was on pinpointing the most accurate kinematic representations, with particular attention to the 1 and 2 DOF models.

We further enriched our analysis with VAE and ICA techniques, visualizing the motion axes derived from these methods. The primary evaluation metric employed was the reconstruction loss, quantified by the MSE, and applied to a validation subset making up 10% of the total data. The goal was to validate the efficiency of our autoencoder-based kinematic optimizer, especially in light of the incorporation of ICA and VAE regularization techniques [11], thereby advancing our understanding and application of these advanced regularization methods in the context of kinematic optimization.

5.1.3 Results

The performance evaluation of our autoencoder-based kinematic optimizer is central to this section. We focus on the enhancements achieved through the incorporation of ICA and VAE regularization techniques. The evaluation employs data from a hand testbench and a knee joint dataset, aiming to identify all joint axes and solve the corresponding inverse kinematics problem [11].

In the hand testbench experiments, three autoencoder variants were assessed: the standard Autoencoder (AE), the ICA-augmented Autoencoder (AE+ICA), and the VAE. The experiments had dual objectives: to validate the model using both simulated and actual measurement data. The decoder model's axis parameters were initialized randomly for both scenarios. Figure 5.5 illustrates the training progression for hand model joint optimization. The AE+ICA variant exhibited the highest error, while the AE variant demonstrated superior performance, achieving the lowest losses [11].

Turning to the knee joint, its complex structure and multiple DOFs necessitated a detailed evaluation. We assessed the performance of our optimizer across three distinct models, each representing 1 DOF, 2 DOFs, and 3 DOFs. Figure 5.6 visualizes the training progression for these knee joint models. A summary of the MSE values for each model across different DOFs is provided in Table 5.1.

Lastly, all model variants, including AE, AE+ICA, and VAE, provided valid solutions for both forward and inverse kinematics due to their low reconstruction errors. For further analysis, we focused on comparing the joint trajectories derived from AE and AE+ICA, using Wilhelm et al.'s dataset [11]. Figure 5.7 illustrates this

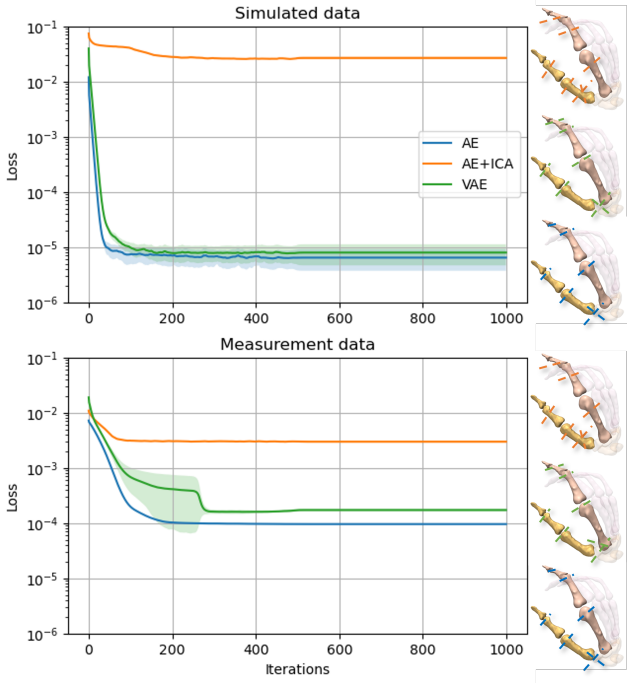

Figure 5.5 Training progression for hand model joint optimization across three independent runs for both simulated and actual measurement data. The MSE loss is plotted for AE (blue), AE+ICA (orange), and VAE (green). Adjacent hand models illustrate the trained joint axes, emphasized using dotted lines in the respective model colors [11].

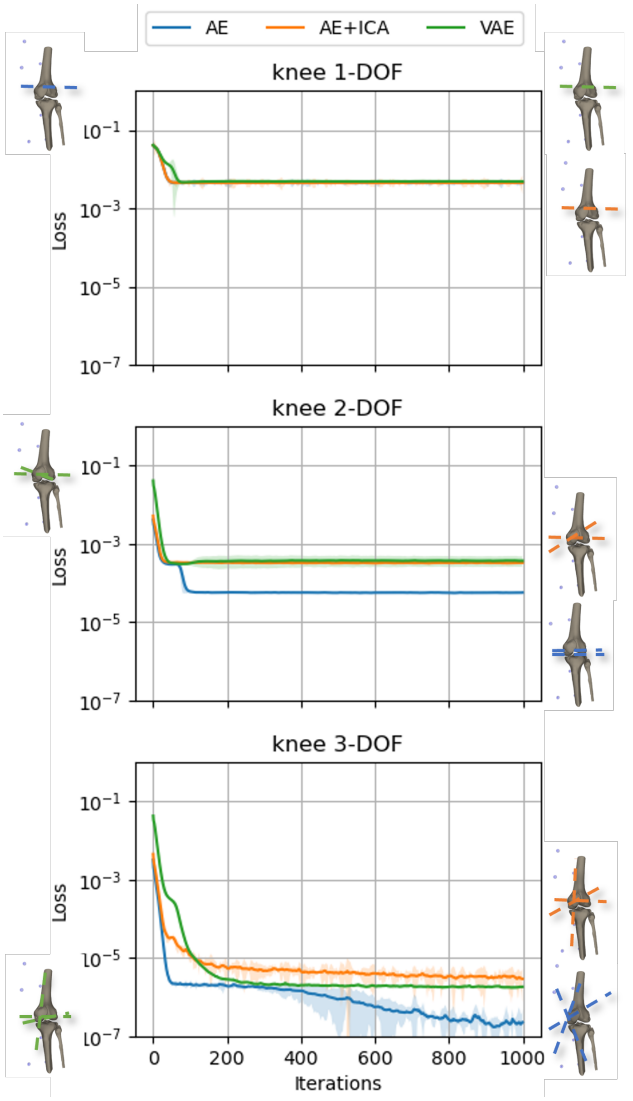

Figure 5.6 Training progression for knee joint models across three independent runs, evaluated using MSE loss on Wilhelm et al.'s validation dataset [11]. The models include the standard AE (blue), AE+ICA (orange), and VAE (green). Adjacent knee models illustrate the derived joint axes [11].

comparison. The AE+ICA method distinctly separated the flexion axis from the other two axes, whereas the AE method showed coupled trajectories, particularly during high flexion angles [11].

5.1.4 Discussion on Autoencoder Kinematics

In this section, we investigate the implications of our experimental findings, focusing on the performance and adaptability of the autoencoder-based kinematic optimizer. The optimizer's performance is particularly noteworthy when enhanced with ICA and VAE techniques [11].

Our experiments spanned two primary domains: a hand testbench and a knee joint model. For the hand testbench, the standard AE and VAE models demonstrated excellent performance in reconstructing simulated data, with errors around 1×10^{-5}. However, these results indicate room for improvement, as errors below 1×10^{-10} are generally expected for simulated data. The identified joint axes closely aligned with the predefined anatomical axes, reinforcing the model's accuracy. On the other hand, the ICA-augmented

Table 5.1 Mean MSE values for each variant across different models, averaged over three independent training runs.

Model	AE	AE+ICA	VAE
Hand	$9.6e-05$	$3.0e-03$	$1.6e-04$
Knee 1-DOF	$4.5e-03$	$4.5e-03$	$4.6e-03$
Knee 2-DOF	$5.6e-05$	$3.2e-04$	$3.1e-04$
Knee 3-DOF	$1.6e-07$	$2.8e-06$	$1.7e-06$

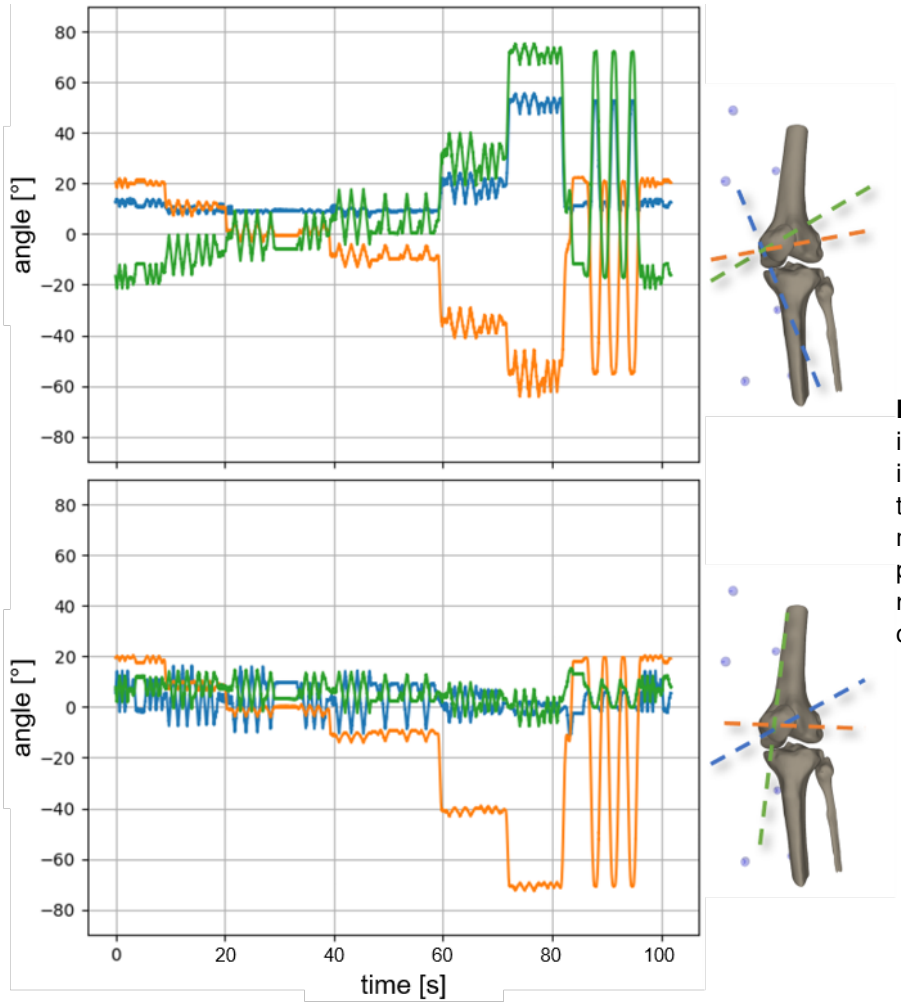

Figure 5.7 Joint trajectory comparison for the 3-DOF knee joint using Wilhelm et al.'s data [11]. The top graph represents the AE-based method, while the bottom graph depicts the AE+ICA approach. Corresponding joint axes are color-coded [11].

model faced challenges in decoupling inherently independent axes. For models with several independent single axes, the methods AE and VAE are therefore to be preferred.

In the context of the knee joint, our models were evaluated across different DOFs. The AE+ICA model excelled in anatomical interpretability, effectively decoupling joint axes in multi-DOF models. The AE model, while precise, may compromise on this interpretability. The VAE model showed robustness, particularly in handling noisy datasets, due to its probabilistic treatment of both input and output spaces. For models with several coupled axes, such as the knee joint, the ICA method is preferred to ensure interpretability.

Our work also presents a comparison between AE and AE+ICA in terms of joint trajectories for the 3-DOF knee joint model. The AE+ICA model's ability to differentiate between the flexion axis and other axes aligns well with anatomical expectations, whereas the AE model's strategy may not always be biomechanically intuitive and interpretable.

The integration of autoencoders in kinematic optimization resonates with existing literature. For instance, the importance of precise trajectory planning highlighted by Li et al. [271] aligns with our objectives. Similarly, the adaptability emphasized by Sundaralingam and Hermans [272] is evident in our AE and AE+ICA models.

Our approach diverges by introducing the efficacy of ICA and VAE as regularization techniques, offering new avenues for kinematic optimization [273, 274].

A limitation of this study is its reliance on only two validation datasets, which may not capture the variability in joint movements across different populations. Additionally, the models make certain assumptions about joint constraints and movement redundancies, which may limit their broader applicability. Future work should aim for a more comprehensive evaluation to validate the derived joint parameters against established systems.

5.1.5 Conclusion on Autoencoder based Kinematics

In this section, we have recaptured the work originally presented in the paper, focusing on a versatile autoencoder-based kinematic optimizer [11]. This optimizer is capable of solving both forward and inverse kinematics across a range of models and datasets. Its architecture is both simple and efficient, making it an innovative contribution to kinematic optimization. The methodology has been particularly effective in identifying surrogate kinematic models with low reconstruction errors for anatomically distinct joints, such as the hand and the knee.

A notable strength of the optimizer is its ability to interpret and identify axes of compromise, a capability particularly apparent in its handling of the knee joint across various degrees of freedom. This attribute enhances the detailed analysis of biomechanical systems, showcasing the optimizer's adaptability and durability. These results confirm the usefulness of this approach in the fields of biomechanics and robotics and point to possible areas for further research and development in these fields.

This segment of the research establishes a robust foundation for the kinematic optimization of previously unidentified biomechanical models. It also facilitates a meaningful comparison between diverse modeling approaches based on their accuracy in reconstructing measured data. Despite its strengths, the current methodology is confined to kinematic considerations and does not extend to more sophisticated model optimization techniques. To address these more complex aspects, advanced methods are developed in the subsequent Section.

5.2 Model-Free Proximal Policy Optimization for Dynamic Optimization

While differentiable physics-based models offer gradient-based optimization techniques, they often face challenges in backpropagating to relevant dynamic parameters, particularly in complex biomechanical systems [166, 167]. This limitation is especially pronounced in robotic applications, where the systems are frequently treated as black boxes. To address this, model-free solutions like evolutionary algorithms and reinforcement learning have gained prominence, as they effectively bridge the "reality gap" between simulated and real-world behavior [168].

Recent advancements in reinforcement learning-based optimization techniques have shown promising results across various domains, from quantum control [169] to thermal power unit efficiency [170]. These techniques offer a viable alternative to traditional differentiable models, particularly when the focus shifts from kinematic constraints to the definition of select dynamic parameters like stiffness and damping characteristics [171, 172].

The primary contribution of this section is the introduction of a novel reinforcement learning-based optimization procedure designed to minimize the divergence between measurement data and model output. This approach enhances the model's predictive capabilities and is particularly well-suited for complex systems where differentiable models fall short. Grounded in state-of-the-art reinforcement learning techniques, specifically proximal policy optimization [275], this work aims to provide a robust and accurate method for system identification and parameter optimization, thereby advancing the field of robotic control and optimization algorithms.

5.2.1 Reinforcement Learning-Based System Identification: Model Generation and Initial Setup

The process of model generation is outlined in Figure 5.8, which serves as a comprehensive guide for creating a biomechanical model suitable for reinforcement learning-based optimization.

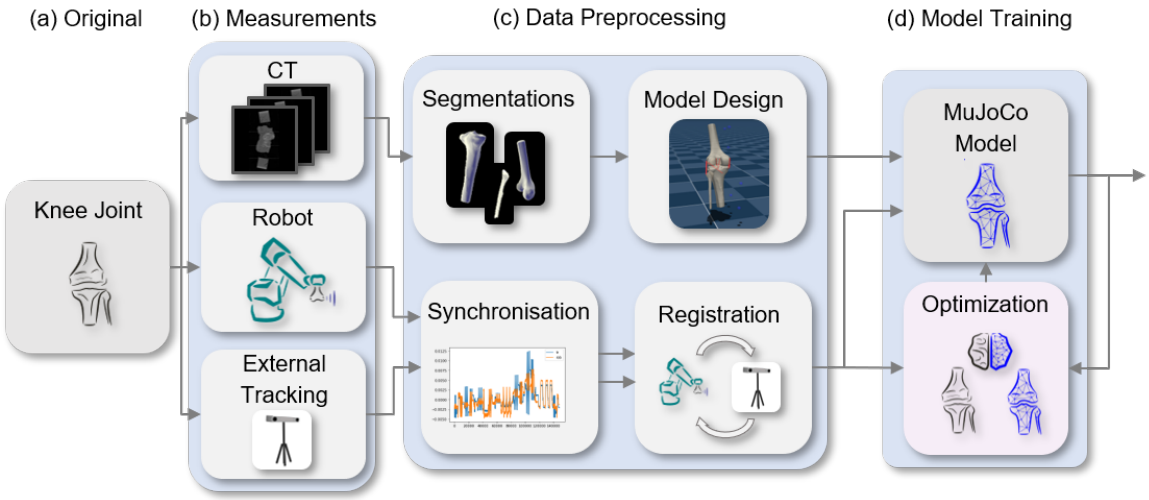

Figure 5.8 Workflow for generating the biomechanical model. The model is initially created based on segmented CT data and synchronized robot and tracking data. Further optimization is performed based on the measurement data [12].

Model generation begins with the acquisition of multimodal data, including CT scans for geometry and dynamic recordings of position, forces, and torques. This raw data is then processed to create an initial model using the MuJoCo physics engine [266]. The model incorporates segmented bones and annotated attachment points for tendons and ligaments, with properties estimated based on existing literature [276, 277]. The dynamic data is temporally synchronized and transformed into the model's coordinate system. This enables model manipulation and sets the stage for the reinforcement learning-based parameter optimization.

The initial model comprises four primary bones, simplified into two rigid bodies for computational efficiency. Convex collision meshes are generated to simulate realistic bone-to-bone interactions [278]. Attachment points for significant ligaments are marked and serve as the basis for the model's dynamic properties. These properties, encapsulated in the parameter vector ψ, are set as learnable parameters for subsequent optimization.

Reinforcement Learning-Based Parameter Adaptation

The challenge of parameter optimization in non-differentiable simulators is addressed by formulating it as a reinforcement learning problem. The objective is to minimize the divergence between the simulated motion x_{Sim} and the measured motion x_{Mea}, under the same measured force-torque FT_{Mea}.

$$\min_{\psi} \left[x_{\text{Sim}}(FT_{\text{Mea}}, \psi, t) - x_{\text{Mea}}(FT_{\text{Mea}}, t)\right]^2 \tag{5.7}$$

The reward function incorporates both the desired motion behavior and the stability of the process:

$$\text{reward}(t) = 1 + \lambda \left[x_{\text{Sim}}(t) - x_{\text{Mea}}(t)\right]^2 \tag{5.8}$$

Here, λ serves as a hyperparameter that balances between robust training and asymptotic behavior.

In this setup, the actor in the reinforcement learning framework selects a set of parameters ψ at the beginning of each trajectory and maintains it throughout, unlike traditional Reinforcement Learning (RL) where actions are state-dependent. This is formalized as:

$$\pi_{\psi}(a_{\tau}) = \text{const.} \; \forall \; t \in \tau \tag{5.9}$$

The optimization problem can thus be expressed as maximizing the expected reward over trajectories τ:

$$\max_{\psi} U(\psi) = \sum_{\tau} P(\tau, \psi) R(\tau) \tag{5.10}$$

The gradient for this optimization problem aligns closely with traditional policy gradient methods:

$$\hat{g} = \hat{\mathbb{E}}_t \left[\nabla_{\psi} \log \pi_{\psi}(a_\tau) \hat{A}_t \right] \tag{5.11}$$

PPO is employed for this parameter optimization, given its robust training procedure and enhanced asymptotic behavior. The full parameter optimization algorithm is shown in Algorithm 1.

Algorithm 1 Proposed algorithm for system identification [12]. Derived from Schulman et al. [275].

Initialize policy parameters ψ_0, initial value function parameters η_0
while not converged **do**
  Initialize empty set of local trajectories $\mathbb{D}$.
  while Number of max timesteps $t_{\max}$ not reached **do**
    Sample a trajectory from the measurement τ_{mea}.
    Generate the local parameters $\psi = \pi_{\psi}$ and update the simulator.
    Set the simulator in position $x_{\mathrm{Sim},t_0} = x_{\mathrm{Mea},t_0}$.
    Simulate by using FT_{Mea} and collect $x_{\mathrm{Sim},t}$.
    Append collected trajectory to $\mathbb{D}$.
  end while
  Compute rewards-to-go $\hat{R}_t$.
  Compute advantage estimates $\hat{A}_t$ for all collected timesteps.
  Update the policy by maximizing the PPO-Clip objective:
  $\psi_{\mathrm{new}} = \underset{\psi}{\mathrm{argmax}} \sum_{\tau \in \mathbb{D}} \sum_{t=0}^{T} \left(\frac{\pi_{\psi}(a_\tau)}{\pi_{\psi_{\mathrm{old}}}(a_\tau)} \hat{A}^{\pi_{\psi_{\mathrm{old}}}}(s_t, a_\tau), g(\epsilon, \hat{A}^{\pi_{\psi_{\mathrm{old}}}}(s_t, a_\tau) \right)$,
  with $g(\epsilon, A) = \begin{cases} (1+\epsilon)A & \text{if } A \geq 0 \\ (1-\epsilon)A & \text{otherwise} \end{cases}$
  Update the value function by regression:
  $\eta_{\mathrm{new}} = \underset{\eta}{\mathrm{argmin}} \sum_{\tau \in \mathbb{D}} \sum_{t=0}^{T} \left(V_{\eta}(s_t) - \hat{R}_t \right)^2$
end while

To address the increased policy gradient variance arising from constant parameters over long trajectories, the measurement data is segmented into smaller, randomly selected regions to form localized measurement trajectories τ_{mea}. The simulation model is initialized at the start of each local series, and parameters are generated via the stochastic policy $\pi_{\psi}(a_\tau)$. The motion trajectory x_{sim} is then simulated using the parameterized model and measured force-torque data. Simulation termination occurs if instability or excessive velocity is detected. The policy gradient is subsequently computed using an additional value function V_{η} to calculate the advantage, thereby minimizing update variance.

Validation of Parameter Optimizer: Experimental Setup and Data Sources

Our validation approach for the parameter optimizer is implemented through two distinct experimental setups. In the first setup, we utilize a simplified surrogate model of a knee joint, designed to create a controlled environment for assessing the optimizer's effectiveness. As illustrated in Figure 5.9 b, the model features a double plate structure linked by a central rotational joint, with diagonally arranged tendons. This configuration is intended to mimic basic dynamics of the knee joint. We generate simulated measurement data from this model, allocating 90% for training purposes and 10% for validation. The primary goal is to test the optimizer's ability to precisely identify parameters and reconstruct trajectories.

The second part of our validation employs real-world data, sourced from Wilhelm et al. [9]. Unlike the surrogate model, this dataset lacks a ground truth, challenging the optimizer to identify plausible parameters

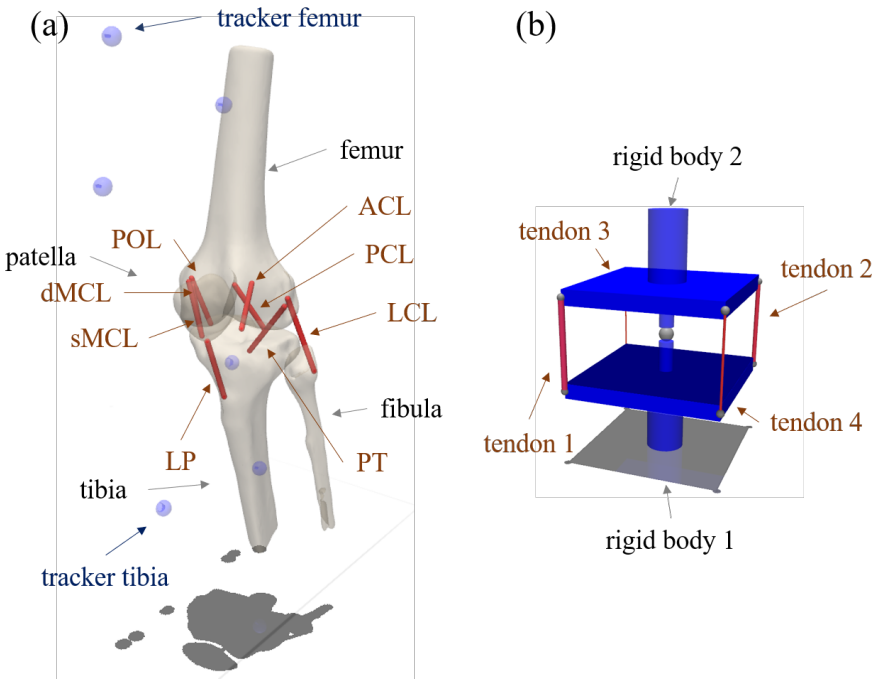

Figure 5.9 Figure (a) depicts the MuJoCo-simulated knee joint model, illustrating results from CT segmentation and the pinpointing of ligament attachment sites. This visual emphasizes key skeletal structures alongside the tendons and ligaments vital to the knee's dynamic and kinematic properties. Figure (b) presents a schematic of the simplified surrogate plate model, comprising two plates linked by four tendons around a central rotational joint. Applied external forces and torques to the upper plate induce simulated movements, forming the basis for the optimization dataset [12].

based on an initial approximation of the knee joint model. The tests were conducted at various flexion angles and had a total recording duration of 23 minutes, providing a robust dataset for further model identification.

5.2.2 Adaptive System Calibration with Simulated Environments

The efficacy of the optimization algorithm was evaluated within a simulated framework, utilizing the simplified Mujoco model illustrated in Figure 5.9 b, which was crafted to mirror the controlled conditions of experimental setups accurately. Through a sequence of five distinct training sessions, the algorithm's capability to precisely identify unknown parameters within the simulation was assessed. The training duration extended over 10000 iterations, with λ set to 1, considering the system exhibited no stability issues. Figure 5.10 systematically showcases the findings from these experimental runs. Figure 5.10 presents the optimization results from five distinct training iterations. Specifically, Panel (a) illustrates the trajectory of the MSE parameter across these iterations. Panel (b) compares the initial output of the system with actual empirical data, while Panel (c) shows the system's output at the end of the training process. In these graphical representations, dotted lines indicate the empirical data targeted for approximation, and solid lines depict the outputs from the simulation model at both the initial and final stages.

The results show a significant decrease in the MSE from values above 1×10^3 to below 1×10^2. This reduction underscores the optimizer's capability to fine-tune simulation parameters to closely match experimental data. The comparison of system outputs before and after optimization, as depicted in Panels (b) and (c), initially reveals discrepancies between the model predictions and the actual data. However, the post-optimization results in Panel (c) demonstrate an excellent alignment, with the MSE optimized to below 5×10^{-4}. This precision illustrates the optimizer's effectiveness in minimizing errors and its ability to generate validation trajectories that closely replicate real-world phenomena, emphasizing the value of computational models in accurately simulating physical systems.

An in-depth review of the parameter adjustment over the course of training for the plate model is provided in Figure 5.11, offering insights into how each parameter evolved during the optimization process.

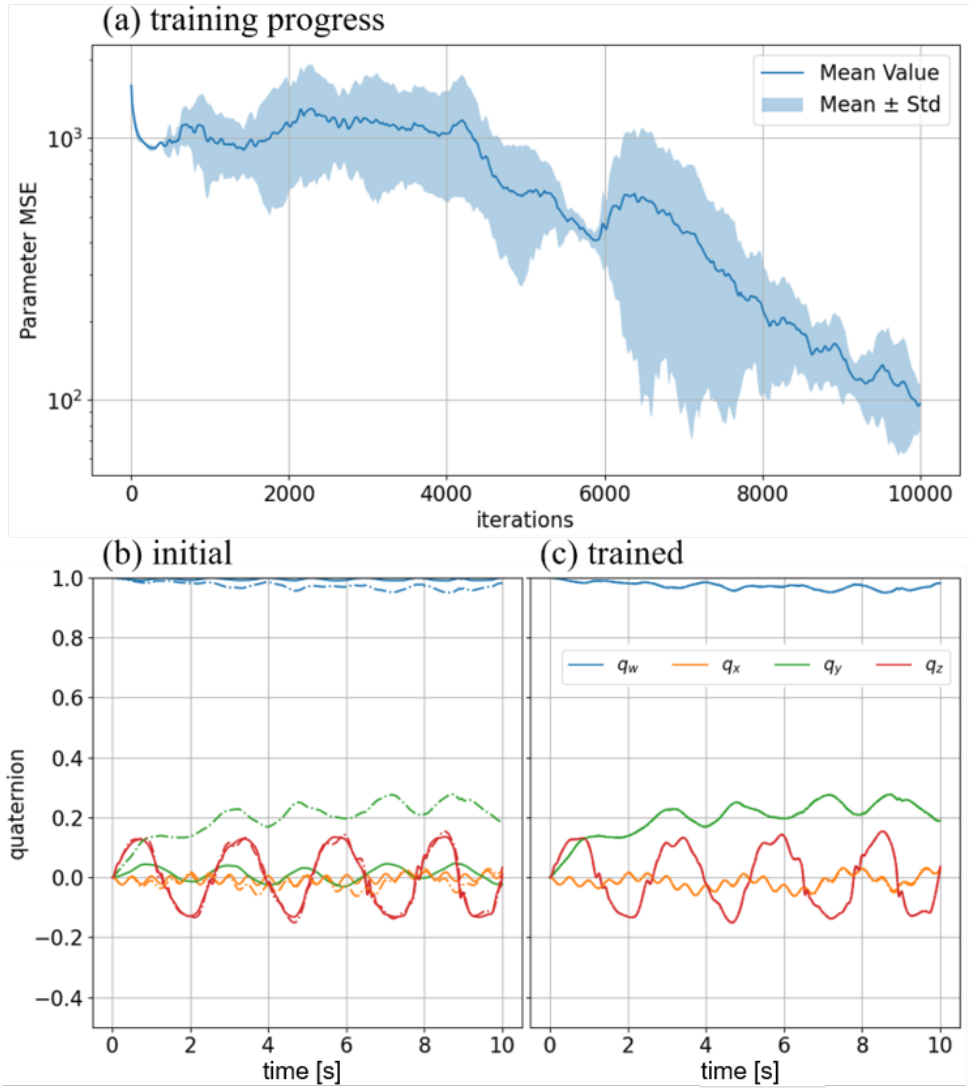

Figure 5.10 Outcomes of plate optimization across five independent training sessions are depicted. Panel (a) displays the MSE parameter evolution throughout the training iterations. Panel (b) illustrates the initial system response in comparison with the actual measurements, while panel (c) demonstrates the final system response after completion of the training. Dotted lines represent the ground truth measurements targeted for fitting, whereas solid lines indicate the simulation model's current output for plot (b) and (c) [12].

Figure 5.11 presents the optimization trajectory for parameters within the plate system over five training sessions. It plots the evolution of stiffness and damping parameters, with the actual values used in data synthesis marked in red. This analysis reveals the optimizer's success in closely estimating the true parameters, especially in determining stiffness values. However, a persistent variance in damping values, particularly for tendon-2, suggests minor challenges in achieving complete accuracy, highlighting areas for further refinement in the optimizer's approach.

5.2.3 Automatic System Adaptation for Real-World Data

Transitioning to the application of our detailed knee model, as depicted in Figure 5.9 (a), to real-world datasets revealed stability challenges within the simulation model. These challenges necessitated careful adjustments to the λ parameter, striking a delicate balance between ensuring system stability and maintaining the precision of measurements.

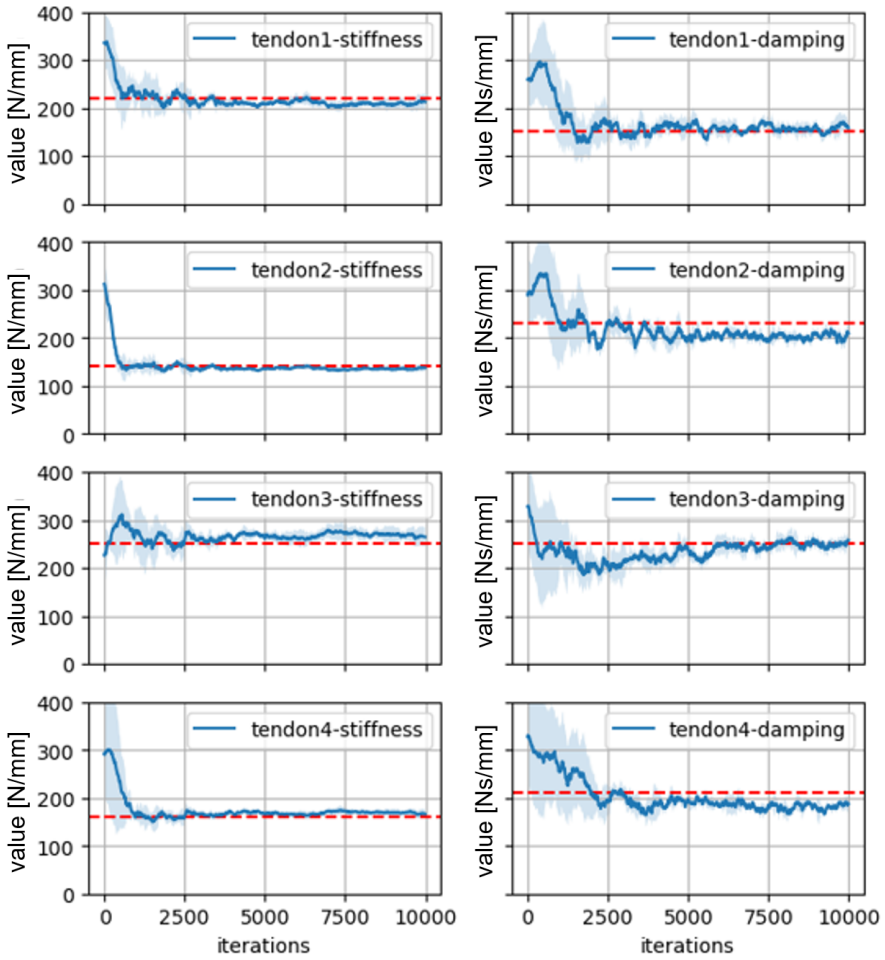

Figure 5.11 Parameter optimization results for the plate system during five individual training runs. The graph shows the stiffness and damping values evolving over time, with the true values used for data synthesis marked in red [12].

In our efforts to refine the balance between system parameters, we evaluated the effectiveness of the algorithm for automatic system identification by varying the λ values through five distinct training iterations, specifically examining λ values of 1, 2, 10, 20, 50. These iterations were thoroughly analyzed to determine the optimal training approach. The PPO algorithm supported this investigation, targeting precise identification of the knee model's system dynamics, as illustrated in Figure 5.12. Training was methodically carried out in segments of up to 50 time steps, using measurement data until the system either reached instability or exceeded a predefined critical velocity of v_{crit} = 20 m/s.

This training evidenced marked improvements in simulation stability and extended episode lengths across the spectrum of λ values. Notably, exceedingly high λ values, such as λ = 50, corresponded with reduced episode lengths and heightened training instability. Conversely, a λ value of 20 exhibited optimal performance in terms of validation dataset simulation accuracy. Lesser λ values, namely 1,2, showed minimal enhancements in performance.

The optimizer's refinement of motion trajectories was rigorously assessed against a hold-out validation set, encompassing measurement trajectories previously unutilized during training. This assessment contrasted initial simulation outcomes against those from the optimized model, underscoring the accuracy of the system identification method. As depicted in Figure 5.13, this comparison illustrates significant enhancements in aligning simulation outputs with empirical data, particularly evident in the improved correlation for position and quaternion trajectories.

Initially, discrepancies between the model's predictions and actual measurements highlighted early simulation inaccuracies. Post-training outcomes, however, demonstrate a considerable reduction in validation error

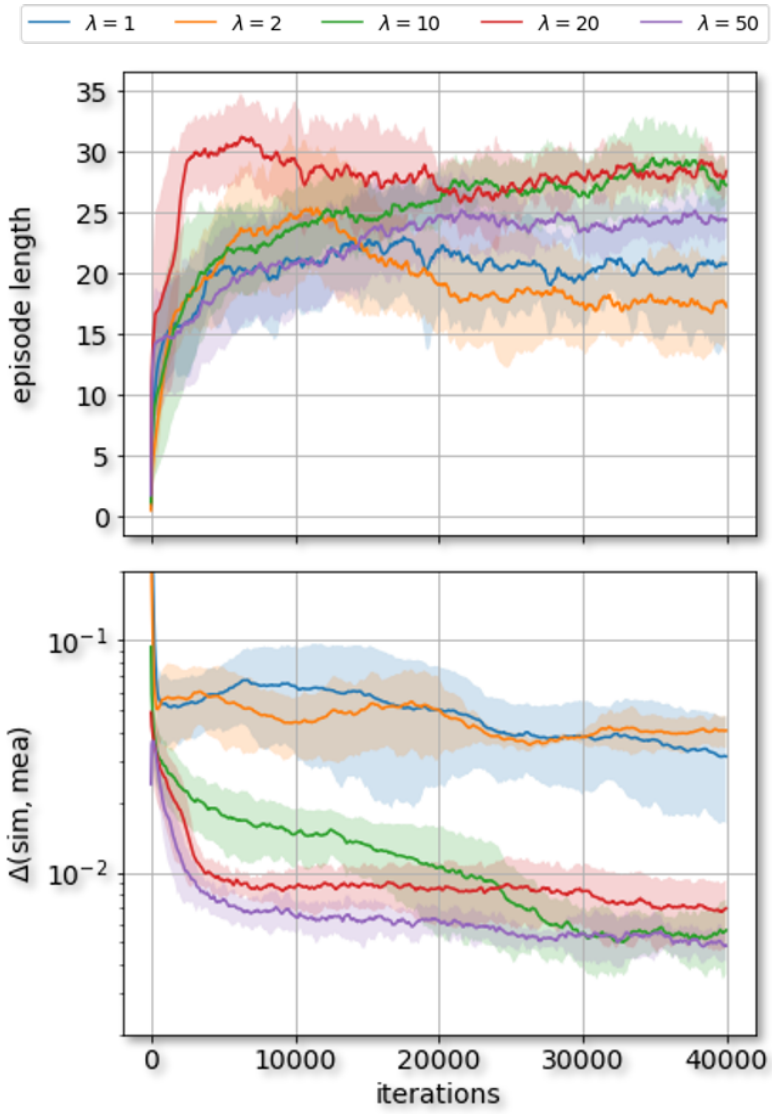

Figure 5.12 Illustrating the progress in system identification training for the knee joint across varied λ values. Displayed are the simulation trajectories' average lengths (top) and the per-time-step mean error between measurements and simulation outcomes (bottom), detailed as mean ± standard deviation [12].

and a closer approximation of actual motion trajectories by the optimized model. Nonetheless, discrepancies in certain trajectory components underscore the complexities and limitations inherent in accurately modeling dynamic systems, signaling areas for further refinement and optimization in our approach to achieving more precise and reliable simulation results for real-world applications.

5.2.4 Discussion on the Reinforcement Optimizer

This section evaluated a reinforcement learning-based optimizer for system identification in both simulated and real-world settings. The optimizer demonstrated robust performance in the simulated environment, effectively minimizing both immediate and long-term prediction errors.

In real-world applications, the optimizer's efficacy was notably influenced by the hyperparameter λ, with a value of 20 proving optimal. This highlights the importance of hyperparameter tuning for real-world performance. The optimizer utilizes PPO to adapt existing models to measured data, thereby extending simulation duration and system stability. This narrows the gap between simulated and real-world data, enhancing the model's general applicability.

The study confirms the optimizer's utility in complex, potentially non-differentiable systems and sets the stage for future research aimed at improving its robustness and accuracy. It also reiterates the limitations

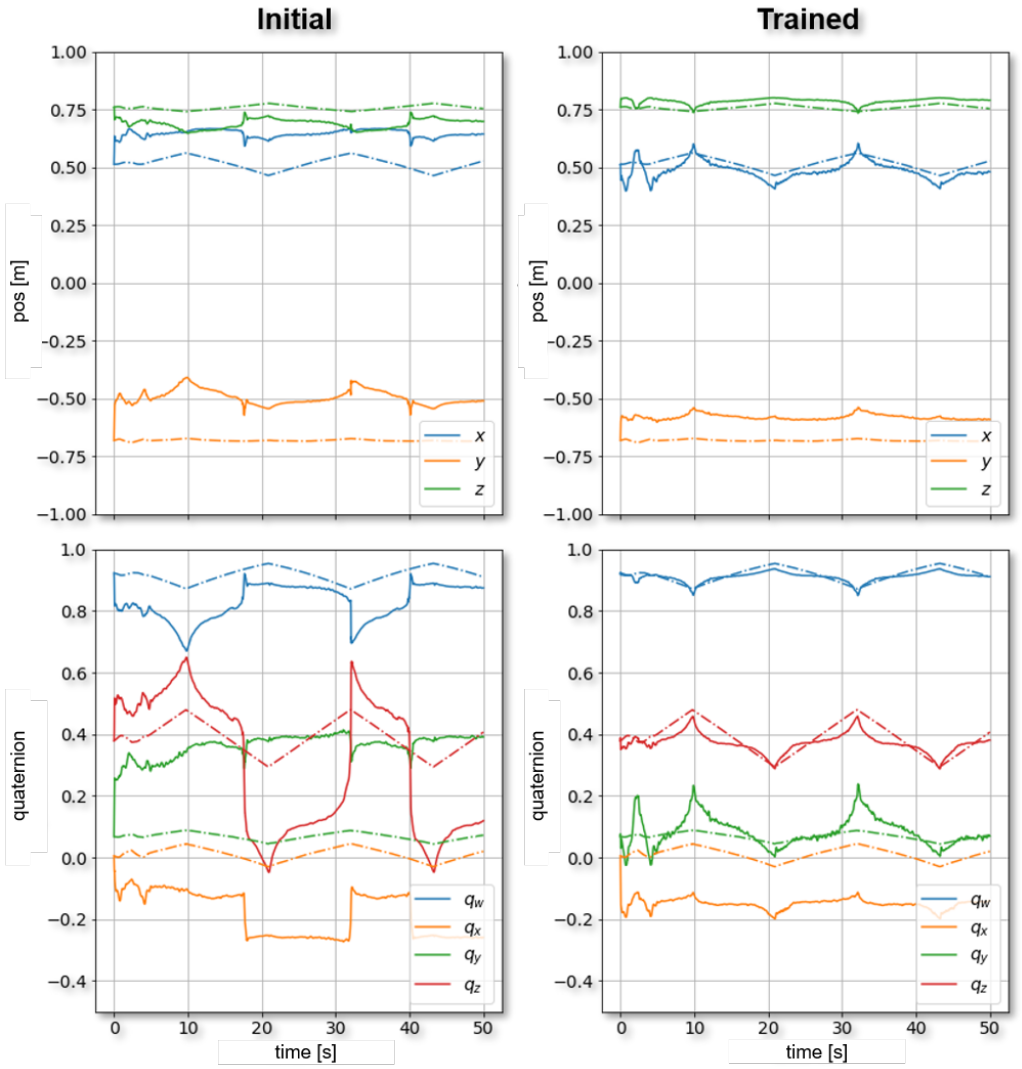

Figure 5.13 Comparing simulated motion trajectories with actual data over a 50-second validation period, focusing on position data (top) and quaternion trajectories (bottom). Solid lines represent simulation outputs; dotted lines denote empirical data from the robotic knee testbench, illustrating initial predictions versus optimized model predictions [12].

discussed earlier, such as the challenges posed by cadaveric experiments, the simplifications in the initial model, and the inherent constraints of the simulated environment.

Limitations

Although the proposed parameter optimizer presents notable advancements, its applicability is restricted. It is effective only when the system model is explicitly known and the range of parameters can be realistically narrowed. Furthermore, successful parameter identification critically depends on the adequacy of the collected data variety, which must support unambiguous parameter determination. However, even with an optimal data scenario, limitations of the algorithm persist, and it cannot be assured that it will correctly identify system parameters for every scenario.

Moreover, the identification and modeling of real models for complex joints like the knee remain significant challenges in research. The optimizer described herein merely facilitates approximate solutions, provided the fundamental prerequisites are adequately met. Although the solutions demonstrated using MuJoCo represent a preliminary step forward, they omit crucial joint components such as the menisci and other

soft tissues. Consequently, the parameters optimized are specific to the current model and do not directly translate to more complex or realistic models.

Conclusions

This section has introduced a reinforcement learning-based optimizer that utilizes proximal policy optimization for system identification in both simulated and real-world knee models. While the optimizer demonstrates high predictive accuracy, it encounters difficulties in uniquely identifying system parameters. This methodology offers exciting prospects for research into complex kinematic systems and underscores the significance of hyperparameter tuning. Future efforts will aim to improve the optimizer's robustness and focus on the necessary prerequisites for data collection to achieve unique parameter identification. Additionally, work will extend to developing personalized models, broadening the application of this technology.

6 Conclusions

This dissertation addresses the central research question: How can an adaptive, multidisciplinary system for analyzing and predicting joint health be effectively developed in the context of orthopedic patient care? The primary objective of the studies presented was to integrate cutting-edge developments in medical informatics, robotics, and orthopedics. This integration led to the creation of a comprehensive toolkit aimed at enhancing patient outcomes. The effectiveness of this toolkit is demonstrated through various individual studies conducted as part of this research.

The framework presented in Figure 6.1 consists of four main components, all of which contribute to a collaborative approach to orthopaedic care. Chapter 2 introduces the concept of wearable technology and describes preoperative gait analysis using inertial measurement units (IMUs) and postoperative rehabilitation using an innovative finger exoskeleton. Chapter 3 addresses planning and prediction algorithms that include important features such as bone tumor detection and limb alignment, which are crucial for efficient preoperative planning. Chapter 4 focuses on robotic test platforms designed for accurate simulation of joint dynamics and includes specialized test benches for knee and hand joint analysis. Subsequently, Chapter 5 examines model optimization, completing the development of the framework. Collectively, these chapters introduce a versatile, integrated toolset that serves both clinicians and researchers in the field of orthopedics, enhancing their capabilities in joint health analysis.

Drawing an analogy to the Kalman filter, a well-established recursive algorithm for state estimation cited in [279], this dissertation similarly adopts an iterative enhancement approach in its structure. Analogous to the prediction phase of the Kalman filter, the Planning and Prediction Algorithms (Chapter 3) generate forecasts based on existing datasets and models. These forecasts are enriched with inputs from diverse sources, such as data from Robotic Testing Platforms (Chapter 4) and Wearable Technology (Chapter 2), improving the accuracy of the predictions. The refinement of these forecasts mirrors the Kalman filter's update phase and is executed by the Model Optimization Algorithms (Chapter 5). This cyclical process of prediction and refinement, incorporating empirical data from the testing platforms, progressively refines the initial forecasts. This methodology highlights the dissertation's effective and flexible framework in tackling the complexities of human joint management.

The integration of medical informatics, robotics, and orthopedics offers an innovative approach to patient care and research. Medical informatics serves as the foundation of this strategy, facilitating data-driven decision-making; robotics enhances precision and automation, particularly in data collection and mechanical testing; and orthopedics provides essential clinical insights, focusing on the specific needs and treatment outcomes of patients. This multidisciplinary integration extends beyond the limits of each individual field, enabling a more thorough analysis of joint health, improving preoperative planning, and enables the creation of personalized treatment strategies. This approach not only addresses existing research gaps but also provides a broader view of joint health, equipping clinicians and researchers with an advanced toolkit to improve patient care.

6.1 Contributions

This research was initiated in response to the increasing age of the global population [14] and the vital need to maintain mobility and joint health to ensure a high quality of life [15]. Additionally, the growing shortage of healthcare workers [17] and demographic shifts underscore the urgent need for technological interventions and automation to address care shortages. The thesis aims to harness the capabilities of AI and robotics to improve joint healthcare. It proposes the use of robotic wearables for objective patient data collection and the automation of rehabilitation processes to reduce the burden on orthopedic surgeons. This includes

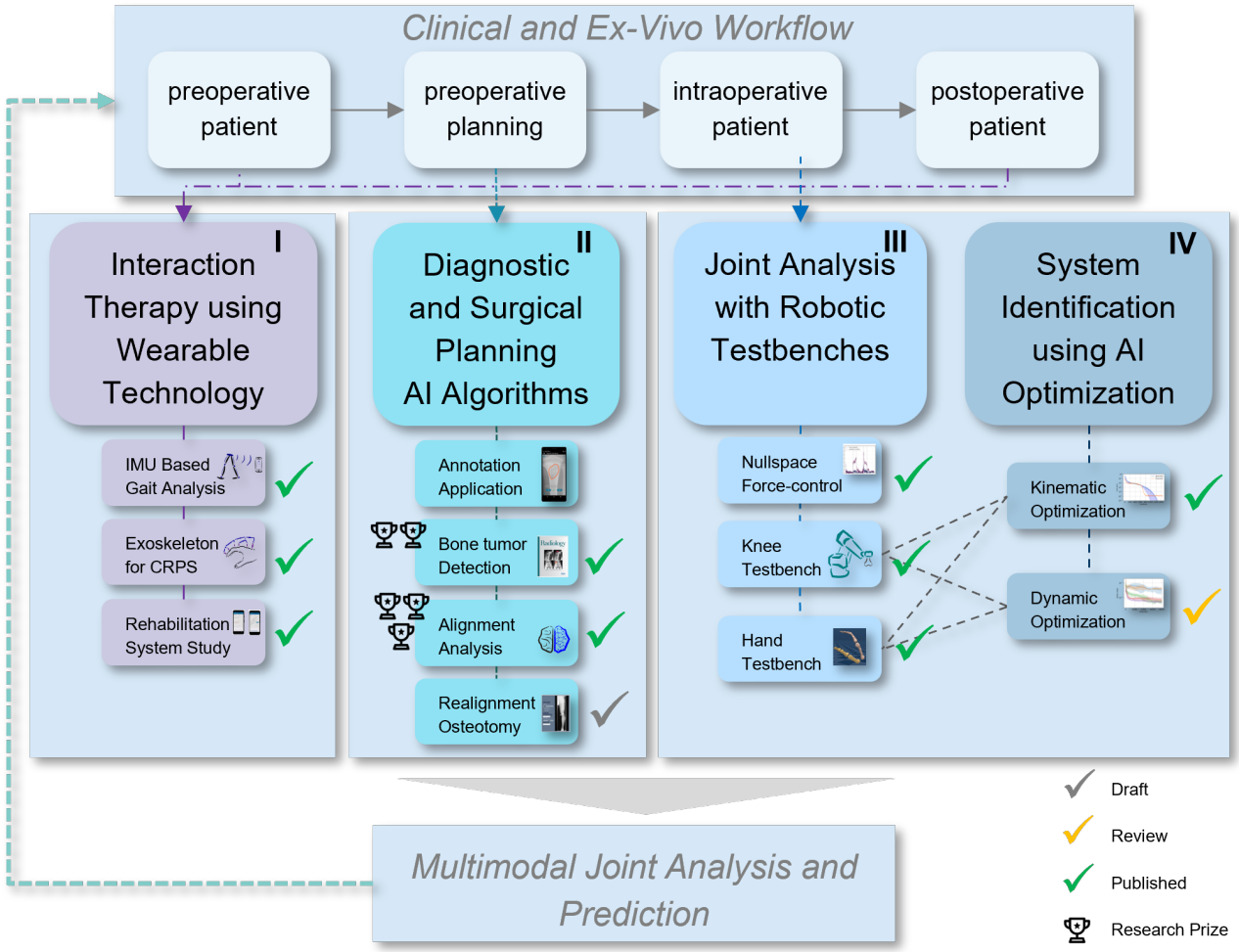

Figure 6.1 The contributions in a clinical context, starting with 1) wearables, 2) diagnostics and planning, 3) robotic test benches and 4) optimization. Each contribution is organized according to its main topic and the connections between the topics are visualized by dashed lines. The most important links to the clinical workflow are indicated by the connection to the clinical context at the top. In addition, the corresponding publication status and any research awards are indicated for each article.

enhancing joint analysis through robotic testbenches and employing AI-based optimization for personalized treatment planning.

The thesis envisions a seamless integration of robotics and AI into orthopedic care, spanning from preoperative assessments to postoperative recovery. A comprehensive framework was developed, incorporating a multimodal joint analysis toolkit for clinical use. This toolkit includes gait analysis, preoperative planning, intraoperative support through robotic testbenches, and postoperative rehabilitation assistance with exoskeletons and optimization algorithms. This integration represents an advancement in delivering orthopedic care, enhancing both the precision of treatments and the efficiency of recovery processes.

Additionally, the thesis underwent extensive verification and validation, with experiments conducted to demonstrate the practicality and effectiveness of the developed tools. These experiments validated the relevance and feasibility of the methods for clinical application, underscoring the reliability and efficacy of the proposed technologies and methodologies. The collective achievements documented in this thesis represent advancements in orthopedic care, effectively meeting its objectives and making a meaningful contribution to the field.

6.2 Addressing Objectives and Research Questions

This thesis employs a multidisciplinary approach to tackle essential objectives and research questions aimed at improving orthopedic care, guiding its contributions toward advancements in both technological innovations and clinical practices. The research investigates the complexities of orthopedic biomechanics, with a special emphasis on hand and knee joints. It establishes a robust foundation that not only broadens our understanding but also supports the development of an innovative, adaptive, multimodal framework designed to address these complexities ([9, 10]).

In addressing the first research question, the integration of wearable and robotic technologies into clinical orthopaedic workflows, this thesis has demonstrated how real-time objective data can be collected and utilized for the prevention and rehabilitation of joint diseases. By leveraging IMUs for gait analysis and exoskeleton technologies for finger rehabilitation ([1–3]), the research underlines the potential of these technologies to provide critical insights into patient mobility and rehabilitation progress, thereby advancing personalized orthopaedic care.

The potential benefits and challenges of using AI for image analysis in orthopedic diagnostics and surgical planning, as outlined in the second research question, have been extensively evaluated. The development of diagnostic algorithms for data annotation, bone tumor detection ([4]), and limb alignment ([6]) represent significant strides towards integrating AI into the clinical workflow. These advancements not only improve the accuracy and reliability of diagnostics but also underscore the challenges of clinical implementation, including data privacy concerns and the need for algorithmic transparency.

The development and application of specialized robotic testbenches for biomechanical research advance the investigation into the comprehensive analysis of human joints, addressing the third research question. These testbenches incorporate sophisticated control algorithms capable of executing multiple tasks with precision, prioritizing specific functions while dynamically adjusting to the unique biomechanical structures encountered. This adaptability is illustrated by the introduction of a null-space control system for the knee testbench ([8]), which demonstrates an innovative approach to managing complex, variable tasks. The capabilities of these testbenches extend beyond traditional methodologies, enabling high-resolution in-depth ex-vivo experimentation. They open new avenues for the detailed exploration of the mechanical properties and dynamic behaviors of knee and hand joints ([9, 10]), with the hand testbench, in particular, offering fundamental insights into hand mechanics and generating comprehensive, previously inaccessible multimodal datasets. This work not only underscores the complexity of human joints but also highlights the critical role that robotics plays in enhancing our understanding and improving the management of orthopedic conditions. Through these advancements, the thesis contributes significantly to the field, offering a refined understanding of joint mechanics and the potential for improved diagnostic and therapeutic strategies in orthopedics.

Finally, the thesis addresses the application of AI algorithms to biomechanical systems for improved modeling of joint behavior, tackling the fourth research question. Through the development of optimization techniques, such as kinematic model optimization ([11]), and reinforcement-based optimization ([12]), this research proposes new methodologies for the accurate and efficient analysis of joint kinematics and dynamics. These contributions not only advance the theoretical framework for biomechanical modeling but also promise to enhance the precision of clinical diagnostics and interventions.

6.3 Limitations

This dissertation advances the multidisciplinary analysis and prediction of joint health. However, it is essential to recognize its limitations in order to achieve a balanced understanding and identify future research directions.

The framework, while innovative, exhibits a degree of modular isolation. Each module, designed to address specific aspects of joint health, operates effectively on its own. However, this independence results in a lack of an integrated, cohesive approach. Such modular isolation potentially limits the ability to achieve a holistic understanding and treatment of joint health. This is particularly evident in the framework's focus

on specific joints, primarily the knee and hand. While this specialization allows for targeted solutions, it restrictively narrows the framework's applicability and universality, limiting its utility across a diverse range of joint types. Integrating the various components of the framework presents its own set of challenges. For instance, the planning algorithms, a critical component of the framework, do not seamlessly interface with the multimodal joint analysis and wearable technology. This lack of integration can lead to inefficiencies and reduced effectiveness. Furthermore, one key projects underpinning the framework in Wilhelm et al. [12] is still pending peer review. The outcomes of these reviews are uncertain, and the possibility of significant revisions or rejection could impact the framework's robustness and reliability.

Another limitation lies in the absence of clinical validation of parts of the presented contributions. Although the framework shows promise in controlled ex-vivo settings, parts of it have not been validated in clinical environments. This raises questions about its practical applicability and effectiveness in real-world healthcare scenarios. Additionally, the computational demands of certain algorithms, especially those involved in planning and predictive modeling, are substantial. This high computational intensity could hinder the real-time application of these algorithms in clinical settings, where rapid processing and responsiveness are often crucial. In summary, although the thesis contributes to the field of orthopaedics, these limitations need to be addressed in order to fully exploit the potential of the proposed framework.

6.4 Achievements

The research and methodologies presented in this thesis have made significant contributions to the field of orthopedics, influencing both academic discourse and practical applications. The widespread impact of this work is evident from achievements in various areas, showcasing its relevance and effectiveness in addressing real-world challenges.

Notably, the development of a bone tumor detection algorithm stands out, which has gained significant recognition in the healthcare sector. This includes receiving the trainee research prize at the RSNA 2020, the best abstract award at DKSMR 2021, and being featured on the Radiology journal's cover in September 2021. Such recognitions not only underline the algorithm's innovation but also its pivotal role in enhancing radiological and oncological practices. Additionally, this work has inspired new AI-based projects at our university, further demonstrating its influence in advancing medical diagnostics AI research. The presented surgical planning algorithm has also received several awards, including the Digitization Award at DKOU 2023 [280], a second prize for the best paper at AGA 2023 and the award for the best poster at OT Digital 2023. These awards reflect the algorithm's novel approach to surgical planning and its potential to surgical procedures. In addition, this work has driven the development of a new exoskeleton frame that is making a major contribution to wearable technology in orthopaedics, particularly in rehabilitation and improving mobility. Releasing data from robotic test rigs as open source will support a culture of collaboration and knowledge sharing that is essential for future advances in biomechanical modeling. Furthermore, the introduction of a comprehensive framework for data collection and prediction applicable to different joints is an essential step towards personalized, precise and efficient orthopaedic treatments. This framework underlines the comprehensive contribution of this work to clinical orthopaedics and improves treatment methods.

In summary, the influence of this work extends beyond academic circles as it paves the way for practical innovation and encourages further research in orthopaedics. The various achievements of this work, which have been recognized with prestigious awards, have had a profound impact on the medical community and represent a significant advance in orthopaedic research and practice.

6.5 Future Directions in Orthopedic Robotics and AI

This dissertation establishes a foundational base for future advancements in orthopedics through the integration of robotics and AI, identifying pivotal areas for research progression. There exists a notable opportunity for the enhancement of robotic wearables in orthopedics, emphasizing the need for improve-

ments in ergonomics, user engagement, and durability. The execution of extensive clinical trials and the application of machine learning for predictive diagnostics stand out as critical steps for advancing these technologies, aiming to elevate patient care by early identification of joint issues.

The advancement of AI in orthopaedics represents transformative potential for clinical workflows and requires refined AI models for customized treatment options as well as addressing privacy and computational efficiency concerns to promote the clinical integration of AI. Investigating the long-term effectiveness of AI and robotic wearables, ethical guidelines for AI in decision making and its extension to telemedicine are essential areas for comprehensive studies. In addition, the personalization of treatment plans through advanced modeling for customized prosthetics and consideration of individual biomechanics signals a significant shift towards optimizing patient-specific care. This approach, which is being extended to various orthopaedic conditions, could significantly improve the effectiveness of treatment. In addition, research into adaptable, modular robotic systems and the integration of AI into the development of orthopaedic implants will significantly impact patient outcomes, highlighting the importance of understanding the psychological and social impact of these technologies on patients.

The need for interdisciplinary collaboration is emphasized as a key driver for innovation, with contributions from clinicians, bioengineers and computer scientists enriching orthopaedic technology development. Such synergistic efforts are expected to lead to breakthroughs in orthopaedic care, highlighting the multi-faceted approach required to advance this field.

Core Publications

[1] **Nikolas Wilhelm**, Carina M. Micheler, et al. “Development and Evaluation of a Cost-effective IMU System for Gait Analysis: Comparison with Vicon and VideoPose3D Algorithms”. In: *Current Directions in Biomedical Engineering* 9.1 (Sept. 2023), pp. 254–257. DOI: 10.1515/cdbme-2023-1064. URL: https://doi.org/10.1515/cdbme-2023-1064.

[2] **Nikolas Wilhelm**, Thomas Dickmann, et al. “An Adaptive Mechatronic Exoskeleton for Force-Controlled Finger Rehabilitation”. In: *Frontiers in Robotics and AI* 8 (2021). ISSN: 2296-9144. DOI: 10.3389/frobt.2021.716451. URL: https://www.frontiersin.org/article/10.3389/frobt.2021.716451.

[3] **Nikolas Wilhelm**, Sami Haddadin, et al. “Development of an Exoskeleton Platform of the Finger for Objective Patient Monitoring in Rehabilitation”. In: *Sensors* 22.13 (June 2022), p. 4804. DOI: 10.3390/s22134804. URL: https://doi.org/10.3390/s22134804.

[4] Claudio E. von Schacky, **Nikolas Wilhelm**, et al. “Multitask Deep Learning for Segmentation and Classification of Primary Bone Tumors on Radiographs”. In: *Radiology* 301.2 (Nov. 2021), pp. 398–406. DOI: 10.1148/radiol.2021204531. URL: https://doi.org/10.1148/radiol.2021204531.

[5] Claudio E. von Schacky, **Nikolas Wilhelm**, et al. “Development and evaluation of machine learning models based on X-ray radiomics for the classification and differentiation of malignant and benign bone tumors”. In: *European Radiology* 32.9 (Apr. 2022), pp. 6247–6257. DOI: 10.1007/s00330-022-08764-w. URL: https://doi.org/10.1007/s00330-022-08764-w.

[6] **Nikolas Wilhelm**, Claudio E. von Schacky, et al. “Multicentric development and validation of a multi-scale and multi-task deep learning model for comprehensive lower extremity alignment analysis”. In: *Artificial Intelligence in Medicine* (2024), p. 102843. ISSN: 0933-3657. DOI: https://doi.org/10.1016/j.artmed.2024.102843. URL: https://www.sciencedirect.com/science/article/pii/S093336572400085X.

[7] **Nikolas Wilhelm**, Claudio E. von Schacky, et al. “Fully Automated Planning of Medial Open Wedge High Tibial Osteotomy on Weight Bearing Anterior Posterior Long Leg Radiographs via Artificial Intelligence – A Multicentric Development and Validation Study”. In: *The American Journal of Sports Medicine* (2024). Planned submission, Unsubmitted manuscript.

[8] **Nikolas Wilhelm**, Rainer Burgkart, et al. “Exploiting null space potentials to control arm robots compliantly performing nonlinear tactile tasks”. In: *International Journal of Advanced Robotic Systems* 16.6 (2019), p. 1729881419885473. DOI: 10.1177/1729881419885473. eprint: https://doi.org/10.1177/1729881419885473.

[9] **Nikolas Wilhelm**, Constantin von Deimling, et al. “Validation of a Robotic Testbench for Evaluating Biomechanical Effects of Implant Rotation in Total Knee Arthroplasty on a Cadaveric Specimen”. In: *Sensors* 23.17 (Aug. 2023), p. 7459. DOI: 10.3390/s23177459. URL: https://doi.org/10.3390/s23177459.

[10] **Nikolas Wilhelm**, Claudio Glowalla, et al. “Design and Implementation of a Robotic Testbench for Analyzing Pincer Grip Execution in Human Specimen Hands”. Accepted for the 2024 IEEE International Conference on Robotics and Automation (ICRA). Munich, Germany, 2024.

[11] **Nikolas Wilhelm**, Sami Haddadin, et al. “Accurate Kinematic Modeling using Autoencoders on Differentiable Joints”. Accepted for the 2024 IEEE International Conference on Robotics and Automation (ICRA). Munich, Germany, 2024.

[12] **Nikolas Wilhelm**, Rainer Burgkart, et al. “System Identification of the Human Knee by Adaption of Plausible Models using Reinforcement Learning in Robotic Data Acquisition”. In: (2024). Only GitHub Version available.

[13] **Nikolas WIlhelm**, Victor Schaack, et al. “An Adaptive Robotic Exoskeleton for Comprehensive Force-Controlled Hand Rehabilitation”. In: *2024 IEEE/RSJ International Conference on Intelligent Robots and Systems (IROS)*. IEEE, Oct. 2024, pp. 170–177. DOI: 10.1109/iros58592.2024.10802093. URL: http://dx.doi.org/10.1109/IROS58592.2024.10802093.

References

[14] Statistisches Bundesamt (Destatis). *Long-term care projection: 1.8 million more people in need of long-term care expected until 2055*. https://www.destatis.de/EN/Press/2023/03/PE23_124_12.html. Accessed: 2023-11-07. 2023.

[15] My-Linh N Luong, Rebecca J Cleveland, et al. "Social determinants and osteoarthritis outcomes". In: *Aging Health* 8.4 (Aug. 2012), pp. 413–437. DOI: 10.2217/ahe.12.43. URL: https://doi.org/10.2217/ahe.12.43.

[16] Julian Wangler and Michael Jansky. "Promotion of Exercise and Health for Older People in Primary Care: A Qualitative Study on the Potential, Experiences and Strategies of General Practitioners in Germany". In: *Journal of Prevention* 44.4 (Mar. 2023), pp. 477–490. DOI: 10.1007/s10935-023-00730-6. URL: https://doi.org/10.1007/s10935-023-00730-6.

[17] Lydia Malin, Anika Jansen, et al. *Fachkraefteengpaesse in Unternehmen: Fachkraeftesicherung in Deutschland - diese Potenziale gibt es noch*. KOFA-Studien 2/2019. –Kompetenzzentrum Fachkraeftesicherung (KOFA), Institut der deutschen Wirtschaft (IW) / German Economic Institute, 2019. URL: https://EconPapers.repec.org/RePEc:zbw:iwkofa:22019.

[18] Kerstin Denecke and Claude R. Baudoin. "A Review of Artificial Intelligence and Robotics in Transformed Health Ecosystems". In: *Frontiers in Medicine* 9 (July 2022). ISSN: 2296-858X. DOI: 10.3389/fmed.2022.795957. URL: http://dx.doi.org/10.3389/fmed.2022.795957.

[19] In: *Nature* 610.7931 (Oct. 2022), S9–S9. ISSN: 1476-4687. DOI: 10.1038/d41586-022-03210-9. URL: http://dx.doi.org/10.1038/d41586-022-03210-9.

[20] Andrew P. Kurmis and Jamie R. Ianunzio. "Artificial intelligence in orthopedic surgery: evolution, current state and future directions". In: *Arthroplasty* 4.1 (Mar. 2022). ISSN: 2524-7948. DOI: 10.1186/s42836-022-00112-z. URL: http://dx.doi.org/10.1186/s42836-022-00112-z.

[21] Simon J. Federer and Gareth G. Jones. "Artificial intelligence in orthopaedics: A scoping review". In: *PLOS ONE* 16.11 (Nov. 2021). Ed. by Thippa Reddy Gadekallu, e0260471. ISSN: 1932-6203. DOI: 10.1371/journal.pone.0260471. URL: http://dx.doi.org/10.1371/journal.pone.0260471.

[22] Lena Petersson, Ingrid Larsson, et al. "Challenges to implementing artificial intelligence in healthcare: a qualitative interview study with healthcare leaders in Sweden". In: *BMC Health Services Research* 22.1 (July 2022). ISSN: 1472-6963. DOI: 10.1186/s12913-022-08215-8. URL: http://dx.doi.org/10.1186/s12913-022-08215-8.

[23] Marius Niculescu, Octavia-Sorina Hoțaru, et al. "Challenges of Integrating New Technologies for Orthopedic Doctors to Face up to Difficulties during the Pandemic Era". In: *Healthcare* 11.11 (2023). ISSN: 2227-9032. DOI: 10.3390/healthcare11111524. URL: https://www.mdpi.com/2227-9032/11/11/1524.

[24] Nicola Maffulli, Hugo C. Rodriguez, et al. "Artificial intelligence and machine learning in orthopedic surgery: a systematic review protocol". In: *Journal of Orthopaedic Surgery and Research* 15.1 (Oct. 2020). ISSN: 1749-799X. DOI: 10.1186/s13018-020-02002-z. URL: http://dx.doi.org/10.1186/s13018-020-02002-z.

[25] Hamid Naghibi Beidokhti, Dennis Janssen, et al. “A comparison between dynamic implicit and explicit finite element simulations of the native knee joint”. In: *Medical Engineering & Physics* 38.10 (Oct. 2016), pp. 1123–1130. DOI: 10.1016/j.medengphy.2016.06.001. URL: https://doi.org/10.1016/j.medengphy.2016.06.001.

[26] Juan C. Mora, Rene Przkora, et al. “Knee osteoarthritis: pathophysiology and current treatment modalities”. In: *Journal of pain research* 11 (Oct. 2018). 30323653[pmid], pp. 2189–2196. ISSN: 1178-7090. DOI: 10.2147/JPR.S154002. URL: https://www.ncbi.nlm.nih.gov/pubmed/30323653.

[27] Robert J. Cooper, Ruth K. Wilcox, et al. “Finite element models of the tibiofemoral joint: A review of validation approaches and modelling challenges”. In: *Medical Engineering & Physics* 74 (Dec. 2019), pp. 1–12. DOI: 10.1016/j.medengphy.2019.08.002. URL: https://doi.org/10.1016/j.medengphy.2019.08.002.

[28] Michael T. Hirschmann and Werner Müller. “Complex function of the knee joint: the current understanding of the knee”. In: *Knee Surgery, Sports Traumatology, Arthroscopy* 23.10 (May 2015), pp. 2780–2788. DOI: 10.1007/s00167-015-3619-3. URL: https://doi.org/10.1007/s00167-015-3619-3.

[29] Frank R. Noyes, John F. Cummings, et al. “The diagnosis of knee motion limits, subluxations, and ligament injury”. In: *The American Journal of Sports Medicine* 19.2 (Mar. 1991), pp. 163–171. DOI: 10.1177/036354659101900212. URL: https://doi.org/10.1177/036354659101900212.

[30] Werner Müller. *The Knee*. Springer Berlin Heidelberg, 1983. DOI: 10.1007/978-3-642-61763-8. URL: https://doi.org/10.1007/978-3-642-61763-8.

[31] A Menschik et al. “Mechanik des Kniegelenkes. i”. In: *Zeitschrift fur Orthopadie und ihre Grenzgebiete* (1974).

[32] W Müller. “Neuere Aspekte der funktionellen Anatomie des Kniegelenkes”. In: *Hefte zur Unfallheilkunde* (1977), pp. 131–7.

[33] N ARDEN and M NEVITT. “Osteoarthritis: Epidemiology”. In: *Best Practice & Research Clinical Rheumatology* 20.1 (Feb. 2006), pp. 3–25. DOI: 10.1016/j.berh.2005.09.007. URL: https://doi.org/10.1016/j.berh.2005.09.007.

[34] Joseph A Buckwalter, Charles Saltzman, et al. “The Impact of Osteoarthritis”. In: *Clinical Orthopaedics and Related Research* 427 (Oct. 2004), S6–S15. DOI: 10.1097/01.blo.0000143938.30681.9d. URL: https://doi.org/10.1097/01.blo.0000143938.30681.9d.

[35] Behzad Heidari. “Knee osteoarthritis prevalence, risk factors, pathogenesis and features: Part I”. In: *Caspian journal of internal medicine* 2.2 (2011). 24024017[pmid], pp. 205–212. ISSN: 2008-6164. URL: https://www.ncbi.nlm.nih.gov/pubmed/24024017.

[36] Hilal Maradit Kremers, Dirk R Larson, et al. “Prevalence of Total Hip and Knee Replacement in the United States”. In: *The Journal of Bone and Joint Surgery-American Volume* 97.17 (Sept. 2015), pp. 1386–1397. DOI: 10.2106/jbjs.n.01141. URL: https://doi.org/10.2106/jbjs.n.01141.

[37] Philippa Bowland, E Ingham, et al. “Review of the biomechanics and biotribology of osteochondral grafts used for surgical interventions in the knee”. In: *Proceedings of the Institution of Mechanical Engineers, Part H: Journal of Engineering in Medicine* 229.12 (Nov. 2015), pp. 879–888. DOI: 10.1177/0954411915615470. URL: https://doi.org/10.1177/0954411915615470.

[38] F. Persson, A. Turkiewicz, et al. “The risk of symptomatic knee osteoarthritis after arthroscopic meniscus repair vs partial meniscectomy vs the general population”. In: *Osteoarthritis and Cartilage* 26.2 (Feb. 2018), pp. 195–201. DOI: 10.1016/j.joca.2017.08.020. URL: https://doi.org/10.1016/j.joca.2017.08.020.

[39] Alec A. Macaulay, Dean C. Perfetti, et al. “Anterior Cruciate Ligament Graft Choices”. In: *Sports Health* 4.1 (2012). PMID: 23016071, pp. 63–68. DOI: 10.1177/1941738111409890. eprint: https://doi.org/10.1177/1941738111409890. URL: https://doi.org/10.1177/1941738111409890.

[40] Amulya Bharat. *Hand Bone Anatomy: Human Diagram Download*. http://www.amulyabharat.com/hand-bone-anatomy-human-diagram-download/. Accessed: 2024-06-13.

[41] Visakha K. Nanayakkara, Giuseppe Cotugno, et al. “The Role of Morphology of the Thumb in Anthropomorphic Grasping: A Review”. In: *Frontiers in Mechanical Engineering* 3 (June 2017). ISSN: 2297-3079. DOI: 10.3389/fmech.2017.00005. URL: http://dx.doi.org/10.3389/fmech.2017.00005.

[42] S. M. Hadi Sadati, S. Elnaz Naghibi, et al. “A Geometry Deformation Model for Braided Continuum Manipulators”. In: *Frontiers in Robotics and AI* 4 (2017). ISSN: 2296-9144. DOI: 10.3389/frobt.2017.00022. URL: https://www.frontiersin.org/articles/10.3389/frobt.2017.00022.

[43] Qiang Zhan, Chao Zhang, et al. “Measurement and Description of Human Hand Movement”. In: *MATEC Web of Conferences* 114 (2017). Ed. by P. Liu and X. Tu, p. 04002. DOI: 10.1051/matecconf/201711404002. URL: https://doi.org/10.1051/matecconf/201711404002.

[44] Aoife MacMahon, Sandesh S. Rao, et al. “Preoperative Patient Optimization in Total Joint Arthroplasty—The Paradigm Shift from Preoperative Clearance: A Narrative Review”. In: *HSS Journal®: The Musculoskeletal Journal of Hospital for Special Surgery* 18.3 (July 2021), pp. 418–427. ISSN: 1556-3324. DOI: 10.1177/15563316211030923. URL: http://dx.doi.org/10.1177/15563316211030923.

[45] Nathanael D. Heckmann and Nathan T. Glusenkamp. “Linkage Between Databases in Joint Arthroplasty and Orthopaedics: The Way Forward?” In: *Journal of Bone and Joint Surgery* 104.Suppl 3 (Oct. 2022), pp. 33–38. ISSN: 1535-1386. DOI: 10.2106/jbjs.22.00563. URL: http://dx.doi.org/10.2106/JBJS.22.00563.

[46] Eleni-Rosalina Andrinopoulou, Michael O Harhay, et al. “Reflection on modern methods: Dynamic prediction using joint models of longitudinal and time-to-event data”. In: *International Journal of Epidemiology* 50.5 (Mar. 2021), pp. 1731–1743. ISSN: 1464-3685. DOI: 10.1093/ije/dyab047. URL: http://dx.doi.org/10.1093/ije/dyab047.

[47] *Vicon Motion Capture System*. https://www.vicon.com/. Accessed: 2023-01-13. 2021.

[48] *OptiTrack Motion Capture System*. https://optitrack.com/. Accessed: 2023-01-13. 2021.

[49] James G. Richards. “The measurement of human motion: A comparison of commercially available systems”. In: *Human Movement Science* 18.5 (1999), pp. 589–602. ISSN: 0167-9457. DOI: https://doi.org/10.1016/S0167-9457(99)00023-8. URL: http://www.sciencedirect.com/science/article/pii/S0167945799000238.

[50] PAUL DEVITA, TIBOR HORTOBAGYI, et al. “Gait adaptations before and after anterior cruciate ligament reconstruction surgery”. In: *Medicine &amp Science in Sports &amp Exercise* 29.7 (July 1997), pp. 853–859. DOI: 10.1097/00005768-199707000-00003. URL: https://doi.org/10.1097/00005768-199707000-00003.

[51] Steffi L. Colyer, Murray Evans, et al. “A Review of the Evolution of Vision-Based Motion Analysis and the Integration of Advanced Computer Vision Methods Towards Developing a Markerless System”. In: *Sports Medicine - Open* 4.1 (June 2018). DOI: 10.1186/s40798-018-0139-y. URL: https://doi.org/10.1186/s40798-018-0139-y.

[52] Justin Amadeus Albert, Victor Owolabi, et al. “Evaluation of the Pose Tracking Performance of the Azure Kinect and Kinect v2 for Gait Analysis in Comparison with a Gold Standard: A Pilot Study”. In: *Sensors* 20.18 (Sept. 2020), p. 5104. DOI: 10.3390/s20185104. URL: https://doi.org/10.3390/s20185104.

[53] Georgios Pavlakos, Xiaowei Zhou, et al. “Coarse-to-Fine Volumetric Prediction for Single-Image 3D Human Pose”. In: *CoRR* abs/1611.07828 (2016). arXiv: 1611.07828. URL: http://arxiv.org/abs/1611.07828.

[54] Bugra Tekin, Pablo Márquez-Neila, et al. “Fusing 2D Uncertainty and 3D Cues for Monocular Body Pose Estimation”. In: *CoRR* abs/1611.05708 (2016). arXiv: 1611.05708. URL: http://arxiv.org/abs/1611.05708.

[55] Julieta Martinez, Rayat Hossain, et al. “A simple yet effective baseline for 3d human pose estimation”. In: *CoRR* abs/1705.03098 (2017). arXiv: 1705.03098. URL: http://arxiv.org/abs/1705.03098.

[56] Xiao Sun, Jiaxiang Shang, et al. “Compositional Human Pose Regression”. In: *CoRR* abs/1704.00159 (2017). arXiv: 1704.00159. URL: http://arxiv.org/abs/1704.00159.

[57] Haoshu Fang, Yuanlu Xu, et al. *Learning Pose Grammar to Encode Human Body Configuration for 3D Pose Estimation*. 2017. eprint: arXiv:1710.06513.

[58] Georgios Pavlakos, Xiaowei Zhou, et al. “Ordinal Depth Supervision for 3D Human Pose Estimation”. In: *CoRR* abs/1805.04095 (2018). arXiv: 1805.04095. URL: http://arxiv.org/abs/1805.04095.

[59] Wei Yang, Wanli Ouyang, et al. “3D Human Pose Estimation in the Wild by Adversarial Learning”. In: *CoRR* abs/1803.09722 (2018). arXiv: 1803.09722. URL: http://arxiv.org/abs/1803.09722.

[60] Diogo C. Luvizon, David Picard, et al. “2D/3D Pose Estimation and Action Recognition using Multitask Deep Learning”. In: *CoRR* abs/1802.09232 (2018). arXiv: 1802.09232. URL: http://arxiv.org/abs/1802.09232.

[61] Dario Pavllo, Christoph Feichtenhofer, et al. “3D human pose estimation in video with temporal convolutions and semi-supervised training”. In: *Conference on Computer Vision and Pattern Recognition (CVPR)*. 2019.

[62] Catalin Ionescu, Dragos Papava, et al. “Human3.6M: Large Scale Datasets and Predictive Methods for 3D Human Sensing in Natural Environments”. In: *IEEE Transactions on Pattern Analysis and Machine Intelligence* 36 (2014), pp. 1325–1339.

[63] Thomas Seel, Joerg Raisch, et al. “IMU-Based Joint Angle Measurement for Gait Analysis”. In: *Sensors* 14.4 (2014), pp. 6891–6909. ISSN: 1424-8220. DOI: 10.3390/s140406891. URL: https://www.mdpi.com/1424-8220/14/4/6891.

[64] Christopher G. Goetz, Barbara C. Tilley, et al. “Movement Disorder Society-sponsored revision of the Unified Parkinson’s Disease Rating Scale (MDS-UPDRS): Scale presentation and clinimetric testing results”. In: *Movement Disorders* 23.15 (Nov. 2008), pp. 2129–2170. DOI: 10.1002/mds.22340. URL: https://doi.org/10.1002/mds.22340.

[65] A.M. Sabatini, C. Martelloni, et al. “Assessment of Walking Features From Foot Inertial Sensing”. In: *IEEE Transactions on Biomedical Engineering* 52.3 (Mar. 2005), pp. 486–494. DOI: 10.1109/tbme.2004.840727. URL: https://doi.org/10.1109/tbme.2004.840727.

[66] Steven T. Moore, Hamish G. MacDougall, et al. “Long-term monitoring of gait in Parkinson’s disease”. In: *Gait Posture* 26.2 (July 2007), pp. 200–207. DOI: 10.1016/j.gaitpost.2006.09.011. URL: https://doi.org/10.1016/j.gaitpost.2006.09.011.

[67] Benoit Mariani, Constanze Hoskovec, et al. “3D gait assessment in young and elderly subjects using foot-worn inertial sensors”. In: *Journal of Biomechanics* 43.15 (Nov. 2010), pp. 2999–3006. DOI: 10.1016/j.jbiomech.2010.07.003. URL: https://doi.org/10.1016/j.jbiomech.2010.07.003.

[68] John R. Rebula, Lauro V. Ojeda, et al. “Measurement of foot placement and its variability with inertial sensors”. In: *Gait Posture* 38.4 (Sept. 2013), pp. 974–980. DOI: 10.1016/j.gaitpost.2013.05.012. URL: https://doi.org/10.1016/j.gaitpost.2013.05.012.

[69] Naoki Kitagawa and Naomichi Ogihara. “Estimation of foot trajectory during human walking by a wearable inertial measurement unit mounted to the foot”. In: *Gait Posture* 45 (Mar. 2016), pp. 110–114. DOI: 10.1016/j.gaitpost.2016.01.014. URL: https://doi.org/10.1016/j.gaitpost.2016.01.014.

[70] Alison C. Jones and Ruth K. Wilcox. “Finite element analysis of the spine: Towards a framework of verification, validation and sensitivity analysis”. In: *Medical Engineering & Physics* 30.10 (Dec. 2008), pp. 1287–1304. DOI: 10.1016/j.medengphy.2008.09.006. URL: https://doi.org/10.1016/j.medengphy.2008.09.006.

[71] Stephen J. Piazza and Scott L. Delp. “Three-Dimensional Dynamic Simulation of Total Knee Replacement Motion During a Step-Up Task”. In: *Journal of Biomechanical Engineering* 123.6 (July 2001), pp. 599–606. DOI: 10.1115/1.1406950. URL: https://doi.org/10.1115/1.1406950.

[72] Darryl D. D Lima, Peter C. Chen, et al. “Polyethylene Contact Stresses, Articular Congruity, and Knee Alignment”. In: *Clinical Orthopaedics and Related Research* 392 (Nov. 2001), pp. 232–238. DOI: 10.1097/00003086-200111000-00029. URL: https://doi.org/10.1097/00003086-200111000-00029.

[73] Mohammad Atarod, Joshua M. Rosvold, et al. “A Novel Testing Platform for Assessing Knee Joint Mechanics: A Parallel Robotic System Combined with an Instrumented Spatial Linkage”. In: *Annals of Biomedical Engineering* 42.5 (Feb. 2014), pp. 1121–1132. DOI: 10.1007/s10439-014-0985-9. URL: https://doi.org/10.1007/s10439-014-0985-9.

[74] Christian H. Heinrichs, Dominik Knierzinger, et al. “Validation of a novel biomechanical test bench for the knee joint with six degrees of freedom”. In: *Biomedical Engineering / Biomedizinische Technik* 63.6 (Nov. 2018), pp. 709–717. DOI: 10.1515/bmt-2016-0255. URL: https://doi.org/10.1515/bmt-2016-0255.

[75] M. Frey, R. Burgkart, et al. “Optimised robot-based system for the exploration of elastic joint properties”. In: *Medical & Biological Engineering & Computing* 42.5 (Sept. 2004), pp. 674–678. DOI: 10.1007/bf02347550. URL: https://doi.org/10.1007/bf02347550.

[76] M. Prado and Jorge Horacio. “Development of a high-performance-6-DoF biomechanical joint analysis system based on an industrial robot”. In: *mediaTUM*. 2012.

[77] C. von Deimling. “Tactile Scanning of Human Joints - Insights into Multidimensional Biomechanics”. In: *mediaTUM*. 2021.

[78] Alexander Synek, Marcus Settles, et al. “Multi-body simulation of a human thumb joint by sliding surfaces”. In: *2012 4th IEEE RAS and EMBS International Conference on Biomedical Robotics and Biomechatronics (BioRob)*. 2012, pp. 379–384. DOI: 10.1109/BioRob.2012.6290755.

[79] Dan Hu, David Howard, et al. “Biomechanical Analysis of the Human Finger Extensor Mechanism during Isometric Pressing”. In: *PLoS ONE* 9.4 (Apr. 2014). Ed. by Steve Milanese, e94533. DOI: 10.1371/journal.pone.0094533. URL: https://doi.org/10.1371/journal.pone.0094533.

[80] Maximilian Melzner, Lucas Engelhardt, et al. “Electromyography-Based Validation of a Musculoskeletal Hand Model”. en. In: *J Biomech Eng* 144.2 (Feb. 2022).

[81] Ashish D. Nimbarte, Rodrigo Kaz, et al. “Finger joint motion generated by individual extrinsic muscles: A cadaveric study”. In: *Journal of Orthopaedic Surgery and Research* 3.1 (July 2008). DOI: 10.1186/1749-799x-3-27. URL: https://doi.org/10.1186/1749-799x-3-27.

[82] Joonho Chang, Andris Freivalds, et al. “Investigation of index finger triggering force using a cadaver experiment: Effects of trigger grip span, contact location, and internal tendon force”. en. In: *Appl Ergon* 65 (July 2017), pp. 183–190.

[83] Pilwon Heo, Gwang Min Gu, et al. “Current hand exoskeleton technologies for rehabilitation and assistive engineering”. In: *International Journal of Precision Engineering and Manufacturing* 13.5 (2012), pp. 807–824. ISSN: 2234-7593. DOI: 10.1007/s12541-012-0107-2.

[84] Aladine A. Elsamadicy, Siyun Yang, et al. “Prevalence and Cost Analysis of Complex Regional Pain Syndrome (CRPS): A Role for Neuromodulation”. In: *Neuromodulation: Technology at the Neural Interface* 21.5 (Sept. 2017), pp. 423–430. DOI: 10.1111/ner.12691. URL: https://doi.org/10.1111/ner.12691.

[85] David Epstein, Anne Mason, et al. “The hospital costs of care for stroke in nine European countries”. In: *Health Economics* 17.S1 (Jan. 2008), S21–S31. DOI: 10.1002/hec.1329. URL: https://doi.org/10.1002/hec.1329.

[86] David J. Reinkensmeyer, Jeremy L. Emken, et al. “Robotics, motor learning, and neurologic recovery”. In: *Annual review of biomedical engineering* 6 (2004), pp. 497–525. ISSN: 1523-9829. DOI: 10.1146/annurev.bioeng.6.040803.140223.

[87] E. Taub, N. E. Miller, et al. “Technique to improve chronic motor deficit after stroke”. In: *Archives of physical medicine and rehabilitation* 74.4 (1993), pp. 347–354. ISSN: 0003-9993.

[88] Victor W. Mark and Edward Taub. “Constraint-induced movement therapy for chronic stroke hemiparesis and other disabilities”. In: *Restorative Neurology and Neuroscience* 22.3-5 (2004), pp. 317–336. ISSN: 0922-6028.

[89] James L. Patton and Ferdinando A. Mussa-Ivaldi. “Robot-assisted adaptive training: custom force fields for teaching movement patterns”. In: *IEEE transactions on bio-medical engineering* 51.4 (2004), pp. 636–646. ISSN: 0018-9294. DOI: 10.1109/TBME.2003.821035.

[90] Zan Yue, Xue Zhang, et al. “Hand Rehabilitation Robotics on Poststroke Motor Recovery”. In: *Behavioural neurology* 2017 (2017). DOI: 10.1155/2017/3908135.

[91] Inseong Jo and Joonbum Bae. “Design and control of a wearable and force-controllable hand exoskeleton system”. In: *Mechatronics* 41 (2017), pp. 90–101. ISSN: 09574158. DOI: 10.1016/j.mechatronics.2016.12.001.

[92] Festo AG & Co. KG. *ExoHand*. Esslingen, 2012. URL: https://www.festo.com/group/de/cms/10233.htm (visited on 12/13/2020).

[93] A. Wege, K. Kondak, et al. “Mechanical design and motion control of a hand exoskeleton for rehabilitation”. In: *IEEE International Conference Mechatronics and Automation, 2005* 1 (2005), 155–159 Vol. 1.

[94] A. Chiri, F. Giovacchini, et al. “HANDEXOS: Towards an exoskeleton device for the rehabilitation of the hand”. In: *2009 IEEE/RSJ International Conference on Intelligent Robots and Systems*. IEEE, 2009, pp. 1106–1111. ISBN: 978-1-4244-3803-7. DOI: 10.1109/IROS.2009.5354376.

[95] Jeongsoo Lee, Minhyuk Lee, et al. “Development of a Hand Exoskeleton System for Quantitative Analysis of Hand Functions”. In: *Journal of Bionic Engineering* 15.5 (2018), pp. 783–794. ISSN: 1672-6529. DOI: 10.1007/s42235-018-0066-0.

[96] Jamshed Iqbal, Hamza Khan, et al. “A novel exoskeleton robotic system for hand rehabilitation – Conceptualization to prototyping”. In: *Biocybernetics and Biomedical Engineering* 34.2 (2014), pp. 79–89. ISSN: 02085216. DOI: 10.1016/j.bbe.2014.01.003.

[97] Mine Sarac, Massimiliano Solazzi, et al. “Design and kinematic optimization of a novel underactuated robotic hand exoskeleton”. In: *Meccanica* 52.3 (Oct. 2016), pp. 749–761. DOI: 10.1007/s11012-016-0530-z. URL: https://doi.org/10.1007/s11012-016-0530-z.

[98] Roberto Conti, Enrico Meli, et al. “Kinematic synthesis and testing of a new portable hand exoskeleton”. In: *Meccanica* 52.11-12 (2017), pp. 2873–2897. ISSN: 1572-9648. DOI: 10.1007/s11012-016-0602-0.

[99] A. L. Shoushtari, P. Dario, et al. “A review on the evolvement trend of robotic interaction control”. In: *Ind. Robot* 43 (2016), pp. 535–551.

[100] Neville Hogan. “Impedance Control: An Approach to Manipulation: Part I—Theory”. In: *Journal of Dynamic Systems, Measurement, and Control* 107.1 (1985), p. 1. ISSN: 00220434. DOI: 10.1115/1.3140702.

[101] Andrea Calanca, Riccardo Muradore, et al. “A Review of Algorithms for Compliant Control of Stiff and Fixed-Compliance Robots”. In: *IEEE/ASME Transactions on Mechatronics* 21.2 (2016), pp. 613–624. ISSN: 1083-4435. DOI: 10.1109/TMECH.2015.2465849. (Visited on 02/06/2018).

[102] J. E. Colgate and J. M. Brown. “Factors affecting the Z-Width of a haptic display”. In: *Proceedings of the 1994 IEEE International Conference on Robotics and Automation*. IEEE Comput. Soc. Press, 1994, pp. 3205–3210. ISBN: 0-8186-5330-2. DOI: 10.1109/ROBOT.1994.351077.

[103] M. H. Raibert and J. J. Craig. “Hybrid Position/Force Control of Manipulators”. In: *Journal of Dynamic Systems, Measurement, and Control* 103.2 (1981), p. 126. ISSN: 00220434. DOI: 10.1115/1.3139652.

[104] Christoph Schuetz, Julian Pfaff, et al. “Motion planning for redundant manipulators in uncertain environments based on tactile feedback: Sept. 28, 2015 - Oct. 2, 2015, Hamburg, Germany”. In: *IEEE/RSJ International Conference on Intelligent Robots and Systems*. 2015, pp. 6387–6394. DOI: 10.1109/IROS.2015.7354290. (Visited on 12/01/2017).

[105] M. Kazemi, Y. Dabiri, et al. “Recent Advances in Computational Mechanics of the Human Knee Joint”. In: *Computational and Mathematical Methods in Medicine* 2013 (2013), pp. 1–27. DOI: 10.1155/2013/718423. URL: https://doi.org/10.1155/2013/718423.

[106] Mika E. Mononen, Petri Tanska, et al. “A Novel Method to Simulate the Progression of Collagen Degeneration of Cartilage in the Knee: Data from the Osteoarthritis Initiative”. In: *Scientific Reports* 6.1 (Feb. 2016). DOI: 10.1038/srep21415. URL: https://doi.org/10.1038/srep21415.

[107] R. Shirazi and A. Shirazi-Adl. “Computational biomechanics of articular cartilage of human knee joint: Effect of osteochondral defects”. In: *Journal of Biomechanics* 42.15 (Nov. 2009), pp. 2458–2465. DOI: 10.1016/j.jbiomech.2009.07.022. URL: https://doi.org/10.1016/j.jbiomech.2009.07.022.

[108] Mikko S. Venäläinen, Mika E. Mononen, et al. “Quantitative Evaluation of the Mechanical Risks Caused by Focal Cartilage Defects in the Knee”. In: *Scientific Reports* 6.1 (Nov. 2016). DOI: 10.1038/srep37538. URL: https://doi.org/10.1038/srep37538.

[109] Qingen Meng, John Fisher, et al. “The effects of geometric uncertainties on computational modelling of knee biomechanics”. In: *Royal Society Open Science* 4.8 (Aug. 2017), p. 170670. DOI: 10.1098/rsos.170670. URL: https://doi.org/10.1098/rsos.170670.

[110] Piotr Łuczkiewicz, Karol Daszkiewicz, et al. “Influence of meniscus shape in the cross sectional plane on the knee contact mechanics”. In: *Journal of Biomechanics* 48.8 (June 2015), pp. 1356–1363. DOI: 10.1016/j.jbiomech.2015.03.002. URL: https://doi.org/10.1016/j.jbiomech.2015.03.002.

[111] Qingen Meng, Zhongmin Jin, et al. “Computational investigation of the time-dependent contact behaviour of the human tibiofemoral joint under body weight”. In: *Proceedings of the Institution of Mechanical Engineers, Part H: Journal of Engineering in Medicine* 228.11 (Nov. 2014), pp. 1193–1207. DOI: 10.1177/0954411914559737. URL: https://doi.org/10.1177/0954411914559737.

[112] Hamid Naghibi Beidokhti, Dennis Janssen, et al. “The influence of ligament modelling strategies on the predictive capability of finite element models of the human knee joint”. In: *Journal of Biomechanics* 65 (Dec. 2017), pp. 1–11. DOI: 10.1016/j.jbiomech.2017.08.030. URL: https://doi.org/10.1016/j.jbiomech.2017.08.030.

[113] Azhar A. Ali, Michael D. Harris, et al. “Combined measurement and modeling of specimen-specific knee mechanics for healthy and ACL-deficient conditions”. In: *Journal of Biomechanics* 57 (May 2017), pp. 117–124. DOI: 10.1016/j.jbiomech.2017.04.008. URL: https://doi.org/10.1016/j.jbiomech.2017.04.008.

[114] Lasse P. Räsänen, Petri Tanska, et al. “The effect of fixed charge density and cartilage swelling on mechanics of knee joint cartilage during simulated gait”. In: *Journal of Biomechanics* 61 (Aug. 2017), pp. 34–44. DOI: 10.1016/j.jbiomech.2017.06.041. URL: https://doi.org/10.1016/j.jbiomech.2017.06.041.

[115] Joyce Van den Broeck, Evie Vereecke, et al. “Segmentation accuracy of long bones”. In: *Medical Engineering & Physics* 36.7 (July 2014), pp. 949–953. DOI: 10.1016/j.medengphy.2014.03.016. URL: https://doi.org/10.1016/j.medengphy.2014.03.016.

[116] E. Peña, B. Calvo, et al. “A three-dimensional finite element analysis of the combined behavior of ligaments and menisci in the healthy human knee joint”. In: *Journal of Biomechanics* 39.9 (Jan. 2006), pp. 1686–1701. DOI: 10.1016/j.jbiomech.2005.04.030. URL: https://doi.org/10.1016/j.jbiomech.2005.04.030.

[117] Yasin Y. Dhaher, Scott L. Delp, et al. “The use of basis functions in modelling joint articular surfaces: application to the knee joint”. In: *Journal of Biomechanics* 33.7 (July 2000), pp. 901–907. DOI: 10.1016/s0021-9290(00)00024-5. URL: https://doi.org/10.1016/s0021-9290(00)00024-5.

[118] G.A. Ateshian, L.J. Soslowsky, et al. “Quantitation of articular surface topography and cartilage thickness in knee joints using stereophotogrammetry”. In: *Journal of Biomechanics* 24.8 (Jan. 1991), pp. 761–776. DOI: 10.1016/0021-9290(91)90340-s. URL: https://doi.org/10.1016/0021-9290(91)90340-s.

[119] J. Wismans, F. Veldpaus, et al. “A three-dimensional mathematical model of the knee-joint”. In: *Journal of Biomechanics* 13.8 (Jan. 1980), pp. 677–685. DOI: 10.1016/0021-9290(80)90354-1. URL: https://doi.org/10.1016/0021-9290(80)90354-1.

[120] Andrew E. Anderson, Benjamin J. Ellis, et al. “Effects of idealized joint geometry on finite element predictions of cartilage contact stresses in the hip”. In: *Journal of Biomechanics* 43.7 (May 2010), pp. 1351–1357. DOI: 10.1016/j.jbiomech.2010.01.010. URL: https://doi.org/10.1016/j.jbiomech.2010.01.010.

[121] K. Stentz-Olesen, E. T. Nielsen, et al. “Validation of static and dynamic radiostereometric analysis of the knee joint using bone models from CT data”. In: *Bone & Joint Research* 6.6 (June 2017), pp. 376–384. DOI: 10.1302/2046-3758.66.bjr-2016-0113.r3. URL: https://doi.org/10.1302/2046-3758.66.bjr-2016-0113.r3.

[122] Liming Shu, Ko Yamamoto, et al. “A subject-specific finite element musculoskeletal framework for mechanics analysis of a total knee replacement”. In: *Journal of Biomechanics* 77 (Aug. 2018), pp. 146–154. DOI: 10.1016/j.jbiomech.2018.07.008. URL: https://doi.org/10.1016/j.jbiomech.2018.07.008.

[123] K. S. Halonen, C. M. Dzialo, et al. “Workflow assessing the effect of gait alterations on stresses in the medial tibial cartilage - combined musculoskeletal modelling and finite element analysis”. In: *Scientific Reports* 7.1 (Dec. 2017). DOI: 10.1038/s41598-017-17228-x. URL: https://doi.org/10.1038/s41598-017-17228-x.

[124] Jiang Yao, Sarah L. Lancianese, et al. “Magnetic resonance image analysis of meniscal translation and tibio-menisco-femoral contact in deep knee flexion”. In: *Journal of Orthopaedic Research* 26.5 (2008), pp. 673–684. DOI: 10.1002/jor.20553. URL: https://doi.org/10.1002/jor.20553.

[125] K.S. Halonen, M.E. Mononen, et al. “Deformation of articular cartilage during static loading of a knee joint – Experimental and finite element analysis”. In: *Journal of Biomechanics* 47.10 (July 2014), pp. 2467–2474. DOI: 10.1016/j.jbiomech.2014.04.013. URL: https://doi.org/10.1016/j.jbiomech.2014.04.013.

[126] Marco Viceconti, Sigbjorn Olsen, et al. “Extracting clinically relevant data from finite element simulations”. In: *Clinical Biomechanics* 20.5 (June 2005), pp. 451–454. DOI: 10.1016/j.clinbiomech.2005.01.010. URL: https://doi.org/10.1016/j.clinbiomech.2005.01.010.

[127] C.G. Peterfy, E. Schneider, et al. “The osteoarthritis initiative: report on the design rationale for the magnetic resonance imaging protocol for the knee”. In: *Osteoarthritis and Cartilage* 16.12 (Dec. 2008), pp. 1433–1441. DOI: 10.1016/j.joca.2008.06.016. URL: https://doi.org/10.1016/j.joca.2008.06.016.

[128] Alex Krizhevsky, Ilya Sutskever, et al. “ImageNet Classification with Deep Convolutional Neural Networks”. In: *Advances in Neural Information Processing Systems*. Ed. by F. Pereira, C. J. C. Burges, et al. Vol. 25. Curran Associates, Inc., 2012, pp. 1097–1105. URL: https://proceedings.neurips.cc/paper/2012/file/c399862d3b9d6b76c8436e924a68c45b-Paper.pdf.

[129] Kaiming He, Xiangyu Zhang, et al. “Deep Residual Learning for Image Recognition”. In: *CoRR* abs/1512.03385 (2015). arXiv: 1512.03385. URL: http://arxiv.org/abs/1512.03385.

[130] Tom B. Brown, Benjamin Mann, et al. *Language Models are Few-Shot Learners*. 2020. arXiv: 2005.14165 [cs.CL].

[131] Andrew W. Senior, Richard Evans, et al. “Improved protein structure prediction using potentials from deep learning”. In: *Nature* 577.7792 (Jan. 2020), pp. 706–710. DOI: 10.1038/s41586-019-1923-7. URL: https://doi.org/10.1038/s41586-019-1923-7.

[132] Philipp Tschandl, Christoph Rinner, et al. “Human–computer collaboration for skin cancer recognition”. In: *Nature Medicine* 26.8 (June 2020), pp. 1229–1234. DOI: 10.1038/s41591-020-0942-0. URL: https://doi.org/10.1038/s41591-020-0942-0.

[133] Scott Mayer McKinney, Marcin Sieniek, et al. “International evaluation of an AI system for breast cancer screening”. In: *Nature* 577.7788 (Jan. 2020), pp. 89–94. DOI: 10.1038/s41586-019-1799-6. URL: https://doi.org/10.1038/s41586-019-1799-6.

[134] Aleksei Tiulpin, Stefan Klein, et al. “Multimodal Machine Learning-based Knee Osteoarthritis Progression Prediction from Plain Radiographs and Clinical Data”. In: *Scientific Reports* 9.1 (Dec. 2019). DOI: 10.1038/s41598-019-56527-3. URL: https://doi.org/10.1038/s41598-019-56527-3.

[135] Kaiming He, Georgia Gkioxari, et al. “Mask R-CNN”. In: *CoRR* abs/1703.06870 (2017). arXiv: 1703.06870. URL: http://arxiv.org/abs/1703.06870.

[136] Zhaoye Zhou, Gengyan Zhao, et al. “Deep convolutional neural network for segmentation of knee joint anatomy”. In: *Magnetic Resonance in Medicine* 80.6 (May 2018), pp. 2759–2770. DOI: 10.1002/mrm.27229. URL: https://doi.org/10.1002/mrm.27229.

[137] Nicholas Bien, Pranav Rajpurkar, et al. “Deep-learning-assisted diagnosis for knee magnetic resonance imaging: Development and retrospective validation of MRNet”. In: *PLOS Medicine* 15.11 (Nov. 2018), pp. 1–19. DOI: 10.1371/journal.pmed.1002699. URL: https://doi.org/10.1371/journal.pmed.1002699.

[138] Justus Schock, Daniel Truhn, et al. “Automated Analysis of Alignment in Long-Leg Radiographs by Using a Fully Automated Support System Based on Artificial Intelligence”. In: *Radiology: Artificial Intelligence* 3.2 (Mar. 2021), e200198.

[139] R G Marx, P Grimm, et al. “Reliability of lower extremity alignment measurement using radiographs and PACS”. In: *Knee Surg. Sports Traumatol. Arthrosc.* 19.10 (Mar. 2011), p. 1693.

[140] Adrian V Specogna, Trevor B Birmingham, et al. “Reliability of lower limb frontal plane alignment measurements using plain radiographs and digitized images”. en. In: *J. Knee Surg.* 17.4 (Oct. 2004), pp. 203–210.

[141] Loı¨c Duron, Alexis Ducarouge, et al. “Assessment of an AI Aid in Detection of Adult Appendicular Skeletal Fractures by Emergency Physicians and Radiologists: A Multicenter Cross-sectional Diagnostic Study”. In: *Radiology* 300.1 (July 2021), pp. 120–129.

[142] Justin D Krogue, Kaiyang V Cheng, et al. “Automatic Hip Fracture Identification and Functional Subclassification with Deep Learning”. In: *Radiology: Artificial Intelligence* 2.2 (Mar. 2020), e190023.

[143] Takaaki Urakawa, Yuki Tanaka, et al. “Detecting intertrochanteric hip fractures with orthopedist-level accuracy using a deep convolutional neural network”. In: *Skeletal Radiol.* 48.2 (Feb. 2019), pp. 239–244.

[144] Joy T Wu, Ken C L Wong, et al. “Comparison of Chest Radiograph Interpretations by Artificial Intelligence Algorithm vs Radiology Residents”. In: *JAMA Netw Open* 3.10 (Oct. 2020), e2022779–e2022779.

[145] Alexander Tack, Bernhard Preim, et al. “Fully automated Assessment of Knee Alignment from Full-Leg X-Rays employing a “YOLOv4 And Resnet Landmark regression Algorithm” (YARLA): Data from the Osteoarthritis Initiative”. en. In: *Comput. Methods Programs Biomed.* 205 (June 2021), p. 106080.

[146] Dror Paley. *Principles of Deformity Correction* -. Berlin, Heidelberg: Springer, 2014. ISBN: 978-3-642-59373-4.

[147] Steffen Schröter, Christoph Ihle, et al. “Digital planning of high tibial osteotomy. Interrater reliability by using two different software”. In: *Knee Surg. Sports Traumatol. Arthrosc.* 21.1 (Jan. 2013), pp. 189–196.

[148] Murilo Barroso Matos, José Leonardo Rocha de Faria, et al. “Evaluation of intraobserver and interobserver reliability of mechanical axis alignment measure of the lower limb through the panoramic radiograph in patients in the preoperative and postoperative periods of total knee arthroplasty”. In: *Open J. Orthop.* 10.09 (2020), pp. 221–233.

[149] G A Schmale, A F Bayomy, et al. “The reliability of full-length lower limb radiographic alignment measurements in skeletally immature youth”. en. In: *J. Child. Orthop.* (Jan. 2019).

[150] Diederik P Kingma and Max Welling. *Auto-Encoding Variational Bayes*. 2014. arXiv: 1312.6114 [stat.ML].

[151] Ian J. Goodfellow, Jean Pouget-Abadie, et al. *Generative Adversarial Networks*. 2014. arXiv: 1406.2661 [stat.ML].

[152] Kaiming He, Haoqi Fan, et al. “Momentum Contrast for Unsupervised Visual Representation Learning”. In: *CoRR* abs/1911.05722 (2019). arXiv: 1911.05722. URL: http://arxiv.org/abs/1911.05722.

[153] Sayantan Bhadra, Weimin Zhou, et al. *Medical image reconstruction with image-adaptive priors learned by use of generative adversarial networks*. 2020. eprint: arXiv:2001.10830.

[154] Tian Qi Chen, Yulia Rubanova, et al. “Neural Ordinary Differential Equations”. In: *CoRR* 1806.07366 (2018). arXiv: 1806.07366. URL: http://arxiv.org/abs/1806.07366.

[155] Raşit Koeker, Cemil Oez, et al. “A study of neural network based inverse kinematics solution for a three-joint robot”. In: *Robotics and Autonomous Systems* 49.3 (2004). Patterns and Autonomous Control, pp. 227–234. ISSN: 0921-8890. DOI: https://doi.org/10.1016/j.robot.2004.09.010. URL: https://www.sciencedirect.com/science/article/pii/S0921889004001666.

[156] Adrian-Vasile Duka. “Neural Network based Inverse Kinematics Solution for Trajectory Tracking of a Robotic Arm”. In: *Procedia Technology* 12 (2014), pp. 20–27. DOI: 10.1016/j.protcy.2013.12.451. URL: https://doi.org/10.1016/j.protcy.2013.12.451.

[157] Guanwu Jiang, Minzhou Luo, et al. “A Precise Positioning Method for a Puncture Robot Based on a PSO-Optimized BP Neural Network Algorithm”. In: *Applied Sciences* 7.10 (Sept. 2017), p. 969. DOI: 10.3390/app7100969. URL: https://doi.org/10.3390/app7100969.

[158] Takeyuki Ono, Ryosuke Eto, et al. “Analysis and control of a Stewart platform as base motion compensators - Part I: Kinematics using moving frames”. In: *Nonlinear Dynamics* 107.1 (Nov. 2021), pp. 51–76. DOI: 10.1007/s11071-021-06767-8. URL: https://doi.org/10.1007/s11071-021-06767-8.

[159] Guoxin Fang, Yingjun Tian, et al. “Efficient Jacobian-Based Inverse Kinematics With Sim-to-Real Transfer of Soft Robots by Learning”. In: *IEEE/ASME Transactions on Mechatronics* 27.6 (Dec. 2022), pp. 5296–5306. DOI: 10.1109/tmech.2022.3178303. URL: https://doi.org/10.1109/tmech.2022.3178303.

[160] Franziska Meier, Austin Wang, et al. *Differentiable and Learnable Robot Models*. 2022. DOI: 10.48550/ARXIV.2202.11217. URL: https://arxiv.org/abs/2202.11217.

[161] Lukas Mölschl, Jakob J. Hollenstein, et al. *Differentiable Forward Kinematics for TensorFlow 2*. 2023. DOI: 10.48550/ARXIV.2301.09954. URL: https://arxiv.org/abs/2301.09954.

[162] Martín Abadi, Ashish Agarwal, et al. *TensorFlow: Large-Scale Machine Learning on Heterogeneous Systems*. Software available from tensorflow.org. 2015. URL: https://www.tensorflow.org/.

[163] Martin Kubovčiék, Iveta Dirgová Luptáková, et al. “Signal Novelty Detection as an Intrinsic Reward for Robotics”. In: *Sensors* 23.8 (Apr. 2023), p. 3985. DOI: 10.3390/s23083985. URL: https://doi.org/10.3390/s23083985.

[164] Masatoshi Nagano, Tomoaki Nakamura, et al. “Spatio-temporal categorization for first-person-view videos using a convolutional variational autoencoder and Gaussian processes”. In: *Frontiers in Robotics and AI* 9 (Sept. 2022). DOI: 10.3389/frobt.2022.903450. URL: https://doi.org/10.3389/frobt.2022.903450.

[165] Midhun M S and James Kurian. “Task level disentanglement learning in robotics using VAE”. In: *International journal of electrical and computer engineering systems* 13.7 (Sept. 2022), pp. 561–568. DOI: 10.32985/ijeces.13.7.8. URL: https://doi.org/10.32985/ijeces.13.7.8.

[166] Keenon Werling, Dalton Omens, et al. *Fast and Feature-Complete Differentiable Physics for Articulated Rigid Bodies with Contact*. 2021. DOI: 10.48550/ARXIV.2103.16021. URL: https://arxiv.org/abs/2103.16021.

[167] Jonas Degrave, Michiel Hermans, et al. “A Differentiable Physics Engine for Deep Learning in Robotics”. In: *Frontiers in Neurorobotics* 13 (Mar. 2019). DOI: 10.3389/fnbot.2019.00006. URL: https://doi.org/10.3389/fnbot.2019.00006.

[168] Luzius Brodbeck, Simon Hauser, et al. “Morphological Evolution of Physical Robots through Model-Free Phenotype Development”. In: *PLOS ONE* 10.6 (June 2015). Ed. by Josh Bongard, e0128444. DOI: 10.1371/journal.pone.0128444. URL: https://doi.org/10.1371/journal.pone.0128444.

[169] V. V. Sivak, A. Eickbusch, et al. “Model-Free Quantum Control with Reinforcement Learning”. In: *Physical Review X* 12.1 (Mar. 2022). DOI: 10.1103/physrevx.12.011059. URL: https://doi.org/10.1103/physrevx.12.011059.

[170] Xianyuan Zhan, Haoran Xu, et al. “DeepThermal: Combustion Optimization for Thermal Power Generating Units Using Offline Reinforcement Learning”. In: *Proceedings of the AAAI Conference on Artificial Intelligence* 36.4 (June 2022), pp. 4680–4688. DOI: 10.1609/aaai.v36i4.20393. URL: https://doi.org/10.1609/aaai.v36i4.20393.

[171] Andrew S. Morgan, Daljeet Nandha, et al. “Model Predictive Actor-Critic: Accelerating Robot Skill Acquisition with Deep Reinforcement Learning”. In: *2021 IEEE International Conference on Robotics and Automation (ICRA)*. IEEE, May 2021. DOI: 10.1109/icra48506.2021.9561298. URL: https://doi.org/10.1109/icra48506.2021.9561298.

[172] Yusheng Wang, Yidong Lou, et al. “A Tightly-Coupled Framework for Large-Scale Map Construction With Multiple Non-Repetitive Scanning LiDARs”. In: *IEEE Sensors Journal* 22.4 (Feb. 2022), pp. 3626–3636. DOI: 10.1109/jsen.2022.3142041. URL: https://doi.org/10.1109/jsen.2022.3142041.

[173] J. Michael McCarthy and Gim Song Soh. *Geometric Design of Linkages*. Vol. 11. New York, NY: Springer New York, 2011. ISBN: 978-1-4419-7891-2. DOI: 10.1007/978-1-4419-7892-9.

[174] Frank Birklein and Violeta Dimova. “Complex regional pain syndrome–up-to-date”. In: *PAIN Reports* 2.6 (Nov. 2017), e624. DOI: 10.1097/pr9.0000000000000624. URL: https://doi.org/10.1097/pr9.0000000000000624.

[175] “Quick DASH, Questionnaire (13-Item Short Version)”. In: *Encyclopedia of Quality of Life and Well-Being Research*. Ed. by Alex C. Michalos. Dordrecht: Springer Netherlands, 2014, pp. 5382–5382. ISBN: 978-94-007-0753-5. DOI: 10.1007/978-94-007-0753-5_103382. URL: https://doi.org/10.1007/978-94-007-0753-5_103382.

[176] Andre Esteva, Alexandre Robicquet, et al. “A guide to deep learning in healthcare”. In: *Nature Medicine* 25.1 (Jan. 2019), pp. 24–29. DOI: 10.1038/s41591-018-0316-z. URL: https://doi.org/10.1038/s41591-018-0316-z.

[177] Dinggang Shen, Guorong Wu, et al. “Deep Learning in Medical Image Analysis”. In: *Annual Review of Biomedical Engineering* 19.1 (June 2017), pp. 221–248. DOI: 10.1146/annurev-bioeng-071516-044442. URL: https://doi.org/10.1146/annurev-bioeng-071516-044442.

[178] Geert Litjens, Thijs Kooi, et al. “A survey on deep learning in medical image analysis”. In: *Medical Image Analysis* 42 (Dec. 2017), pp. 60–88. DOI: 10.1016/j.media.2017.07.005. URL: https://doi.org/10.1016/j.media.2017.07.005.

[179] Veronika Cheplygina, Marleen de Bruijne, et al. “Not-so-supervised: A survey of semi-supervised, multi-instance, and transfer learning in medical image analysis”. In: *Medical Image Analysis* 54 (May 2019), pp. 280–296. DOI: 10.1016/j.media.2019.03.009. URL: https://doi.org/10.1016/j.media.2019.03.009.

[180] Lena Maier-Hein, Matthias Eisenmann, et al. “Why rankings of biomedical image analysis competitions should be interpreted with care”. In: *Nature Communications* 9.1 (Dec. 2018). DOI: 10.1038/s41467-018-07619-7. URL: https://doi.org/10.1038/s41467-018-07619-7.

[181] Muhammad Fermi Pasha -, Saravanesh Supramaniam -, et al. “An Android-based Mobile Medical Image Viewer and Collaborative Annotation: Development Issues and Challenges”. In: *International Journal of Digital Content Technology and its Applications* 6.1 (Jan. 2012), pp. 208–217. DOI: 10.4156/jdcta.vol6.issue1.26. URL: https://doi.org/10.4156/jdcta.vol6.issue1.26.

[182] Pinar Alper, Khalid Belhajjame, et al. “LabelFlow Framework for Annotating Workflow Provenance”. In: *Informatics* 5.1 (Feb. 2018), p. 11. DOI: 10.3390/informatics5010011. URL: https://doi.org/10.3390/informatics5010011.

[183] Flutter. *Flutter: Beautiful native apps in record time.* Accessed: 2023-03-25. 2023. URL: https://flutter.dev.

[184] Tsung-Yi Lin, Michael Maire, et al. “Microsoft COCO: Common Objects in Context”. In: *CoRR* abs/1405.0312 (2014). arXiv: 1405.0312. URL: http://arxiv.org/abs/1405.0312.

[185] Magdalena Bloier, Florian Hinterwimmer, et al. “Detection and Segmentation of Heterogeneous Bone Tumours in Limited Radiographs”. In: *Current Directions in Biomedical Engineering* 8.2 (Aug. 2022), pp. 69–72. DOI: 10.1515/cdbme-2022-1019. URL: https://doi.org/10.1515/cdbme-2022-1019.

[186] *A Multi-Task Deep Learning Model for Simultaneous Detection, Segmentation and Classification of Bone Tumors on Radiographs*. https://www.rsna.org/annual-meeting/awards-recognition/trainee-research-prize. Accessed: 2021-01-22. 2021.

[187] Saeid Safiri, Ali-Asghar Kolahi, et al. “Global, regional and national burden of osteoarthritis 1990-2017: a systematic analysis of the Global Burden of Disease Study 2017”. In: *Annals of the Rheumatic Diseases* 79.6 (May 2020), pp. 819–828. DOI: 10.1136/annrheumdis-2019-216515. URL: https://doi.org/10.1136/annrheumdis-2019-216515.

[188] Zhenwu Cao, Xiujun Mai, et al. “Unicompartmental Knee Arthroplasty vs High Tibial Osteotomy for Knee Osteoarthritis: A Systematic Review and Meta-Analysis”. In: *J. Arthroplasty* 33.3 (Mar. 2018), pp. 952–959.

[189] Joseph N Liu, Avinesh Agarwalla, et al. “High Tibial Osteotomy and Medial Meniscus Transplant”. en. In: *Clin. Sports Med.* 38.3 (July 2019), pp. 401–416.

[190] Patricia M Lutz, Philipp W Winkler, et al. “Complex patellofemoral reconstruction leads to improved physical and sexual activity in female patients suffering from chronic patellofemoral instability”. en. In: *Knee Surg. Sports Traumatol. Arthrosc.* 29.9 (Sept. 2021), pp. 3017–3024.

[191] Kent T Yamaguchi, Edward C Cheung, et al. “Effects of Anterior Closing Wedge Tibial Osteotomy on Anterior Cruciate Ligament Force and Knee Kinematics”. In: *Am. J. Sports Med.* 46.2 (Feb. 2018), pp. 370–377.

[192] Elliot Sappey-Marinier, Cécile Batailler, et al. “Mechanical alignment for primary TKA may change both knee phenotype and joint line obliquity without influencing clinical outcomes: a study comparing restored and unrestored joint line obliquity”. In: *Knee Surg. Sports Traumatol. Arthrosc.* (July 2021).

[193] Xiaoyu Liu, Zhenxian Chen, et al. “High Tibial Osteotomy: Review of Techniques and Biomechanics”. en. In: *J. Healthc. Eng.* 2019 (May 2019).

[194] Matthew L Brown, Julie C McCauley, et al. “Osteochondritis Dissecans Lesion Location Is Highly Concordant With Mechanical Axis Deviation”. In: *Am. J. Sports Med.* 48.4 (Mar. 2020), pp. 871–875.

[195] Byoung-Yoon Hwang, Sung-Jae Kim, et al. “Risk Factors for Medial Meniscus Posterior Root Tear”. In: *Am. J. Sports Med.* 40.7 (July 2012), pp. 1606–1610.

[196] Yi-Lun Wang, Tuo Yang, et al. “Association Between Tibial Plateau Slopes and Anterior Cruciate Ligament Injury: A Meta-analysis”. en. In: *Arthroscopy* 33.6 (June 2017), 1248–1259.e4.

[197] Justin M Webb, Lucy J Salmon, et al. “Posterior Tibial Slope and Further Anterior Cruciate Ligament Injuries in the Anterior Cruciate Ligament–Reconstructed Patient”. In: *Am. J. Sports Med.* 41.12 (Dec. 2013), pp. 2800–2804.

[198] Florian B Imhoff, Victor Funke, et al. “The complexity of bony malalignment in patellofemoral disorders: femoral and tibial torsion, trochlear dysplasia, TT–TG distance, and frontal mechanical axis correlate with each other”. In: *Knee Surg. Sports Traumatol. Arthrosc.* 28.3 (Mar. 2020), pp. 897–904.

[199] Jakob Ackermann, Gergo Merkely, et al. “The Effect of Mechanical Leg Alignment on Cartilage Restoration With and Without Concomitant High Tibial Osteotomy”. en. In: *Arthroscopy* 36.8 (Aug. 2020), pp. 2204–2214.

[200] Qiang Zheng, Sphoorti Shellikeri, et al. “Deep Learning Measurement of Leg Length Discrepancy in Children Based on Radiographs”. en. In: *Radiology* 296.1 (July 2020), pp. 152–158.

[201] Yu-Cheng Yeh, Chi-Hung Weng, et al. “Deep learning approach for automatic landmark detection and alignment analysis in whole-spine lateral radiographs”. en. In: *Sci Rep* 11.1 (Apr. 2021), p. 7618.

[202] Willem Paul Gielis, Hassan Rayegan, et al. “Predicting the mechanical hip-knee-ankle angle accurately from standard knee radiographs: a cross-validation experiment in 100 patients”. en. In: *Acta Orthop* 91.6 (June 2020), pp. 732–737.

[203] Thong Phi Nguyen, Dong-Sik Chae, et al. “Intelligent analysis of coronal alignment in lower limbs based on radiographic image with convolutional neural network”. en. In: *Comput Biol Med* 120 (Mar. 2020), p. 103732.

[204] Thomas G Dietterich. “Ensemble methods in machine learning”. In: *Multiple Classifier Systems: First International Workshop, MCS 2000 Cagliari, Italy, June 21–23, 2000 Proceedings 1*. Springer. 2000, pp. 1–15.

[205] Prem N. Ramkumar, Michael Pang, et al. “Meaningless Applications and Misguided Methodologies in Artificial Intelligence–Related Orthopaedic Research Propagates Hype Over Hope”. In: *Arthroscopy: The Journal of Arthroscopic &amp Related Surgery* 38.9 (Sept. 2022), pp. 2761–2766. DOI: 10.1016/j.arthro.2022.04.014. URL: https://doi.org/10.1016/j.arthro.2022.04.014.

[206] Sebastian Simon, Gilbert M Schwarz, et al. “Fully automated deep learning for knee alignment assessment in lower extremity radiographs: a cross-sectional diagnostic study”. en. In: *Skeletal Radiol* 51.6 (Nov. 2021), pp. 1249–1259.

[207] R. Kyle Martin, Christophe Ley, et al. “Artificial intelligence and machine learning: an introduction for orthopaedic surgeons”. In: *Knee Surgery, Sports Traumatology, Arthroscopy* 30.2 (Sept. 2021), pp. 361–364. DOI: 10.1007/s00167-021-06741-2. URL: https://doi.org/10.1007/s00167-021-06741-2.

[208] Sunho Ko, Ayoosh Pareek, et al. “Artificial intelligence in orthopedics: three strategies for deep learning with orthopedic specific imaging”. In: *Knee Surgery, Sports Traumatology, Arthroscopy* 30.3 (Jan. 2022), pp. 758–761. DOI: 10.1007/s00167-021-06838-8. URL: https://doi.org/10.1007/s00167-021-06838-8.

[209] Yun Pei, Wenzhuo Yang, et al. “Automated measurement of hip-knee-ankle angle on the unilateral lower limb X-rays using deep learning”. en. In: *Phys Eng Sci Med* 44.1 (Nov. 2020), pp. 53–62.

[210] Matthias J. Feucht, Philipp W. Winkler, et al. “Isolated high tibial osteotomy is appropriate in less than two-thirds of varus knees if excessive overcorrection of the medial proximal tibial angle should be avoided”. In: *Knee Surgery, Sports Traumatology, Arthroscopy* 29.10 (July 2020), pp. 3299–3309. DOI: 10.1007/s00167-020-06166-3. URL: https://doi.org/10.1007/s00167-020-06166-3.

[211] Michael Tanzer and Asim M Makhdom. “Preoperative Planning in Primary Total Knee Arthroplasty”. en. In: *J Am Acad Orthop Surg* 24.4 (Apr. 2016), pp. 220–230.

[212] Marc-Daniel Ahrend, Heiko Baumgartner, et al. “Influence of axial limb rotation on radiographic lower limb alignment: a systematic review”. en. In: *Arch Orthop Trauma Surg* (Oct. 2021).

[213] Kenichi Goshima, Takeshi Sawaguchi, et al. “Large opening gaps, unstable hinge fractures, and osteotomy line below the safe zone cause delayed bone healing after open-wedge high tibial osteotomy”. In: *Knee Surgery, Sports Traumatology, Arthroscopy* 27.4 (Dec. 2018), pp. 1291–1298. ISSN: 1433-7347. DOI: 10.1007/s00167-018-5334-3. URL: http://dx.doi.org/10.1007/s00167-018-5334-3.

[214] A Miniaci, F T Ballmer, et al. “Proximal tibial osteotomy. A new fixation device”. en. In: *Clin Orthop Relat Res* 246 (Sept. 1989), pp. 250–259.

[215] Matthias J. Feucht, Philipp Minzlaff, et al. “Degree of axis correction in valgus high tibial osteotomy: proposal of an individualised approach”. In: *International Orthopaedics* 38.11 (July 2014), pp. 2273–2280. ISSN: 1432-5195. DOI: 10.1007/s00264-014-2442-7. URL: http://dx.doi.org/10.1007/s00264-014-2442-7.

[216] Ali Leylavi Shoushtari, Paolo Dario, et al. “A review on the evolvement trend of robotic interaction control”. In: *Industrial Robot: An International Journal* 43.5 (2016), pp. 535–551. DOI: 10.1108/IR-02-2016-0073. (Visited on 01/29/2018).

[217] Christopher Schindlbeck and Sami Haddadin. “Unified passivity-based Cartesian force/impedance control for rigid and flexible joint robots via task-energy tanks”. In: *2015 IEEE International Conference on Robotics and Automation (ICRA)*. IEEE, May 2015. DOI: 10.1109/icra.2015.7139036. URL: http://dx.doi.org/10.1109/ICRA.2015.7139036.

[218] Neville Hogan. “Impedance Control: An Approach to Manipulation: Part II—Implementation”. In: *Journal of Dynamic Systems, Measurement, and Control* 107.1 (1985), p. 8. ISSN: 00220434. DOI: 10.1115/1.3140713.

[219] I. D. Walker. “The use of kinematic redundancy in reducing impact and contact effects in manipulation”. In: *Proceedings*. Los Alamitos, Calif and Piscataway, NJ: IEEE Computer Society Press, 1990, pp. 434–439. ISBN: 0-8186-9061-5. DOI: 10.1109/ROBOT.1990.126016.

[220] O. Khatib. “A unified approach for motion and force control of robot manipulators: The operational space formulation”. In: *IEEE Journal on Robotics and Automation* 3.1 (Feb. 1987), pp. 43–53. ISSN: 0882-4967. DOI: 10.1109/JRA.1987.1087068.

[221] William D. Fisher and M. Shahid Mujtaba. “Hybrid Position/Force Control: A Correct Formulation”. In: *The International Journal of Robotics Research* 11.4 (1992), pp. 299–311. ISSN: 0278-3649. DOI: 10.1177/027836499201100403.

[222] Alexander Dietrich, Christian Ott, et al. “An overview of null space projections for redundant, torque-controlled robots”. In: *The International Journal of Robotics Research* 34.11 (2015), pp. 1385–1400. DOI: 10.1177/0278364914566516. eprint: https://doi.org/10.1177/0278364914566516. URL: https://doi.org/10.1177/0278364914566516.

[223] J. Sandoval, G. Poisson, et al. “A new kinematic formulation of the RCM constraint for redundant torque-controlled robots”. In: *2017 IEEE/RSJ International Conference on Intelligent Robots and Systems (IROS)*. Sept. 2017, pp. 4576–4581. DOI: 10.1109/IROS.2017.8206326.

[224] Chae An and J. Hollerbach. “Kinematic stability issues in force control of manipulators”. In: *Proceedings. 1987 IEEE International Conference on Robotics and Automation*. Institute of Electrical and Electronics Engineers, 1987, pp. 897–903. DOI: 10.1109/ROBOT.1987.1087933.

[225] H. Zhang. “Kinematic stability of robot manipulators under force control”. In: *Robotics and Automation, IEEE International Conference On, ’89*. Los Alamitos: IEEE Computer Society Press, 1989, pp. 80–85. ISBN: 0-8186-1938-4. DOI: 10.1109/ROBOT.1989.99971.

[226] Alain Liégeois. “Automatic Supervisory Control of the Configuration and Behavior of Multibody Mechanisms”. In: *IEEE Transactions on Systems, Man, and Cybernetics* 7.12 (1977), pp. 868–871. ISSN: 0018-9472. DOI: 10.1109/TSMC.1977.4309644.

[227] B. Nemec and L. Zlajpah. “Force control of redundant robots in unstructured environment”. In: *IEEE Transactions on Industrial Electronics* 49.1 (2002), pp. 233–240. ISSN: 02780046. DOI: 10.1109/41.982267.

[228] Hamid Sadeghian, Mehdi Keshmiri, et al. “Null-space impedance control with disturbance observer”. In: *2012 IEEE/RSJ International Conference on Intelligent Robots and Systems*. IEEE, 2012, pp. 2795–2800. ISBN: 978-1-4673-1736-8. DOI: 10.1109/IROS.2012.6385690.

[229] Jaeheung Park and Oussama Khatib. “Robot multiple contact control”. In: *Robotica* 26.05 (2008), p. 126. ISSN: 0263-5747. DOI: 10.1017/S0263574708004281.

[230] Robert Platt, Muhammad Abdallah, et al., eds. *Multiple-priority impedance control: (ICRA) ; 9 - 13 May 2011, Shanghai, China*. Piscataway, NJ: IEEE, 2011. ISBN: 9781612843865. DOI: 10.1109/ICRA.2011.5980228.

[231] M. W. Gertz, Jin-Oh Kim, et al. “Exploiting redundancy to reduce impact force”. In: *Intelligent Robots and Systems ’91: Proceedings IROS ’91*. New York: Institute of Electrical and Electronics Engineers, 1991, pp. 179–184. ISBN: 0-7803-0067-X. DOI: 10.1109/IROS.1991.174446.

[232] W. J. Chung, I. H. Kim, et al. “Null-space dynamics-based control of redundant manipulators in reducing impact”. In: *Control Engineering Practice* 5.9 (1997), pp. 1273–1282. ISSN: 09670661. DOI: 10.1016/S0967-0661(97)84366-3.

[233] Felix Sygulla, Christoph Schuetz, et al. “Adaptive motion control in uncertain environments using tactile feedback”. In: *International Conference on Advanced Intelligent Mechatronics (AIM)*. Ed. by IEEE. Piscataway, NJ: IEEE, 2016, pp. 1277–1284. ISBN: 978-1-5090-2065-2. DOI: 10.1109/AIM.2016.7576946.

[234] Benjamin J. Fregly, Thor F. Besier, et al. “Grand challenge competition to predict in vivo knee loads”. In: *Journal of Orthopaedic Research* 30.4 (Dec. 2011), pp. 503–513. DOI: 10.1002/jor.22023. URL: https://doi.org/10.1002/jor.22023.

[235] Yuhua Song, Richard E. Debski, et al. “A three-dimensional finite element model of the human anterior cruciate ligament: a computational analysis with experimental validation”. In: *Journal of Biomechanics* 37.3 (Mar. 2004), pp. 383–390. DOI: 10.1016/s0021-9290(03)00261-6. URL: https://doi.org/10.1016/s0021-9290(03)00261-6.

[236] Darryl D. D’Lima, Nikolai Steklov, et al. “In vivo contact stresses during activities of daily living after knee arthroplasty”. In: *Journal of Orthopaedic Research* 26.12 (June 2008), pp. 1549–1555. DOI: 10.1002/jor.20670. URL: https://doi.org/10.1002/jor.20670.

[237] Thomas P Andriacchi and Annegret Mündermann. “The role of ambulatory mechanics in the initiation and progression of knee osteoarthritis”. In: *Current Opinion in Rheumatology* 18.5 (Sept. 2006), pp. 514–518. DOI: 10.1097/01.bor.0000240365.16842.4e. URL: https://doi.org/10.1097/01.bor.0000240365.16842.4e.

[238] Leena Sharma. “The Role of Knee Alignment in Disease Progression and Functional Decline in Knee Osteoarthritis”. In: *JAMA* 286.2 (July 2001), p. 188. DOI: 10.1001/jama.286.2.188. URL: https://doi.org/10.1001/jama.286.2.188.

[239] S.A. Banks and W.A. Hodge. “Accurate measurement of three-dimensional knee replacement kinematics using single-plane fluoroscopy”. In: *IEEE Transactions on Biomedical Engineering* 43.6 (June 1996), pp. 638–649. DOI: 10.1109/10.495283. URL: https://doi.org/10.1109/10.495283.

[240] Horacio Martinez, Constantin von Deimling, et al. “Real-time 3D visualization in an open architecture of a robotic application in the biomechanics”. In: *2012 IEEE International Conference on Robotics and Biomimetics (ROBIO)*. IEEE, Dec. 2012, pp. 709–717. DOI: 10.1109/robio.2012.6491174. URL: https://doi.org/10.1109/robio.2012.6491174.

[241] Chung Hui James Tan, Tim Saier, et al. “Effect of three remplissage techniques on tendon coverage and shoulder kinematics: a navigated robotic biomechanical study”. In: *BMC Musculoskeletal Disorders* 17.1 (Jan. 2016). DOI: 10.1186/s12891-015-0856-z. URL: https://doi.org/10.1186/s12891-015-0856-z.

[242] Johan Bellemans, William Colyn, et al. “The Chitranjan Ranawat Award: Is Neutral Mechanical Alignment Normal for All Patients?: The Concept of Constitutional Varus”. In: *Clinical Orthopaedics &amp Related Research* 470.1 (Jan. 2012), pp. 45–53. DOI: 10.1007/s11999-011-1936-5. URL: https://doi.org/10.1007/s11999-011-1936-5.

[243] S M Howell, J D Roth, et al. “Kinematic Alignment in Total Knee Arthroplasty: Definition, History, Principle, Surgical Technique, and Results of an Alignment Option for TKA”. In: *Arthropaedia* 1 (2014), pp. 44–53.

[244] J.R.B. Hutt, M.-A. LeBlanc, et al. “Kinematic TKA using navigation: Surgical technique and initial results”. In: *Orthopaedics &amp Traumatology: Surgery &amp Research* 102.1 (Feb. 2016), pp. 99–104. DOI: 10.1016/j.otsr.2015.11.010. URL: https://doi.org/10.1016/j.otsr.2015.11.010.

[245] C. Rivière, F. Iranpour, et al. “Alignment options for total knee arthroplasty: A systematic review”. In: *Orthopaedics &amp Traumatology: Surgery &amp Research* 103.7 (Nov. 2017), pp. 1047–1056. DOI: 10.1016/j.otsr.2017.07.010. URL: https://doi.org/10.1016/j.otsr.2017.07.010.

[246] J M Landsmeer. “Anatomical and functional investigations on the articulation of the human fingers”. en. In: *Acta Anat Suppl (Basel)* 25.24 (1955), pp. 1–69.

[247] N K Fowler and A C Nicol. “Interphalangeal joint and tendon forces: normal model and biomechanical consequences of surgical reconstruction”. en. In: *J Biomech* 33.9 (Sept. 2000), pp. 1055–1062.

[248] Scott F M Duncan, Caitlin E Saracevic, et al. “Biomechanics of the hand”. en. In: *Hand Clin* 29.4 (Oct. 2013), pp. 483–492.

[249] Benjamin I Binder-Markey and Wendy M Murray. “Incorporating the length-dependent passive-force generating muscle properties of the extrinsic finger muscles into a wrist and finger biomechanical musculoskeletal model”. en. In: *J Biomech* 61 (June 2017), pp. 250–257.

[250] M Mirakhorlo, N Van Beek, et al. “A musculoskeletal model of the hand and wrist: model definition and evaluation”. en. In: *Comput Methods Biomech Biomed Engin* 21.9 (Sept. 2018), pp. 548–557.

[251] Lucas Engelhardt, Maximilian Melzner, et al. “A new musculoskeletal AnyBody™ detailed hand model”. en. In: *Comput Methods Biomech Biomed Engin* (Dec. 2020), pp. 1–11.

[252] Angélica Vargas, Karla Chiapas-Gasca, et al. “Clinical Anatomy of the Hand”. In: *Reumatologıéa Clıénica* 8 (Dec. 2012), pp. 25–32. DOI: 10.1016/j.reuma.2012.10.004. URL: https://doi.org/10.1016/j.reuma.2012.10.004.

[253] Benjamin Vedder. *VESC - Open Source ESC*. Accessed: 2023-04-17. 2022. URL: %5Curl%7Bhttp://vedder.se/2015/01/vesc-open-source-esc/%7D.

[254] NVIDIA. *Isaac SDK*. Accessed: 2023-04-17. 2022. URL: https://developer.nvidia.com/isaac-sdk.

[255] Xingyu Chen, Yufeng Liu, et al. “MobRecon: Mobile-Friendly Hand Mesh Reconstruction from Monocular Image”. In: *arXiv:2112.02753* (2021).

[256] Aude Billard and Danica Kragic. “Trends and challenges in robot manipulation”. In: *Science* 364.6446 (June 2019). DOI: 10.1126/science.aat8414. URL: https://doi.org/10.1126/science.aat8414.

[257] Joshua Fishman, Samuel Ubellacker, et al. “Dynamic Grasping with a "Soft" Drone: From Theory to Practice”. In: *2021 IEEE/RSJ International Conference on Intelligent Robots and Systems (IROS)*. IEEE, Sept. 2021. DOI: 10.1109/iros51168.2021.9635927. URL: https://doi.org/10.1109/iros51168.2021.9635927.

[258] R.J. Sanchez, E. Wolbrecht, et al. “A pneumatic robot for re-training arm movement after stroke: rationale and mechanical design”. In: *9th International Conference on Rehabilitation Robotics, 2005. ICORR 2005.* 2005, pp. 500–504. DOI: 10.1109/ICORR.2005.1501151.

[259] Joonho Chang, Andris Freivalds, et al. “Investigation of index finger triggering force using a cadaver experiment: Effects of trigger grip span, contact location, and internal tendon force”. In: *Applied Ergonomics* 65 (2017), pp. 183–190. ISSN: 0003-6870. DOI: https://doi.org/10.1016/j.apergo.2017.06.011. URL: https://www.sciencedirect.com/science/article/pii/S0003687017301448.

[260] Dan Hu, David Howard, et al. “Biomechanical Analysis of the Human Finger Extensor Mechanism during Isometric Pressing”. In: *PLOS ONE* 9.4 (Apr. 2014), pp. 1–11. DOI: 10.1371/journal.pone.0094533. URL: https://doi.org/10.1371/journal.pone.0094533.

[261] Peng Gao, Hyeonseung Lee, et al. “Improved Position Estimation Algorithm of Agricultural Mobile Robots Based on Multisensor Fusion and Autoencoder Neural Network”. In: *Sensors* 22.4 (2022). ISSN: 1424-8220. DOI: 10.3390/s22041522. URL: https://www.mdpi.com/1424-8220/22/4/1522.

[262] Jensen K. Henry, Jeffrey W. Hoffman, et al. “The Impact of Progressive Collapsing Foot Deformity on Foot &amp Ankle Kinematics and Plantar Pressure During Simulated Gait”. In: *Foot and Ankle Orthopaedics* 7.1 (Jan. 2022), 2473011421S0023. DOI: 10.1177/2473011421s00237. URL: https://doi.org/10.1177/2473011421s00237.

[263] Xiyang Sun, Yingtao Liu, et al. “A neuromechanical model for Drosophila larval crawling based on physical measurements”. In: *BMC Biology* 20.1 (June 2022). DOI: 10.1186/s12915-022-01336-w. URL: https://doi.org/10.1186/s12915-022-01336-w.

[264] H Josephs, RL Huston, et al. “Dynamics of Mechanical Systems”. In: *Applied Mechanics Reviews* 56.2 (Mar. 2003), B22–B23. DOI: 10.1115/1.1553436. URL: https://doi.org/10.1115/1.1553436.

[265] Leo Dorst, Chris Doran, et al., eds. *Applications of Geometric Algebra in Computer Science and Engineering*. Birkhäuser Boston, 2002. DOI: 10.1007/978-1-4612-0089-5. URL: https://doi.org/10.1007/978-1-4612-0089-5.

[266] Emanuel Todorov, Tom Erez, et al. “MuJoCo: A physics engine for model-based control”. In: *2012 IEEE/RSJ International Conference on Intelligent Robots and Systems*. IEEE. 2012, pp. 5026–5033. DOI: 10.1109/IROS.2012.6386109.

[267] Adam Paszke, Sam Gross, et al. “PyTorch: An Imperative Style, High-Performance Deep Learning Library”. In: *Advances in Neural Information Processing Systems 32*. Curran Associates, Inc., 2019, pp. 8024–8035. URL: http://papers.neurips.cc/paper/9015-pytorch-an-imperative-style-high-performance-deep-learning-library.pdf.

[268] Pierre Baldi. “Autoencoders, Unsupervised Learning, and Deep Architectures”. In: *Proceedings of ICML Workshop on Unsupervised and Transfer Learning*. Ed. by Isabelle Guyon, Gideon Dror, et al. Vol. 27. Proceedings of Machine Learning Research. Bellevue, Washington, USA: PMLR, July 2012, pp. 37–49. URL: https://proceedings.mlr.press/v27/baldi12a.html.

[269] A. Hyvaerinen and E. Oja. “Independent component analysis: algorithms and applications”. In: *Neural Networks* 13.4 (2000), pp. 411–430. ISSN: 0893-6080. DOI: https://doi.org/10.1016/S0893-6080(00)00026-5. URL: https://www.sciencedirect.com/science/article/pii/S0893608000000265.

[270] Diederik P Kingma and Max Welling. *Auto-Encoding Variational Bayes*. 2013. DOI: 10.48550/ARXIV.1312.6114. URL: https://arxiv.org/abs/1312.6114.

[271] Bai Li, Tankut Acarman, et al. “Optimization-Based Trajectory Planning for Autonomous Parking With Irregularly Placed Obstacles: A Lightweight Iterative Framework”. In: *IEEE Transactions on Intelligent Transportation Systems* 23.8 (2022), pp. 11970–11981. DOI: 10.1109/TITS.2021.3109011.

[272] Balakumar Sundaralingam and Tucker Hermans. “Relaxed-rigidity constraints: kinematic trajectory optimization and collision avoidance for in-grasp manipulation”. In: *Autonomous Robots* 43.2 (June 2018), pp. 469–483. DOI: 10.1007/s10514-018-9772-z. URL: https://doi.org/10.1007/s10514-018-9772-z.

[273] Filip Maric, Matthew Giamou, et al. “Riemannian Optimization for Distance Geometric Inverse Kinematics”. In: *CoRR* abs/2108.13720 (2021). arXiv: 2108.13720. URL: https://arxiv.org/abs/2108.13720.

[274] Bai Li, Yakun Ouyang, et al. “Mixed-Integer and Conditional Trajectory Planning for an Autonomous Mining Truck in Loading/Dumping Scenarios: A Global Optimization Approach”. In: *IEEE Transactions on Intelligent Vehicles* 8.2 (2023), pp. 1512–1522. DOI: 10.1109/TIV.2022.3214777.

[275] John Schulman, Filip Wolski, et al. “Proximal Policy Optimization Algorithms”. In: *CoRR* 1707.06347 (2017). arXiv: 1707.06347. URL: http://arxiv.org/abs/1707.06347.

[276] David A. Warrell, Timothy M. Cox, et al. *Oxford Textbook of Medicine*. Oxford University Press, May 2010. ISBN: 9780199204854. DOI: 10.1093/med/9780199204854.001.1. URL: https://doi.org/10.1093/med/9780199204854.001.1.

[277] Constantinos N. Maganaris and John P. Paul. “In vivo human tendon mechanical properties”. In: *The Journal of Physiology* 521.1 (Nov. 1999), pp. 307–313. DOI: 10.1111/j.1469-7793.1999.00307.x. URL: https://doi.org/10.1111/j.1469-7793.1999.00307.x.

[278] Khaled Mamou, E Lengyel, et al. “Volumetric hierarchical approximate convex decomposition”. In: *Game Engine Gems 3*. AK Peters, 2016, pp. 141–158.

[279] R. E. Kalman. “A New Approach to Linear Filtering and Prediction Problems”. In: *Journal of Basic Engineering* 82.1 (Mar. 1960), pp. 35–45. DOI: 10.1115/1.3662552. URL: https://doi.org/10.1115/1.3662552.

[280] DGOU. *Forschungspreis Digitalisierung in Orthopaedie und Unfallchirurgie*. https://dgou.de/preise-stipendien/preise/versorgungsforschung/forschungspreis-digitalisierung-in-o-und-u. Accessed: 2024-03-22. 2023.

Acknowledgments

I would like to acknowledge the use of ChatGPT, an AI language model developed by OpenAI, which assisted with language editing of this manuscript. All suggestions provided by the tool were carefully reviewed and verified by me, and the final interpretations and conclusions remain my own.

A Abbreviations and Acronyms

ACL Anterior Cruciate Ligament

ADC Analog to Digital

AE Autoencoder

AI Artificial Intelligence

AMA Ankle Mechanical Axis

CAD Computer Aided Design

CI Confidence Intervall

CMC Carpometacarpal Joint

CNN Convolutional Neural Network

COCO Common Objects in Context

CRPS Chronic Regional Pain Syndrome

CT Computer Tomography

DASH Disabilities of the Arm, Shoulder and Hand

DIP Distal Interphalangeal Joint

DL Deep Learning

DOF Degree of Freedom

EXP Exposure in Vivo

FE Finite Element

FSR Force Sensing Resistor

GAN Generative Adversarial Network

HD High Definition

ICA Independent Component Analysis

ICC Inter Class Correlation

IP Interphalangeal

IMU Internal Measurement Unit

IoU Intersection over Union

IP Interphalangeal Joint

JLCA Joint Line Convergence Angle

KJL Knee Joint Line

KJLO Knee Joint Line Obliquity

LLR Long Leg Radiograph

MAD Mechanical Axis Deviation

MCP Metacarpophalangeal Joint

mFTA Mechanical Femorotibial Angle

ML Machine Learning

mLDFA Medial Lateral Distal Femoral Angle

mLDTA Medial Lateral Distal Tibial Angle

mLPFA Medial Lateral Patellar Femoral Angle

mMPTA Medial Proximal Tibial Angle

MoCo Momentum Contrastive

mow-HTO medial opening wedge High Tibia Osteotomy

MPJPE Mean Per-Joint Position Error

MRI Magnet Resonance Imaging

MS Multi Scale

MSD Mean Squared Deviation

MSE Mean Squared Error

MS-TrainSim Multi Scale Training Simulation

MuJoCo Multiple Joints in Contact

OA Osteoathritis

OI Osteoarthritis Initiative

OS Orthopedic Surgeon

PCL Posterior Cruciate Ligament

PIP Proximal Phalangeal Joint

PPO Proximal Policy Optimization

PROM Patient-Reported Outcome Measures

PWM pulse width modulation

RL Reinforcement Learning

RMS Root Mean Square

RMSE Root Mean Square Error

ROM Range of Motion

SC Single Scale

SD Storage Device

SDK Software Development Kit

SLA Stereolithography

TDA Total Deviation Angle

TKA Total Knee Arthroplasty

TP Tibia Plateau

UHD Ultra High Definition

VAE Variational Autoencoder

VESC Vedder electric velocity controller

List of Symbols

$(\boldsymbol{S}_x\boldsymbol{J})^{\#}$	Reduced Jacobian for position control.
α	Step size in null space control equations.
$\boldsymbol{\delta x}, \boldsymbol{\delta f}$	Position and force error vectors in Cartesian task space.
$\dot{\boldsymbol{q}}, \ddot{\boldsymbol{q}}$	First and second derivatives of the minimum coordinates $\boldsymbol{q}$ with respect to time, representing the velocities and accelerations of the finger joints.
$\boldsymbol{\tau}_c$	Control torque.
$\boldsymbol{F}_{\text{sum}}$	Sum of external forces acting on a body, calculated for each finger joint.
$\boldsymbol{g}_x, \boldsymbol{g}_f$	Linear control functions for position and force, respectively.
$\boldsymbol{I}$	Identity matrix.
$\boldsymbol{J}$	Jacobian matrix.
$\boldsymbol{J}_p$	Translatory Jacobian at the impact point.
$\boldsymbol{J}_x$	Position-selected Jacobian matrix.
$\boldsymbol{M}_{\text{sum}}$	Sum of moments (torques) acting on a body, calculated for each finger joint.
$\boldsymbol{N}$	Null space matrix, facilitating orthogonal projection of the Jacobian.
$\boldsymbol{N}_f$	Specialized null space matrix for filtering position-controlled joint velocities in force-prioritized control architecture.
$\boldsymbol{n}_f$	Normalized force vector.
$\boldsymbol{N}_x$	Null space matrix of the reduced Jacobian $\boldsymbol{J}_x$.
$\boldsymbol{p}$	Translation vector.
$\boldsymbol{q}$	Quaternion representing orientation.
$\boldsymbol{q} = (\alpha, \beta, \gamma)^T$	Minimum coordinates for the dynamic finger model, representing the angular positions of the three finger joints.
$\boldsymbol{S}_x, \boldsymbol{S}_f$	Selector matrices for position and force, respectively.
$\delta\ddot{f}, \delta\ddot{f}_{\{x,y,z\}}$	Dynamics differentiated and solved for control variables in stability and decoupling analyses.
δf	Scalar force error between the desired and actual forces.
$\dot{\boldsymbol{q}}_c$	Control joint velocity.
$\dot{\boldsymbol{u}}_t, \dot{\boldsymbol{u}}_j, \dot{\boldsymbol{u}}_n$	Velocity inputs in task, joint, and null spaces, respectively.
$\dot{\boldsymbol{x}}_t$	Task space velocity.
$\dot{f}_a$	Actual force rate at the tool center point.
$\dot{x}_p$	Contact space velocity.
$\dot{x}_f, \dot{y}_f, \dot{z}_f$	Direction-dependent force-driven velocities.
η_0	Initial value function parameters for reinforcement learning-based parameter adaptation.
$\hat{A}_t$	Advantage estimate at time t, used for computing the policy gradient.
$\hat{g}$	Estimated gradient for optimization in policy gradient methods.
$\hat{X}_{\text{mea}}$	Reconstructed data from the differentiable forward kinematics model.
λ (AE context)	Weighting factor balancing the reconstruction loss and KL-divergence in the VAE loss function.

λ (RL context)	Hyperparameter in the reinforcement learning framework balancing robust training and asymptotic behavior.
$\mathbb{D}$	Set of local trajectories collected during reinforcement learning optimization.
$\mathcal{L}(X_{\text{mea}}, \hat{X}_{\text{mea}})$	Loss function representing the reconstruction error between measured data X_{mea} and reconstructed data $\hat{X}_{\text{mea}}$.
MSE	Mean Squared Error, a common measure of reconstruction error in autoencoders.
NN_Ψ	Neural network modeling the inverse kinematics.
reward_t	Reward function at time t, incorporating desired motion behavior and process stability.
μ_i, σ_i^2	Mean and variance of the i-th component in the probabilistic distribution encoded by a VAE.
$\pi_\psi(a_\tau)$	Policy in the reinforcement learning framework, determining the set of parameters ψ for each trajectory τ.
${}_I\boldsymbol{F}_i$	External forces acting on body i, described in the inertial reference frame I.
${}_I\boldsymbol{J}_{T,i}^T$	Transposed Jacobian matrix for translation, relating joint velocities to linear velocities of body i in the inertial frame I.
${}_{K_i}\boldsymbol{\omega}_i$	Angular velocity of body i, described in the body-fixed coordinate frame K_i.
${}_{K_i}\boldsymbol{J}_{R,i}^T$	Transposed Jacobian matrix for rotation, relating joint velocities to angular velocities of body i in the body-fixed frame K_i.
${}_{K_i}\boldsymbol{L}_i$	Angular momentum of body i, described in the body-fixed coordinate frame K_i.
${}_{K_i}\boldsymbol{M}_i$	Moments (torques) acting on body i, described in the body-fixed coordinate frame K_i.
ψ	Parameter vector encapsulating the model's dynamic properties, set as learnable parameters for optimization.
Ψ^*, Θ^*	Optimized parameters of the autoencoder, including both the neural network parameters Ψ and the kinematic parameters Θ.
ψ_0	Initial policy parameters for the reinforcement learning-based parameter adaptation.
τ_{mea}	Localized measurement trajectories, used for segmenting measurement data into smaller regions.
axis_i	Axis vector representing the orientation of a hinge joint.
$\text{cov}(q_i, q_j)$	Covariance between components q_i and q_j of the encoded representation.
position_i	Position of the rotational axis of a hinge joint.
Θ	Joint parameters in the forward kinematics model visualization.
FT_{Mea}	Measured force-torque, used as input for both simulated and measured motions.
k_n	Kinematic variable related to contact stiffness.
L_{ICA}	ICA-inspired regularization term aimed at encouraging feature independence by penalizing the covariance of the encoded representations.
L_{KL}	KL-divergence in the VAE framework, quantifying the difference between the encoded distribution and a prior distribution.
L_{rec}	Reconstruction loss in the VAE framework, measuring the difference between the measured data and its reconstruction from the encoded distribution.

L_{VAE}	Overall loss function for a VAE, combining the reconstruction loss L_{rec} and the KL-divergence L_{KL}.
$M_1 - M_3$	Unknown torques at the finger joints, representing either resistance to motion or actuation torque applied by the patient.
$n_{f_x}, n_{f_y}, n_{f_z}$	Cartesian components of the normal force vector.
$P(\tau, \psi)$	Probability of trajectory τ under parameters ψ.
Q	Joint angles derived from pose measurements.
R	Rotation matrix.
$R(\tau)$	Reward associated with trajectory τ.
T, d, c	Scalar variables for time constant, dimensionless damping, and stiffness, respectively.
$T_j(q_i)$	Transformation matrix dependent on joint positions q_i.
T_{eff}	Transformation matrix from the base to the end effector in a kinematic chain.
T_{b_i}	Transformation matrix related to rigid body b_i.
T_{o-b_i}	Transformation matrix representing the position of body b_i relative to an origin frame o.
$U(\psi)$	Expected reward over trajectories τ, optimized by selecting parameters ψ.
V_η	Value function used to calculate the advantage and minimize update variance in policy gradient computation.
X_{mea}	Dataset of pose measurements.
x_{Mea}	Measured motion, used as a reference for optimizing the simulation.
x_{Sim}	Simulated motion, dependent on measured force-torque FT_{Mea} and dynamic parameters ψ.